BIODEGRADABLE NANO- AND MICROPARTICLES FOR GENE DELIVERY AND IMMUNE ACTIVATION

by

Joel C. Sunshine

A dissertation submitted to Johns Hopkins University in conformity with the requirements for the degree of Doctor of Philosophy

Baltimore, Maryland

May 2013

Abstract

This thesis discusses the development of biodegradable polymers, nanoparticles, and microparticles for gene delivery and immune activation. The bulk of this thesis focuses on trying to understand basic principles important to the development of polymer-based gene delivery nanoparticles and acellular artificial antigen presenting cells (aAPC) for CD8+ T cell activation, In addition to the basic work, these technologies can be applied to many areas of human health and I have focused on applications in cancer and ophthalmology.

The root cause of many diseases has a genetic component, from single gene disorders like hemophilia to multifactorial disorders like cancer. As a result, gene therapy has enormous therapeutic potential if it can be done safely and efficiently. The vast majority of the effort into gene therapy has been directed at co-opting viruses as vectors for gene delivery, as viruses have evolved to be supremely efficient at getting their genetic information into foreign cells, but viral gene therapy has been hampered by high profile setbacks in clinical trials, owing to the potential for insertional mutagenesis and overly aggressive host immune responses to the vector. Theoretically, non-viral gene therapy should overcome these limitations by reducing the host response, enabling unlimited cargo capacity, and should be easier to produce and standardize. However, non-viral gene therapy has thus far been unable to achieve the required high transfection efficacies seen with viruses. A class of synthetic cationic polymers, poly(ß-amino)esters (PBAEs), have shown promise, but in order to develop next-generation synthetic polymer vectors for gene delivery, a deeper understanding of the relationship between polymer design and functional outcomes is required. In this thesis, I investigated structure-

function relationships within a library of PBAEs that we developed, with an eye towards investigating the impact of polymer properties on critical barriers to intracellular delivery. To extend this work, we looked to develop PBAEs for non-viral gene delivery to the eye, by investigating how different particle formulations might enable differential delivery to ocular cell types, and by performing a pilot study looking at *in vivo* gene delivery to the mouse retina via subretinal injection. We found that polymer hydrophobicity was a critical dimension that significantly effected polymer vector performance. We also found that the amine termini of PBAEs were critical to vector function at the level of nanoparticle uptake even though they did not substantially alter any putative key nanoparticle properties. We found that polymer formulations that worked well for one cell class worked well for another cell type within that class but may not work well for a different cell class, and demonstrated that PBAEs could engender high levels of gene expression in the mouse retina.

Tumor immunotherapy requires the activation of cytotoxic T lymphocytes (CTLs) against tumor-specific targets. This activation process occurs *in vivo* through the interaction of activated antigen presenting cells (APCs) with CD8+ T-cells in the lymph nodes. As an alternative to inducing biological APCs to create the targeted response of interest in the CD8+ T cell population, acellular artificial antigen presenting cells (aAPC) have been designed that mimic biological APC by presenting proteins for signal 1 (antigen specificity) and signal 2 (costimulation) on the surface of spherical particles. When activated, biological APCs undergo significant changes to surface composition AND surface morphology; however, in the quest to mimic this process and engender immune responses with aAPCs, the focus has been squarely on the changes to surface

protein composition. We hypothesized that artificial antigen presenting cell (aAPC) shape (or morphology) is a critical parameter that modulates T-cell activation and proliferation. We hypothesized that high aspect ratio ellipsoidal aAPCs, rather than spherical aAPCs, might enable increased contact between aAPCs and T-cells, result in enhanced T-cell activation *in vitro*, and mediate enhanced aAPC-based tumor killing *in vivo* in melanoma mouse models. To this end, we fabricated ellipsoidal aAPCs using PLGA microparticles, and tested the effects of shape on T-cell activation and tumor prevention by aAPCs *in vitro* and *in vivo*. We found that ellipsoidal aAPCs were substantially more efficient than their spherical counterparts at CTL activation, that increased aspect ratio resulted in increased activation, and that ellipsoidal aAPCs reduced / delayed tumor growth and increased mouse survival as compared to spherical and non-cognate controls in a melanoma tumor prevention study *in vivo*.

Thesis Committee

Jordan J. Green, Ph.D. *(primary advisor, reader)*

Assistant Professor, Department of Biomedical Engineering

Johns Hopkins University School of Medicine

Jonathan P. Schneck, M.D. Ph.D.

Professor, Department of Pathology,

Johns Hopkins University School of Medicine

Hai-Quan Mao, Ph.D. *(reader)*

Associate Professor, Department of Materials Science and Engineering,

Johns Hopkins University School of Medicine

Kevin J. Yarema, Ph.D.

Associate Professor, Department of Biomedical Engineering,

Johns Hopkins University School of Medicine

Acknowledgments

This work could not be completed without the guidance, support, and energy of many people who I would like to thank from the bottom of my heart.

I would like to thank my mentor, Dr. Jordan Green, for his constant guidance, energy and enthusiasm. I could not have found a better mentor than Dr. Green, always offering helpful advice and productive discussions both about the science in the lab but also about life in general. He always encouraged exploration of new and novel ideas. I truly appreciate how much he truly cares about what is best for me. I will try my best to model my mentorship and future leadership after his style.

Equally important to my Ph.D. experience, both scientifically and personally, were the amazing members of the Green Group. To Corey Bishop, Nupura Bhise, Jay Kim, Kristen Kozielski, Ron Shmueli, and Stephany Tzeng – you guys were the best labmates I could possibly ask for. From our ping-pong sessions, extended lunches, movie outings, and fantastic conversations about life, to the always-productive scientific discussions and helpful advice, I thank you for a wonderful experience and am glad to have made life-long friends.

I would like to thank my thesis committee, Dr. Jonathan Schneck, Dr. Hai-Quan Mao, and Dr. Kevin Yarema for their support and encouragement throughout this process. I am incredibly grateful for their time, energy, and enthusiasm.

I would like to thank my family. To my parents, Phil and Margot, and siblings, Josh and Avi, I thank you for your support, excitement and unconditional love. To my in-laws, Henry and Rachel, I thank you for being the best parents-in-law I could possibly have, and for being a source of fantastic advice for all thing medical and scientific. Last,

but certainly not least, I would like to thank my wife, Sarah, for her support, patience, and boundless energy. You have made this experience all that much more sweet.

Contents

1 Table of Contents

List of tables

List of figures

1 Chapter 1: Introduction to the thesis

1.1 Objectives

Gene therapy has the potential to treat a wide variety of diseases, but the development of gene delivery in the clinic has been hampered by high profile setbacks with viral gene delivery. Non-viral gene therapy, however, has thus far been unable to achieve the required high transfection efficacies seen with viruses. A class of synthetic cationic polymers, poly(ß-amino)esters (PBAEs), have shown promise, but in order to develop next-generation synthetic polymer vectors for gene delivery, a deeper understanding of the relationship between polymer design and functional outcomes is required. We hypothesized that understanding how polymer chemical structure relates to the barriers inherent to intracellular gene delivery will help to optimize our gene delivery formulations and will enhance our understanding of the pivotal barriers to successful non-viral, polymer based gene delivery. To that end, I synthesized a library of degradable end-modified poly(β-amino ester)s and investigated structure-function relationships and how polymer properties such as hydrophobicity and buffering capacity relates to non-viral gene delivery efficacy (**Aim 1**). We hypothesize that polymer structure can be tuned so that polymeric gene delivery nanoparticles have specific efficacy in one type of cell over another type of cell. To investigate this, we used the gene delivery library to deliver DNA to three different, interrelated cell types – human umbilical vein endothelial cells (HUVECs), human retinal endothelial cells (HRECs), and retinal pigment epithelial cells (RPEs). This allowed us to examine the ability of diverse, but structurally related library of PBAEs, to deliver genes to two endothelial cell types (HUVEC and HREC) and one

epithelial cell type (RPE) which is also found in the retina (**Aim 2a**). We were also interested in extending this study to investigate whether we could use this technology for *in vivo* delivery to the RPE (**Aim 2b**).

The critical component of cancer immunotherapy revolves around the activation of anti-tumor cytotoxic T cells (CTL) by antigen presenting cells (APCs). Artificial antigen presenting cells (aAPC) have been designed to mimic true APC by presenting proteins for signal 1 (antigen specificity) and signal 2 (costimulation) on the surface of spherical particles. We hypothesized that artificial antigen presenting cell (aAPC) shape is a critical parameter that modulates T-cell activation and proliferation. We hypothesized that high aspect ratio ellipsoidal aAPCs, rather than spherical aAPCs, might enable increased contact between aAPCs and T-cells, result in enhanced T-cell activation *in vitro*, and mediate enhanced aAPC-based tumor killing *in vivo* in melanoma mouse models. To this end, we fabricated ellipsoidal aAPCs using PLGA microparticles, and tested the effects of shape on T-cell activation and tumor prevention by aAPCs *in vitro* and *in vivo* (**Aim 3**). The specific aims defined for this thesis were as follows:

Aim 1. Synthesize a library of degradable end-modified poly(β-amino ester)s and investigate structure function relationships and the impact of polymer properties on non-viral gene delivery.

a. Synthesize a library of degradable end-modified poly(β-amino ester)s
b. Investigation of structure-function relationships such as the effect of base polymer hydrophobicity and end-group modification

c. Characterize key members of the library with respect to the barriers to intracellular gene delivery

Aim 2. Optimize gene delivery for ocular applications *in vitro* and *in vivo*

a. Deliver DNA to HUVECs, HRECs, and RPEs *in vitro* to optimize gene delivery for ocular applications and examine the performance of the library across multiple cell types with an eye towards identifying if the polymers display cell type specificity
b. As a proof of concept, deliver DNA to the RPE *in vivo* using a subretinal injection model

Aim 3. Fabricate novel biodegradable microparticles with varying shapes as aAPCs and measure their efficacy at stimulating T-cells *in vitro* and *in vivo*.

a. Construction and characterization of biodegradable ellipsoidal aAPCs
b. Evaluate *in vitro* interactions and efficacy of ellipsoidal aAPCs
    1) Determine how shape and formulation affects T-cell activation, proliferation, and function
    2) Mechanistic analysis of aAPC shape in interaction with T-cells
c. Evaluate *in vivo* interactions and efficacy of ellipsoidal aAPCs

1.2 Summary of contributions

The major contributions and accomplishments of this thesis work are:

Chapter 2. State of the Art

- **Sunshine JC**, Bishop CJ, Green JJ. "Advances in polymeric and inorganic vectors for nonviral nucleic acid delivery." *Therapeutic Delivery*. 2011; 2(4):493-521
- **Sunshine, J.C.**, Green, J.J. Nanoengineering Approaches to the Design of Artificial Antigen Presenting Cells. *Nanomedicine* (2013).

Chapter 3.

- **Sunshine JC**, Bhise NB, Green JJ. "Degradable polymers for gene delivery." *Conference Proceedings IEEE Engineering in Medicine and Biology Society*. 2009; 1:2412-5.
- Green JJ, **Sunshine JC,** Bhise N, Shmueli RB, Tzeng SY. "Multicomponent Degradable Cationic Polymers." U.S. Patent P-10753-02. Filed: May 17, 2010.
- **Poster Presentation - Sunshine JC**, Bhise N, Shmueli R, Divi S, Rauck B, Green JJ. "High-Throughput Development of Degradable Polymers for Gene Delivery" presented at the Johns Hopkins NanoBio Symposium. Baltimore, MD. May 18, 2009.
- **Poster Presentation - Sunshine JC**, Bhise N, Akanda M, Shmueli R, Li D, Green JJ. "Biphasic degrading polymers for intracellular delivery" presented at the 10th US-Japan Symposium on Drug Delivery Systems. Maui, HI. Dec. 16-20, 2009

- **Poster Presentation - Sunshine JC**, Bhise N, Shmueli R, Li D, Akanda M, Green JJ. “Bioreducible Cationic Polymers for Gene Delivery: Backbone, End-Capping Still Matters” presented at the Johns Hopkins NanoBio Symposium. Baltimore, MD. April 29, 2010.

Chapter 4.

- **Sunshine JC**, Akanda MI, Li D, Kozielski KL, and Green JJ. “Effects of Base Polymer Hydrophobicity and End-Group Modification on Polymeric Gene Delivery.” *Biomacromolecules*. 2011; 12(10),3592–3600

Chapter 5.

- **Sunshine JC**, Peng DY, Green JJ. “Uptake and transfection with polymeric nanoparticles are dependent on polymer end-group structure, but largely independent of nanoparticle physical and chemical properties.” *Molecular Pharmaceutics*. 2012; 9(11),3375-3383
- **Poster Presentation -** Peng DY, **Sunshine JC**, Green JJ. "Characterization of Degradable Poly(ester amines) and Poly(amidoamines)for Non-viral Gene Delivery" presented at the Annual Meeting of the Biomedical Engineering Society. Austin, TX. October 6-9, 2010, and at the 2011 INBT Annual Symposium, Baltimore, MD. May 13, 2011.

Chapter 6.

- Shmueli RB*, **Sunshine JC***, Xu Z, Duh EJ, Green JJ. “Gene delivery nanoparticles specific for human microvasculature and microvasculature.”

Nanomedicine: NBM. 2012; 8(7):1200-7. * These authors contributed equally to this manuscript

- **Poster Presentation -** Shmueli R, **Sunshine JC**, Duh E, Green JJ. "Non-viral Gene Delivery for Microvasculature and Macrovasculature," presented at the Wilmer Eye Institute Research Day, Baltimore, MD. April 15, 2011.

Chapter 7.

- **Sunshine JC***, Sunshine SB*, Handa JT, Green JJ. "Poly(β-amino ester)-Nanoparticle Mediated Transfection Of Retinal Pigment Epithelial Cells *in vitro* and *in vivo*." *PLoS ONE*. 2012; 7(5), e37543. * These authors contributed equally to this manuscript
- **Poster Presentation - Sunshine JC**, Sunshine SB, Handa JT, Green JJ. "Transfection of Retinal Pigment Epithelial Cells with a Combinatorial Library of Poly(beta-amino)esters" presented at the Wilmer Eye Institute Research Day, Baltimore, MD. April 15, 2011, and at ARVO (Association for Research in Vision and Opthalmology), Ft. Lauderdale, FL. May 1-5, 2011.

Chapter 8.

- **Sunshine JC***, Perica KP*, Schneck JP, Green JJ. "Particle shape dependence of CD8+ T cell activation by artificial antigen presenting cells." *Biomaterials*. 2013. * These authors contributed equally to this manuscript
- Green JJ, Perica K, Schneck J, **Sunshine JC**. "Artificial Cells of Defined and Dynamic Size and Shape." U.S. Prov. Patent. Filed: December 15, 2011

- **Poster Presentation - Sunshine JC**, Perica K, Schneck JP, Green JJ. "Particle shape matters for T-cell activation by artificial Antigen Presenting Cells (aAPC)" presented at the 2012 INBT Annual Symposium, Baltimore, MD. May 4, 2012.
- **Talk - Sunshine JC**, Perica K, Schneck JP, Green JJ. "T-cell activation by artificial antigen presenting cells (aAPC): Effects of particle shape" presented at the 86th ACS Colloid and Surface Science Symposium, Baltimore, MD. Jun. 10-13, 2012.
- **Talk - Sunshine JC**, Perica K, Schneck JP, Green JJ. "Shape-dependence of T-cell induction by artificial Antigen Presenting Cells (aAPC)" presented at the 10th US-Japan Symposium on Drug Delivery Systems. Maui, HI. Dec. 16-20, 2011.
- **Talk - Sunshine JC**, Perica K, Schneck JP, Green JJ. "Non-Spherical Artificial Antigen Presenting Cells for Tumor Immunotherapy" presented at the Society for Biomaterials. Boston, MA. Apr. 10-13, 2013.

Chapter 9.

- **Sunshine JC**, Green JJ. "Nanoengineering approaches to the design of artificial antigen presenting cells." *Nanomedicine*. 2013; 8(7), 1173-1189

Other Peer-Reviewed Publications

- Bhise N, Gray R, **Sunshine JC**, Htet S, Ewald A, Green JJ. "The relationship between terminal functionalization and molecular weight of a gene delivery polymer and transfection efficacy in mammary epithelial 2-D cultures and 3-D organotypic cultures." *Biomaterials*. 2010; 31(31):8088-96

- Bhise N, Shmueli RB, **Sunshine JC**, Tzeng SY, Green JJ. "Drug delivery strategies for therapeutic angiogenesis and antiangiogenesis." *Expert Opinion on Drug Delivery*. 2011; 8(4):485-504
- Tzeng SY, Guerrero-Cázares H, Martinez EE, **Sunshine JC**, Quiñones-Hinojosa A, Green JJ. "Non-Viral Gene Delivery Nanoparticles based on Poly(beta-amino) esters for Treatment of Glioblastoma." *Biomaterials*. 2011; 32(23):5402-10
- Bishop, CJ, Ketola, TM, Tzeng, SY, **Sunshine, JC**, Urtti, A, Lemmetyinen, H, Vuorimaa-Laukkanen, E., Yliperttula, M., Green, J.J. The Effect and Role of Carbon Atoms in Poly(beta-amino ester)s for DNA Binding and Gene Delivery. *Journal of the American Chemical Society* (2013).

1.3 Outline of the Thesis

This thesis describes the development and characterization of a PBAE library with respect to structure function relationships within the library and polymer properties related to intracellular barriers to entry. It also describes optimization of the PBAE library for use in ocular applications both *in vitro* and *in vivo*. Finally, the development, characterization, and optimization of a biodegradable, non-spherical, acellular artificial Antigen Presenting Cell (aAPC) system for tumor immunotherapy is discussed.

Chapter 2 presents an overview of the current state of the art techniques and nanotechnology platforms developed for cationic polymer-based non-viral gene delivery vectors and for artificial antigen presentation on acellular substrates. Chapter 3 reports the development of initial PBAE vectors and their performance in trasfection of cancer cells and non-cancerous fibroblasts. The effect of small changes in molecular structure on transfection efficiency is discussed. Chapter 4 describes the synthesis of the PBAE library in full, and details structure-function relationships within the library, particularly focusing on the relationship of base polymer hydrophobicity to transfection and cytotoxicity. Chapter 5 details an investigation into PBAE polymer and nanoparticle properties relevant to the barriers to intracellular delivery; in particular, the particle size, charge, binding affinity, polymer buffering capacity, polymer degradation rate were studied as they related to particle uptake, cell transfection and cytotoxicity.

Chapter 6 reports the performance of the polymer library across three related cell types – two endothelial cell types (human umbilical vein endothelial cells or HUVECs, and human retinal endothelial cells or HRECs) and 2 ocular cell types (the HRECs and retinal pigment epithelial cells or RPEs). Of particular interest, the performance of the

library was highly correlated between the 2 endothelial cell types (HUVEC and HREC), but not very highly correlated between the epithelial cell type (RPE) and either endothelial cell type. Chapter 7 describes an initial, pilot, *in vitro* and *in vivo* study to determine the feasibility of using PBAEs for gene delivery to the retinal pigment epithelium.

Chapter 8 describes the development of a biodegradable, non-spherical, acellular aAPC system for tumor immunotherapy. Spherical and ellipsoidal aAPCs were synthesized and characterized by SEM, fluorimetry, and confocal imaging, and were tested *in vitro* for their comparative ability to induce cognate-peptide specific T cell proliferation at a variety of particle doses, protein densities, and particle aspect ratios. The aAPCs were then compared in a tumor-prevention model *in vivo.*

Chapter 9 presents concluding remarks and suggests future directions to be pursued for building on the work described herein. This includes preliminary work on using PBAEs for transfection of dendritic cells for genetic vaccine delivery, the development of nanoscale biodegradable aAPCs, and suggestions to improve the current generation of artificial antigen presenting cells using nanoengineering approaches.

2 Chapter 2: State of the Art

2.1 Cationic Polymers for Non-viral Nucleic Acid Delivery

Nucleic acid therapies have enormous potential in the clinic, from treatment of specific genetic diseases such as cystic fibrosis [1], Leber hereditary optic neuropathy [2], hemoglobinopathies [3, 4] and hemophilia [5], to the treatment of cancer [6, 7] and cardiovascular disease [8] and the use of genetic vaccines [9]. Additionally, nucleic acid delivery plays a crucial role in cellular engineering and basic biomedical research, through the ability to knock in and knock down genes and proteins in the lab, as well as in the creation of induced-pluripotent stem-cells (iPSCs) by viral [10, 11] and non-viral [12] methods.

The central challenge for effective therapy using nucleic acids is finding a safe and effective delivery system [13]. With regards to gene therapy, since viral gene therapy can have serious safety concerns [14], recent efforts have focused on non-viral methods.

There are several barriers to cellular entry and delivery of the nucleic acid cargo that challenge the development of an effective delivery vehicle (**Fig. 2.1**). The vehicle needs to form a stable complex with its nucleic acid cargo, protect it from degradation extracellularly, arrive at the cell of interest, get internalized (typically via either receptor-mediated endocytosis and or non-specific endocytic pathways), escape endo-lysosomal degradation, release its cargo, and harmlessly degrade or otherwise be removed.

This chapter contains excerpts from an article that was published as Sunshine JC, Bishop CJ, Green JJ. "Advances in polymeric and inorganic vectors for nonviral nucleic acid delivery." *Therapeutic Delivery*. 2011; 2(4):493-521.

After escaping the endosomal compartment and making it into the cytoplasm, DNA and agRNA need to make it to the nucleus. This is among the largest challenges remaining to non-viral gene delivery. Recently, several groups have shown that it takes between 30 and 100 times more DNA delivered to the cytoplasm than it does to the nucleus to give the same level of gene expression, even in dividing cells [15]. Dividing cells are more easily transfected because mitosis-associated nuclear envelope breakdown greatly enhances nuclear localization of plasmids and transfection efficiency; however this is not a requirement - plasmids can enter the nuclei through nuclear pore complexes (NPCs) in the absence of cell division, although significantly less efficiently [16].

Yet simply getting to the nucleus is not the end of the line. Cohen et al showed that cells transfected with lipofectamine or polyethylenimine contained between 75 and 50,000 plasmids/nucleus [17]. They also noted that a subpopulation of cells that contained only 3x the average number of cells had 100x the expression of the rest of the population, indicating that downstream processes aside from nuclear importation are also crucial [17].

Various cationic polymer systems have been utilized for nucleic acid delivery. A wide range of structures have been explored, including linear and branched non-degradable polycations as well as biodegradable and bioreducible polycations and oligosacharides. Some of the most commonly use polymer structures are shown in **Fig. 2.2**. All of these polymers have secondary or tertiary amino groups, a portion of which are protonated at neutral pH, which enables electrostatic interaction with the anionic nucleic acid.

Poly-l-lysine (PLL) was the first polymeric gene transfection agent developed, and was shown to condense DNA into small complexes with rod (25-50 nm) or toroidal (40 to 80 nm) structure [18]. PLL can be synthesized by several-step polymerization of ε,N-benzyloxycarbonyl-α,N-carboxy-L-lysine anhydride[19]. PLL is limited by its high cytotoxicity and lack of bio-degradability, so various groups since then have conjugated PLL to a variety of other molecules such as poly-ethylene glycol (PEG)[20], targeting ligands such as asialoorosomucoid [21], transferring [22], galactose [23, 24], lactose [25], folate [26], and endosomolytic groups like histidine [27].

Poly(ethylenimine) (PEI) was the second polymeric transfection agent developed [28]. Branched PEI (b-PEI) can be synthesized from aziridine monomers under acidic conditions, and linear PEI (l-PEI) can be synthesized by the hydrolysis of poly(2-proplyl-2-oxazoline)[29], or by polymerization of aziridine monomers at lower temperatures [30]. Compared to later generation nucleic acid delivery agents, PEI is extremely cytotoxic, leading to necrosis and apoptosis [31]. The high proportion of nitrogen atoms provides for a strong buffering effect ("the proton sponge effect") that is advantageous for endosomal escape, as described below. 25 kDa b-PEI has been shown to be an efficient transfection reagent with reduced toxicity as compared to higher molecular weight b-PEI [32]. For delivery of shorter nucleic acids (e.g. mRNA) only low molecular weight PEI (2 kDa or less) leads to efficient biological effect, as complexes with higher molecular weight PEI are too stable and do not release the nucleic acid into the cytoplasm [33].

Poly(lactide-co-glycolide) (PLGA) microspheres have been used extensively in nucleic acid delivery for their utility in and their relative biocompatibility and biodegradability. PLGA is synthesized by co-polymerization of glycolic acid and lactic

acid with various catalysts, and hydrolytically degradable. Microparticles can be formed from pre-made polymer by emulsion evaporation, emulsion diffusion, solvent displacement and salting out techniques, and particle size depends on the formulation conditions and molecular weight of the starting material [34]. Both the polymer and its degradation products are well tolerated in animal studies [35, 36].

As opposed to mostly linear, cross-linked, or other branched systems, dendrimers such as poly(amido amine) (PAMAM) dendrimers are synthesized iteratively to produce nanoscale structures characterized by dendritic connectivity and radial symmetry. Advantages of dendrimeric systems include precise, nanoscale, structural control, densely modifiable surface chemistry (for addition of targeting ligands, modification of surface charge etc), and high charge density for complexation and buffering. PAMAM dendrimers were first synthesized in the mid 1980s [37]. Typically, ethyenediamine or ammonia are used as cores and allowed to undergo repeating two-step reactions whereby methyl acrylate is added by Michael addition to all the primary amines, and then the ester groups are amidated by a large excess of ethylenediamine to produce primary amine termini. They have been extensively studied for gene delivery [38, 39] as well as oligonucleotide delivery [40-43]. Interestingly, thermal degradation of the dendrimers was shown to increase transfection efficacy [44].

Poly(β-amino ester)s (PBAE) are synthesized by Michael addition of either primary or bis(secondary) aliphatic amines to diacrylate compounds [45], and their simple chemistry leads them naturally to a combinatorial approach to synthesis and screening of polymer libraries[46-50]. They are hydrolytically degradable at the

backbone ester linkages, and their tertiary amines along the backbone allow for buffering of the endosome.

2.1.1 Physical Requirements

When designing gene therapy vectors it is important to note that physical properties such as size, aspect ratio, molecular weight, surface area, shape, polydispersity, zeta potential, and others, can have an impact on cytotoxicity and delivery [51]. To meet certain barrier requirements for gene delivery, surface modifications can be used to modify the physical properties of the delivery system to improve circulation time and solubility (i.e., PEGylation) [52] [cb1], localization (i.e., folic acid, RGD) [53], biostability (i.e., zeta potential: amine or carboxylic groups) [52], cytotoxicity (addition of carboxyl or hydroxyl groups) [54, 55], internalization, and inhibition of reticuloendothelial system clearance [56, 57].

2.1.1.1 Shape

Recently, manipulation of particle shape has come into focus as a new method for modulating drug delivery [58]. Local shape of the particle where it made contact with the cell and not the overall shape dictated whether or not it was internalized by a macrophage [59]. Elongated particles have been shown to circulate longer and avoid phagocytosis more effectively than spherical particles [60], however, spherical particles are much more efficiently internalized into target tissues as compared to elongated particles [61]. Seeking to take advantage of this property, a group has recently constructed PLGA-based shape shifting particles (one way, from ellipsoid to spherical) in response to temperature,

pH, or a chemical signal and demonstrated efficient uptake of the spheres as compared to the ellipsoids (**Fig. 2.3**) [62].

Other nanoparticle morphologies may prove worthwhile investigating to assess cytotoxicity and nucleic acid delivery as potential vectors. DeSimone used soft lithography using polydimethylsiloxane and perfluoropolyether to make a mold enabling nanoparticle replication in a non-wetting template. Using this, nanoparticles with diverse shapes synthesizable (i.e., 200 nm trapezoidal particles, 200 x 800 nm bar particles, 3 μm arrow particles, and 2.5 x 1 μm^2 hexnut particles with 1 μm holes) [63].

2.1.1.2 Size

Polymer nanoparticles have been developed with a wide variety of sizes for different purposes. Nanoparticles of approximately 100 nm show prolonged blood circulation and a relatively low rate of mononuclear-phagocyte system uptake [64]. Particles with a 1-5 μm diameter are likely to be trapped in the liver and phagocytosed by Kupffer cells [62]. Particles larger than 5 μm are likely to be trapped in the capillary beds [62]. When NPs are greater than 200 nm they are likely to be filtered in the spleen, whereas the NPs less than 100 nm are likely to leave the blood vessels through fenestrations in the endothelial lining [62]. NPs that are ~50-200 nm have been known to accumulate in tumors by the enhanced permeability and retention (EPR) effect (as a result of leaky vasculature and the absence of a draining lymphatic system) [65, 66]. It has been suggested that the particles must not exceed 300 nm to take advantage of the EPR effect [67]. Sizes smaller than 50 nm are likely to enter most cells and sizes smaller than 20 nm can extravasate [66, 68]. The glomerular apparatus' capillary wall has

fenestrations of approximately 4–5 nm and it has been reported that nanoparticles >8 nm cannot be filtered through the glomerular filtration system, which would increase circulation half-life [69].

2.1.1.3 Charge

When particles have neutral or slightly negative zeta potentials, they have a greater propensity to escape the reticuloendothelial system (RES) of the body and avoid nonspecific interaction with other biological milieu [70, 71]. However, when zeta potentials are positive, nanoparticles are more easily able to bind negatively charged cell membranes of target cells [72]. For example, the maximum zeta potentials of lysine-, arginine-, and histidine modified nanoemulsions were reported at 50 (highest transfection efficiency), 43, and 7 mV (lowest transfection efficiency), respectively [73]. On the other hand, NPs with positive zeta potentials can have greater affinity for anionic proteoglycans on the surface of cell membranes which can enhance cell contact and promote cellular uptake and internalization [74].

Some nanoparticles may be more or less cytotoxic depending on their charge (i.e., AuNPs are less cytotoxic when anionic [75]. It is important to consider zeta potentials when complexing nucleic acids via ionic interactions. The interaction must be strong enough to condense the nucleic acid to protect against restriction enzymes. It is important to note that zeta potentials of nanoparticles can switch signs when in the presence of serum and this should be considered in the design process [76, 77].

2.1.1.4 Biocompatibility

Biocompatibility is crucial for maintaining an appropriate host response during gene therapy. In depth assessments and characterizations are required to elucidate the physicochemical differences responsible for low cytotoxicity and acceptable viability.

PEI lacks degradable linkages and is too toxic for therapeutic applications, inducing both apopotosis and necrosis in an endothelial cell model [78]. PEI's efficacy and cytotoxicity are both often positively correlated with the molecular weight used, so low molecular weight PEI, while possessing reduced cytotoxicity, also is typically less efficacious (cite). As a result, a number of investigators have synthesized an array of degradable PEIs consisting of LMW PEIs and degradable cross-linkers, in the hopes of achieving higher efficacy with the reduced cytotoxicity of low molecular weight PEIs [79, 80].

Other groups have focused on developing new, biodegradable polymers for non-viral gene delivery, which we will review here by method of degradation. Biodegradable polymers should be able to both reduce the cytotoxicity associated with the transfection reagent as well and potentially improve dissocation of the vector from its cargo to allow the cargo to be utilized intracellularly.

Multiple strategies have been formulated using ester bonds to allow hydrolytic cleavage of the polymer. Amine containing hydrolyzable polymers have been utilized which are effective gene delivery agents with significantly decreased cytotoxicity as compared to non-degradable polymers such as poly(ethylenimine) (PEI) [28] and poly(lysine) (PLL) [18]. These structures include poly(lactide-*co*-glycolide) (PLGA) [81],

hyperbranched poly(amino ester)s [82], poly(lactic acid) (PLA) [36], and linear poly(β-amino ester)s (PBAE) [45], among others.

PBAEs are synthesized by simple Michael addition of primary or bis-secondary amines with diacrylate esters [45, 83]. Libraries of PBAEs have been developed for gene-vector screening [46-50]. Studies have shown that amine-terminated PBAEs are more effective at pDNA transfection than acrylate-terminated versions. Modification of the polymer ends with different amines can lead to virus-like efficacy in human primary cells *in vitro* (**Fig. 2.4**) [84]. Tuning of polymer end group leads to significant differences in transfection efficacy, and the optimal endgroup for each cell type appears to be cell-type specific [85, 86]. PBAEs also have been shown to be non-toxic to human primary cells *in vitro* [87] and in mice *in vivo* [88, 89].

2.1.1.5 "Stealth" properties

After intravenous administration, a variety of serum proteins bind to the surface of the nanoparticles, which are recognized by the scavenger receptor on the macrophage cell surface and internalized, leading to a significant loss of nanoparticles from the circulation [90]. Addition of hydrophilic moieties, like poly(ethylene glycol) (PEG), poly(N-(2-hydroxypropyl-methacrylamide) (pHPMA), and various oligosaccharides, have been shown to increase solubility, prolong circulation time, neutralize zeta potential, and reduce interactions with the environment within the bloodstream due to a higher tolerance against incubation with serum proteins [91, 92]. One disadvantage of this approach is that while it may stabilize the polyplex in serum and reduce cytotoxicity, it may also interfere with complexation and reduce transfection efficiencies depending on

the extent of addition [93]. Modification of the surface of preformed particles with PEG/pHPMA that can bind to exposed surface amino groups has been shown to alleviate this problem [91, 94]. Recently, Name et al. showed that adding PEG to PAMAM dendrimers via bis-aryl hydrazone bond linkages into the vector significantly enhanced the buffering capacity of the vector even with a high degree of PEGylation [95]. PEG can be added to a variety of nanoparticles and can be further modified to provide targeting [96-99], or can be attached by degradable bonds (such as matrix metaloproteinases (MMP)) that can be cleaved to expose underlying functionalities [100-104].

2.1.2 Nucleic Acid Complexation

Polymers for nucleic acid delivery typically rely on electrostatic interaction between the cationic polymer and the anionic phosphate backbone of nucleic acid substrate. For polymer:DNA complexes, requirements include condensation of the plasmid to an appropriate scale for internalization, neutralization of the negatively charged phosphate backbone of the DNA, and protection of DNA from degradation both intra- and extracellularly [105, 106]. Sufficient cationic charge is crucial to condense DNA, but it is also correlated with increased cytotoxicity, and higher DNA binding affinity may lead to decreased DNA release and reduced transport through the cytoplasm [107]. Alternatively, hydrolytically degradable nanoparticles can be formed through encapsulation of DNA by non-cationic polymers such as PLGA. These particles degrade to release their nucleic acid cargo and the size of the particlecan be controlled in the nanometer to micrometer range, depending on the method of particle formation used. Methods have been developed to protect the cargo from destruction during these

processes [81] but are still limited by low encapsulation efficiency and potential DNA degradation in the hydrolyzing polymer core [108].

Chitosan can form nanoparticles through a process called ionotropic gelation. Upon exposure to multivalent polyanions such as sodium tripolyphosphate (TPP), nanoparticles spontaneously form via linkages between the phosphate groups of TPP and the amino groups of chitosan [109]. Chitosan has been optimized to allow for the encapsulation of both hydrophilic and hydrophobic drugs and has been utilized in nucleic acid delivery [110, 111], most successfully as hybrid co-polymers with various polycations [112-114]. Chitosan is a versatile nucleic acid delivery agent, with recent work demonstrating the successful delivery of anti-sense oligodeoxynucleotides (asODN) using a folic acid (FA) conjugated hydroxypropyl-chitosan carrier, resulting in 35% inhibition of tumor growth [53], hepatocyte targeted gene delivery using a galactosylated chitosan-graft-polyethylenimine (GC-g-PEI)/DNA complexes-loaded poly(organophosphazene) thermosensitive biodegradable hydrogel [115], and siRNA [116].

2.1.3 Cellular Targeting

By utilizing a targeting moiety, smaller dosages can elicit comparable therapeutic responses while minimizing side effects and reducing the cost of therapy [117]. There are two types of targeting; passive and active. Passive targeting utilizes natural processes such as the enhanced permeability and retention effect, which utilizes the leaky tumor vasculature and lack of efficient lymphatic drainage in a solid tumor to lead to passive accumulation of drug at the tumor site, given sufficient circulation time [118]. Active

targeting consists of an additional ligand to assist in localization or internalization such as antibodies or their fragments (i.e., J591 against prostate-specific membrane antigens [119], anti-HER2 (Trastuzumab) [120], etc) [121], folic acid([122]), sugars (i.e., galactose, mannose, and lactose) [123], peptides (RGD) [124, 125], transferrin [126], and nucleic acid aptamers [127], Large target moieties, however, may hamper the internalization and or gene unpacking and may be disadvantageous and thus removing the target moiety at the cell surface may be worthwhile [117]. Targeting moieties are typically attached chemically but can be physically adsorped to the delivery system as well [128]. Interestingly, it has been shown that biodistribution of cargo at the accumulation site is independent of the presence of targeting ligands [66]**.** If there is preference for a tumor site and the targeting ligand is not a factor then the EPR effect is likely responsible for the biodistribution. The reason for improved functionality when targeting ligands are used appears to be due to an increase in cell internalization and specificity of the nanoparticles rather than tissue localization. Non-targeted nanoparticles have a propensity to end up in the extracellular space and tumor-associated macrophages [66].

Cationic polymers have been modified with targeting ligands for various applications. For example, the addition of lung surfactant to ternary nanoparticles for aerosol-based gene therapy enhances gene delivery to the lung, resulting in 12-fold higher transfection compared to pure nanoparticles and 30-fold higher compared to polyethylenimine [129]. Insulin adsorption significantly increased gene expression of PEI-pDNA nanoparticles up to 16-fold on alveolar epithelial cells but not on bronchial epithelial cells [130].

2.1.4 Endosomal Escape

In the early experiments with non-viral gene delivery, non-degradable polycations, including poly(l-lysine) (PLL), polyethylenimine (PEI) were used. A major advantage of PEI is the "proton sponge" effect due to PEI's extensive buffering capacity. When PEI:DNA complexes gain entry to the endosome, the secondary and tertiary amines in PEI function tobuffer acidification of the endosome. This causes an influx of negatively charged chloride ions into the endosome to maintain electroneutrality as protons are continually pumped into the endosome. Eventually, this leads to osmotic swelling and rupture of the endosomes and release of the vector and cargo into the cytoplasm. This mechanism has been widely explored for gene and siRNA delivery [28, 131]. This concept has also been extended and heavily used in the design of next-generation biodegradable vectors which also contain this buffering capacity.

Another widely used buffering moiety is the imidazole ring of histidine. It is a weak base with a (pKa ~ 6) capable of buffering the endosome. For example, a poly(phosphazene) based polymer has been histidylated, and the resulting polymer showed improved transfection and reduced cytotoxicity when compared to the histidine-free polymer and branched PEI [132].

Newer methods for endosomal escape involve functionalizing a polymer with peptides that enhance endosomal release. Melittin enables release of nonviral gene transfer particles into the cytoplasm and also enhances their transport into the nucleus, possibly via the cationic cluster KRKR near the C terminus of the peptide [133]. Modifying melittin either by reversible acetylation of a lysine residue in melittin [134] or

replacement of two glutamines with glutamic acids which get neutralized at acidic pH [135] takes advantage of the acidification of the endosome to induce membrane lysis only in the endosomal compartment and reduces the cytotoxicity associated with use. Functionalizing polylysine with polyethylene glycol and a pH-responsive melittin peptide was shown to be an efficient siRNA delivery agent [136].

Anionic fusogenic peptides, such as INF1-4, INF7, E5, and E5WYG, contain glutamate residues that protonate under acidic conditions (pH 5-5.5) in the endosome, triggering a conformational change from a random coil to alpha-helix, leading to membrane disruption [137-139]. Adding these peptides to polymeric vehicles was shown to enhance the endosomal escape rate constant by two orders of magnitude [140].

2.1.5 Release of Cargo / Degradation

Nucleic acids must be released from the vector to have an effect. This can be done by taking advantage of the redox potential gradient [141], acidic environment of the endosome [142], MMPs [143, 144], photocatalysis [145], and hydrolytic degradation of the carrier [45, 146, 147]. It has been shown that plasmid unpacking can be a limiting step with regards to gene expression for sufficiently large polymer constructs [148].

2.1.5.1 Bioreducible polymers

Using bioreducible polymers via incoporation of disulfide linkages takes advantage of the relative reducing environment of the intracellular space. Intracellular reduction of the disulfide bond occurs via the glutathione (GSH) pathway. GSH is regenerated from its oxidized form by glutathione reductase, and is an important

component in a multitude of pathways as well as playing a major function as part of cellular defense against oxidative stress. Disulfide bonds are stable extracellularly, preventing particle breakdown before the nano-complex reaches the cell surface, whereas the reducing environment of the intracellular space allows for enhanced polymer breakdown and nucleic acid release [149-153].

Disulfide bonds have been shown to degrade intracellularly within 3 hours [154]. When cell lines with different intrinsic glutathione levels were compared, increased cellular GSH levels were associated with improved transfection of mRNA polyplexes. No clear trend was observed for plasmid DNA or siRNA containing complexes; rather, the cell line which demonstrated the best DNA transfection was the fastest dividing cell line [155].

Enhancing release of the pDNA cargo can lead to dramatic gains in transfection efficiency. Carlisle et al condensed pDNA with thiolated polyethylenimine (PEI-SH) and surface-coated the resulting nanoparticles using thiol-reactive poly[*N*-(2-hydroxypropyl)methacrylamide] (PHPMA) with 2-pyridyldisulfanyl or maleimide groups, forming reducible disulphide-linked or stable thioether-linked coatings, respectively. Interestingly, disulfide-linked complexes showed 40-100-fold higher transfection activity than thioether-linked ones, demonstrating the utility of the bioreducible approach in enhancing pDNA release [103]. Chen et al synthesized a series of reducible hyperbranched poly(amido amine)s and found that reducible polymers were able to achieve nearly 200-fold higher transfection as compared to control polymers [156].

Combination of hydrolyzable and bioreducible functional groups as a single polymer might also help further tune the release profile[157].

Reducible polymers have also been used to deliver siRNA. Histidine containing reducible polycations based on CH(6)K(3)H(6)C monomers (His6 RPCs) were examined for their utility in delivering siRNA. Co-delivery of EGFP siRNA with pEGFP plasmid DNA reduced reporter gene expression by 85%. Interestingly, while as with most polymer systems, larger polymer size correlated with increased DNA transfection efficiency, effective delivery of siRNA was only possible with smaller polymers (36-80k) [158].

Low molecular weight PEI has also been crosslinked via disulfide linkages to show reduced cytotoxicity and equivalent DNA transfection efficacy to higher MW PEI [159]. In another study, reducible poly(amido ethylenimine) (SS-PAEI) was synthesized by addition copolymerization of triethylenetetramine and cystamine bis-acrylamide (poly(TETA/CBA)) and used as a carrier for siRNA. Under normal conditions they demonstrated significantly higher suppression of VEGF with poly(TETA/CBA) than linear-polyethylenimine. The addition of dl-buthionine sulfoxamine, which reduces intracellular level of reduced glutathione reduced the RNAi activity level of poly(TETA/CBA) formulation to that of L-PEI, showing that reduction of the polymer was crucial to gene knockdown [160].

Jere et al used a reducible polyspermine (RPS) carrier composed of multiple spermine units with disulfide linkages and showed improved efficacy in gene delivery and in gene knockdown compared to 25K PEI. RPS delivered anti-Akt1 sh/si/ssiRNA and altered the cancer cell survival, proliferation and metastasis to different extents depending on the nature of siRNA treatment [161].

2.1.5.2 Acid labile linkages

Acid labile linkages would also be useful for endosomal escape and for enhanced cargo release into the cytoplasm, as they take advantage of the acidification of the endosome to allow for release of the cargo. Acid labile acetal and ketal bond bearing polycations were recently developed for this purpose. Oligoethylenimines linked by either acid-degradable ketal or acetal linkers in a copolymer with 5 kDa PEG formed complexes with half-lives of 3 min at pH 5.0, and 5 h (OEI-MK) or 3.5 h (OEI-BAA) at physiological pH 7.4 [102]. Acid-reversible PEGylation was shown to improve polyplex compatibility and transfection efficiency [101].

Reversibly shielded polyplexes (polycation and PEG linked via acylhydrazides or pyridylhydrazines) exhibited up to 2 log orders of magnitude higher gene expression in vitro and 1 log magnitude higher gene expression in an in vivo mouse model, compared to the stably shielded control polyplexes [100].

2.1.6 Nuclear Translocation

Diffusion of DNA > 250 bp is significantly reduced in the cellular milieu compared with in solution due to involvement of the actin cytoskeleton [162]. The nuclear pore complex (NPC) forms a selective permeability barrier, allowing free diffusion of molecules (e.g. ions, small proteins, and metabolites) with a mass/size less than about 40 kDa/10 nm proteins [163]. Macromolecules greater than ~40 kDa are transported actively across the nuclear envelope through the nuclear pore complexes (NPCs) using soluble transport factors or carrier molecules (β-karyopherins) that cycle between the cytoplasm and nucleus [164]. In the classical case, nuclear localization

signals (NLS) are recognized by importin-α, which then binds to importin-β, and this complex is allowed through the NPC. Once inside the nucleus, the importin-β binding domain is released by binding to RanGTP and the cargo is released [164]. By electron microscopy and gold nanoparticles complexed to NLSs, Panté and Kann were able to show that the largest rigid particle to achieve nuclear entry through NPCs was ~39 nm in diameter including NLSs [165].

Strategies for obtaining access to the nucleus have relied primarily on diffusion through the cytoplasm and presentation of NLS to allow pDNA access to the nucleus [166]. Numerous groups have tried to complex synthetic or naturally occurring NLS peptides with the delivered DNA, with variable efficacy [167], and the ones which have been successful may be due to the peptides inducing improved nanoparticle complexation and not increased nuclear import [166]. A single NLS has been shown to be sufficient to carry the DNA through the NLS [168], but the addition of hundreds of NLS sequences to a plasmid lead to no nuclear localization of the plasmids [169], since multiple NLS sites might lead to the machinery attempting to pull a single plasmid through through multiple NPC at the same time, as well as potentially inhibit translation.

Two of the best characterized NLSs are the classical NLS from SV40 Large T-antigen (PKKKRKV) and the bipartite NLS in which the classical NLS is split into two halves (typically KKKX5−20RK). Proteins containing these NLS are bound by importins which allow access to the nucleus via the nuclear pore complex (NPC) [170]. Plasmids containing as little as 72 bp of the SV40 enhancer target to the nucleus of most cells within several hours, due to the enhancer containing binding sites for a number of

ubiquitously expressed mammalian transcription factors, each of which functions in the nucleus and contains an NLS [171].

2.1.7 Conclusions and Future Directions

Polymeric and inorganic based-vectors for nucleic acid delivery need to overcome many crucial barriers to entry in the delivery process, and a variety of novel approaches have been investigated to overcome those challenges. A wide array of materials have been investigated for their potential in this area, including degradable and non-degradable cationic polymers, oligo- and polysaccharides, among many others, each with unique properties and potential advantages.

Firstly, the vector must be stably complexed to the nucleic acid cargo and needs to stay compacted until cellular entry. The size, shape, surface charge, and surface functionality of the nanoparticles are crucial to efficient delivery, increased circulation time, and specific cellular entry of the nanoparticles. Size is a crucial parameter in determining the passive biodistribution of the nanoparticle delivery system, and charge shielding / PEGylation has been shown to improve circulation time and increase accumulation at tumor sites as a result of the EPR effect. Various groups have synthesized particles of different shapes and even developed shape-shifting particles whose shape-change can be triggered by pH, heat, and light.

The vast majority of delivery systems achieve cellular entry via endocytosis. For delivery of isRNA, interaction with TLR7 in the endosome is the end-goal, so nanoparticles should be designed to remain in the endosome and present the isRNA to TLR7 there. For siRNA and all DNA based systems, there needs to be a mechanism for

endosomal escape. The classical mechanism employed by non-viral vectors involves the proton-sponge effect, but novel endosomolytic peptides and acid triggered exposure of hydrophobic residues have also been utilized to engineer endosomal escape. Hydrolysis, bioreduction, and photolysis have been utilized extensively to reduce toxicity and promote unpacking of the cargo intracellularly. Trafficking DNA-based cargo to the nucleus remains an area of need, mostly relying on diffusion to bring the DNA to the nucleus and NLS sequences to allow nuclear import via the NPC.

There is a major need for fundamental understanding of how cationic polymer structure plays a role in overcoming the barriers to gene and nucleic acid delivery outlined above. The cationic-polymer based gene delivery component of my thesis focuses extensively on attempting to further describe structure-function relationships that we were able to extract from our combinatorial library approach to developing PBAE vectors for gene delivery (**Aim 1**). In addition, understanding how and why polymers work well in one cell type and not in another may help point the way to the generalizability of in vitro results, and may enable more efficient design of gene delivery vectors for particular applications (**Aim 2**).

2.2 Next Generation Artificial Antigen Presenting Cells for Tumor Immunotherapy

Synthetic biomaterials and particles can be engineered to be 'biomimetic', where they act similarly in an organism to natural biological molecules and cells. This biological mimicry can be beneficial for wound healing and regenerative medicine, new types of advanced therapeutics, coatings on medical devices, and other applications. One particular area where biomimetic particles have significant potential to advance medicine is in the field of tumor immunotherapy.

The main goal of tumor immunotherapy is to encourage the body's own immune responses to aberrant cells. The recognition that there are tumor-infiltrating immune cells, T lymphocytes or T cells, and the identification of the genes that are targeted by T cells in melanoma, led to the identification of tumor antigens for immunotherapy [172, 173] .Tumor antigens are specific biological molecules that are present at the nanoscale on the surfaces of cancer cells, but are not present on the surfaces of healthy cells. Numerous human tumor antigens recognized by T cells have now been identified and these antigens are promising targets for tumor immunotherapy[174].

A variety of approaches for tumor immunotherapy have been investigated, with the most common approach involving natural biological antigen presenting cells interacting with T cells. However, there are challenges with these approaches including efficacy, safety, cost, and general flexibility. If there was an off-the-shelf synthetic product that was relatively easy to manufacture, biocompatible and safe, and could engender strong and specific T-cell responses against an antigen, it would be a boon for the treatment of

many types of cancer as well as being beneficial for the treatment of other diseases such as infectious diseases[175]. To construct such an off-the-shelf synthetic product, biomimetic acellular artificial antigen presenting cells, there are many important design parameters to consider.

Much of the focus to date has in the development of aAPCs has centered on the identity of the surface-presented proteins used to target the T cell population and induce a response. Spherical, cell-sized (2-10 μm), isotropic (homogeneous surface presentation) aAPCs that present some of the same protein signals on their surface as biological antigen presenting cells (APCs) have been developed and well characterized, and are already attractive options for *ex vivo* T cell proliferation and have shown *in vivo* efficacy in mouse models[175-183].

2.2.1 How Biological Antigen Presenting Cells Work

Antigens on a tumor cell are recognized by a T cell by its T cell receptor (TCR). To accomplish this, naïve T cells must be directed to productively respond to TCR binding by antigen presenting cells that present specific antigen to T cells via major histocompatability complex (MHC) molecules. There are two classes of MHCs with different functions and that present different peptides. MHC class II molecules present peptides obtained via the endosomal-lysosomal route and serve to present peptides which come from outside the cell; thus presentation of non-self peptides in class II MHC is crucial to mediating the immune response to extracellular pathogens. MHC class I molecules, on the other hand, bind to peptides generated by the proteasome, and are used generally used to present peptides whose source is internal to the cell; thus presentation

of peptides in class II MHC is crucial to mediating the immune response to intracellular pathogens and cancer. Class I MHC function to activate $CD8^+$ T-cells or cytotoxic T-lymphocytes (CTL), whose primary function within the adaptive immune system is the recognition and killing of infected or cancerous cells within the body. There is a strong argument that class I MHC restricted tumor antigens that can be recognized by CTLs make the best "tumor rejection antigens", as class I MHC are present in all cells, CTLs are the primary effector arm of the immune response against cancer, and the fact that loss of HLA class I expression in cancer patients is strongly associated with disease progression[184]. Thus, control over $CD8^+$ T cell fate is critical to the success of tumor immunotherapy.

T cell fate is be dictated not only by the antigen recognized, but the context in which the antigen is recognized (**Fig. 2.5**). Naïve T cells that recognize pMHC (pMHC), without co-stimulation by secondary signals, are directed to become unresponsive to further stimuli (anergy) or die, which allows for T cell tolerance to form outside the immune organs. Professional APCs, like DCs, in addition to presenting peptide antigen-in-MHC on the surface (which is termed **signal 1**), provide secondary signals to the T cell in two main ways. Principally, recognition dependent activation is modulated by expression of surface molecules such as B7.1 that interact with other surface molecules on the T cell surface such as CD28 (termed **signal 2**) [185]. Secretable immunostimulatory factors like cytokines also serve to help direct T cell fate; these are often termed **signal 3**[186]. In addition to the identities of the molecules involved in the process, the interaction between a biological APC and a T cell requires close apposition of membranes over a large area of surface contact, and results in large-scale protein

rearrangements and the subsequent formation of the immune synapse (**Fig. 2.6a**, IS)[187, 188].

2.2.2 Artificial aAPCs

Artificial antigen presenting cells (aAPCs) are a promising, but relatively early-stage concept that relies on cell-sized constructs mostly for *ex vivo* expansion. Currently, the more commonly used approach for T cell immunotherapy involves the use of *ex vivo*-expanded autologous tumor-specific T cells [189, 190]. Other currently used approaches involve pulsing autologous, *in vitro* expanded and activated dendritic cells (DCs) with synthetic peptide epitopes from tumor associated antigens (TAA) or the TAA themselves for induction of tumor-specific CTLs [191]. However, these approaches are often unsuccessful and lead to induction of a T cell response that is unable to recognize the tumor cells. Isolation of specific T-cell subsets has been greatly aided by the development of peptide specific tetramers / multimers that consist of pMHC (or HLA) arranged into a multimeric particle by linking 4 (or more) HLA molecules to an avidin-derivative core [192, 193]. One major advantage of the "streptamers" is that function of the T cell is preserved following selection, whereas with tetramers, the selected T cell population shows impaired function [193]. Alternative approaches involve transfecting or transducing DCs with DNA or RNA to produce the TAA[194], or inserting conventional or chimeric T cell receptors into T cells to impart the desired specificity[195, 196].

As an alternative to the conventional approach of accessing native antigen presenting cells and using them to direct the immune response, there has been increasing interest in developing particle systems that can substitute for the function of the

biological APC. These particles as a class are termed artificial antigen presenting cells (aAPC). Recent advances in the development of cell-based aAPCs was recently reviewed by Turtle et al[183] and is outside our scope here.

An ideal aAPC system would provide the same signals (antigen recognition, surface constimulation, and secretable factors) to the T cell target as the biological APCs (**Fig. 2.5**). aAPC have been generated by coupling proteins that deliver Signal 1 and 2 to the surface of particles made from a range of materials, including liposomes [180, 197], magnetic [198-201], polystyrene [181], and degradable polymeric particles [178, 202, 203]. Each material has its own advantages and disadvantages for their use as aAPCs. Liposomes have fluid membranes that closely mimic biological membranes and can be used for delivery of drugs, but are substantially less stable than hard particles. Magnetic particles are of particular interest for *ex vivo* T cell expansion, because they can be readily removed from the expanded T cell population before re-infusion. Biodegradable particles can be useful for their release properties, and are be very biocompatible so may be very suitable for in vivo applications, but present challenges to extended surface presentation. Artificial aAPCs have been mostly investigated for their immunostimulatory properties towards CD4+ or CD8+ T-cells. However, it is important to note that the same bioengineering approaches can be used to potentially synthesize killer aAPCs which kill targeted T cell subsets to eliminate auto-reactive clones that are responsible for auto-immune disease [204, 205] or to generate aAPCs which stimulate and expand natural killer T (NKT) cells [206, 207].

2.2.3 Signal 1 and 2 – Antigen presentation and costimulation

One of the advantages with a synthetic approach is the ability to pattern the surface with defined surface molecules and specified ratios. This allows the precise study of the effects of those particular protein sets in isolation or in combination. The biological recognition signal consists strictly of pMHC and TCR, so TCR-subset-specific aAPC systems have utilized surface pMHC or pMHC multimers (dimers[208] or tetramers[209]) for the purpose of targeting. The vast majority of aAPC systems tested, however, instead use anti-CD3 mAb as their targeting ligand. CD3 itself is a co-receptor that is part of the TCR complex regardless of TCR antigen specificity, and when used in aAPC systems, is used to stimulate the TCR of any T cell in an antigen-independent fashion.

The first study detailing the use of HLA molecules in a completely artificial system to activate T cells was published in 1978 by Engelhard et al, who showed that CTL induction was possible using 100-nm phospholipid vesicles presenting on their surface purified HLA antigens [180]. The critical finding of this study revealed that CTL activation was very sensitive to the density of antigen presented. The highest level of CTL function was elicited by liposomes containing 20 molecules per vesicle (2000 molecules/μm^2), which was the lowest density tested in this initial study. Higher density vesicles (100 and 400 molecules per vesicle or 10000 and 40000 molecules/μm^2) showed lower maximal levels of function. For optimal function, however, this system required a high ratio of liposomes to target cells (100 liposomes / target cell).

Multiple biological molecules can function as “signal 2” and can induce positive costimulation or negactive costimulation (repression) depending on their identity. These

surface molecules interact dynamically to modulate the response to TCR triggering. Studies with polystyrene microparticles have helped to identify the importance of co-stimulation to effective aAPC function. Polystyrene (PS) microparticles functionalized with anti-TCR antibody and B7-1 showed that co-stimulation by B7-1 is sufficient for the induction of effector function in $CD4^+$ and $CD8^+$ T cells [210], but that $CD8^+$ responses were transient in nature and required higher density of costimulatory molecules on the surface than that required by $CD4^+$ cells. In addition, ICAM-1 (critical for cell-cell adhesion and the major component of the pSMAC) was shown to also be able to provide co-stimulation for $CD8^+$ T cell activation and synergize with B7-1 for induction of IL-2 production, but failed to do so for $CD4^+$ T cells [211].

2.2.4 Signal 3 – Cytokine release

One of the advantages of a biodegradable aAPC system compared to a non-degradable aAPC system is that the biodegradable system can be engineered to release soluble factors from within the aAPC in addition to presenting factors that are attached to the aAPC surface. In addition, for in vivo administration, biodegradable aAPC would offer the promise of avoiding in vivo accumulation and increasing biocompatability, as the eventual dissolution of the particle would allow for complete elimination of the system from the body.

One major difficulty with constructing biodegradable aAPC is that degradation of the particle tends to lead to loss of surface function. Initial work by Shalabi et al showed that polyglycolic acid (PGA) microparticle could be used to release immunomodulatory compounds, and could also be made into and aAPC by irreversible absorption of anti-

CD3 and anti-CD28 onto the surface [212]. Subsequently, using a novel method which relies on the incorporation of avidin-palmitic acid conjugates into the surface of the poly(lactic-co-glycolic) acid (PLGA) particles [213], Steenblock et al. were able to develop a PLGA-based biodegradable aAPC which could stably present ligand on its surface in solution for over 20 days [177]. This method relies on the hydrophobic chain of the palmitic acid partitioning into the hydrophobic PLGA core, while the avidin partitions to the surface of the particles and is available to bind biotinylated anti-CD3 and anti-CD28 antibody.

In addition, because PLGA is biodegradable, IL-2 could be released from the particle core, allowing the aAPC to incorporate cytokine signaling (signal 3) in addition to antigen recognition and surface co-stimulation (**Fig. 2.5**). Importantly, paracrine release of IL-2 from the particles resulted in superior T cell expansion compared to exogenous administration of equivalent amounts of cytokine [177]. Paracrine delivery of IL-2 upon T cell contact resulted in increased IL-2 in the contact region and increased proliferation of CD8+ T cells in vitro 10-fold compared to bulk IL-2 administration. Additionally, these responses appear to require sustained release of low levels of IL-2 and depend on close contact between the aAPC and T cell [178].

2.2.5 Particle size as a critical parameter

Polysytrene particles have been extensively studies as platforms for the development of aAPCs, and studies in this system have enhanced our understanding of critical parameters in designing acellular aAPCs. Perhaps most critically, the effect of particle size on aAPC function was first studied using polystyrene (PS) particles [181].

Testing various sized spherical PS particles with class I MHC immobilized on the surface, Mesher found that 4-5 μm particles provided optimal stimulus. Smaller particles showed decreased stimulation, and this decreased stimulation could not be overcome by increasing the dose of the smaller particles. These results indicated that receptor occupancy over a large surface area of contact is a critical determinant for activation. While efficient and effective nanoscale aAPC might have better properties for *in vivo* applications, such as improved draining to lymph nodes, and reduced likelihood of safety concerns (such as aAPC becoming trapped in a capillary bed), these data point to the potential advantages of microscale aAPCs.

2.2.6 Particle shape

The use of non-spherical particles has generated increasing interest in recent years for biomedical applications. From a biomimetic perspective, the various morphologies of bacterial and viruses are suspected to play a role in their ability to efficiently invade and colonize cells. Generally, the cytoskeleton, its organization, and the physical cues that it can transmit can result in dramatic effects on cell fate [214]. This is seen during the interaction of a T cell with an antigen presenting cell (APC), which is a critical determinant of T cell fate and effector function. With activation, APC such as dendritic cells have major changes in their cell morphology resulting in significant increases in their overall cell surface area facilitating interaction with naïve T cells to direct T cell fate.

A wide variety of shapes have been generated by top-down and bottom up approaches [215, 216]. Particles have been made that mimic the mechanobiology of red-

blood cells, resulting in increased circulation times and dramatically improved their biodistribution profiles [217]. Recent advances in the ability to generate particles with diverse shapes has enabled the study of the effect of shape on cellular internalization, phagocytosis, particle attachment, and circulation half-life [218]. Local particle curvature appears to dictate whether or not the particle will be phagocytosed [219, 220]. In particular, high aspect ratio (AR) ellipsoidal microparticles (in particular, those with AR > 20) have reduced phagocytosis compared to spherical particles, because when the low curvature sides of the particle encounter a phagocytic cell, the low curvature prevents the cell from engulfing the particle. In addition, the shape of the particle also modulates the degree of particle attachment to macrophages independent of the rate it internalizes the particle. In particular, prolate ellipsoids (a>b=c) showed the lowest internalization rates but most efficient particle attachment, when compared to oblate ellipsoids (a=b>c) or spherical particles [221]. Particle shape has also been implicated in increasing circulation time for particles injected into the bloodstream of mice, by aligning with blood flow in a superior fashion to spherical particles and reducing phagocytosis [222, 223].

To date, nearly acellular artificial antigen presenting cell systems have utilized spherical particles in their constructs. However, both the dramatic morphological changes that come with activation of dendritic cells, and the potential improvements in terms of decreased particle internalization and increased particle attachment indicates that particle shape may play a key role in future aAPC systems, and helps to motivate the development of non-spherical artificial antigen presenting cells described herein.

2.2.7 Methods to engineer polymeric aAPC shape

Perhaps the simplest and most accessable method developed for generating non-spherical particles uses a film stretching technique originally developed by Ho et al[224] and more recently adapted to generate polymeric micro- and nanoparticles of varied shape (**Figure 6**) [225]. Polymeric particles are suspended in a solution containing high quantities of poly(vinyl)alcohol (PVA) and some glycerol as a plasticizer, and then the particle solution is cast into a film by pouring onto a leveling table and allowing the water to evaporate over time. This film can then be cut into pieces, and stretched under heating on a stretching device, cooled, and then the particles are removed by dissolving the film. The advantages of this approach are that it does not require complex technology and generation of particles with complex shape is possible. This process lends itself less efficiently to large-scale batch synthesis, and batch-to-batch variability due to inhomogeneous stretching can be a moderate issue; however, the ease of application and the control over equivalent volume in comparison samples made this method an easy choice for our purposes here.

One of the most versatile approaches to generating a vast array of potential shapes is Particle Replication in Nonwetting Templates (PRINT) technology [226]. By using photocurable perfluoropolyether (PFPE) molds and fluorinated surfaces, PRINT is able to produce isolated, harvestable individual particles. It can be used to generate monodisperse micro- and nanoparticles (sub-100 nm) of various polymers such as PLG, poly(pyrrole) and polyethyelene glycol, and can be used to incorporate proteins, DNA, and small molecules into the shaped particles. In addition, particles can be printed that are 100% protein [227].

High AR particles, as noted above, are of considerable interest due to favorable reduction in phagocytosis and increase in cellular binding properties. High AR particles can be generated using PRINT by using a mechanical elongation strategy. This involves fabricating an initial PDMS mold, deforming that mold, and using the deformed mold to generate a new mold [228]. Due to limitations in deformation extent, this process can be repeated in cycles to generate very high aspect ratio particles.

Continuous flow lithography also been developed for synthesis of particles with diverse shapes [229]. In this process, an acrylate oligomer stream containing a photoinitiator is flowed through a PDMS microfluidic device, and the flowing oligomer is exposed to controlled pulses of UV light shined through a transparency mask that is patterned by lithography. The limitation here is that continuous flow lithography cannot readily fabricate sub-3 μm shapes, as the process is limited by polymerization times and the feature sizes that are printable on a transparency mask (polymerization time is inversely related to the size of the transparency mask). A modified stop-polymerize-flow method was suggested to enable synthesis of 1-μm particles.

2.2.8 Conclusion

Acellular aAPC have particularly shown great initial promise for *ex vivo* activation of CTL and have been investigated for *in vivo* applications as well. The development of aAPCs has focused mainly on the choice of proteins to use for surface presentation to T cells when conjugated to various spherical, micro-scale particles. Key recent advances have allowed for the development of acellular aAPCs that incorporate more biological cues than antigen recognition (signal 1) and costimulation (signal 2).

aAPCs have been developed that incorporate secretable cues (cytokines, “signal 3”) and surface geometric cues that operate from the nanoscale to the microscale, such as interfacial geometry, surface protein organization and segregation, and dynamic protein rearrangement. Early work has demonstrated a critical role for particle size, showing that the surface area available for contact is crucial in these systems.

Biodegradable particles offer strong biocompatablility and are useful for release of secretable cues or other immunomodulatory factors. Recent advances in the development of methods for the generation of non-spherical biodegradable particles may enable next-generation aAPC with interfacial geometry that more closely mimics the biological situation.

2.3 Figures

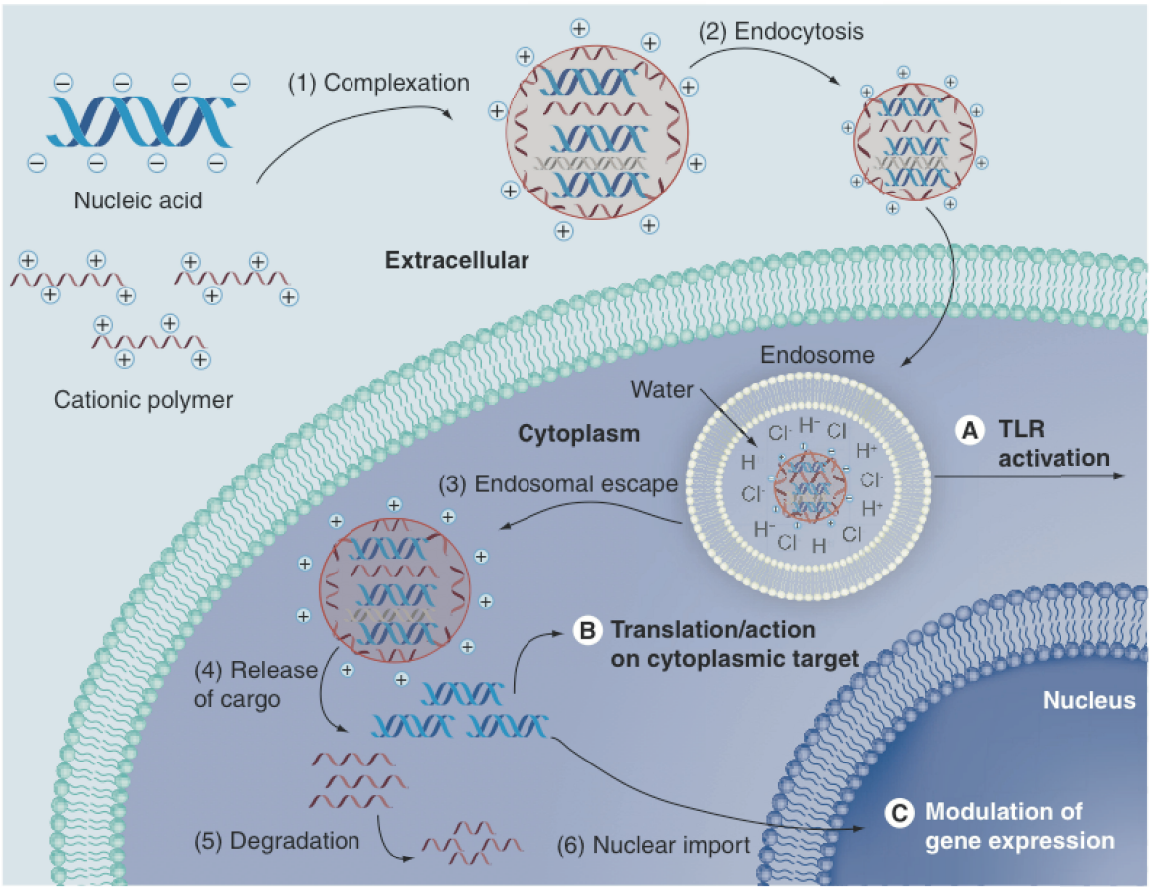

Figure 2.1. Barriers to intracellular nucleic acid delivery. (1) Nucleic acid must be complexed to the nanocarrier and protected from degradation as it makes its way to the target cell. (2) The nanocarrier and cargo must be internalized successfully. (A) TLR7 is localized to the endosome; for isRNA activity, endosomal escape is not required. For other nucleic acid, (3) endosomal escape is required. (B) (4) For cytoplasmic activity, nucleic acid must be released intracellularly. (5) Nanocarrier degradation is not required, but is useful for reduced toxicity. (C) (6) For DNA, shRNA-encoding plasmids, and agRNA, nuclear import is required for successful effect.

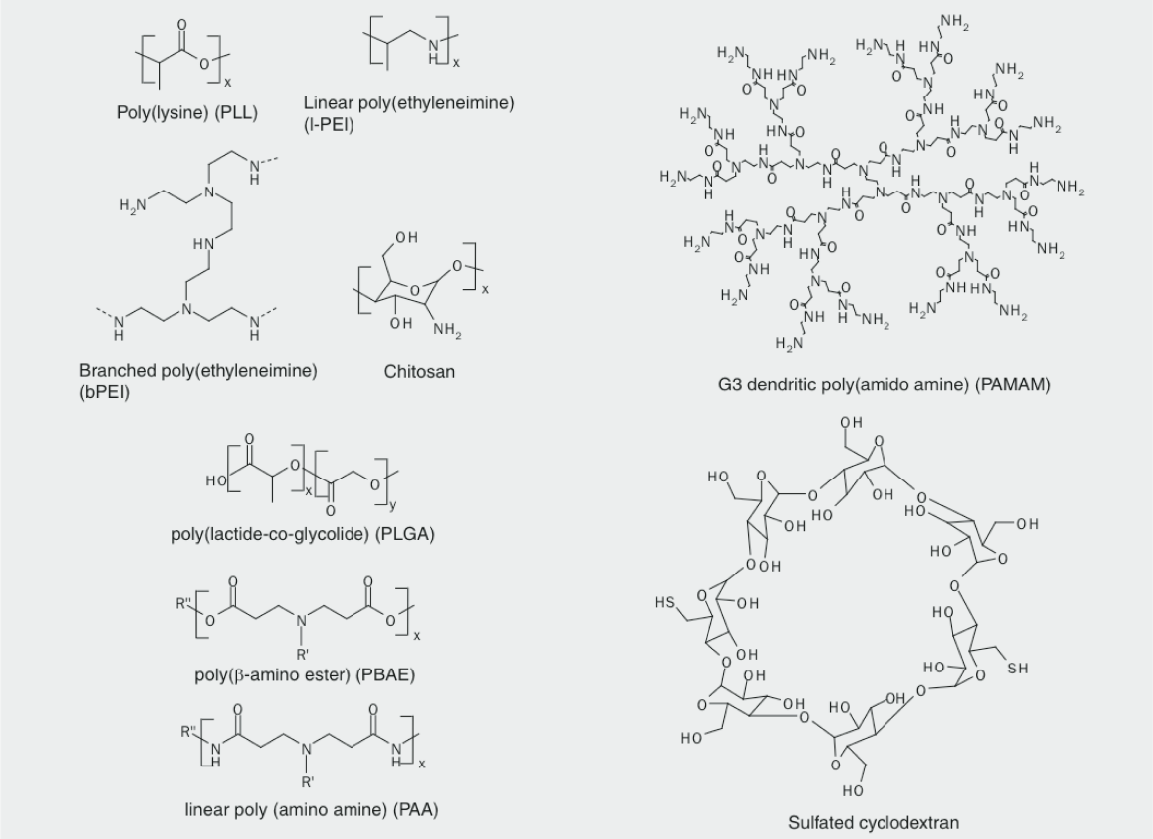

Figure 2.2: Commonly used cationic polymers and polysaccharides used in gene delivery

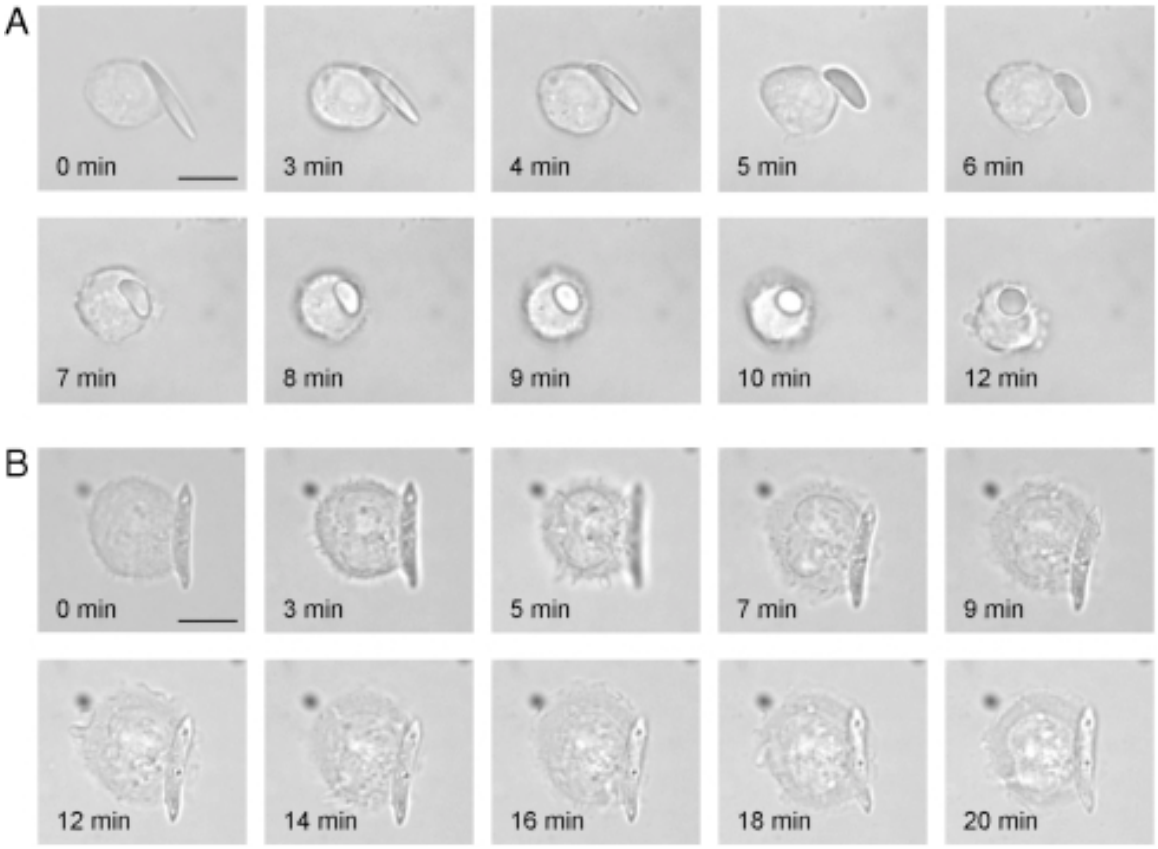

Figure 2.3. Time-lapse video microscopy stills of shape-dependent phagocytosis by macrophage. (A) Shape-switching poly(lactide-co-glycolide)– ester elliptical disk allows macrophage internalization. (B) Poly(lactide-co- glycolide)–ester elliptical disk that does not switch shape prevents internalization. Scale bar: 10 μm. Reproduced with permission from [230].

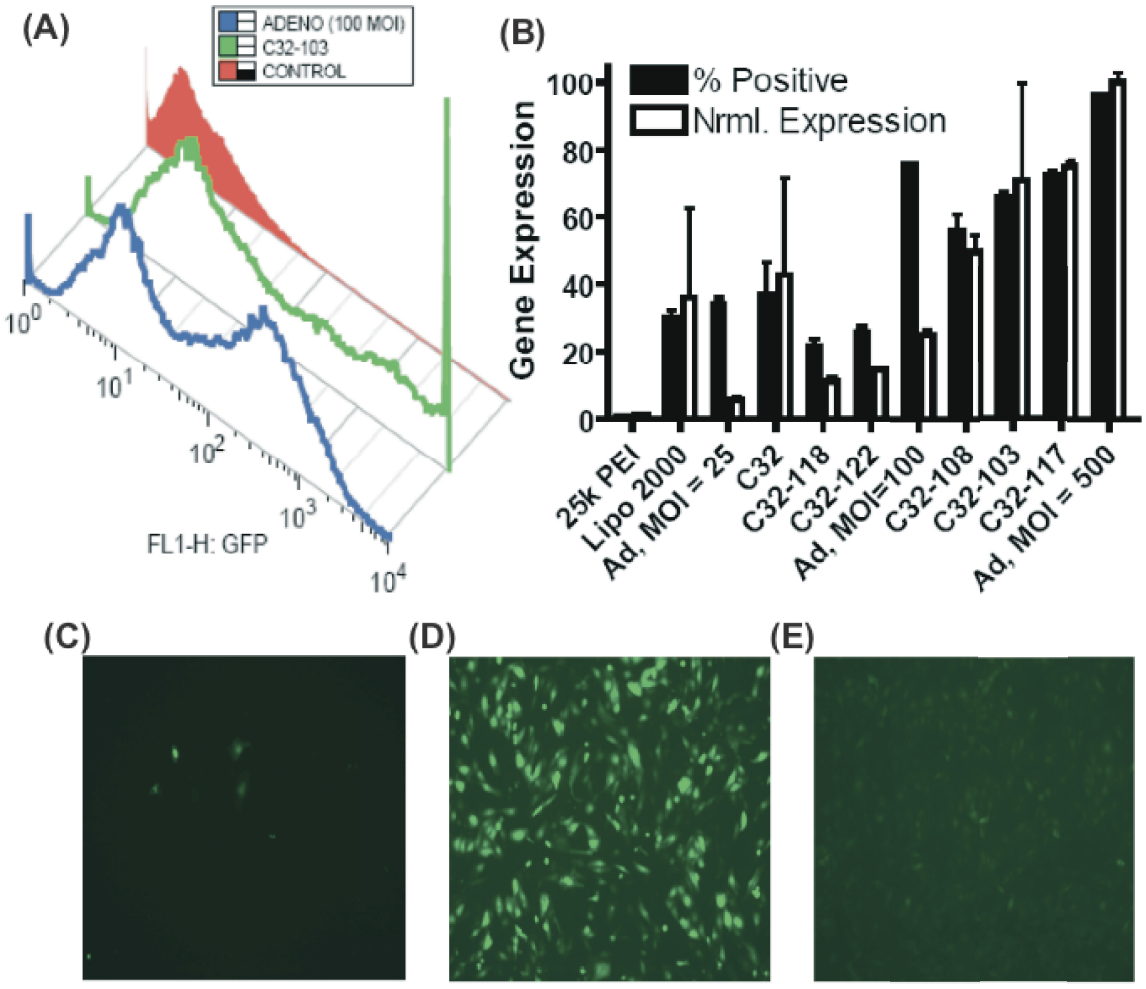

Figure 2.4. Gene expression of poly(β-amino ester)s compared with adenovirus. (A) Gene expression histogram comparing adenovirus, PBAE and negative control. (B) Comparison of various poly(β-amino ester) formulations with adenovirus with respect to % positive cells and normalized expression. Images of GFP+ cells 24 h post-transfection with (C) PEI, (D) C32–103 and (E) 500 MOI adenovirus. GFP: Green fluorescent protein; MOI: Multiplicity of infection; PEI: Poly(ethylenimine). Reproduced with permission from [231].

Figure 2.5: Biological vs. acellular artificial Antigen Presenting Cell schematic: A schematic depicting a biological APC interacting with a T cell (left) and an aAPC interacting with a T cell (right). In the biological setting, the recognition signal ("signal 1") is provided by the interaction of pMHC with the T cell receptor complex, composed of a TCR heterodimer and signaling CD3 chains. Costimulation ("signal 1") occurs through a variety of cell-surface protein mediators; the B7.1:CD28 interaction is often used in aAPC constructs. T cell fate is also determined classically by the cytokine mileau sensed ("signal 3").

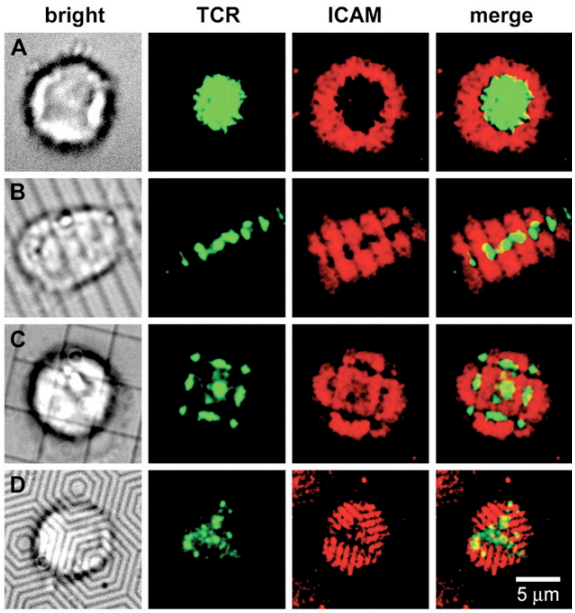

Figure 2.6: **Immune synapse disruption by patterned substrates**. Immune synapse formation is dependant on the shape of the substrate. T cells with fluorescently stained TCRs (green) were added to supported lipid bilayers containing pMHC (unlabeled) and ICAM (red) on the surfaces without patterning (A), with 2-μm parallel lines (B), with 5-μm boxes (C), and with hexagonal lines (D, 1-μm spacing). Reprinted with permission from AAAS from *Science* [232], 2005.

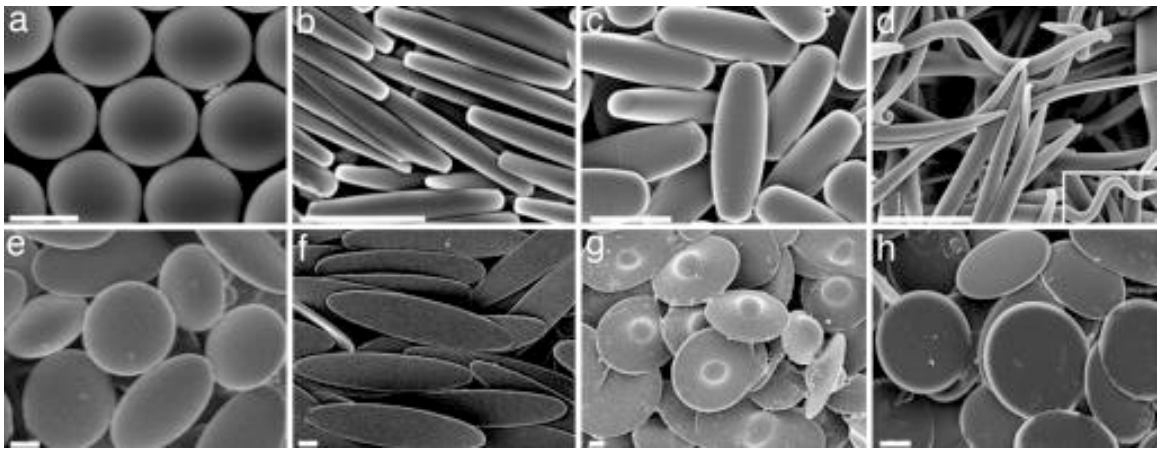

Figure 2.7: **Diverse non-spherical particle shapes**. Diverse shapes can be made using a film stretching method using microparticles (a-h). Adapted with permission from [225], copyright 2011, National Academy of Sciences, USA.

2.4 References

1. Pringle, I.A., S.C. Hyde, and D.R. Gill, *Non-viral vectors in cystic fibrosis gene therapy: recent developments and future prospects.* Expert Opin Biol Ther, 2009. **9**(8): p. 991-1003.
2. Lam, B.L., et al., *Leber hereditary optic neuropathy gene therapy clinical trial recruitment: year 1.* Arch Ophthalmol. **128**(9): p. 1129-35.
3. Sadelain, M., et al., *Strategy for a multicenter phase I clinical trial to evaluate globin gene transfer in beta-thalassemia.* Ann N Y Acad Sci. **1202**: p. 52-8.
4. Perumbeti, A. and P. Malik, *Therapy for beta-globinopathies: a brief review and determinants for successful and safe correction.* Ann N Y Acad Sci. **1202**: p. 36-44.
5. Viiala, N.O., S.R. Larsen, and J.E. Rasko, *Gene therapy for hemophilia: clinical trials and technical tribulations.* Semin Thromb Hemost, 2009. **35**(1): p. 81-92.
6. Phalon, C., D.D. Rao, and J. Nemunaitis, *Potential use of RNA interference in cancer therapy.* Expert Rev Mol Med. **12**: p. e26.
7. Sangro, B., et al., *A phase I clinical trial of thymidine kinase-based gene therapy in advanced hepatocellular carcinoma.* Cancer Gene Ther.
8. Karvinen, H. and S. Yla-Herttuala, *New aspects in vascular gene therapy.* Curr Opin Pharmacol. **10**(2): p. 208-11.
9. Nguyen, D.N., et al., *Polymeric Materials for Gene Delivery and DNA Vaccination.* Advanced Materials, 2009. **21**(8): p. 847-867.
10. Yu, J., et al., *Induced pluripotent stem cell lines derived from human somatic cells.* Science, 2007. **318**(5858): p. 1917-20.
11. Takahashi, K., et al., *Induction of pluripotent stem cells from adult human fibroblasts by defined factors.* Cell, 2007. **131**(5): p. 861-72.
12. Green, J.J., et al., *Nanoparticles for gene transfer to human embryonic stem cell colonies.* Nano Lett, 2008. **8**(10): p. 3126-30.
13. Putnam, D., *Polymers for gene delivery across length scales.* Nat Mater, 2006. **5**(6): p. 439-51.
14. Check, E., *Gene therapy put on hold as third child develops cancer.* Nature, 2005. **433**(7026): p. 561.
15. Miller, A.M. and D.A. Dean, *Tissue-specific and transcription factor-mediated nuclear entry of DNA.* Adv Drug Deliv Rev, 2009. **61**(7-8): p. 603-13.
16. Lam, A.P. and D.A. Dean, *Progress and prospects: nuclear import of nonviral vectors.* Gene Ther. **17**(4): p. 439-47.
17. Cohen, R.N., et al., *Quantification of plasmid DNA copies in the nucleus after lipoplex and polyplex transfection.* J Control Release, 2009. **135**(2): p. 166-74.
18. Laemmli, U.K., *Characterization of DNA condensates induced by poly(ethylene oxide) and polylysine.* Proc Natl Acad Sci U S A, 1975. **72**(11): p. 4288-92.
19. Sela, M., R. Arnon, and I. Jacobson, *Synthesis of Poly-L-Lysine and Poly-L-Lysyl Albumin Via Sigma-N-Trifluoroacetyl-Alpha,N-Carboxy-L-Lysine Anhydride.* Biopolymers, 1963. **1**(6): p. 517-525.

20. Choi, Y.H., et al., *Polyethylene glycol-grafted poly-L-lysine as polymeric gene carrier.* J Control Release, 1998. **54**(1): p. 39-48.
21. Wu, G.Y. and C.H. Wu, *Receptor-mediated in vitro gene transformation by a soluble DNA carrier system.* J Biol Chem, 1987. **262**(10): p. 4429-32.
22. Wagner, E., et al., *Transferrin-Polycation Conjugates as Carriers for DNA Uptake into Cells.* Proceedings of the National Academy of Sciences of the United States of America, 1990. **87**(9): p. 3410-3414.
23. Nishikawa, M., et al., *Targeted delivery of plasmid DNA to hepatocytes in vivo: Optimization of the pharmacokinetics of plasmid DNA galactosylated poly(L-lysine) complexes by controlling their physicochemical properties.* Journal of Pharmacology and Experimental Therapeutics, 1998. **287**(1): p. 408-415.
24. Hashida, M., et al., *Targeted delivery of plasmid DNA complexed with galactosylated poly(L-lysine).* Journal of Controlled Release, 1998. **53**(1-3): p. 301-310.
25. Midoux, P., et al., *Specific Gene-Transfer Mediated by Lactosylated Poly-L-Lysine into Hepatoma-Cells.* Nucleic Acids Research, 1993. **21**(4): p. 871-878.
26. Mislick, K.A., et al., *Transfection of Folate-Polylysine DNA Complexes - Evidence for Lysosomal Delivery.* Bioconjugate Chemistry, 1995. **6**(5): p. 512-515.
27. Midoux, P. and M. Monsigny, *Efficient gene transfer by histidylated polylysine pDNA complexes.* Bioconjugate Chemistry, 1999. **10**(3): p. 406-411.
28. Boussif, O., et al., *A versatile vector for gene and oligonucleotide transfer into cells in culture and in vivo: polyethylenimine.* Proc Natl Acad Sci U S A, 1995. **92**(16): p. 7297-301.
29. Brissault, B., et al., *Synthesis of linear polyethylenimine derivatives for DNA transfection.* Bioconjugate Chemistry, 2003. **14**(3): p. 581-587.
30. Fischer, D., et al., *A novel non-viral vector for DNA delivery based on low molecular weight, branched polyethylenimine: Effect of molecular weight on transfection efficiency and cytotoxicity.* Pharmaceutical Research, 1999. **16**(8): p. 1273-1279.
31. Moghimi, S.M., et al., *A two-stage poly(ethylenimine)-mediated cytotoxicity: implications for gene transfer/therapy.* Mol Ther, 2005. **11**(6): p. 990-5.
32. Wightman, L., et al., *Different behavior of branched and linear polyethylenimine for gene delivery in vitro and in vivo.* Journal of Gene Medicine, 2001. **3**(4): p. 362-372.
33. Bettinger, T., et al., *Peptide-mediated RNA delivery: a novel approach for enhanced transfection of primary and post-mitotic cells.* Nucleic Acids Research, 2001. **29**(18): p. 3882-3891.
34. Astete, C.E. and C.M. Sabliov, *Synthesis and characterization of PLGA nanoparticles.* Journal of Biomaterials Science-Polymer Edition, 2006. **17**(3): p. 247-289.
35. Visscher, G.E., et al., *Biodegradation of and Tissue Reaction to 50-50 Poly(Dl-Lactide-Co-Glycolide) Microcapsules.* Journal of Biomedical Materials Research, 1985. **19**(3): p. 349-365.
36. Shive, M.S. and J.M. Anderson, *Biodegradation and biocompatibility of PLA and PLGA microspheres.* Adv Drug Deliv Rev, 1997. **28**(1): p. 5-24.

37. Tomalia, D.A., et al., *A New Class of Polymers - Starburst-Dendritic Macromolecules.* Polymer Journal, 1985. **17**(1): p. 117-132.
38. Haensler, J. and F.C. Szoka, *Polyamidoamine Cascade Polymers Mediate Efficient Transfection of Cells in Culture.* Bioconjugate Chemistry, 1993. **4**(5): p. 372-379.
39. Navarro, G. and C.T. de ILarduya, *Activated and non-activated PAMAM dendrimers for gene delivery in vitro and in vivo.* Nanomedicine-Nanotechnology Biology and Medicine, 2009. **5**(3): p. 287-297.
40. Bielinska, A., et al., *Regulation of in vitro gene expression using antisense oligonucleotides or antisense expression plasmids transfected using starburst PAMAM dendrimers.* Nucleic Acids Research, 1996. **24**(11): p. 2176-2182.
41. DeLong, R., et al., *Characterization of complexes of oligonucleotides with polyamidoamine starburst dendrimers and effects on intracellular delivery.* Journal of Pharmaceutical Sciences, 1997. **86**(6): p. 762-764.
42. Axel, D.I., et al., *Toxicity, uptake kinetics and efficacy of new transfection reagents: Increase of oligonucleotide uptake.* Journal of Vascular Research, 2000. **37**(4): p. 221-234.
43. Ravina, M., et al., *Knocking Down Gene Expression with Dendritic Vectors.* Mini-Reviews in Medicinal Chemistry, 2010. **10**(1): p. 73-86.
44. Tang, M.X., C.T. Redemann, and F.C. Szoka, *In vitro gene delivery by degraded polyamidoamine dendrimers.* Bioconjugate Chemistry, 1996. **7**(6): p. 703-714.
45. Lynn, D.M. and R. Langer, *Degradable poly(beta-amino esters): Synthesis, characterization, and self-assembly with plasmid DNA.* Journal of the American Chemical Society, 2000. **122**(44): p. 10761-10768.
46. Akinc, A., et al., *Parallel synthesis and biophysical characterization of a degradable polymer library for gene delivery.* J Am Chem Soc, 2003. **125**(18): p. 5316-23.
47. Anderson, D.G., et al., *Structure/property studies of polymeric gene delivery using a library of poly(beta-amino esters).* Mol Ther, 2005. **11**(3): p. 426-34.
48. Anderson, D.G., D.M. Lynn, and R. Langer, *Semi-automated synthesis and screening of a large library of degradable cationic polymers for gene delivery.* Angew Chem Int Ed Engl, 2003. **42**(27): p. 3153-8.
49. Green, J.J., R. Langer, and D.G. Anderson, *A Combinatorial Polymer Library Approach Yields Insight into Nonviral Gene Delivery.* Acc Chem Res, 2008.
50. Lynn, D.M., et al., *Accelerated discovery of synthetic transfection vectors: parallel synthesis and screening of a degradable polymer library.* J Am Chem Soc, 2001. **123**(33): p. 8155-6.
51. Gormley, A.J., and Ghandehari, H, *Evaluation of toxicity of nanostructures in biological systems*, in *Nanotoxicity: From In Vivo and In Vitro Models to Health Risks*, S.C. Sahu, and Casciano, D. A., Editor. 2009, John Wiley & Sons, Ltd: West Sussex. p. 115-159.
52. van Vlerken, L.E., T.K. Vyas, and M.M. Amiji, *Poly(ethylene glycol)-modified nanocarriers for tumor-targeted and intracellular delivery.* Pharm Res, 2007. **24**(8): p. 1405-14.
53. Wang, J.Q., et al., *Reversion of multidrug resistance by tumor targeted delivery of antisense oligodeoxynucleotides in hydroxypropyl-chitosan nanoparticles.* Biomaterials, 2010. **31**(15): p. 4426-4433.

54. Sayes, C.M., et al., *Functionalization density dependence of single-walled carbon nanotubes cytotoxicity in vitro.* Toxicol Lett, 2006. **161**(2): p. 135-42.
55. Zhang, B.L., et al., *Characterization of and biomolecule immobilization on the biocompatible multi-walled carbon nanotubes generated by functionalization with polyamidoamine dendrimers.* Colloids and Surfaces B-Biointerfaces, 2010. **80**(1): p. 18-25.
56. Lee, J.S., et al., *Gold, Poly(beta-amino ester) Nanoparticles for Small Interfering RNA Delivery.* Nano Letters, 2009. **9**(6): p. 2402-2406.
57. Pissuwan, D., T. Niidome, and M.B. Cortie, *The forthcoming applications of gold nanoparticles in drug and gene delivery systems.* J Control Release, 2009.
58. Champion, J.A., Y.K. Katare, and S. Mitragotri, *Particle shape: A new design parameter for micro- and nanoscale drug delivery carriers.* Journal of Controlled Release, 2007. **121**(1-2): p. 3-9.
59. Champion, J.A. and S. Mitragotri, *Role of target geometry in phagocytosis.* Proceedings of the National Academy of Sciences of the United States of America, 2006. **103**(13): p. 4930-4934.
60. Geng, Y., et al., *Shape effects of filaments versus spherical particles in flow and drug delivery.* Nature Nanotechnology, 2007. **2**(4): p. 249-255.
61. Muro, S., et al., *Control of endothelial targeting and intracellular delivery of therapeutic enzymes by modulating the size and shape of ICAM-1-targeted carriers.* Molecular Therapy, 2008. **16**(8): p. 1450-1458.
62. Yoo, J.W. and S. Mitragotri, *Polymer particles that switch shape in response to a stimulus.* Proceedings of the National Academy of Sciences of the United States of America, 2010. **107**(25): p. 11205-11210.
63. Jeong, W., M.E. Napier, and J.M. DeSimone, *Challenging nature's monopoly on the creation of well-defined nanoparticles.* Nanomedicine, 2010. **5**(4): p. 633-639.
64. Li, S.D. and L. Huang, *Pharmacokinetics and biodistribution of nanoparticles.* Molecular Pharmaceutics, 2008. **5**(4): p. 496-504.
65. Tang, C., et al., *Nanoparticles and Cellular Carriers - Allies in Cancer Imaging and Cellular Gene Therapy?* Stem Cells.
66. Phillips, M.A., M.L. Gran, and N.A. Peppas, *Targeted Nanodelivery of Drugs and Diagnostics.* Nano Today. **5**(2): p. 143-159.
67. Reilly, R.M., *Carbon nanotubes: Potential benefits and risks of nanotechnology in nuclear medicine.* Journal of Nuclear Medicine, 2007. **48**(7): p. 1039-1042.
68. Sekhon, B.S. and S.R. Kamboj, *Inorganic nanomedicine-Part 1.* Nanomedicine. **6**(4): p. 516-522.
69. Tong, R. and J.J. Cheng, *Anticancer polymeric nanomedicines.* Polymer Reviews, 2007. **47**(3): p. 345-381.
70. Bonoiu, A.C., et al., *Nanotechnology approach for drug addiction therapy: gene silencing using delivery of gold nanorod-siRNA nanoplex in dopaminergic neurons.* Proc Natl Acad Sci U S A, 2009. **106**(14): p. 5546-50.
71. Son, S. and W.J. Kim, *Biodegradable nanoparticles modified by branched polyethylenimine for plasmid DNA delivery.* Biomaterials. **31**(1): p. 133-43.

72. Sokolova, V., et al., *An outer shell of positively charged poly(ethyleneimine) strongly increases the transfection efficiency of calcium phosphate/DNA nanoparticles.* Journal of Materials Science. **45**(18): p. 4952-4957.
73. Liu, C.H. and S.Y. Yu, *Cationic nanoemulsions as non-viral vectors for plasmid DNA delivery.* Colloids Surf B Biointerfaces. **79**(2): p. 509-15.
74. Ortiz Mellet, C., J.M. Benito, and J.M. Garcia Fernandez, *Preorganized, macromolecular, gene-delivery systems.* Chemistry. **16**(23): p. 6728-42.
75. Goodman, C.M., et al., *Toxicity of gold nanoparticles functionalized with cationic and anionic side chains.* Bioconjug Chem, 2004. **15**(4): p. 897-900.
76. Green, J.J., R. Langer, and D.G. Anderson, *A combinatorial polymer library approach yields insight into nonviral gene delivery.* Accounts of Chemical Research, 2008. **41**(6): p. 749-759.
77. Arsianti, M., et al., *Assembly of polyethylenimine-based magnetic iron oxide vectors: insights into gene delivery.* Langmuir. **26**(10): p. 7314-26.
78. Godbey, W.T., K.K. Wu, and A.G. Mikos, *Poly(ethylenimine)-mediated gene delivery affects endothelial cell function and viability.* Biomaterials, 2001. **22**(5): p. 471-480.
79. Kloeckner, J., E. Wagner, and M. Ogris, *Degradable gene carriers based on oligomerized polyamines.* Eur J Pharm Sci, 2006. **29**(5): p. 414-25.
80. Jere, D., et al., *Degradable polyethylenimines as DNA and small interfering RNA carriers.* Expert Opinion on Drug Delivery, 2009. **6**(8): p. 827-834.
81. Ando, S., et al., *PLGA microspheres containing plasmid DNA: Preservation of supercoiled DNA via cryopreparation and carbohydrate stabilization.* Journal of Pharmaceutical Sciences, 1999. **88**(1): p. 126-130.
82. Lim, Y., et al., *Cationic hyperbranched poly(amino ester): a novel class of DNA condensing molecule with cationic surface, biodegradable three-dimensional structure, and tertiary amine groups in the interior.* J Am Chem Soc, 2001. **123**(10): p. 2460-1.
83. Green, J.J., et al., *Poly(beta-amino esters): procedures for synthesis and gene delivery.* Methods Mol Biol, 2009. **480**: p. 53-63.
84. Green, J.J., et al., *Combinatorial modification of degradable polymers enables transfection of human cells comparable to adenovirus.* Adv. Mater., 2007. **19**(19): p. 2836-2842.
85. Sunshine, J., et al., *Small molecule end group of linear polymer determine cell-type gene delivery efficacy.* Advanced Materials, 2009. **21(48)**: p. 4947-4951.
86. Zugates, G.T., et al., *Gene delivery properties of end-modified poly(beta-amino ester)s.* Bioconjug Chem, 2007. **18**(6): p. 1887-96.
87. Green, J.J., et al., *Biodegradable polymeric vectors for gene delivery to human endothelial cells.* Bioconjugate Chemistry, 2006. **17**: p. 1162-1169.
88. Anderson, D.G., et al., *A polymer library approach to suicide gene therapy for cancer.* Proc Natl Acad Sci U S A, 2004. **101**(45): p. 16028-33.
89. Huang, Y.H., et al., *Nanoparticle-delivered suicide gene therapy effectively reduces ovarian tumor burden in mice.* Cancer Research, 2009. **69**(15): p. 6184-91.

90. Opanasopit, P., M. Nishikawa, and M. Hashida, *Factors affecting drug and gene delivery: Effects of interaction with blood components.* Critical Reviews in Therapeutic Drug Carrier Systems, 2002. **19**(3): p. 191-233.
91. Ogris, M., et al., *PEGylated DNA/transferrin-PEI complexes: reduced interaction with blood components, extended circulation in blood and potential for systemic gene delivery.* Gene Therapy, 1999. **6**(4): p. 595-605.
92. Harada, A., et al., *Effective tolerance to serum proteins of head-tail type polycation vectors by PEGylation at the periphery of the head block.* Biomacromolecules. **11**(4): p. 1036-42.
93. Petersen, H., et al., *Polyethylenimine-graft-poly(ethylene glycol) copolymers: Influence of copolymer block structure on DNA complexation and biological activities as gene delivery system.* Bioconjugate Chemistry, 2002. **13**(4): p. 845-854.
94. Subr, V., et al., *Coating of DNA/poly(L-lysine) complexes by covalent attachment of poly[N-(2-hydroxypropyl)methacrylamide].* Biomacromolecules, 2006. **7**(1): p. 122-130.
95. Yuan, Q., W.A. Yeudall, and H. Yang, *PEGylated Polyamidoamine Dendrimers with Bis-Aryl Hydrazone Linkages for Enhanced Gene Delivery.* Biomacromolecules. **11**(8): p. 1940-7.
96. Liu, Y., et al., *A leptin derived 30-amino-acid peptide modified pegylated poly-L-lysine dendrigraft for brain targeted gene delivery.* Biomaterials. **31**(19): p. 5246-57.
97. Chen, Y., J.J. Wu, and L. Huang, *Nanoparticles targeted with NGR motif deliver c-myc siRNA and doxorubicin for anticancer therapy.* Mol Ther. **18**(4): p. 828-34.
98. Liu, Z., et al., *Preparation of carbon nanotube bioconjugates for biomedical applications.* Nat Protoc, 2009. **4**(9): p. 1372-82.
99. Davis, M.E., *The First Targeted Delivery of siRNA in Humans via a Self-Assembling, Cyclodextrin Polymer-Based Nanoparticle: From Concept to Clinic.* Molecular Pharmaceutics, 2009. **6**(3): p. 659-668.
100. Walker, G.F., et al., *Toward synthetic viruses: endosomal pH-triggered deshielding of targeted polyplexes greatly enhances gene transfer in vitro and in vivo.* Mol Ther, 2005. **11**(3): p. 418-25.
101. Knorr, V., M. Ogris, and E. Wagner, *An acid sensitive ketal-based polyethylene glycol-oligoethylenimine copolymer mediates improved transfection efficiency at reduced toxicity.* Pharm Res, 2008. **25**(12): p. 2937-45.
102. Knorr, V., et al., *Acetal linked oligoethylenimines for use as pH-sensitive gene carriers.* Bioconjug Chem, 2008. **19**(8): p. 1625-34.
103. Carlisle, R.C., et al., *Polymer-coated polyethylenimine/DNA complexes designed for triggered activation by intracellular reduction.* J Gene Med, 2004. **6**(3): p. 337-44.
104. Murthy, N., et al., *Design and synthesis of pH-responsive polymeric carriers that target uptake and enhance the intracellular delivery of oligonucleotides.* J Control Release, 2003. **89**(3): p. 365-74.

105. Abdelhady, H.G., et al., *Direct real-time molecular scale visualisation of the degradation of condensed DNA complexes exposed to DNase I.* Nucleic Acids Research, 2003. **31**(14): p. 4001-4005.
106. Lechardeur, D., et al., *Metabolic instability of plasmid DNA in the cytosol: A potential barrier to gene transfer.* Gene Therapy, 1999. **6**(4): p. 482-497.
107. Schaffer, D.V., et al., *Vector unpacking as a potential barrier for receptor-mediated polyplex gene delivery.* Biotechnology and Bioengineering, 2000. **67**(5): p. 598-606.
108. Walter, E., et al., *Microencapsulation of DNA using poly(DL-lactide-co-glycolide): stability issues and release characteristics.* Journal of Controlled Release, 1999. **61**(3): p. 361-374.
109. Shu, X.Z. and K.J. Zhu, *Chitosan/gelatin microspheres prepared by modified emulsification and ionotropic gelation.* J Microencapsul, 2001. **18**(2): p. 237-45.
110. Weecharangsan, W., et al., *Chitosan lactate as a nonviral gene delivery vector in COS-1 cells.* Aaps Pharmscitech, 2006. **7**(3): p. -.
111. Zhao, X., et al., *Thiolated trimethyl chitosan nanocomplexes as gene carriers with high in vitro and in vivo transfection efficiency.* Journal of Controlled Release, 2010. **144**(1): p. 46-54.
112. Lou, Y.L., et al., *Poly(ethylene imine)-g-chitosan using EX-810 as a spacer for nonviral gene delivery vectors.* Journal of Biomedical Materials Research Part A, 2009. **88A**(4): p. 1058-1068.
113. Rethore, G., et al., *Preparation of Chitosan/Polyglutamic Acid Spheres Based on the Use of Polystyrene Template as a Nonviral Gene Carrier.* Tissue Engineering Part C-Methods, 2009. **15**(4): p. 605-613.
114. Yuan, X.D., et al., *The Development and Mechanism Studies of Cationic Chitosan-Modified Biodegradable PLGA Nanoparticles for Efficient siRNA Drug Delivery.* Pharmaceutical Research, 2010. **27**(7): p. 1285-1295.
115. Jiang, H.L., et al., *Galactosylated Chitosan-g-PEI/DNA Complexes-loaded Poly(organophosphazene) Hydrogel as a Hepatocyte Targeting Gene Delivery System.* Archives of Pharmacal Research, 2010. **33**(4): p. 551-556.
116. Opanasopit, P., et al., *Nucleic Acid Delivery with Chitosan Hydroxybenzotriazole.* Oligonucleotides, 2010. **20**(3): p. 127-136.
117. Bauhuber, S., et al., *Delivery of Nucleic Acids via Disulfide-Based Carrier Systems.* Advanced Materials, 2009. **21**(32-33): p. 3286-3306.
118. Greish, K., *Enhanced permeability and retention (EPR) effect for anticancer nanomedicine drug targeting.* Methods Mol Biol. **624**: p. 25-37.
119. Moffatt, S. and R.J. Cristiano, *PEGylated J591 mAb loaded in PLGA-PEG-PLGA tri-block copolymer for targeted delivery: in vitro evaluation in human prostate cancer cells.* Int J Pharm, 2006. **317**(1): p. 10-3.
120. Liu, Y., et al., *A strategy for precision engineering of nanoparticles of biodegradable copolymers for quantitative control of targeted drug delivery.* Biomaterials.
121. Pissuwan, D., et al., *Targeted destruction of murine macrophage cells with bioconjugated gold nanorods.* Journal of Nanoparticle Research, 2007. **9**(6): p. 1109-1124.

122. Dauty, E., et al., *Intracellular delivery of nanometric DNA particles via the folate receptor.* Bioconjugate Chemistry, 2002. **13**(4): p. 831-839.
123. Hashida, M., et al., *Cell-specific delivery of genes with glycosylated carriers.* Adv Drug Deliv Rev, 2001. **52**(3): p. 187-96.
124. Kunath, K., et al., *Integrin targeting using RGD-PEI conjugates for in vitro gene transfer.* J. Gene Med., 2003. **5**: p. 588-599.
125. Green, J.J., et al., *Electrostatic ligand coatings of nanoparticles enable ligand-specific gene delivery to human primary cells.* Nano Letters, 2007. **7**(4): p. 874-9.
126. Ogris, M., et al., *Tumor-targeted gene therapy: strategies for the preparation of ligand-polyethylene glycol-polyethylenimine/DNA complexes.* J. Controlled Release, 2003. **91**(1-2): p. 173-181.
127. Levy-Nissenbaum, E., et al., *Nanotechnology and aptamers: applications in drug delivery.* Trends in Biotechnology, 2008. **26**(8): p. 442-9.
128. Shmueli, R.B., D.G. Anderson, and J.J. Green, *Electrostatic surface modifications to improve gene delivery.* Expert Opin Drug Deliv, 2010. **7**(4): p. 535-50.
129. Nguyen, J., et al., *Nanocomposites of lung surfactant and biodegradable cationic nanoparticles improve transfection efficiency to lung cells.* Journal of Controlled Release, 2009. **140**(1): p. 47-54.
130. Elfinger, M., et al., *Self-Assembly of Ternary Insulin-Polyethylenimine (PEI)-DNA Nanoparticles for Enhanced Gene Delivery and Expression in Alveolar Epithelial Cells.* Biomacromolecules, 2009. **10**(10): p. 2912-2920.
131. Akinc, A., et al., *Exploring polyethylenimine-mediated DNA transfection and the proton sponge hypothesis.* Journal of Gene Medicine, 2005. **7**(5): p. 657-663.
132. Yang, Y.X., et al., *Histidylated cationic polyorganophosphazene/DNA self-assembled nanoparticles for gene delivery.* International Journal of Pharmaceutics, 2008. **353**(1-2): p. 277-282.
133. Ogris, M., et al., *Melittin enables efficient vesicular escape and enhanced nuclear access of nonviral gene delivery vectors.* J Biol Chem, 2001. **276**(50): p. 47550-5.
134. Rozema, D.B., et al., *Endosomolysis by masking of a membrane-active agent (EMMA) for cytoplasmic release of macromolecules.* Bioconjugate Chemistry, 2003. **14**(1): p. 51-57.
135. Boeckle, S., et al., *Melittin analogs with high lytic activity at endosomal pH enhance transfection with purified targeted PEI polyplexes.* Journal of Controlled Release, 2006. **112**(2): p. 240-248.
136. Meyer, M., et al., *Breathing Life into Polycations:â€‰ Functionalization with pH-Responsive Endosomolytic Peptides and Polyethylene Glycol Enables siRNA Delivery.* Journal of the American Chemical Society, 2008. **130**(11): p. 3272-3273.
137. Murata, M., et al., *Modification of the N-terminus of membrane fusion-active peptides blocks the fusion activity.* Biochem Biophys Res Commun, 1991. **179**(2): p. 1050-5.
138. Midoux, P., R. Mayer, and M. Monsigny, *Membrane permeabilization by alpha-helical peptides: a flow cytometry study.* Biochim Biophys Acta, 1995. **1239**(2): p. 249-56.

139. Wagner, E., et al., *Influenza virus hemagglutinin HA-2 N-terminal fusogenic peptides augment gene transfer by transferrin-polylysine-DNA complexes: toward a synthetic virus-like gene-transfer vehicle.* Proc Natl Acad Sci U S A, 1992. **89**(17): p. 7934-8.
140. Moore, N.M., et al., *The effect of endosomal escape peptides on in vitro gene delivery of polyethylene glycol-based vehicles.* J Gene Med, 2008. **10**(10): p. 1134-49.
141. Hwang, C., A.J. Sinskey, and H.F. Lodish, *Oxidized redox state of glutathione in the endoplasmic reticulum.* Science, 1992. **257**(5076): p. 1496-502.
142. Mellman, I., *Endocytosis and molecular sorting.* Annu Rev Cell Dev Biol, 1996. **12**: p. 575-625.
143. Gross, J. and C.M. Lapiere, *Collagenolytic activity in amphibian tissues: a tissue culture assay.* Proc Natl Acad Sci U S A, 1962. **48**: p. 1014-22.
144. Coussens, L.M., B. Fingleton, and L.M. Matrisian, *Matrix metalloproteinase inhibitors and cancer: trials and tribulations.* Science, 2002. **295**(5564): p. 2387-92.
145. Niidome, Y., et al., *Pulsed-Laser Induced Fragmentation and Dissociation of DNA Immobilized on Gold Nanoparticles.* Molecular Crystals and Liquid Crystals, 2006. **445**: p. 201 - 206.
146. Jon, S., D.G. Anderson, and R. Langer, *Degradable poly(amino alcohol esters) as potential DNA vectors with low cytotoxicity.* Biomacromolecules, 2003. **4**(6): p. 1759-1762.
147. Jewell, C.M., et al., *Release of plasmid DNA from intravascular stents coated with ultrathin multilayered polyelectrolyte films.* Biomacromolecules, 2006. **7**(9): p. 2483-2491.
148. Schaffer, D.V. and D.A. Lauffenburger, *Optimization of cell surface binding enhances efficiency and specificity of molecular conjugate gene delivery.* J Biol Chem, 1998. **273**(43): p. 28004-9.
149. Lin, C. and J.F. Engbersen, *The role of the disulfide group in disulfide-based polymeric gene carriers.* Expert Opin Drug Deliv, 2009. **6**(4): p. 421-39.
150. Lin, C., et al., *Disulfide-containing poly(beta-amino ester)s for gene delivery.* J Control Release, 2006. **116**(2): p. e79-81.
151. Lin, C., et al., *Linear poly(amido amine)s with secondary and tertiary amino groups and variable amounts of disulfide linkages: synthesis and in vitro gene transfer properties.* J Control Release, 2006. **116**(2): p. 130-7.
152. Piest, M., et al., *Novel poly(amido amine)s with bioreducible disulfide linkages in their diamino-units: structure effects and in vitro gene transfer properties.* J Control Release, 2008. **130**(1): p. 38-45.
153. Saito, G., J.A. Swanson, and K.D. Lee, *Drug delivery strategy utilizing conjugation via reversible disulfide linkages: Role and site of cellular reducing activities.* Advanced Drug Delivery Reviews, 2003. **55**(2): p. 199-215.
154. Lee, Y., et al., *Visualization of the degradation of a disulfide polymer, linear poly(ethylenimine sulfide), for gene delivery.* Bioconjug Chem, 2007. **18**(1): p. 13-8.
155. Manickam, D.S., et al., *Effect of innate glutathione levels on activity of redox-responsive gene delivery vectors.* J Control Release. **141**(1): p. 77-84.

156. Chen, J., C. Wu, and D. Oupicky, *Bioreducible hyperbranched poly(amido amine)s for gene delivery.* Biomacromolecules, 2009. **10**(10): p. 2921-7.
157. Sunshine, J., N. Bhise, and J.J. Green, *Degradable polymers for gene delivery.* Conf Proc IEEE Eng Med Biol Soc, 2009. **2009**: p. 2412-5.
158. Stevenson, M., et al., *Delivery of siRNA mediated by histidine-containing reducible polycations.* J Control Release, 2008. **130**(1): p. 46-56.
159. Gosselin, M.A., W.J. Guo, and R.J. Lee, *Efficient gene transfer using reversibly cross-linked low molecular weight polyethylenimine.* Bioconjugate Chemistry, 2001. **12**(6): p. 989-994.
160. Hoon Jeong, J., et al., *Reducible poly(amido ethylenimine) directed to enhance RNA interference.* Biomaterials, 2007. **28**(10): p. 1912-7.
161. Jere, D., et al., *Akt1 silencing efficiencies in lung cancer cells by sh/si/ssiRNA transfection using a reductable polyspermine carrier.* Biomaterials, 2009. **30**(8): p. 1635-47.
162. Dauty, E. and A.S. Verkman, *Actin cytoskeleton as the principal determinant of size-dependent DNA mobility in cytoplasm: A new barrier for non-viral gene delivery.* Journal of Biological Chemistry, 2005. **280**(9): p. 7823-7828.
163. Pouton, C.W., et al., *Targeted delivery to the nucleus.* Advanced Drug Delivery Reviews, 2007. **59**(8): p. 698-717.
164. Stewart, M., *Molecular mechanism of the nuclear protein import cycle.* Nature Reviews Molecular Cell Biology, 2007. **8**(3): p. 195-208.
165. Pante, N. and M. Kann, *Nuclear pore complex is able to transport macromolecules with diameters of similar to 39 nm.* Molecular Biology of the Cell, 2002. **13**(2): p. 425-434.
166. Lam, A.P. and D.A. Dean, *Progress and prospects: nuclear import of nonviral vectors.* Gene Therapy, 2010. **17**(4): p. 439-447.
167. van der Aa, M.A.E.A., et al., *An NLS peptide covalently linked to linear DNA does not enhance transfection efficiency of cationic polymer based gene delivery systems.* Journal of Gene Medicine, 2005. **7**(2): p. 208-217.
168. Zanta, M.A., P. Belguise-Valladier, and J.P. Behr, *Gene delivery: A single nuclear localization signal peptide is sufficient to carry DNA to the cell nucleus.* Proceedings of the National Academy of Sciences of the United States of America, 1999. **96**(1): p. 91-96.
169. Sebestyen, M.G., et al., *DNA vector chemistry: The covalent attachment of signal peptides to plasmid DNA.* Nature Biotechnology, 1998. **16**(1): p. 80-85.
170. McLane, L.M. and A.H. Corbett, *Nuclear Localization Signals and Human Disease.* Iubmb Life, 2009. **61**(7): p. 697-706.
171. Miller, A.M., et al., *Identification of Protein Cofactors Necessary for Sequence-specific Plasmid DNA Nuclear Import.* Molecular Therapy, 2009. **17**(11): p. 1897-1903.
172. Kawakami, Y., et al., *Cloning of the gene coding for a shared human melanoma antigen recognized by autologous T cells infiltrating into tumor.* Proc Natl Acad Sci U S A, 1994. **91**(9): p. 3515-9.
173. van der Bruggen, P., et al., *A gene encoding an antigen recognized by cytolytic T lymphocytes on a human melanoma.* Science, 1991. **254**(5038): p. 1643-7.

174. Novellino, L., C. Castelli, and G. Parmiani, *A listing of human tumor antigens recognized by T cells: March 2004 update.* Cancer Immunol Immunother, 2005. **54**(3): p. 187-207.
175. Oelke, M., et al., *Ex vivo induction and expansion of antigen-specific cytotoxic T cells by HLA-Ig-coated artificial antigen-presenting cells.* Nat Med, 2003. **9**(5): p. 619-24.
176. Durai, M., et al., *In vivo functional efficacy of tumor-specific T cells expanded using HLA-Ig based artificial antigen presenting cells (aAPC).* Cancer Immunol Immunother, 2009. **58**(2): p. 209-20.
177. Steenblock, E.R. and T.M. Fahmy, *A comprehensive platform for ex vivo T-cell expansion based on biodegradable polymeric artificial antigen-presenting cells.* Mol Ther, 2008. **16**(4): p. 765-72.
178. Steenblock, E.R., et al., *An artificial antigen-presenting cell with paracrine delivery of IL-2 impacts the magnitude and direction of the T cell response.* J Biol Chem, 2011. **286**(40): p. 34883-92.
179. Maus, M.V., et al., *Ex vivo expansion of polyclonal and antigen-specific cytotoxic T lymphocytes by artificial APCs expressing ligands for the T-cell receptor, CD28 and 4-1BB.* Nat Biotechnol, 2002. **20**(2): p. 143-8.
180. Engelhard, V.H., et al., *Induction of secondary cytotoxic T lymphocytes by purified HLA-A and HLA-B antigens reconstituted into phospholipid vesicles.* Proc Natl Acad Sci U S A, 1978. **75**(11): p. 5688-91.
181. Mescher, M.F., *Surface contact requirements for activation of cytotoxic T lymphocytes.* J Immunol, 1992. **149**(7): p. 2402-5.
182. Curtsinger, J., et al., *Artificial cell surface constructs for studying receptor-ligand contributions to lymphocyte activation.* J Immunol Methods, 1997. **209**(1): p. 47-57.
183. Turtle, C.J. and S.R. Riddell, *Artificial antigen-presenting cells for use in adoptive immunotherapy.* Cancer J, 2010. **16**(4): p. 374-81.
184. Gilboa, E., *The makings of a tumor rejection antigen.* Immunity, 1999. **11**(3): p. 263-70.
185. Jenkins, M.K., et al., *CD28 delivers a costimulatory signal involved in antigen-specific IL-2 production by human T cells.* J Immunol, 1991. **147**(8): p. 2461-6.
186. Curtsinger, J.M., et al., *Inflammatory cytokines provide a third signal for activation of naive CD4+ and CD8+ T cells.* J Immunol, 1999. **162**(6): p. 3256-62.
187. Grakoui, A., et al., *The immunological synapse: a molecular machine controlling T cell activation.* Science, 1999. **285**(5425): p. 221-7.
188. Lee, K.H., et al., *T cell receptor signaling precedes immunological synapse formation.* Science, 2002. **295**(5559): p. 1539-42.
189. Rosenberg, S.A., et al., *Use of tumor-infiltrating lymphocytes and interleukin-2 in the immunotherapy of patients with metastatic melanoma. A preliminary report.* N Engl J Med, 1988. **319**(25): p. 1676-80.
190. Dudley, M.E., et al., *Cancer regression and autoimmunity in patients after clonal repopulation with antitumor lymphocytes.* Science, 2002. **298**(5594): p. 850-4.

191. Kurokawa, T., M. Oelke, and A. Mackensen, *Induction and clonal expansion of tumor-specific cytotoxic T lymphocytes from renal cell carcinoma patients after stimulation with autologous dendritic cells loaded with tumor cells.* Int J Cancer, 2001. **91**(6): p. 749-56.
192. Altman, J.D., et al., *Phenotypic analysis of antigen-specific T lymphocytes.* Science, 1996. **274**(5284): p. 94-6.
193. Neudorfer, J., et al., *Reversible HLA multimers (Streptamers) for the isolation of human cytotoxic T lymphocytes functionally active against tumor- and virus-derived antigens.* J Immunol Methods, 2007. **320**(1-2): p. 119-31.
194. Nguyen, D.N., et al., *Polymeric Materials for Gene Delivery and DNA Vaccination.* Advanced Materials, 2009. **21**(8): p. 847-867.
195. Rosenberg, S.A., *Raising the bar: the curative potential of human cancer immunotherapy.* Sci Transl Med, 2012. **4**(127): p. 127ps8.
196. Morgan, R.A., et al., *Cancer regression in patients after transfer of genetically engineered lymphocytes.* Science, 2006. **314**(5796): p. 126-9.
197. Giannoni, F., et al., *Clustering of T cell ligands on artificial APC membranes influences T cell activation and protein kinase C theta translocation to the T cell plasma membrane.* J Immunol, 2005. **174**(6): p. 3204-11.
198. Oelke, M., et al., *Ex vivo induction and expansion of antigen-specific cytotoxic T cells by HLA-Ig-coated artificial antigen-presenting cells.* Nat Med, 2003. **9**(5): p. 619-25. PMID: 12074385.
199. Ugel, S., et al., *In vivo administration of artificial antigen-presenting cells activates low-avidity T cells for treatment of cancer.* Cancer Res, 2009. **69**(24): p. 9376-84.
200. Levine, B.L., et al., *Effects of CD28 costimulation on long-term proliferation of CD4+ T cells in the absence of exogenous feeder cells.* J Immunol, 1997. **159**(12): p. 5921-30.
201. Maus, M.V., et al., *HLA tetramer-based artificial antigen-presenting cells for stimulation of CD4+ T cells.* Clin Immunol, 2003. **106**(1): p. 16-22.
202. Han, H., et al., *A novel system of artificial antigen-presenting cells efficiently stimulates Flu peptide-specific cytotoxic T cells in vitro.* Biochem Biophys Res Commun, 2011. **411**(3): p. 530-5.
203. Steenblock, E.R. and T.M. Fahmy, *A comprehensive platform for ex vivo T-cell expansion based on biodegradable polymeric artificial antigen-presenting cells.* Mol Ther, 2008. **16**(4): p. 765-72. PMID: 18334990.
204. Schutz, C., et al., *Killer artificial antigen-presenting cells: a novel strategy to delete specific T cells.* Blood, 2008. **111**(7): p. 3546-52.
205. Schutz, C., et al., *Killer artificial antigen-presenting cells: the synthetic embodiment of a 'guided missile'.* Immunotherapy, 2010. **2**(4): p. 539-50.
206. Webb, T.J., et al., *Ex vivo induction and expansion of natural killer T cells by CD1d1-Ig coated artificial antigen presenting cells.* J Immunol Methods, 2009. **346**(1-2): p. 38-44.
207. Sun, W., et al., *Connecting the dots: artificial antigen presenting cell-mediated modulation of natural killer T cells.* J Interferon Cytokine Res, 2012. **32**(11): p. 505-16.

208. O'Herrin, S.M., et al., *Antigen-specific blockade of T cells in vivo using dimeric MHC peptide.* J Immunol, 2001. **167**(5): p. 2555-60.
209. Pareja, E., et al., *The tetramer model: a new view of class II MHC molecules in antigenic presentation to T cells.* Tissue Antigens, 1997. **50**(5): p. 421-8.
210. Deeths, M.J. and M.F. Mescher, *B7-1-dependent co-stimulation results in qualitatively and quantitatively different responses by CD4+ and CD8+ T cells.* Eur J Immunol, 1997. **27**(3): p. 598-608.
211. Deeths, M.J. and M.F. Mescher, *ICAM-1 and B7-1 provide similar but distinct costimulation for CD8+ T cells, while CD4+ T cells are poorly costimulated by ICAM-1.* Eur J Immunol, 1999. **29**(1): p. 45-53.
212. Shalaby, W.S., et al., *Absorbable microparticulate cation exchanger for immunotherapeutic delivery.* J Biomed Mater Res B Appl Biomater, 2004. **69**(2): p. 173-82.
213. Fahmy, T.M., et al., *Surface modification of biodegradable polyesters with fatty acid conjugates for improved drug targeting.* Biomaterials, 2005. **26**(28): p. 5727-36.
214. Fletcher, D.A. and R.D. Mullins, *Cell mechanics and the cytoskeleton.* Nature, 2010. **463**(7280): p. 485-92.
215. Merkel, T.J., et al., *Scalable, Shape-Specific, Top-Down Fabrication Methods for the Synthesis of Engineered Colloidal Particles.* Langmuir, 2010. **26**(16): p. 13086-13096.
216. Glotzer, S.C. and M.J. Solomon, *Anisotropy of building blocks and their assembly into complex structures.* Nature Materials, 2007. **6**(8): p. 557-562.
217. Merkel, T.J., et al., *Using mechanobiological mimicry of red blood cells to extend circulation times of hydrogel microparticles.* Proc Natl Acad Sci U S A, 2011. **108**(2): p. 586-91.
218. Champion, J.A., Y.K. Katare, and S. Mitragotri, *Particle shape: a new design parameter for micro- and nanoscale drug delivery carriers.* J Control Release, 2007. **121**(1-2): p. 3-9.
219. Champion, J.A. and S. Mitragotri, *Role of target geometry in phagocytosis.* Proc Natl Acad Sci U S A, 2006. **103**(13): p. 4930-4.
220. Champion, J.A. and S. Mitragotri, *Shape induced inhibition of phagocytosis of polymer particles.* Pharm Res, 2009. **26**(1): p. 244-9.
221. Sharma, G., et al., *Polymer particle shape independently influences binding and internalization by macrophages.* J Control Release, 2010. **147**(3): p. 408-12.
222. Muro, S., et al., *Control of endothelial targeting and intracellular delivery of therapeutic enzymes by modulating the size and shape of ICAM-1-targeted carriers.* Mol Ther, 2008. **16**(8): p. 1450-8.
223. Geng, Y., et al., *Shape effects of filaments versus spherical particles in flow and drug delivery.* Nat Nanotechnol, 2007. **2**(4): p. 249-55.
224. Ho, C.C., et al., *Preparation of Monodisperse Ellipsoidal Polystyrene Particles.* Colloid and Polymer Science, 1993. **271**(5): p. 469-479.
225. Champion, J.A., Y.K. Katare, and S. Mitragotri, *Making polymeric micro- and nanoparticles of complex shapes.* Proc Natl Acad Sci U S A, 2007. **104**(29): p. 11901-4.

226. Rolland, J.P., et al., *Direct fabrication and harvesting of monodisperse, shape-specific nanobiomaterials.* J Am Chem Soc, 2005. **127**(28): p. 10096-100.
227. Kelly, J.Y. and J.M. DeSimone, *Shape-specific, monodisperse nano-molding of protein particles.* J Am Chem Soc, 2008. **130**(16): p. 5438-9.
228. Wang, Y., et al., *Generation of a library of particles having controlled sizes and shapes via the mechanical elongation of master templates.* Langmuir, 2011. **27**(2): p. 524-8.
229. Dendukuri, D., et al., *Continuous-flow lithography for high-throughput microparticle synthesis.* Nat Mater, 2006. **5**(5): p. 365-9.
230. Yoo, J.W. and S. Mitragotri, *Polymer particles that switch shape in response to a stimulus.* Proc Natl Acad Sci U S A, 2010. **107**(25): p. 11205-10.
231. Green, J.J., et al., *Combinatorial modification of degradable polymers enables transfection of human cells comparable to adenovirus.* Advanced Materials, 2007. **19**(19): p. 2836-2842.
232. Mossman, K.D., et al., *Altered TCR signaling from geometrically repatterned immunological synapses.* Science, 2005. **310**(5751): p. 1191-3.

3 Chapter 3: Degradable Polymers for Gene Delivery

Gene delivery has great potential, both as a therapeutic to treat disease on the genetic level and as a technology to enable regenerative medicine. The central challenge is finding a safe and effective delivery system. As viral gene therapy can have serious safety concerns, many recent efforts have focused on non-viral methods that utilize biomaterials. Many materials have been shown effective for delivering genes in vitro including cationic lipids, sugars, peptides, and polymers [1-3].

One of the lead delivery polymers is polyethylenimine (PEI), which due its cationic structure, can be very effective for binding DNA and forming gene delivery particles [4]. PEI is also particularly effective at promoting endosomal escape of PEI/DNA particles through the proton sponge mechanism [5, 6]. This is critical to prevent lysosomal degradation of the DNA and to enable efficient delivery of the DNA to the cytoplasm. This endosomal escape mechanism has been used in the design of other synthetic gene delivery polymers, including polylysine-based polymers that contain an imidazole group in the side chain [7]. Although PEI shows promise compared to other biomaterials, it also leads to significant cytotoxicity [8] and has lower effectiveness than viral methods.

One newer group of polymers used for gene delivery are poly(β-amino ester)s [9]. They are useful due to their ability to bind DNA, promote cellular uptake, facilitate escape from the endosome, and allow for DNA release in the cytoplasm [10-12]. Unlike PEI, they are readily biodegradable due to their ester linkages, which reduces cytotoxicity

---

This chapter contains excerpts from an article that was published as Sunshine JC, Bhise NB, Green JJ. "Degradable polymers for gene delivery." *Conference Proceedings IEEE Engineering in Medicine and Biology Society*. 2009; 1:2412-5.

[10, 13]. It has been shown that within this class, acrylate-terminated polymers have low gene delivery, whereas amine monomer-terminated polymers have higher delivery [14]. Recently, end-modification with diamine monomers has shown that some of these polymers can rival adenovirus for gene delivery in vitro and are also effective in vivo [15, 16].

Another interesting approach to increase gene delivery effectiveness while reducing cytotoxicity is adding bioreducible linkages to polymers. Disulfide linkages have been added to PEI to produce bioreducible versions with lower cytotoxicity than high molecular weight versions of the parent polymer [17, 18]. Other researchers have shown that bioreducible poly(amido amines) can have higher efficacy than PEI while also having reduced cytotoxicity [19, 20].

It was recently demonstrated that IMR-90 human primary fibroblasts can be reprogrammed to induced pluripotent stem cells with integrating viruses [21]. Reprogramming human differentiated cells into undifferentiated, pluripotent cells could potentially enable a patient to receive a customized cell therapy that is a perfect genetic match.

In this initial study, we investigated how small modifications to the monomer ratio used during polymerization in combination with modifications to end-capping group chemical structure used post-polymerization affects gene delivery. We compared how chemical structure tunes gene delivery efficacy between a cancerous fibroblast line and human primary fibroblasts. In particular, we highlight that small changes to the molecular weight or changes to just the ends of the polymer, while leaving the main chain

of the polymer the same, significantly enhances or decreases the overall delivery of the polymer.

3.1 Materials and Methods

3.1.1 Polymer Synthesis

1,4-butanediol diacrylate (Alfa Aesar), 5-amino-1-pentanol (Alfa Aesar), 1-(3-aminopropyl)-4-methylpiperazine (Lancaster), 1-(3-aminopropyl)pyrrolidine (Acros Organics), 4-aminophenyl disulfide (Sigma-Aldrich), dimethyl sulfoxide (Sigma-Aldrich), 25 kDa polyethylenimine (Sigma-Aldrich), and Lipofectamine 2000 (Invitrogen) were used as received. Polymers were synthesized using a two-step procedure that is described in **Fig. 3.1**. Acrylate-terminated poly(1,4-butanediol diacrylate-co-5-amino-1-pentanol) was first synthesized at two different acrylate monomer to amine monomer molar ratios, 1.05:1 and 1.2:1. For the 1.05:1 ratio, 3532 mg of 1,4-butanediol diacrylate (17.8 mmol) was added to 1754 mg of 5-amino-1-pentanol (17.0 mmol) and for the 1.2:1 ratio, 3532 mg of 1,4-butanediol diacrylate (17.8 mmol) with 1533 mg of 5-amino-1-pentanol (14.8 mmol).

Reactions took place in DMSO (500 mg/mL) in glass vials in the dark under magnetic stirring for 48 hrs at 40°C. As a second step, three amine-containing small molecules were individually conjugated to the ends of each polymer post-polymerization. Reactions were performed by mixing 321 mg of poly(1,4-butanediol diacrylate-co-5-amino-1-pentanol) in DMSO (500 mg/mL) with 800 μL of 0.25 M amine solution. Excess amine is used to fully end-modify the base polymer. Reactions were performed in 1.5 mL tubes in a multi-tube vortexer with constant agitation for 24 hours at room

temperature. Polymers were stored at -20°C with desiccant until use. Polymers were analyzed by gel permeation chromatography using a Waters Breeze System and 3 Styragel Columns (7.8 x 300mm) in series: HR1, HR 3, and HR 4. The eluent was 95% THF/5% DMSO/0.1M piperidine and ran at 1 mL/min.

3.1.2 Cell Culture

COS-7 and IMR-90 cells (ATCC, Manassas, VA) were grown following ATCC recommended protocols and reagents. COS-7s were grown in Dulbecco's Modified Eagle's Medium (DMEM, ATCC) supplemented with 10% fetal bovine serum (ATCC) and 100 units/mL of penicillin and streptomycin (Invitrogen). IMR-90s were grown in Eagle's Minimum Essential Medium (EMEM, ATCC) supplemented with 10% fetal bovine serum (ATCC) and 100 units/mL of penicillin and streptomycin. Cells were subcultured upon confluence and IMR-90s were used prior to passage eight.

3.1.3 Gene Delivery Assays

Cells were plated in white 96-well plates at 15,000 cells in 100 μL per well and allowed to adhere overnight. CMV-Luc

DNA (Elim Biopharmaceuticals, Hayward, CA) was diluted in 25 mM sodium acetate (pH=5) to 0.06 mg/mL. Polymers at 100 mg/ml in DMSO were diluted in 25 mM sodium acetate buffer to concentrations that generate the varying polymer to DNA weight ratios (20, 40, 60, 100). One hundred microliters of diluted polymer solution was mixed vigorously with 100 μL of DNA solution in a 96-well plate using a multichannel pipette. After 10 minutes wait time, 20 μL of each formulation was added to the cells that contained 100 μL of complete media per well. Particles were incubated with the cells for four hours and then removed with a 12-channel aspirator wand. Warm, complete media

was added to the cells (100 μL/well) and they were allowed to grow for two days at 37°C and 5% CO2. Polyethylenimine/DNA particles were formed in a similar manner to the other polymers, except that they were formed at a w/w ratio of 1 (N/P~8) in 150 mM NaCl solution as has been previously described [4, 22]. Lipofectamine 2000 was used following the manufacturer instructions. Forty-eight hours post transfection, gene expression was measured using Bright-Glo luminescence assay kits (Promega), a Synergy 2 multilabel plate reader (Biotek), and a one second read time per well. Protein content per well was measured using the BCA protein assay kit (Pierce) and the Synergy 2 plate reader to measure absorbance at 562 nm.

3.2 Results and discussion

Base acrylate-terminated polymers were synthesized via the conjugate addition of 5-amino-1-pentanol to an excess of 1,4-butanediol diacrylate in a manner similar to that previously described, but at a lower temperature and for a longer reaction time while being dissolved in DMSO [15, 16]. Polymerizations were performed at molar ratios of 1.05:1 and 1.2:1 at 40 °C for 48 hrs. Subsequently, the polymers were end-modified by conjugate addition of 1-(3-aminopropyl)-4-methylpiperazine (Poly 1), 1-(3-aminopropyl)pyrrolidine (Poly 2), or 4-aminophenyl disulfide (Poly 3) to the base polymers at room temperature for 24 hrs (**Fig. 3.1**). Polymers were analyzed by gel permeation chromatography as shown in Table 1. For the 1.2:1 molar ratio, polymers had Mw ~ 6 kDa. At a 1.05:1 molar ratio, the molecular weight was higher, Mw ~ 6.5-8.5 kDa. Gene delivery particles were formed in buffer through self-assembly between the cationic polymers and anionic DNA.

At lower weight ratios (20 and 40 w/w), polymeric particles formed with polymers synthesized at 1.05:1 were generally more efficient for gene delivery than the same polymers formed at 1.2:1. This is likely due to the higher MW of these polymers. In some cases, these changes were dramatic. For example, for Poly 1 at 20 w/w, the 1.05:1 ratio is more than 10-fold as effective as the 1.2:1 ratio with COS-7 cells and 400-fold more effective for IMR-90s. Interestingly, the difference in MW between these two polymers is only ~ 1.5 kDa. However, at higher weight ratios (60 and 100 w/w), this trend is not seen and the effectiveness of both polymer synthesis conditions is comparable. The one exception to this trend is Poly 2, which has comparable delivery between the two synthesis ratios at 60 and 100 w/w in COS-7 cells, but in IMR-90 cells, only the 1.05:1 ratio polymer is effective at any weight ratio tested. Thus small changes to MW may be able to tune delivery properties to alter cell-type specificity.

Certain end-modifying groups also appeared to show cell-type specificity. For example, Poly 3 at 60 w/w or 100 w/w has very high gene delivery to the COS-7 cancerous fibroblasts, but very poor delivery to the IMR-90 human primary fibroblasts. In comparison to Lipofectamine 2000, Poly 3 (1.2:1 ratio and 60 w/w) enables twice the gene expression in COS-7 cells, but over 200-fold less expression in IMR-90s. For transfection of IMR-90s, Poly 1 or Poly 2 at a polymerization ratio of 1.05:1 and polymer to DNA weight ratio of 100 were the most effective. These conditions enabled transfection of human primary fibroblasts in serum-containing media at 8-10 fold the levels of Lipofectamine 2000. Lipofectamine 2000 is a leading-commercially available lipid-based transfection reagent and the polymers presented here can achieve comparable or higher delivery to both cancerous and primary cell types. Compared to 25 kDa

branched polyethylenimine, a leading of-the-shelf gene delivery polymer, the polymers presented here are up to 2-3 orders of magnitude more effective. In all cases, cells remained viable and comparable to untreated controls as determined by visual inspection and relative levels of protein content per well through the BCA assay.

Small molecule amine containing end-groups were chosen to increase DNA binding affinity compared to acrylate terminated polymers and to potentially improve endosomal release of the particles (Poly 1 and Poly 2) or bioreducible release of the DNA (Poly 3). As these small structural modifications also lead to a significant change in cell-type specificity, the end-group may also play an important role in directing particle uptake. We are currently quantifying these mechanisms to better understand structure/function relationships of these materials. Further exploration of polymer structures may lead not only to safe and effective transfection reagents, but also to materials with a natural proclivity to targeting certain types of cells.

3.3 Figures

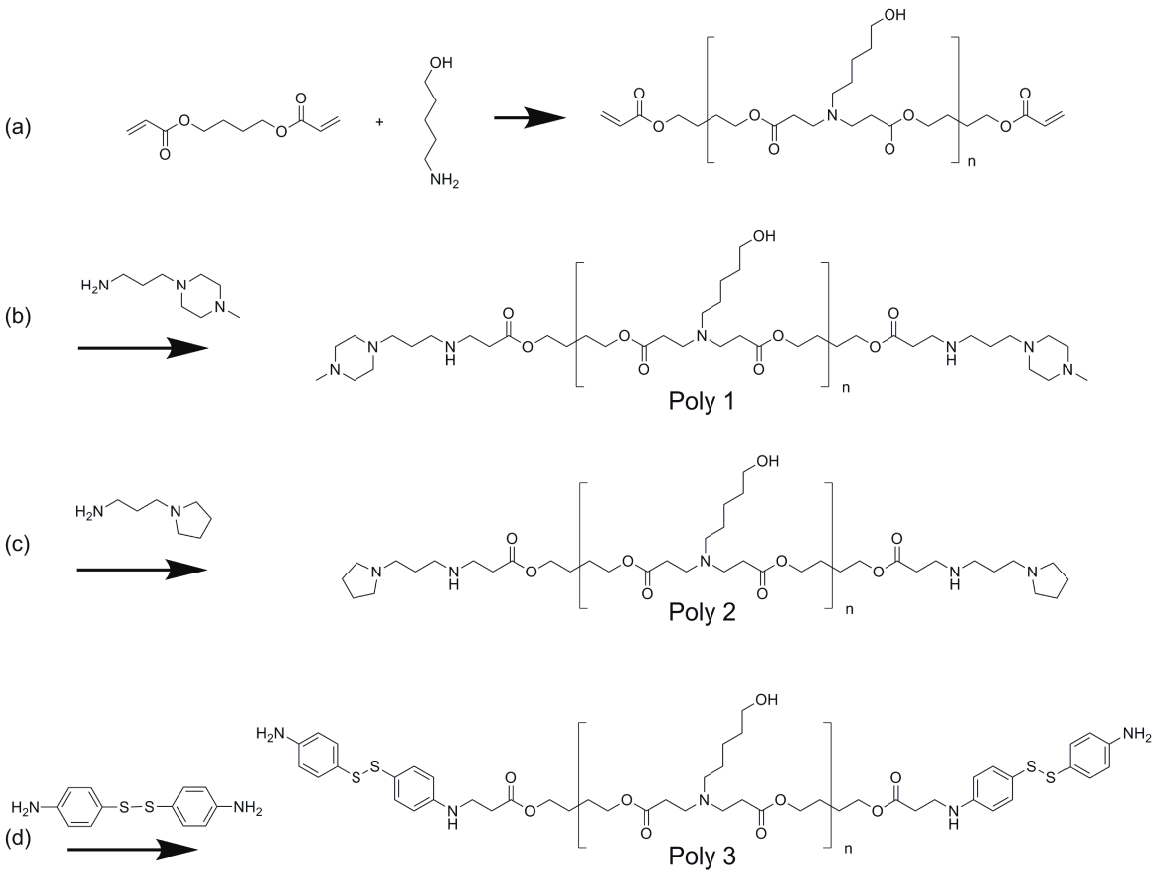

Figure 3.1. Synthesis of degradable gene delivery polymers. (a) 1,4-butanediol diacrylate reacts with 1-amino-5-pentanol to form the acrylate-terminated poly(beta-amino ester) precursor. This react with (b) 1-(3-aminopropyl)-4-methylpiperazine to form Poly 1, (c) 1-(3-aminopropyl)pyrrolidine to form Poly 2, or (d) 4-aminophenyl disulfide to form Poly 3.

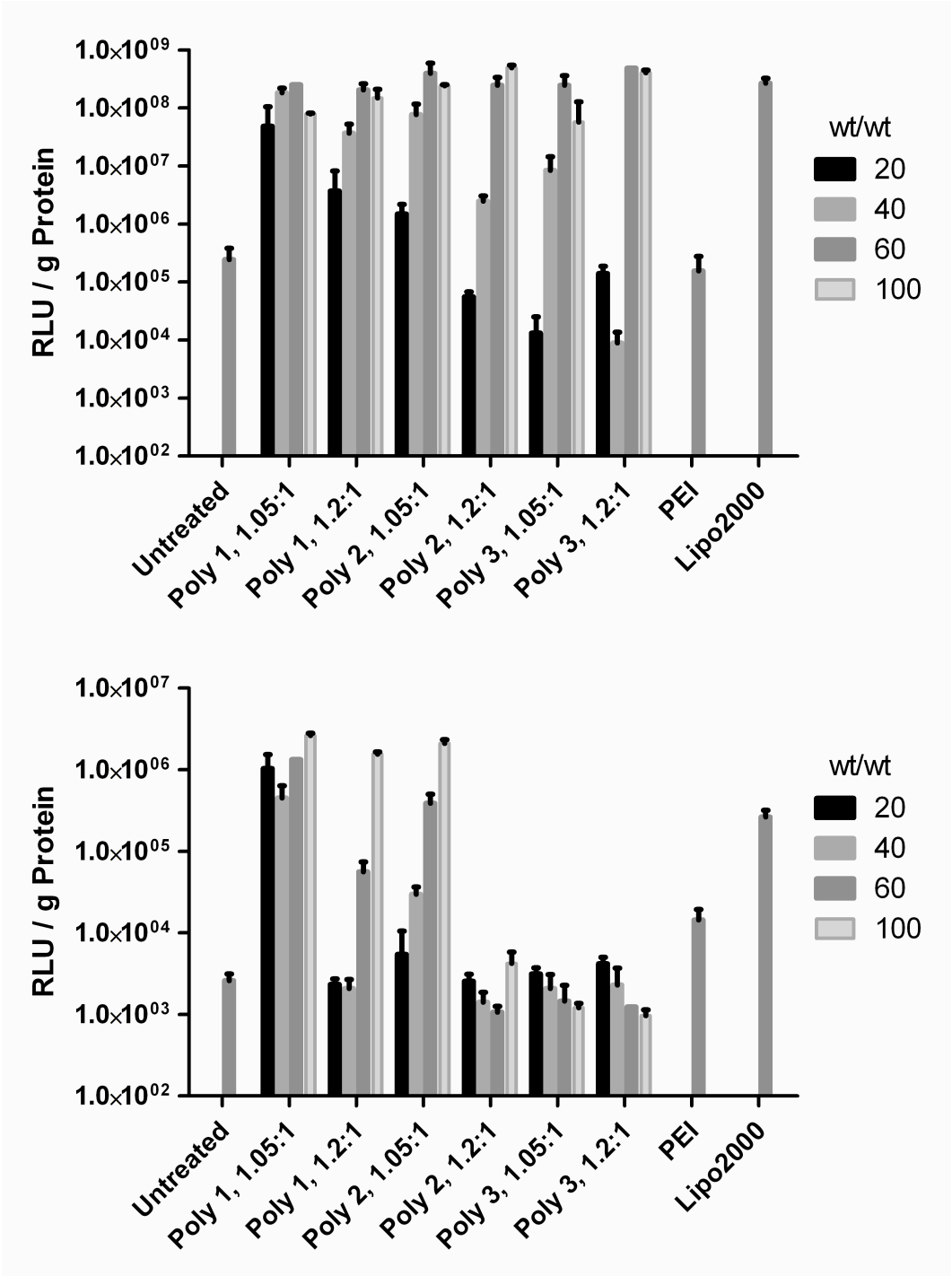

Fig. 3.2. Gene delivery efficacy of Poly 1, Poly 2, Poly 3, and commercial reagents PEI and Lipofectamine 2000 to COS-7 cells (above) and IMR-90 cells (below). Luciferase-encoding DNA is delivered and expression is measured as relative light units per gram protein. Ratio 1.05:1 and 1.2:1 refer to polymerization conditions and wt/wt is the weight ratio of polymer to DNA. Graphs show mean+SD, n=4.

Table 3.1: Polymer Molecular Weight

	Ratio	M_n	M_w	PDI
Poly 1	1.05:1	5415	7696	1.42
	1.2:1	4580	6124	1.34
Poly 2	1.05:1	4249	6459	1.52
	1.2:1	3943	5714	1.45
Poly 3	1.05:1	5680	8521	1.50
	1.2:1	3547	5448	1.54

3.4 References

1. Park, T.G., J.H. Jeong, and S.W. Kim, *Current status of polymeric gene delivery systems.* Advanced Drug Delivery Reviews, 2006. **58**(4): p. 467-486.
2. Pack, D.W., et al., *Design and development of polymers for gene delivery.* Nature Reviews Drug Discovery, 2005. **4**(7): p. 581-593.
3. Pedroso de Lima, M.C., et al., *Cationic lipid-DNA complexes in gene delivery: from biophysics to biological applications.* Advanced Drug Delivery Reviews, 2001. **47**(2-3): p. 277-94.
4. Boussif, O., et al., *A versatile vector for gene and oligonucleotide transfer into cells in culture and in vivo: polyethylenimine.* Proc Natl Acad Sci U S A, 1995. **92**(16): p. 7297-301.
5. Sonawane, N.D., F.C. Szoka, and A.S. Verkman, *Chloride accumulation and swelling in endosomes enhances DNA transfer by polyamine-DNA polyplexes.* Journal of Biological Chemistry, 2003. **278**(45): p. 44826-44831.
6. Akinc, A., et al., *Exploring polyethylenimine-mediated DNA transfection and the proton sponge hypothesis.* Journal of Gene Medicine, 2005. **7**(5): p. 657-663.
7. Putnam, D., et al., *Polymer-based gene delivery with low cytotoxicity by a unique balance of side-chain termini.* Proc Natl Acad Sci U S A, 2001. **98**(3): p. 1200-5.
8. Moghimi, S.M., et al., *A two-stage poly(ethylenimine)-mediated cytotoxicity: implications for gene transfer/therapy.* Mol Ther, 2005. **11**(6): p. 990-5.
9. Green, J.J., D.G. Anderson, and R. Langer, *A combinatorial polymer library yields insights into the field of non-viral gene delivery.* Accounts of Chemical Research, 2007. **41**(6): p. 749-759.
10. Lynn, D.M. and R. Langer, *Degradable poly(beta-amino esters): Synthesis, characterization, and self-assembly with plasmid DNA.* J Am Chem Soc, 2000. **122**: p. 10761-10768.
11. Anderson, D.G., et al., *Structure/property studies of polymeric gene delivery using a library of poly(beta-amino esters).* Molecular Therapy, 2005. **11**(3): p. 426-34.
12. Akinc, A., et al., *Parallel synthesis and biophysical characterization of a degradable polymer library for gene delivery.* Journal of the American Chemical Society, 2003. **125**(18): p. 5316-23.
13. Green, J.J., et al., *Biodegradable polymeric vectors for gene delivery to human endothelial cells.* Bioconjugate Chemistry, 2006. **17**: p. 1162-1169.
14. Akinc, A., et al., *Synthesis of poly(beta-amino ester)s optimized for highly effective gene delivery.* Bioconjugate Chemistry, 2003. **14**(5): p. 979-988.
15. Green, J.J., et al., *Combinatorial modification of degradable polymers enables transfection of human cells comparable to adenovirus.* Advanced Materials, 2007. **19**(19): p. 2836-2842.
16. Zugates, G.T., et al., *Rapid Optimization of Gene Delivery by Parallel End-modification of Poly(beta-amino ester)s.* Mol Ther, 2007. **15**(7): p. 1306-1312.

17. Gosselin, M.A., W.J. Guo, and R.J. Lee, *Efficient gene transfer using reversibly cross-linked low molecular weight polyethylenimine.* Bioconjugate Chemistry, 2001. **12**(6): p. 989-994.
18. Forrest, M.L., J.T. Koerber, and D.W. Pack, *A degradable polyethylenimine derivative with low toxicity for highly efficient gene delivery.* Bioconjug Chem, 2003. **14**(5): p. 934-40.
19. Christensen, L.V., et al., *Reducible poly(amido ethylenimine)s designed for triggered intracellular gene delivery.* Bioconjugate Chemistry, 2006. **17**(5): p. 1233-40.
20. Lin, C., et al., *Bioreducible poly(amido amine)s with oligoamine side chains: synthesis, characterization, and structural effects on gene delivery.* Journal of Controlled Release, 2008. **126**(2): p. 166-74.
21. Yu, J., et al., *Induced pluripotent stem cell lines derived from human somatic cells.* Science, 2007. **318**(5858): p. 1917-20.
22. Sullivan, M.M.O., J.J. Green, and T.M. Przybycien, *Development of a novel gene delivery scaffold utilizing colloidal gold-polyethylenimine conjugates for DNA condensation.* Gene Therapy, 2003. **10**(22): p. 1882-1890.

4 Chapter 4: Effects of Base Polymer Hydrophobicity and End Group Modification on Polymeric Gene Delivery

4.1 Introduction

Gene therapy holds out the promise of specific therapy designed to target the root causes of a plethora of diseases, ranging from single gene diseases such as sickle cell anemia and hemophilia, to diseases with a genetic basis such as cancer, diabetes, and heart disease. Since viruses have long evolved to be exceptionally efficient at getting their genetic information into cells, scientists and clinicians initially took advantage of this to develop viral vector-based gene therapeutics. Unfortunately, the field had significant setbacks when tragedies occurred in clinical trials, including deaths due to excessive immune responses to the viruses, as well as subsequent cancer generation due to insertional mutagenesis [1-3]. The major effort in this field remains in the viral arena – 75% of clinical trials for gene therapy use viral vectors [4]. Due to the potential drawbacks of viral vectors, including their immunogenicity, potential for insertional mutagenesis, small cargo capacity, and difficulty involved in large-scale production, a wide variety of non-viral vectors have been investigated for their nucleic acid delivery efficacy [5, 6]. Among the polymers investigated, poly(beta-amino) esters have particularly shown promise as gene delivery vectors [7-11], with some formulations rivaling adenoviral transfection efficacy in hard to transfect human cell lines [12].

This chapter contains excerpts from an article that was published as Sunshine JC, Akanda MI, Li D, Kozielski KL, and Green JJ. "Effects of Base Polymer Hydrophobicity and End-Group Modification on Polymeric Gene Delivery." *Biomacromolecules*. 2011; 12(10),3592-3600.

Promising recent applications of these polymers include their use in cancer therapy [13-15], as electrostatic coatings on gold nanoparticles for efficient delivery of siRNA [16], as biodegradable hydrogels [17, 18], and as pH-responsive components of polymeric micelles for drug release [19].

Poly(beta-amino) esters (PBAE) are synthesized by simple Michael addition of diacrylates to primary (or bis-secondary) amines. Previous studies have noted that amine-terminated versions of the polymers were far superior to corresponding diacrylate-terminated versions [8], and thus have investigated whether modification of the ends of the polymers would have a dramatic effect on transfection efficacy [20]. Modification of the ends of the polymer has been shown to be important not only with regard to improving the efficacy of a particular polymer backbone, but the particular end group which is optimal appears to be a function of the cell type investigated [21]. There is a relationship between which polymers transfect well in 2D as compared to 3D culture methods, but the relationship is not perfect and some formulations can be better at transfecting cells in 2D monolayer or 3D culture [22]. Some convergence of optimal structure has been previously reported, including that small particle sizes have been associated with improved transfection, and that optimal polymers tend to contain amino-alcohol side chains [23].

One additional advantage of this library approach to vector design is that it can provide the means to productively analyze structure function relationships across a wide or narrow window of potential structures. However, previous studies have not looked at the systematic modification of all three structural and chemical elements that compose the polymer: backbone, side chain, and end-group. Here, we do this and synthesize a new

library of 320 end-modified PBAEs that differ by single carbon changes to the monomers that compose the backbone and side chains and small functional changes to the end-group. In this way we can analyze the contributions of spacer length, side chain length, and overall hydrophobicity / hydrophilicity of the end-modified polymer to the resulting transfection efficacy.

We characterize the transfection efficacy and toxicity of the nanoparticles that these polymers form with DNA through self-assembly. The best performing polymer formulations show superior transfection efficacy to commercially available alternatives with better toxicity profiles, and the data reveal insight into structure function relationships within this polymer library.

4.2 Materials and Methods

4.2.1 Materials

All reagents and solvents were obtained from commercial suppliers and used as received. Monomers were purchased from Acros Organics [1-(3-aminopropyl)-4-methylpiperazine (E8)], Alfa Aesar [3-amino-1-propanol (S3), 4-amino-1-butanol (S4), 5-amino-1-pentanol (S5), 1,4-butanediol diacrylate (B4), 1,6-hexanediol diacrylate (B6), 1-(3-aminopropyl)-4-methylpiperazine (E7)], Fluka [2-(3-aminopropylamino)ethanol (E6)], Monomer-Polymer and Dajac Labs [1,3-propanediol diacrylate (B3), 1,5-pentanediol diacrylate (B5)], Sigma Aldrich [3-aminopropane-1,2-diol (S3o), 1,3-butanediol diacrylate (B3m), 2-(benzoyloxymethyl)-2-ethylpropane-1,3-diyl diacrylate (BL1), ethoxylated bisphenol A diacrylate (BL2), glycerol 1,3-diglycerolate diacrylate (BH1), 1,3-diaminopropane (E1), 4-aminophenyl disulfide (E9),

cystaminedihydrochloride (E10), 2-(1H-imidazol-4-yl)ethanamine (E12)], and TCI America [1,3-diaminopentane (E3), 2-methyl-1,5-diaminopentane (E4), $(PEO)_4$-bis-amine (E5)]. Plasmids (CMV-Luc and CMV-eGFP) were amplified by Aldevron (Fargo, ND) and used as recieved. FuGENE® HD, Lipofectamine™ 2000, and Opti-MEM I were purchased from Invitrogen and used according to manufacturer instructions. CellTiter 96® AQ_{ueous} One MTS assay and the BrightGlo™ assay system were purchased from Promega, and were used according to manufacturer's instructions. Dulbecco's Modified Eagle Medium (DMEM) was purchased from Invitrogen and supplemented with 10% FBS and 1% penicillin/streptomycin.

4.2.2 Polymer Library Synthesis

The library of PBAEs was synthesized by adding primary amines (S) to diacrylate (B) compounds (1.2:1 molar ratio of diacrylate:amine, 5 g total reaction mass) without solvent, stirring at 1000 rpm at 90 °C for 24 hours. In a second step, the base polymers were dissolved in anhydrous DMSO (Sigma Aldrich) at 167 mg/ml. 480 microliters of base polymer at 167 mg/ml (80 mg) was then mixed with 320 microliters of a 0.5M solution of one end-capping amine (E), and allowed to react, while vortexing at 1000 rpm (VWR shaker) at room temperature for 24 hours. Eight diacrylate bases, 4 amino alcohol side chains, and 10 primary-amine containing end-groups were used to synthesize 320 total polymers.

4.2.3 Gel Permeation Chromatography

Organic phase GPC was performed using 94% THF/5% DMSO/1% piperidine (v/v) as the eluent at a flow rate of 1.0 ml/minute in a Waters GPC system equipped with a Waters 717plus autosampler (Waters Corporation, Milford, MA). Three Waters Styragel columns (HR1, HR3, and HR4) were used in series, and the detector (Waters 2414 refractive index detector) and columns were maintained at 40 °C throughout the runs. The molecular weights of the polymers are reported relative to monodisperse polystyrene standards (Shodex, Japan). 100 µl of each sample prepared at 5 mg/ml was injected, and each sample was given 40 minutes to elute off of the column.

4.2.4 ^{1}H-Nuclear Magnetic Resonance (NMR)

All 32 base polymers and at least one representative end-modified polymer for each of the 10 end-modification reactions were characterized on a Bruker spectrometer by 1H-NMR spectroscopy (400 MHz, d6-DMSO); for the complete spectra of all the polymers, see supplementary information. As an example, for base polymer B3-S5: 1.15-1.25 (2H, quint, $NCH_2CH_2C\boldsymbol{H}_2CH_2CH_2OH$), 1.25-1.35 (2H, quint, $NCH_2C\boldsymbol{H}_2CH_2CH_2CH_2OH$), 1.35-1.45 (2H, quint, $NCH_2CH_2CH_2C\boldsymbol{H}_2CH_2OH$), 1.85-1.95 (2H, quint, $CH_2CH_2NCH_2CH_2(COO)CH_2C\boldsymbol{H}_2CH_2(COO)$), 2.3-2.4 (6H, t, $C\boldsymbol{H}_2CH_2NCH_2C\boldsymbol{H}_2(COO)CH_2CH_2CH_2(COO)$ and t, $NC\boldsymbol{H}_2CH_2CH_2CH_2CH_2OH$), 2.6-2.7 (4H, t, $CH_2C\boldsymbol{H}_2NC\boldsymbol{H}_2CH_2(COO)CH_2CH_2CH_2(COO)$), 3.3-3.4 (2H, obsc, $NCH_2CH_2CH_2CH_2C\boldsymbol{H}_2OH$), 4.0-4.1 (4H, t, $CH_2CH_2NCH_2CH_2(COO)C\boldsymbol{H}_2CH_2C\boldsymbol{H}_2(COO)$), 4.1-4.2 (t, $C\boldsymbol{H}_2(COO)CH{=}CH_2$),

4.25-4.35 (br, $NCH_2CH_2CH_2CH_2CH_2O\boldsymbol{H}$), 5.9-6 (d, $COOCH{=}C\boldsymbol{H}_2$), 6.1-6.2 (dd, $COOC\boldsymbol{H}{=}CH_2$), 6.3-6.4 (d, $COOCH{=}C\boldsymbol{H}_2$). For the end-modified polymers, end-modification was verified by the disappearance of the peaks at 5.9-6, 6.1–6.2, and 6.3-6.4 ppm which correspond to the acrylate protons. However, the E9 reactions with base polymers left residual acrylate protons after reaction, indicating incomplete reaction and presence of the acrylate-terminated base polymers. All the other end-modifying amines resulted in complete elimination of acrylate peaks, corresponding to a complete reaction.

Amide formation (peaks at 7.9 ppm corresponding to CO-N***H*** and 3.0-3.2 corresponding to $CONHC\boldsymbol{H}_2$) was noted in a subset of the end-modified polymers, but not in any of the base polymers. Amide formation (quantified by the ratio of peaks corresponding to $CONHC\boldsymbol{H}_2$ and $COOC\boldsymbol{H}_2$) was highest with polymers modified with E1, E3, E4 (two primary amines), was moderate with polymers modified with E6 (one primary, one secondary amine), and was minimal in end modified polymers containing E5, E7, E8, E10, and E12 (**Table 4.1**). Increasing amide formation also resulted in decreased molecular weight of the end-modified polymers (**Fig. 4.1**) with the same pattern (**Fig. 4.2**, linear regression $R^2 = 0.5637$, $p < 0.0001$), indicating that amide formation was the direct cause of the decrease in molecular weight seen with the end-capping step. These trends, however, do not appear to have any impact on the transfection efficacy of the resulting end-modified polymer (**Fig. 4.3**, linear regression $R^2 = 0.0605$, $p > 0.05$; not significant), indicating that small extent of amide bond formation and resulting decrease in molecular weight do not significantly impact the transfection efficacy of the end-modified polymers.

4.2.5 Polymer Solubility

Solubility was measured for a subset of polymers in the buffer used to dissolve the polymers and form the nanoparticles (25 mM sodium acetate (NaAc) in water) through a plate-reader absorbance assay. Ten microliters of 100 mg/ml polymer solution in DMSO was added to 40 microliters of 25 mM NaAc, forming a milky mixture. Absorbance of each well at 620 nm was measured with a plate reader (BioTek Synergy 2). Sequentially, each well was diluted by addition of another 10 microliters of 25 mM NaAc buffer, was mixed by pipetting up and down 5 times, and the resulting well was re-measured with the plate reader. Complete solubility was determined by comparing the absorbance at 620 nm for each well with a reference well containing the same amount of DMSO and 25 mM NaAc, and the result was also confirmed by eye.

4.2.6 Luciferase Transfection and Viability Screening

COS-7 cells were seeded at 15,000 cells/well (50,000 cells/cm^2) into 96-well plates in complete DMEM and allowed to adhere overnight. Polymers were then aliquoted into 96-well U-bottom plates and dissolved in 25 mM sodium acetate buffer (pH 5.2). Separately, CMV-Luc DNA (Elim Biopharm) was diluted and aliquoted out. Diluted polymer was added to CMV-Luc DNA using a multichannel pipette and mixed vigourously by pipetting up and down. Nanoparticles were given 10 minutes to complex, and then were added to cells (20 microliters of nanoparticles added to 100 microliters of fresh complete DMEM). Final particle composition for all polymers was 600 nanograms of CMV-Luc DNA and 36 micrograms of polymer (60 wt/wt polymer:DNA ratio). As positive controls, Lipofectamine™ 2000 (Invitrogen) and FuGENE® HD were prepared

in Optimem I (Invitrogen) according to manufacturer's instructions and added to cells in the concentrations described in the text. After four hours of incubation, the media (and remaining particles) were removed by pipetting, and the media was replaced with fresh warmed DMEM. Twenty four hours after transfection, metabolic activity was assessed by the CellTiter 96® AQ_{ueous} One MTS assay (Promega) and was normalized to untreated control wells. Briefly, 20 microliters of assay reagent was added to cells. Cells were placed back in the incubator for 1 hour, and then absorbance of each well at 590 nm was measured with a plate reader (BioTek Synergy 2). Plates were washed with 1x PBS and fresh media was added to each plate. 48 hours after transfection, luminescence was measured on a plate reader using the BrightGlo™ luciferase assay system. Briefly, 100 microliters of room-temperature assay reagent was added to 100 microliters of media on cells. The plate was swirled for precisely 2 minutes, and then the luminescence was measured.

4.2.7 GFP Transfection and Flow Cytometry

Cell plating, particle formulation, and transfection protocol for the GFP transfection was the same as above, except using EGFP-N1 DNA (Clontech) and particles were formulated at 30, 60, and 90 polymer:DNA wt:wt ratios instead of only 60 wt. 48 hours post transfection, the cells were washed and trypsinized with 30 microliters of 0.25% trypsin-EDTA. 170 microliters of FACS buffer (1x PBS, 2% FBS, 0.5% propidium iodide) was added to cells and the 200 microliters was transferred to Starstedt 96-well round-bottom plates. The plates were centrifuged for 5 minute at 1000 rpm, removed from the centrifuge, and 170 microliters was removed from on top of the cell

pellet. The cell pellet was resuspended in the residual 30 microliters and placed on an Intellicyt high-throughput loader and reader attached to an Accuri C6 flow cytometer. Each well was run dry, and in between each well we included a 1-second PBS wash to minimize well to well contamination. The Hypercyt software was used to discriminate between wells and FlowJo was used for FACS analysis.

4.3 Results and Discussion

4.3.1 Characterization of the Polymer Library

The library of PBAEs was synthesized by adding primary amines to diacrylate compounds (1.2:1 molar ratio of diacrylate:amine) at 90 °C for 24h (**Scheme 4.1a**). These specific monomers were chosen so that single carbon changes to the backbone monomers and to the side chain monomers could be evaluated in the synthetic polymers. In a second step, the base polymers were end-capped by end-capping amines (at 10-fold molar excess of amine to diacrylate termini) at room temperature for 24 hours (**Scheme 4.1b**). These end groups were chosen so that the presence of small molecule functional groups could be evaluated and compared across base polymers with differential structure. Eight diacrylate bases, 4 amino alcohol side chains, and 10 primary-amine containing end-groups were used to synthesize 320 total polymers (**Scheme 4.1c**). In order to more closely match the underlying structure to the naming convention used, we have chosen a separate naming convention from previous studies. Here, the number after "B" (for "base") corresponds to the number of carbons between acrylate groups in the diacrylate, so B3 means than there are 3 CH_2 units between acrylate groups in the diacrylate base. The number after "S" (for "side chain") corresponds to the number of carbons between

the amine group and the hydroxyl group in the side-chain. Previous top-performing base polymers termed “C32”, “C28” [24] correspond to B4-S5 and B4-S4 respectively. The “E” (for “end group”) refers to which end-modifying amine was chosen; they are organized into structurally similar groups but the numbers are simply sequential. The modifier “m” refers to an added methyl group (so B3m has an added methyl group compared to B3) and the modifier “o” to an added hydroxyl group (so S3o has an added hydroxyl group compared to S3). Every base polymer was characterized with respect to its base polymer molecular weight. Weight-averaged molecular weights of the polymers in the library ranged from 2,000 to 48,000, and number-averaged molecular weights ranged from 1,500 to 12,000 (**Fig. 4.4**, **Table 4.2**). While many of the base polymers (8/32) had a weight-averaged molecular weight (Mw) of approximately 10,000 Da (+/- 2,000 Da), some polymers had an especially high Mw (40-50,000 Da, such as B4-S4, B6-S4, and BL2-S3o), and others had an especially low MW (under 3,000, such as BL1-S3 and BH1-S4). The viscosity of the starting monomers appears to have a significant effect on the molecular weight obtained using this synthesis protocol. S3o is relatively more viscous than S3, S4 or S5; polymers synthesized with S3o all had Mw of less than 9,000 Da, except for BL2-S3o. S4 containing polymers with simple hydrocarbon backbones (B3, B3m, B4, B5, B6) all had Mw of greater than 10,000. BL1, BL2, and BH1 all needed to be solvated in order to be effectively mixed with the amino alcohol side chains, and the resulting polymers in general were all smaller than the Mw obtained from the neat synthesis protocol.

4.3.2 Effect of Polymer:DNA ratio

To form nanoparticles, PBAEs were dissolved in 25mM NaAc (pH 5.2) to generate positive charge on the amines and complexed with CMV-Luc DNA at varying polymer:DNA weight ratio (wt/wt). Before screening the entire library at a particular polymer:DNA ratio, we looked at the effect of formulation ratio on polymer transfection efficacy. To do this, we tested a subset of 21 representative polymers for gene delivery at a wide range of wt/wts: 30, 60, 80, 100, 125, and 150 (**Fig. 4.5**, **Table 4.3**). Maximal luminescence was achieved at 60 wt/wt for most polymers tested. However, interestingly for B3-S5 end-modified polymers, maximal luminescence intensity was not achieved until a high 125-150 wt/wt ratio. Since maximal luminescence in general was achieved at 60 wt/wt ratio, we used this wt/wt ratio when subsequently screening the entire library of 320 structures. By testing all polymers at the same weight ratio, the influence of structure can directly be evaluated without the formulation ratio producing possible confounding effects.

4.3.3 Effect of Base Polymer Composition

To evaluate the effect of base-composition of the polymers on transfection efficacy, polymers were allowed to spontaneously form nanoparticles at a fixed weight ratio (60 wt/wt) and then added to COS-7 cells as and examined for transfection efficacy by total well luminescence from BrightGlo (**Fig. 4.6**, **Table 4.4**). To quantify cytotoxicity/cell viability, separate experiments were also conducted in parallel with the same nanoparticles and following the same transfection procedure. Twenty-four hours

after incubation, metabolic activity was assessed by the CellTiter 96® AQ_{ueous} One MTS assay and was normalized to untreated control wells (**Fig. 4.7**, **Table 4.5**).

Previous studies have shown that polymer molecular weight may play a role in transfection efficacy, with increasing molecular weight corresponding to increasing transfection efficacy.[23] At least within this library of polymers, this effect appears to be muted (**Fig. 4.8**), as there was no correlation between increasing molecular weight of the base polymer and increasing average transfection efficacy for all end-modified polymers from the same base polymer (linear regression, $R^2 = 0.003$, $p = 0.7833$),.

Polymers containing simple hydrocarbon backbones were more effective than polymers containing bulkier hydrophobic or hydrophilic backbones. In particular, polymers containing the bulkier hydrophobic backbones (BL1 and BL2) were toxic to the cells at the tested wt/wt and DNA dose, while polymers containing the hydrophilic backbone (BH1) were relatively non-toxic but did not promote transfection.

Single carbon changes to the base polymers in the polymer library produced dramatic results for transfection efficacy. Interplay was found between the relative hydrophobicity and hydrophilicity of the diacrylate and amino alcohols used to synthesize the base polymers. To evaluate the differences seen by this library approach statistically, we converted the luciferase luminescence data for the end-modified polymers containing B3, B3m, B4, B5, and B6 diacrylates and S3o, S3, S4, and S5 side chains to log-scale and performed analysis of variance (GraphPad Prism).

Other studies have looked at modifying cationic polymers with hydrophobic moieties to increase transfection efficacy. Hydrophobic modification of polycations has been shown to be beneficial for gene delivery for a variety of reasons. Increased

hydrophobicity may enhance polymer-DNA binding by providing for physical encapsulation, in addition to charge-charge interactions [25]. Additionally, a general mechanism for uptake of non-viral gene delivery particles results from adsorptive endocytosis; enhancing the hydrophobicity of the polymer could result in increased interaction with the cell membrane and promote this process [25]. Hydrophobic modifications have been also used to improve gene dissociation from the polycation, by decreasing the electrostatic interactions between the cationic polymer and DNA [26, 27], and have been shown to improve the performance of the gene-carrier in the presence of serum [28].

A few excellent recent examples of studies looking at hydrophobic modification of a polycation base polymer show that with hydrophobic modifications, usually some modification improves the product, but too much hydrophobicity can decrease efficacy. N-alkylation of linear polyethyleneimine (PEI) with varying alkyl chain lengths (1, 2, 3, 4, and 8-carbon chains) at 11% of the backbone amines produced dramatic results. Gene delivery to the lung in a mouse model increased 8-, 26-, and 7-fold when modified by 1, 2, or 3 carbons, decreased moderately when modified by 4 carbons, and decreased substantially (200-fold) when modified by 8-carbon chains, as compared to 22 kDa linear PEI [25]. In addition, 11% alkylation produced the most transfection boost with N-ethyl-PEI, as compared to derivatization of 5%, 14%, or 20% of the backbone amines [25]. In other work, poly(amidoamine) (PAMAM) dendrimers were functionalized with 4-8 alkyl chains (12-16 carbons in length) [29]. Cellular uptake was improved by both increasing the amount of functionalization and increasing length of alkyl-chain modification (as

these chains act as a lipid coating for the PAMAM dendrimer), whereas transfection efficacy was optimal with the shortest chain length (12-carbons) [29].

Modification of chitosan, a naturally occurring polycation commonly used as a non-viral gene delivery reagent, with hydrophilic and hydrophobic chains resulted in dramatic effects on the gene delivery properties of this modified polymer. Both modifications enhanced plasmid release and reduced non-specific adsorption, but only modification with the hydrophobic PMLA enhanced cell adsorption and cellular uptake [30].

In comparison to these studies, our study examines how directly modulating the hydrophilic / hydrophobic character of an end-modified cationic polymer (rather than adding hydrophobic moieties to an existing cationic polymer) might modulate transfection efficacy. Presumably, some of the advantages that would be granted to cationic polymers by modifying them with hydrophobic moieties might be conferred to a polymer which at its core was modified to increase its hydrophobicity. In particular, increasing hydrophobic character of the core polymer might increase the ability of that polymer to physically encapsulate the DNA cargo and may also promote adsorptive endocytosis, as in many of the hydrophobic-modified polymer cases [31].

To determine how changing the hydrophobicity of the diacrylate base and the amino alcohol side chain affects the performances of all polymers in the library, we first averaged the log-scale luminescence data for all end-modified polymers with the same base polymer together so that they represent one composite value for each particular base polymer (**Fig. 4.9**). Interestingly, increasing hydrophobicity of either the diacrylate base or the amino alcohol side chain resulted, in general, in increased transfection efficacy.

This trend is shown in the cases of end-capped polymers with B3, B3m, B5, and B6 as backbones and S3o and S3 as side-chains. In the special case of B4-based polymers, only polymer B4-S4 is less effective than otherwise would be predicted. In the case of S4-based polymers, there is biphasic dependence on hydrophobicity with B4-S4 having minimal activity and B3-S4 and B6-S4 having comparable effectiveness. In the case of S5-based polymers, efficacy is high and equivalent across all backbone types.

Closer inspection reveals that there may be some interplay between backbone and side-chain hydrophobicity. Examining the results with respect to increasing amino alcohol side chain hydrophobicity (**Fig. 4.9**), it is clear that the only polymers which included the most hydrophilic side chain (S3o) to achieve significant transfection used the most hydrophobic B6-S3o backbone. For polymers with the S3 side chains, the most effective base polymers incorporated the two most hydrophobic diacrylates (B5, B6). Among the polymers with the most hydrophobic side chain (S5), the most effective end-modified polymers were largely equivalent, although B4-S5 and B5-S5, with intermediate hydrophobicity, were slightly more effective with particular end-groups. S4 has intermediate hydrophobicity and S4-based polymers were shown to have biphasic dependence on backbone hydrophobicity, with the most hydrophilic (B3) or hydrophobic (B6) backbones being optimal compared to the intermediate hydrophobicity backbones (B3m, B4, B5). Overall, there was excellent transfection achieved with all five of these base diacrylates tested. These findings suggest that with increasing side chain hydrophobicity, the requirement for a hydrophobic base diacrylate decreases and also suggests that if we were to test even more hydrophobic side chains that we might notice that incorporating diacrylates with reduced hydrophobicity might be optimal.

For all base diacrylates, the optimal side chain in general was the S5 side chain. However, with increasing base diacrylate hydrophobicity, there is decreasing preference for the most hydrophobic side chain (**Fig. 4.9**). For the least hydrophobic (B3) backbone, there is nearly an order of magnitude increase in transfection efficacy between each increasingly hydrophobic side chain (from 2.94 for B3-S3o to 3.64 for B3-S3 to 4.72 for B3-S4 to 5.55 for B3-S5 in logscale units). For the most hydrophobic (B6) backbone, there is less than an order of magnitude difference in transfection efficacy between the extremes (from 4.49 for B3-S3o to 4.91 for B6-S3 to 4.80 for B6-S4 to 5.40 for B6-S5). This suggests that if we were to test even more hydrophobic base diacrylates, that it is likely that increasing the hydrophobicity of the side chain (by increasing carbon length) may not enhance the gene delivery properties of the resulting end-modified polymer.

To evaluate the relative importance of the base diacrylate and the side chain amino alcohol on the transfection efficacy displayed by the polymer library statistically, we calculated a 2-way ANOVA with our data. In the 2-way ANOVA, the side chains accounted for the largest share of the variance seen (45%, $p < 0.0001$), and the diacrylate used accounted for a smaller, but still highly statistically significant portion of the variance (8.5%, $p < 0.0001$). The interaction between the two groups accounted for an additional 9% of the variance ($p < 0.0001$). This demonstrates that side chain hydrophobicity produced even more dramatic results than increasing base diacrylate hydrophobicity (although both effects are significant). A potential explanation for this discrepancy is that increasing "B" (base diacrylate) hydrophobicity increases spacing between charged nitrogens in the backbone but increasing "S" (side chain) hydrophobicity does not. Thus, increasing the hydrophobicity of the side chains may

yield the advantages associated with increased hydrophobicity without interfering with charge spacing, but increasing the hydrophobicity of the base diacrylate both increases the hydrophobicity and increases the spacing between nitrogens. Also of note, increasing the hydrophobicity of either the backbone or the side chain while holding the same DNA to polymer wt/wt ratio constant effectively decreases the nitrogen to phosphate ratio at the same time, which may affect particle formation and DNA release.

Another way to examine bulk hydrophilicity / hydrophobicity of the polymers is to examine the solubility trends of polymers in the library. We took a subset of polymers which were end-modified with E7 and determined the solubility of the end-modified polymers in the buffer used to dissolve the polymers and form the nanoparticles (25 mM sodium acetate (NaAc) in water). The most hydrophilic polymers (B3-S3-E7 and B3m-S3-E7) were soluble at concentrations exceeding 10 mg/ml, and all polymers tested except for B3m-S4-E7 were completely soluble at 5 mg/ml in 25 mM NaAc (**Table 4.6**).

4.3.4 Effect of End-Modification

End-modification of each polymer backbone significantly modulated its transfection efficacy and toxicity. Polymers formulated with the E9 end group exhibited significant toxicity, almost regardless of the base polymer they were reacted with. Polymers containing E10 and E12 tended to show low transfection efficiencies with a few notable exceptions (B5-S5 and B6-S5 base polymers end modified with E10 and E12 showed transfection efficacies comparable to commercially available transfection reagents Lipofectamine™ 2000 and FuGENE® HD).

To look at how changing side chains affected the performances of all polymers containing a particular end group, we collapsed log-scale luminescence data for all polymers containing the same backbone monomer together into one composite value (**Fig. 4.10**). Among the side chains tested, polymers containing the most hydrophobic amino alcohol (S5) were in general the most effective for transfection of COS-7 cells ($p < 0.01$ vs S4, $p < 0.001$ vs S3, S3o, 1-way ANOVA with Tukey's multiple comparison test) and polymers containing the S4 and S3 side chains were significantly more effective than those containing the S3o side chain ($p < 0.01$ vs S4, $p < 0.05$ vs S3o).

To look at structure-function relationships within the polymer library, using a non-parametric correlation (Spearman), we calculated correlation coefficients and two-tailed p-value comparing each end-modifying amine (**Table 4.7**). The most structurally similar end-modifying amines were also the most highly correlated in this analysis. Performance of polymers containing E1 and E3 end groups (both diamines separated by 3 carbons) was highly correlated ($R = 0.951$, $p = 1.4 \times 10^{-10}$); performance of polymers containing E6, E7 and E8 (one primary amine, one or two secondary/tertiary amines) were also highly correlated (E6 to E8: $R = 0.950$, $p = 6.3 \times 10^{-10}$; E6 to E7: $R = 0.921$, $p = 8.4 \times 10^{-9}$; E7 to E8: $R = 0.918$, $p = 1.23 \times 10^{-8}$). Interestingly, the performance of polymers containing E3 was also highly correlated with the performance of polymers containing E6 and E8 (E3 to E6: $R = 0.930$, $p = 2.8 \times 10^{-9}$; E3 to E8: $R = 0.928$, $p = 3.6 \times 10^{-9}$).

With same base polymers such as B6-S3, it was interesting to find that end-group could significantly modify the overall efficacy from nearly no expression when end-modified with E12, to increased expression that was over 3 log orders higher with B6-S5-E5 and E6, even though neither end-modified polymer was very toxic (**Figs. 4.6 and 4.7**).

This effect is also seen across the whole library. If we average the log-scale luminescence seen with all polymers with the same end-modifying amine (**Fig. 4.11**), we find that all polymers modified with E9 were worse than all other end modified polymers ($p < 0.001$, 1-way ANOVA with Tukey's multiple comparison test), and that E5-end modified polymers were better than E12 end-modified polymers ($p < 0.05$, 1-way ANOVA with Tukey's multiple comparison test). On average, E5 polymers were over 1-log order of magnitude more effective than E12-modified polymers.

To investigate the effects of end-modification further, we synthesized leading end-modified polymers containing all of the diacrylates, the amino alcohol S5, and the end groups E1, E3, E4, E5, E6, E7, and E8, and evaluated their transfection efficacy by flow cytometry at three separate wt/wt ratios (**Fig. 4.12**, **Table 4.8**). For some polymers such as B3m-S5-E5, B3m-S5-E7, B4-S5-E1, B4-S5-E6, B4-S5-E7, B4-S5-E8, etc., optimal transfection occurred at 30 wt/wt, but in almost all of those cases the transfection efficacy did not fall off that significantly from 30 to 60 wt/wt; for some of these, transfection efficacy was relatively consistent in all three formulation conditions, but for others it decreased with increasing wt/wt, often decreasing most dramatically from 60 to 90 wt/wt (3m57, 457, 557). There were also polymers that showed optimal transfection at 60 wt/wt (better than at 30, 90 wt/wt) such as 355 and 454. From a base polymer perspective, B4-S5 was the most efficient (best at 30 wt/wt) and transfection did not drop off with increasing wt/wt ratio. On the other hand, B3-S5 polymers tended to get better at transfection with increasing wt/wt ratio; B5-S5 was optimal at 30 wt/wt and decreased from there; and B6-S5 didn't transfect well at 30 wt/wt but tended to be optimal at 60 wt/wt (and worse again at 90wt/wt). A comparison of the results obtained via the

luciferase assay with the results from flow cytometry indicates the same overall pattern, although there are some differences. Similar findings have been shown in the literature, both with similar polymeric systems and liposomal systems [24, 32]. Differences between in vitro gene delivery assay systems may be due to the fact that they report different things. Luminescence measures a total protein yield per well, whereas flow cytometry highlights a binary separation of the individual cells within a cell population. In cases where a small percentage of cells express a high level of the exogenous gene or where a high percentage of cells express a low level of the exogenous gene, the assay results will diverge. Leading polymers were thoroughly evaluated by using both of these complementary assay methods.

Generally, polymers were optimal or not significantly suboptimal at 60 wt/wt ratio. The top six polymers overall were B3-S5-E1, B3-S5-E5, B3m-S5-E7, B4-S5-E3, B4-S5-E4, and B4-S5-E7; they transfected COS-7s at the following levels when formulated at 60 wt/wt (RLU, %GFP+): 351 ($1.64x10^6$, 64.5%), 355 ($2.02x10^6$, 69.4%), 3m57 ($2.24x10^6$, 67.2%), 453 ($1.97x10^6$, 67.63%), 454 ($1.89x10^6$, 76.6%) and 457 ($5.63x10^5$, 72.5%). These polymers yielded superior efficacy ($p < 0.001$ for both luminescence and fluorescence via 1-way ANOVA of all polymers and using Dunnet's post test) when compared to the positive controls, FuGENE® HD ($7.21x10^5$, 29.9%) and Lipofectamine™ 2000 ($8.07x10^5$, 42.9%).

As compared to other non-viral approaches found in literature, optimized PBAE formulations are superior to most alternatives. PEI complexes were reported to yield 29% transfection and optimized solid lipid nanoparticles were reported to result in 15%

transfection with reduced cytotoxicity as compared to PEI [33]. Electroporation has been reported to yield 71% transfection [34] .

In comparing luminescence to GFP assays as measures of gene delivery efficacy, luminescence based assays offer rapid screening options when flow cytometry is either unavailable or cannot be done in a high-throughput fashion, and can quickly give information regarding the overall transfection level. However, it cannot discriminate between a few very bright cells and many moderately transfected cells.

4.4 Conclusions

In the study presented here, three hundred and twenty end-modified poly(beta-amino)esters (PBAE) were synthesized and tested for gene delivery efficacy in COS-7 cells. This library approach enabled us to not only synthesize and test a large variety of structures rapidly, but provided us with a reasonably robust dataset to analyze for the effect of small structural permutations to the polymer chain. Most PBAE formulations were optimal at 60 wt/wt (polymer:DNA ratio). Optimal PBAE formulations were superior ($p<0.001$) to commercially available non-viral alternatives FuGENE® HD and Lipofectamine™ 2000, as they enabled ~3-fold increased luminescence ($2.2x10^6$ RLU/well vs $8.1x10^5$ RLU/well) and 2-fold increased transfection (76.7% vs 42.9%) as measured by flow cytometry with comparable or reduced toxicity. Increasing hydrophobicity of backbone and side chain tended to increase transfection efficacy, and polymers containing the most hydrophobic side chain (S5) and backbone (B6) tended to perform the best. However, increased hydrophobicity of the backbone reduced the requirement for a hydrophobic side chain, and increased hydrophobicity of the side chain

reduced the requirement for a hydrophobic backbone, suggesting that there might be some optimal total hydrophobicity for cationic polymer-based gene delivery. End-modification of these polymers produced dramatic results, as differences of greater than 3-log orders of transfection efficacy by luminescence was seen with the same base polymer but with different end-groups. These results taken together suggest that balancing hydrophobicity plays a crucial role in transfection efficacy of these polymers, and that optimized end-modified PBAEs are potentially useful non-viral gene delivery reagents.

4.5 Figures

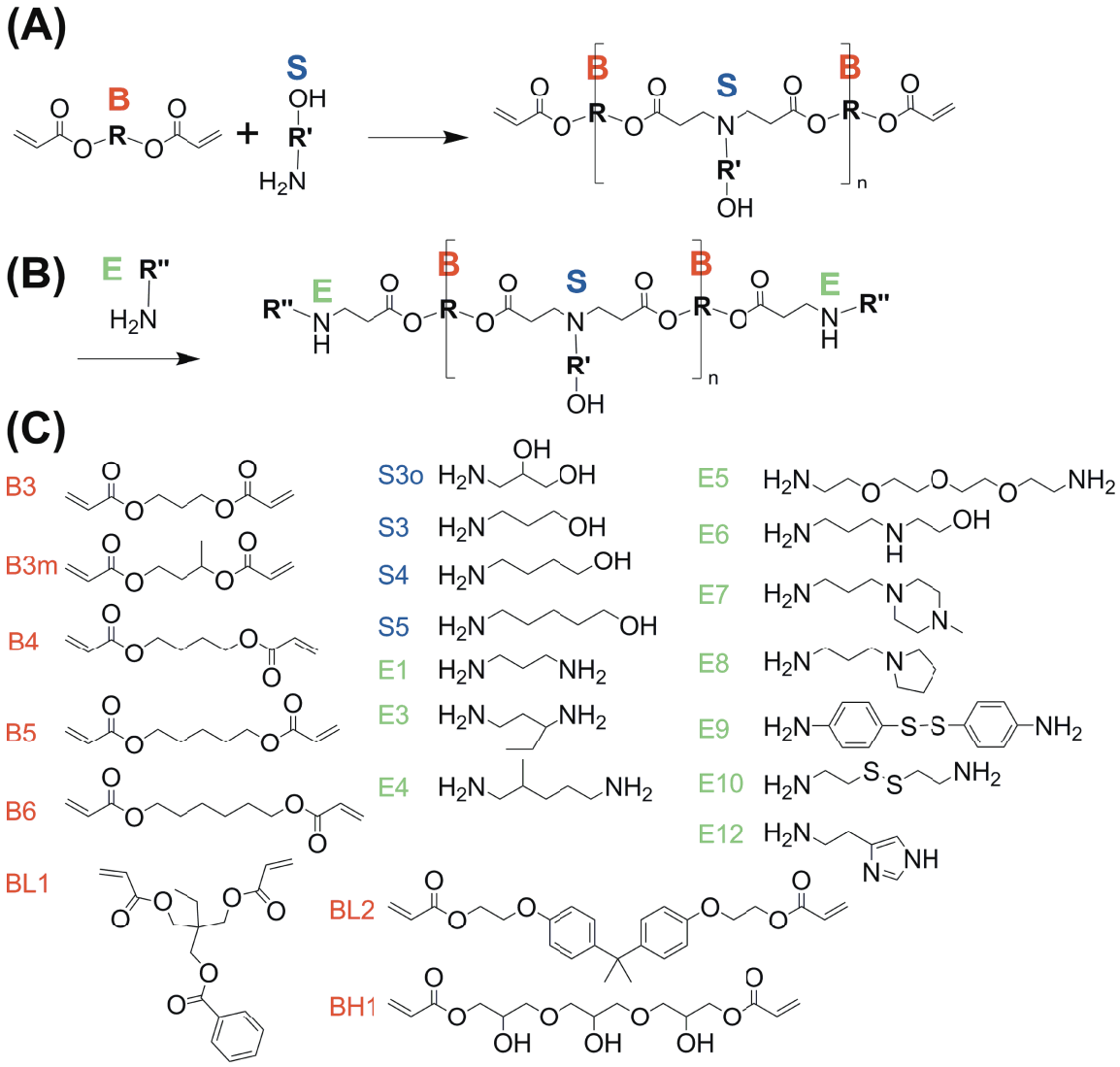

Scheme 4.1. Synthesis of the PBAE library: (a) Diacrylates are reacted with primary amino alcohols by Michael addition with excess diacrylate to form diacrylate-terminated base polymers. (b) Primary amines are added in a second step to form end-modified PBAEs. (c) Library of diacrylates, amino alcohol s, and end-capping amines used in this study are shown.

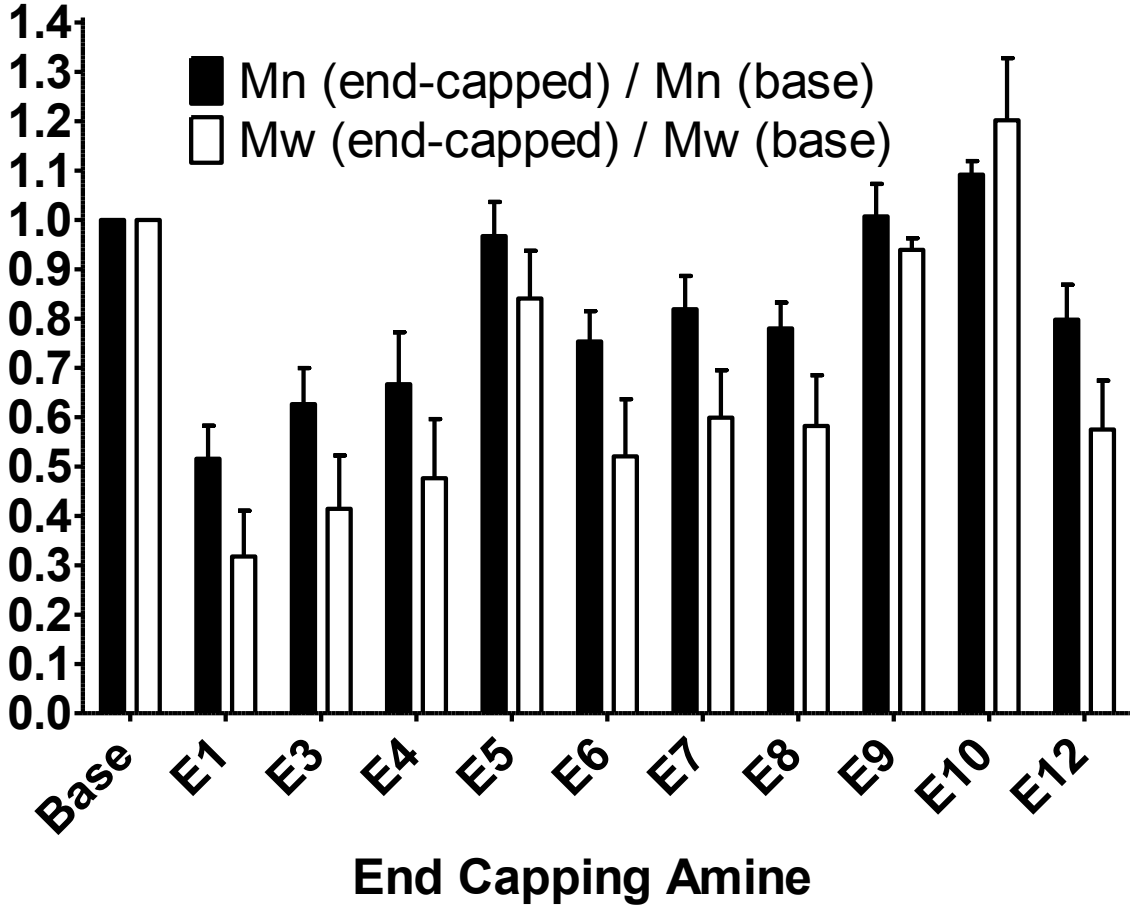

Figure 4.1. **Effect of end-capping on number-averaged and weight-averaged molecular weight.** Relative ratio of number-averaged and weight-averaged molecular weight resulting from end-capping 4 base polymers (B3m-S4, B4-S4, B5-S4, and B4-S5) with the end-capping amines shown at the bottom.

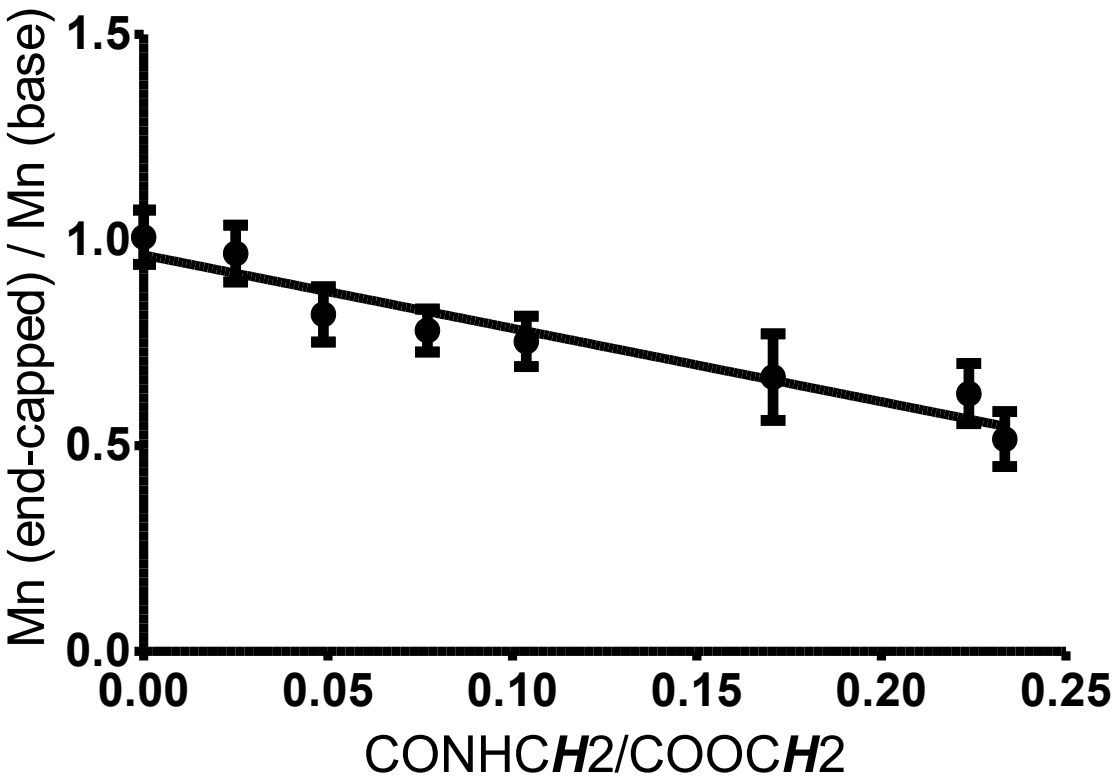

Figure 4.2. **Correlation between amide formation and polymer molecular weight.** There is a negative correlation (linear regression, $R^2 = 0.5637$; $p < 0.0001$) between amide formation, as measured by the ratio ($CONHCH_2$/ $COOCH_2$) and the molecular weight of the resulting polymer; thus, increasing amide formation results in decreased molecular weight.

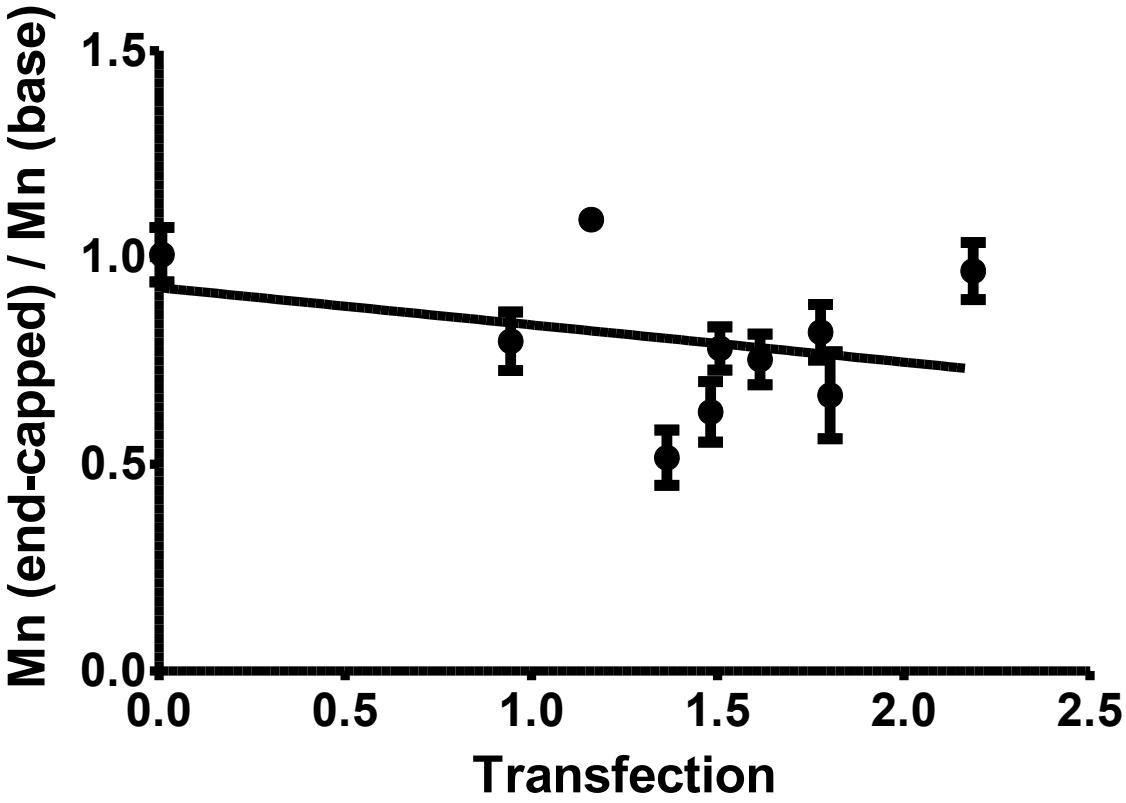

Figure 4.3. Correlation between the decrease in molecular weight of the resulting polymer and the transfection efficacy of the set of polymers with that end-capping amine. For the linear regression, $R^2 = 0.06054$; the correlation is not significant.

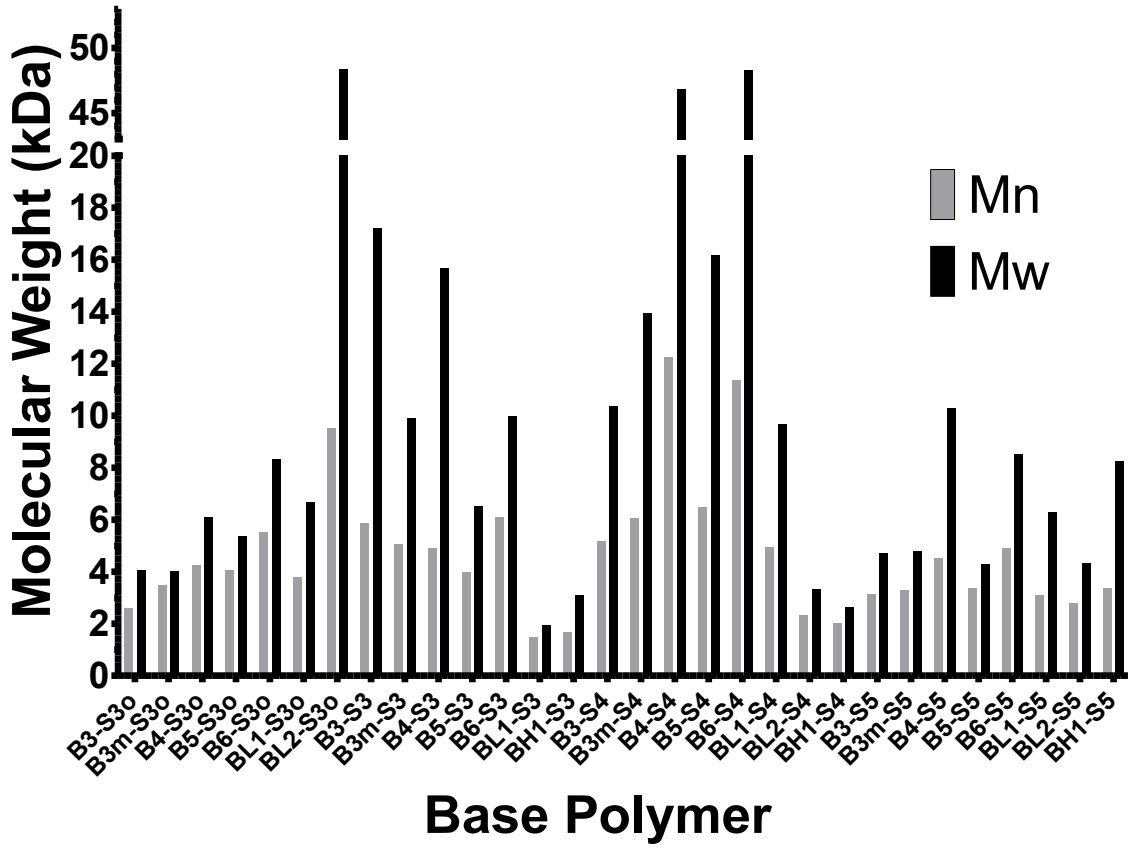

Figure 4.4. Base polymer molecular weight by gel permeation chromatography

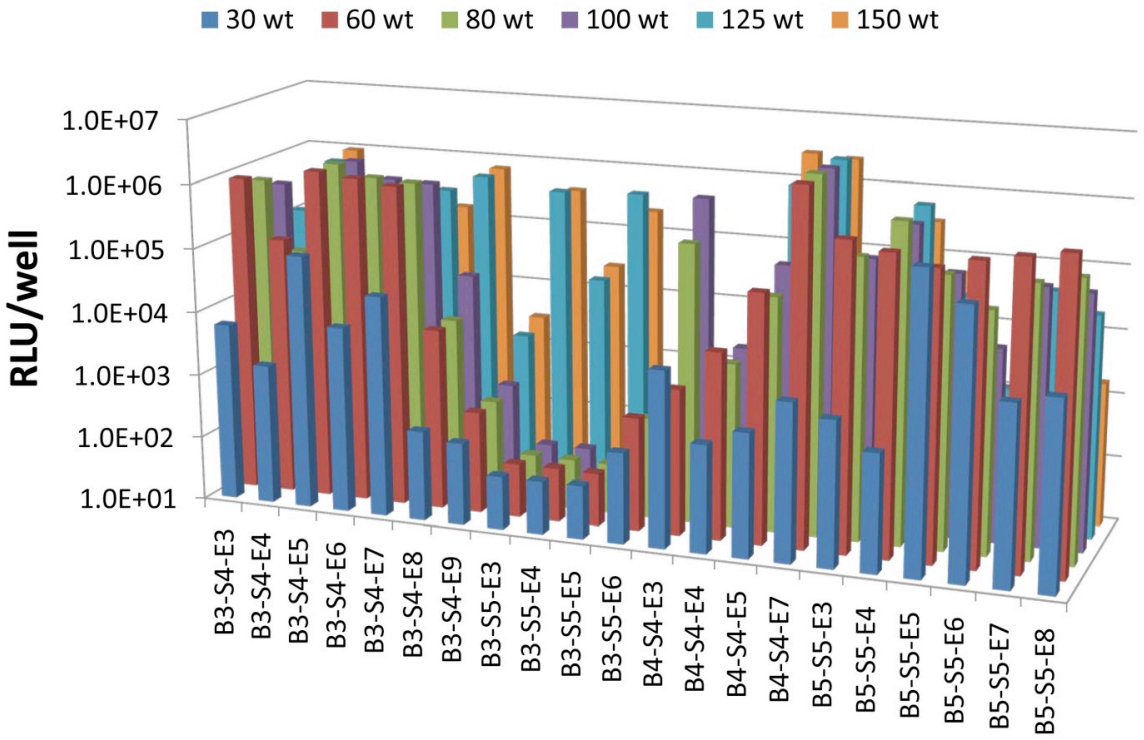

Figure 4.5. Transfection efficacy (average RLU/well, n=4) of representative polymers, formulated at a range of polymer:DNA wt/wt ratios. For most polymers, 60 wt/wt was found to be the optimal polymer:DNA ratio.

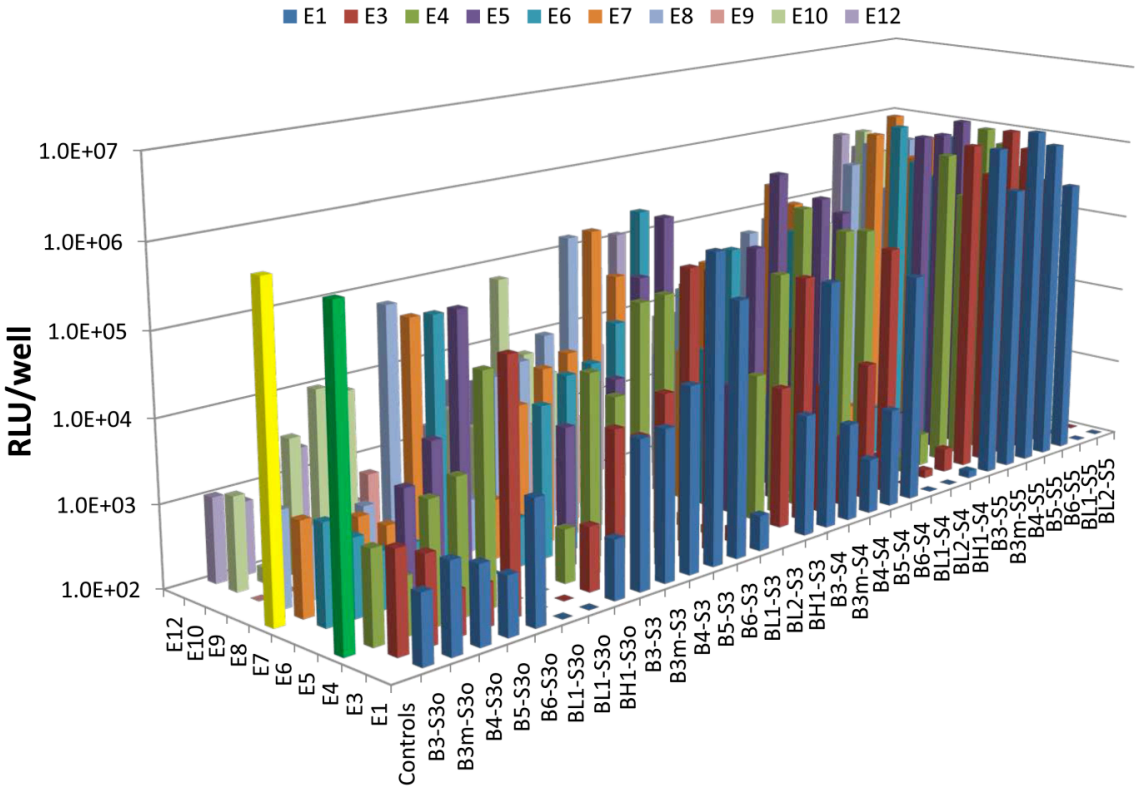

Figure 4.6. Transfection efficacy of polymer library by luminescence. Average luminescence per well, 48 hours post transfection (n=4) with CMV-Luc DNA and polymer library at 60 wt/wt (polymer:DNA). In the control column, the green bar corresponds to FuGENE® HD, and the yellow bar corresponds to Lipofectamine™ 2000.

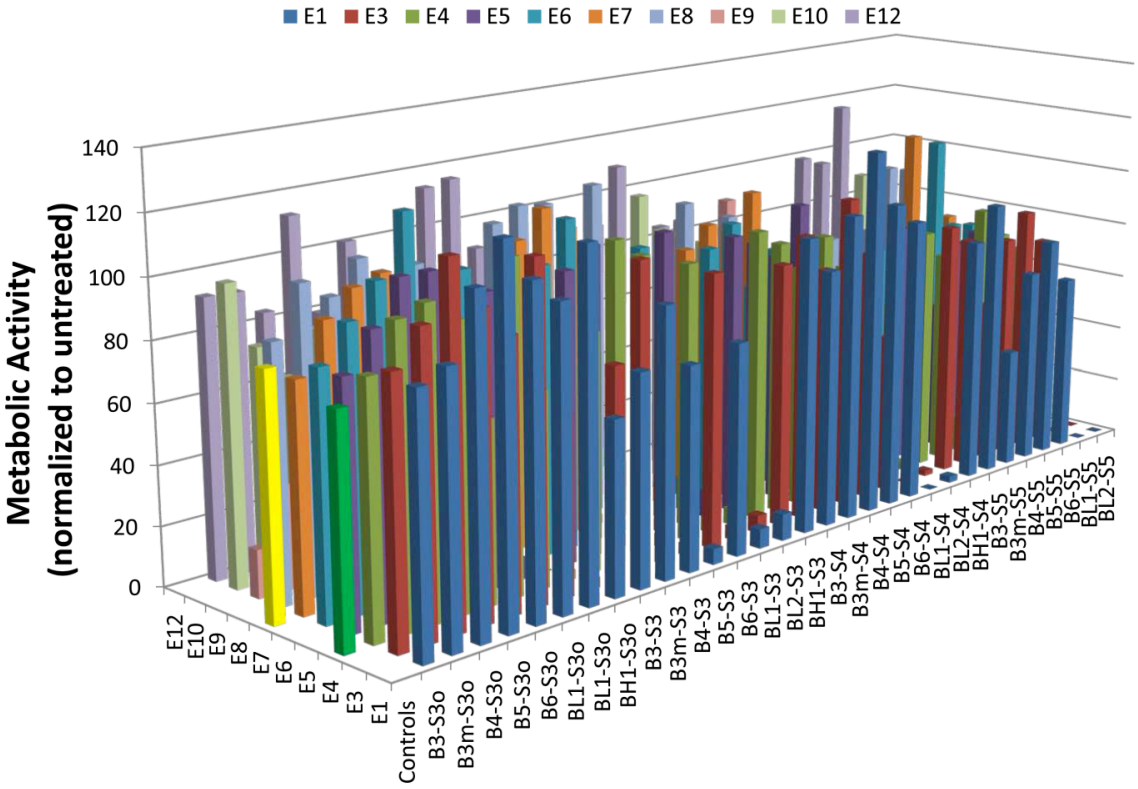

Figure 4.7. Cellular metabolic activity post transfection with the polymer library. Metabolic activity of COS-7 cells 24 hours post-transfection (n=4) with CMV-Luc DNA and polymer library at 60 wt/wt (polymer:DNA)assessed by the CellTiter 96® AQ_{ueous} One MTS assay (n=4) and normalized to untreated control wells. In the control column, the green bar corresponds to FuGENE® HD, and the yellow bar corresponds to Lipofectamine™ 2000.

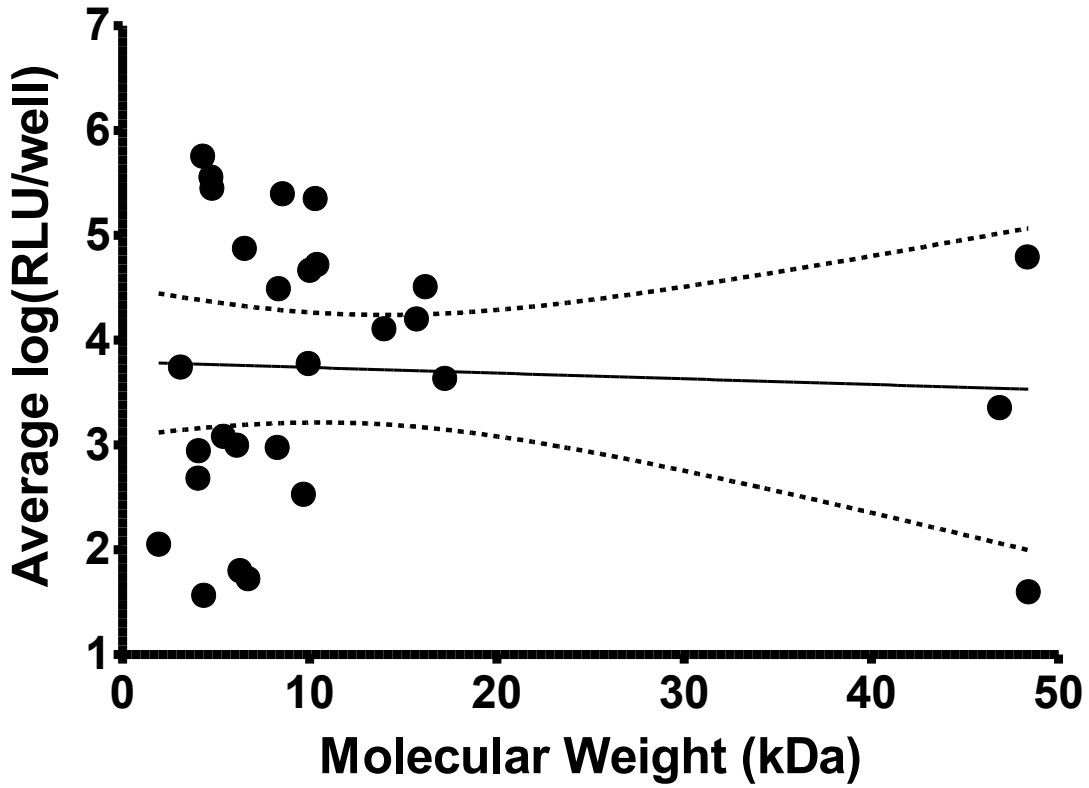

Figure 4.8. Molecular weight vs. transfection efficacy. Base polymer molecular weight vs. average log-scale transfection efficacy for all end-modified polymers from the same base polymer. The solid line is the linear regression line ($R^2 = 0.003$, $p = 0.7833$), and the dashed line is the 95% confidence interval of the regression.

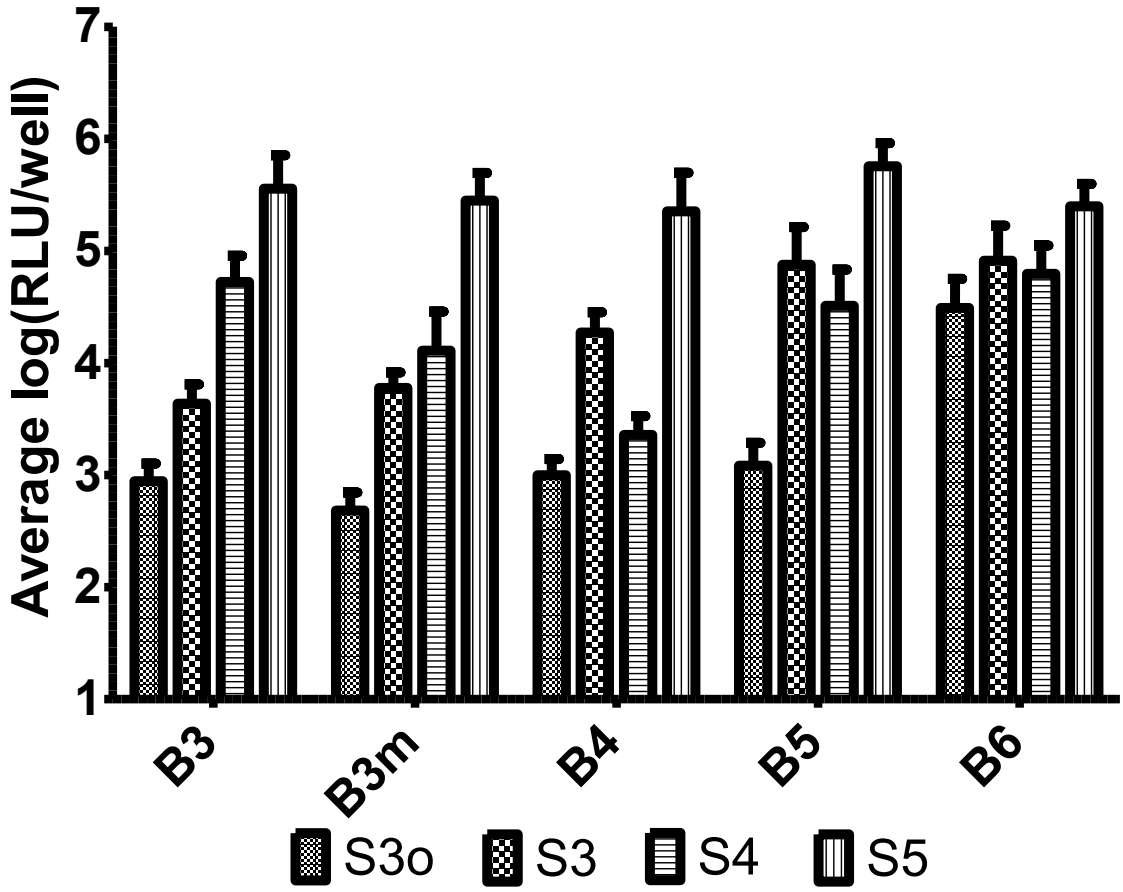

Figure 4.9. Average log-scale luminescence post transfection (mean +/- SE) of end-modified polymers with the same base polymer, plotted with increasing base diacrylate hydrophobicity. As an example, the far left bar represents the average log-scale luminescence post transfection of all polymers containing the base polymer B3-S3o.

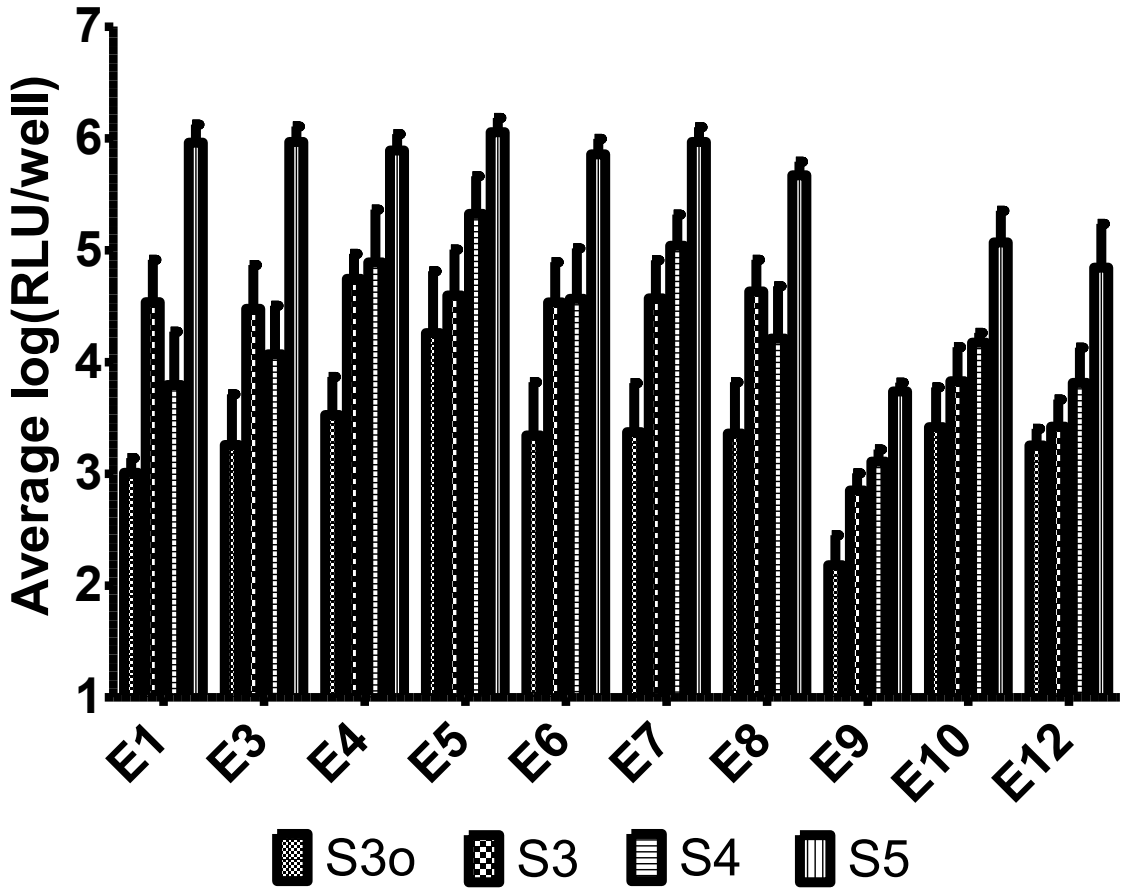

Figure 4.10. Average log-scale luminescence post transfection (mean +/- standard error) of polymers containing the side chain and end group listed. For example, the far left bar represents the average log-scale luminescence post transfection of all polymers containing S3o and E1 (B3S3oE1, B3mS3oE1, B4S3oE1, B5S3oE1, and B6S3oE1).

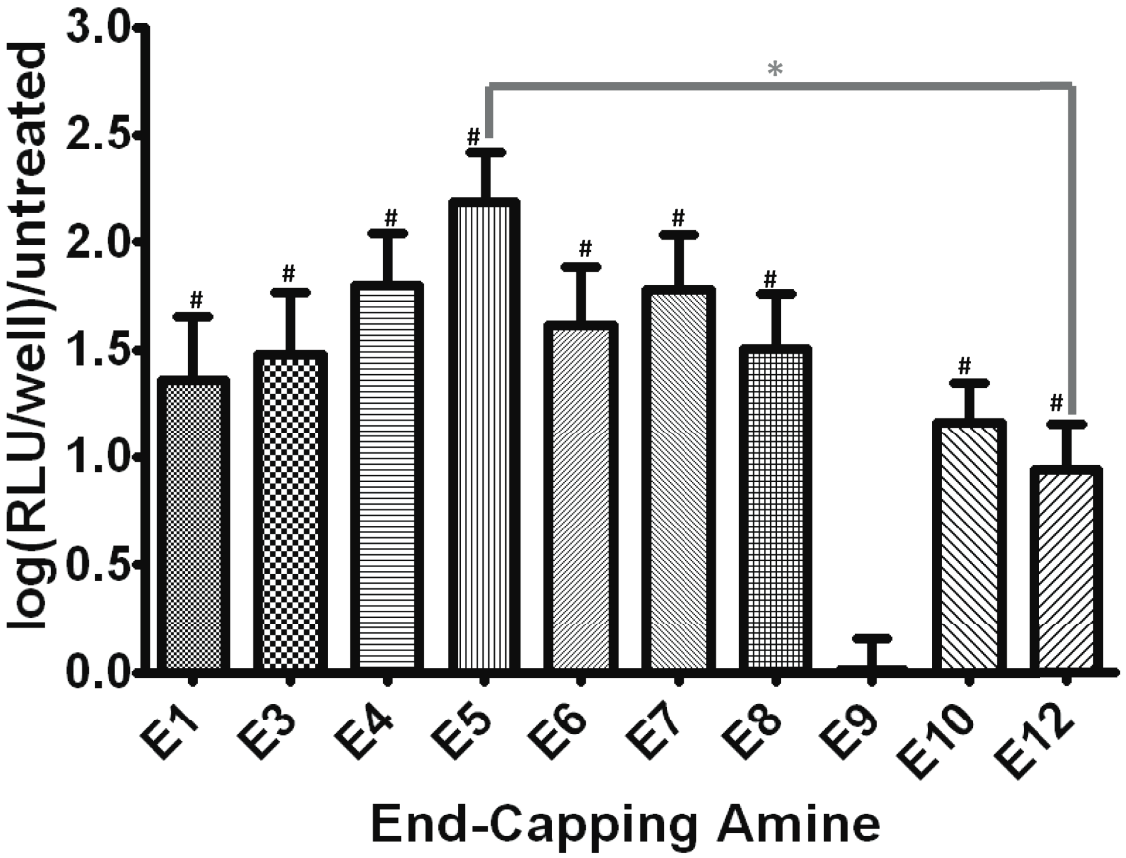

Figure 4.11. Average log-scale luminescence post transfection (mean +/- SE) normalized to the untreated control group of polymers containing the end group listed. For example, the far left bar represents the average log-scale luminescence post transfection of all polymers containing E1. Significant effects (1-way ANOVA, Tukey's multiple comparison test) * $p<0.05$ between E5 and E12, # $p<0.001$ between all E and E9.

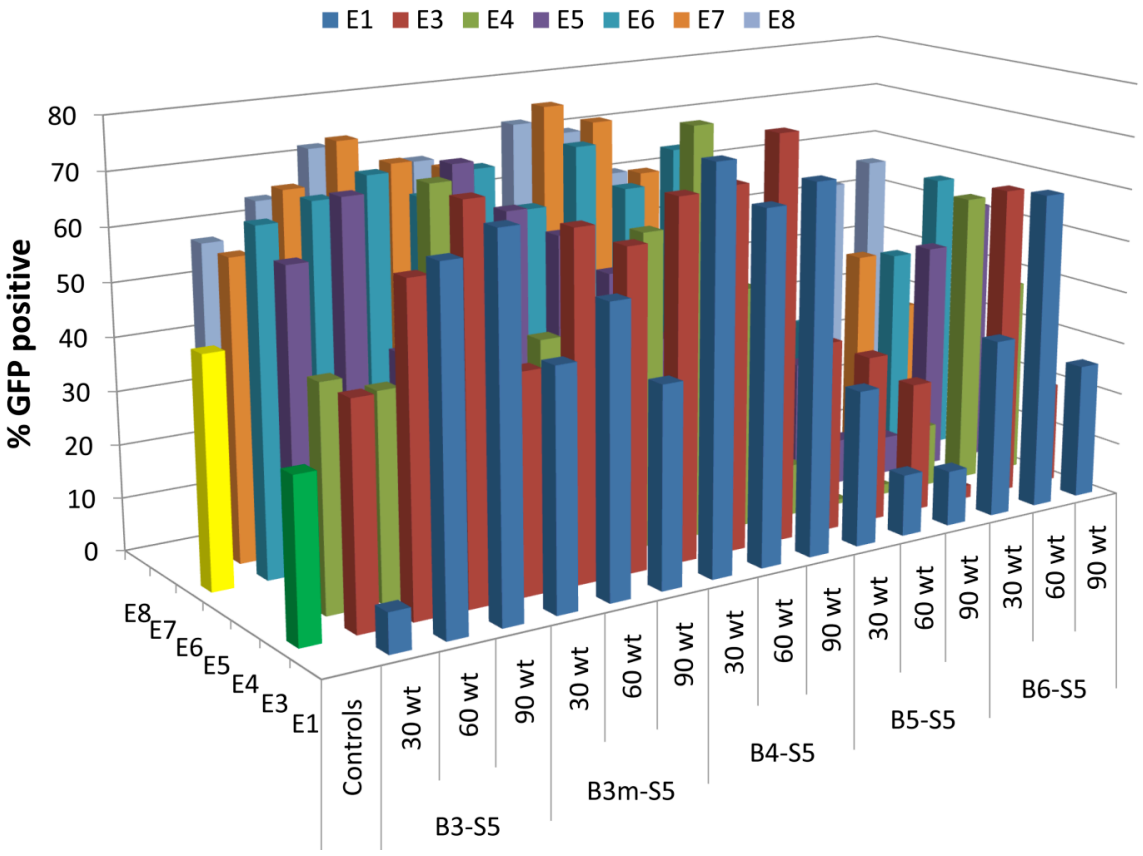

Figure 4.12. Average transfection efficacy by flow cytometry (n=4) of end-modified polymers containing S5. In the control column, the green bar corresponds to FuGENE® HD, and the yellow bar corresponds to Lipofectamine™ 2000.

Table 4.1. Amount of amide formation resulting from end-capping B3-S5 with the end-capping amines on the left. This is quantified as the ratio of the integrals of the peaks corresponding to the CONHC$\boldsymbol{H}_2$ protons which are around 3.0-3.3 ppm, and the COOC$\boldsymbol{H}_2$ protons which are around 4.0 ppm.

	4.0 ppm (COOC$\boldsymbol{H}_2$)	3.0-3.3 ppm (CONHC$\boldsymbol{H}_2$)	Ratio (CONHC$\boldsymbol{H}_2$/COOC$\boldsymbol{H}_2$)
E1	2.27	0.53	0.23348
E3	1.52	0.34	0.223684
E4	2.11	0.36	0.170616
E5	2	0.1	0.05
E6	2.41	0.25	0.103734
E7	2.46	0.12	0.04878
E8	2.47	0.19	0.076923
E9	1.87	0	0
E12	2.35	0	0

Table 4.2. Base polymer molecular weight by gel permeation chromatography

Polymer	Mn	Mw	PDI
B3-S3o	2582	4050	1.568552
B3m-S3o	3494	4023	1.151402
B4-S3o	4265	6101	1.430481
B5-S3o	4069	5383	1.322929
B6-S3o	5537	8320	1.502619
BL1-S3o	3802	6692	1.760126
BL2-S3o	9527	48372	5.077359
B3-S3	5883	17202	2.924018
B3m-S3	5053	9921	1.963388
B4-S3	4921	15695	3.189392
B5-S3	3992	6505	1.629509
B6-S3	6107	9991	1.635991
BL1-S3	1480	1931	1.304732
BH1-S3	1671	3088	1.847995
B3-S4	5189	10383	2.000964
B3m-S4	6075	13967	2.299095
B4-S4	12239	46844	3.827437
B5-S4	6494	16172	2.490299
B6-S4	11351	48325	4.257334
BL1-S4	4959	9656	1.947167
BL2-S4	2334	3318	1.421594
BH1-S4	2018	2648	1.312190
B3-S5	3144	4724	1.502545
B3m-S5	3296	4776	1.449029
B4-S5	4514	10289	2.279353
B5-S5	3352	4277	1.275955

B6-S5	4925	8539	1.733807
BL1-S5	3093	6275	2.028775
BL2-S5	2797	4339	1.551305
BH1-S5	3370	8265	2.452522

Table 4.3. Transfection efficacy (average RLU/well, n=4) of representative polymer formulations, formulated at a range of polymer:DNA wt/wt ratios. Increased blue intensity corresponds to increased luminescence. For most polymers, 60 wt/wt was found to be the optimal polymer:DNA ratio.

	30 wt	60 wt	80 wt	100 wt	125 wt	150 wt
B3-S4-E3	6.05E+03	9.04E+05	6.46E+05	4.25E+05	1.19E+05	2.55E+04
B3-S4-E4	1.53E+03	1.10E+05	5.27E+04	4.07E+05	8.18E+05	9.59E+05
B3-S4-E5	9.46E+04	1.43E+06	1.41E+06	1.19E+06	8.65E+04	1.11E+05
B3-S4-E6	8.15E+03	1.23E+06	9.55E+05	6.81E+05	3.55E+05	7.89E+04
B3-S4-E7	2.84E+04	1.04E+06	8.83E+05	6.44E+05	3.85E+05	1.55E+05
B3-S4-E8	2.54E+02	6.75E+03	6.73E+03	2.44E+04	6.90E+05	7.06E+05
B3-S4-E9	1.92E+02	3.84E+02	3.83E+02	4.72E+02	2.08E+03	2.95E+03
B3-S5-E3	6.73E+01	6.81E+01	6.12E+01	5.87E+01	4.98E+05	3.92E+05
B3-S5-E4	6.70E+01	6.82E+01	6.00E+01	5.93E+01	2.15E+04	2.58E+04
B3-S5-E5	6.73E+01	6.67E+01	5.97E+01	5.87E+01	5.61E+05	2.22E+05
B3-S5-E6	2.57E+02	5.79E+02	3.72E+02	3.25E+02	1.32E+02	3.12E+04
B4-S4-E3	5.47E+03	1.87E+03	2.22E+05	7.98E+05	1.20E+03	7.69E+02
B4-S4-E4	4.75E+02	8.09E+03	3.61E+03	4.29E+03	2.07E+02	1.89E+02
B4-S4-E5	8.43E+02	7.26E+04	4.40E+04	9.46E+04	1.16E+06	2.75E+06
B4-S4-E7	2.83E+03	3.16E+06	3.37E+06	3.08E+06	3.16E+06	2.44E+06
B5-S5-E3	1.79E+03	5.57E+05	2.28E+05	1.52E+05	1.53E+04	1.54E+03
B5-S5-E4	6.73E+02	4.09E+05	8.59E+05	5.62E+05	7.93E+05	3.33E+05
B5-S5-E5	3.92E+05	2.73E+05	1.57E+05	1.16E+05	3.66E+04	5.92E+04
B5-S5-E6	1.31E+05	3.94E+05	5.32E+04	9.79E+03	1.61E+03	2.98E+02
B5-S5-E7	5.86E+03	5.06E+05	1.52E+05	9.44E+04	5.71E+04	2.52E+04
B5-S5-E8	8.00E+03	6.40E+05	2.03E+05	8.57E+04	2.82E+04	1.73E+03

Table 4.4. Average luminescence per well, 48 hrs. post transfection (n=4) with CMV-Luc DNA and polymer library at 60 wt/wt (polymer:DNA). At the left the base polymer is listed; at the top, the end-modifying amine is listed. For example, the cell which is the intersection of B6-S3 and E5 corresponds to B6-S3-E5 formulated at 60 wt/wt. In the control row, the control under E4 corresponds to FuGENE® HD, and the control listed under E7 corresponds to Lipofectamine™ 2000. Increased blue intensity corresponds to increased luminescence.

	E1	E3	E4	E5	E6	E7	E8	E9	E10	E12
Controls			7.21E+05			8.07E+05				
B3-S3o	6.78E+02	1.62E+03	1.29E+03		1.60E+03	1.35E+03	1.41E+03	5.25E+01	1.34E+03	1.05E+03
B3m-S3o	1.20E+03	1.13E+03	4.90E+02		8.69E+02	7.28E+02	7.42E+02	3.95E+01	1.53E+02	7.48E+02
B4-S3o	8.74E+02	3.44E+02	2.91E+03	3.13E+03	4.91E+02	9.59E+02	4.79E+02	1.91E+02	4.26E+03	1.94E+03
B5-S3o	5.14E+02	3.23E+02	4.23E+03	8.76E+03	4.74E+02	6.11E+02	8.30E+02	1.58E+02	1.34E+04	2.20E+03
B6-S3o	3.02E+03	9.65E+04	5.43E+04	2.18E+05	1.62E+05	1.28E+05	1.51E+05	1.30E+03	1.06E+04	5.49E+03
BL1-S3o	4.58E+01	4.45E+01	5.38E+01		7.05E+01	3.25E+01	3.28E+01	3.23E+01	3.93E+01	3.23E+02
BL1-S3o	3.48E+01	3.63E+01	3.88E+01		4.10E+01	4.88E+01	6.88E+01	3.20E+01	3.23E+01	3.53E+01
BH1-S3o	5.30E+02	5.93E+02	4.41E+02		3.84E+02	5.12E+02	4.24E+02	3.73E+01	5.38E+02	3.12E+02
B3-S3	6.22E+03	6.61E+03	2.49E+04	4.69E+03	7.02E+03	5.90E+03	1.09E+04	2.36E+02	2.99E+03	1.51E+03
B3m-S3	6.68E+03	4.42E+03	1.08E+04	1.33E+04	1.36E+04	1.36E+04	1.41E+04	7.77E+02	1.47E+03	4.63E+03
B4-S3	1.76E+04	1.18E+04	1.17E+05	1.21E+04	1.58E+04	1.78E+04	2.46E+04	1.59E+03	8.77E+04	3.81E+03
B5-S3	5.30E+05	2.97E+05	1.23E+05	1.67E+05	4.07E+04	4.49E+05	3.26E+05	4.57E+02	8.67E+03	3.09E+02
B6-S3	1.24E+05	2.33E+05	1.36E+05	7.48E+05	7.66E+05	1.10E+05	1.17E+05	1.36E+03	4.18E+03	2.85E+02
BL1-S3	2.66E+02	1.52E+02	1.25E+02	1.44E+02	1.01E+02	9.90E+01	6.15E+01	7.93E+01	8.28E+01	1.22E+02
BL2-S3										
BH1-S3	3.02E+03	5.42E+03	6.55E+03	4.13E+03	9.71E+03	7.85E+03	5.81E+03	3.93E+03	7.73E+03	4.71E+03
B3-S4	1.07E+05	1.05E+05	1.00E+05	1.82E+05	1.52E+05	8.96E+04	3.48E+04	5.56E+02	2.65E+04	1.17E+05
B3m-S4	1.60E+03	4.06E+03	5.59E+05	1.29E+06	6.68E+03	8.15E+04	1.98E+03	9.25E+02	9.56E+03	2.81E+03
B4-S4	4.75E+02	7.47E+02	1.17E+03	1.25E+04	1.45E+03	1.32E+04	8.22E+02	1.69E+03	9.18E+03	2.94E+03
B5-S4	1.66E+03	5.32E+03	2.24E+05	4.95E+05	1.70E+05	5.73E+05	1.23E+05	1.89E+03	1.75E+04	3.24E+03
B6-S4	6.87E+04	1.32E+05	1.97E+05	2.87E+05	2.66E+05	2.89E+05	1.61E+05	2.10E+03	1.80E+04	3.75E+03
BL1-S4	1.23E+02	1.97E+02	2.55E+02	3.99E+02	4.02E+02	3.54E+02	3.62E+02	3.46E+02	4.26E+02	1.05E+03
BL2-S4	1.83E+01	4.33E+01	3.63E+01	3.58E+01	3.78E+01	6.53E+01	1.42E+02	2.55E+02	6.18E+02	2.35E+03
BH1-S4	7.58E+01	1.26E+02	1.55E+02	1.28E+02	1.79E+02	3.88E+02	6.70E+02	2.44E+02	7.00E+02	1.87E+03
B3-S5	1.64E+06	1.61E+06	1.08E+06	1.67E+06	2.02E+06	1.43E+06	5.05E+05	6.67E+03	3.88E+04	2.00E+04
B3m-S5	4.23E+05	6.14E+05	2.85E+05	1.60E+06	6.17E+05	2.24E+06	8.60E+05	6.63E+03	5.44E+04	6.22E+04
B4-S5	2.15E+06	1.97E+06	1.89E+06	2.13E+06	3.48E+05	5.63E+05	1.87E+05	3.12E+03	3.34E+04	5.19E+03
B5-S5	1.29E+06	1.03E+06	1.07E+06	7.51E+05	1.04E+06	9.00E+05	7.92E+05	8.50E+03	8.19E+05	6.55E+05
B6-S5	3.34E+05	3.47E+05	4.59E+05	4.51E+05	4.35E+05	4.29E+05	3.48E+05	4.10E+03	3.86E+05	3.93E+05
BL1-S5	3.63E+01	6.10E+01	4.90E+01	2.43E+01	2.80E+01	2.70E+01	4.08E+01	8.60E+01	1.91E+02	7.68E+02
BL2-S5	3.63E+01	3.80E+01	3.30E+01	2.25E+01	2.78E+01	1.55E+01	2.20E+01	3.93E+01	6.13E+01	1.93E+02
BH1-S5	5.03E+02	4.32E+02	7.95E+02	1.63E+03	7.99E+02	1.27E+03	5.20E+02	4.76E+02	1.70E+03	4.90E+03

Table 4.5. Metabolic activity of COS-7 cells 24 hr post-transfection (n=4) with CMV-Luc DNA and polymer library at 60 wt/wt (polymer:DNA) assessed by the CellTiter 96® AQ_{ueous} One MTS assay (n=4) and normalized to untreated control wells. At the left the base polymer is listed; at the top, the end-modifying amine is listed. For example, the cell which is the intersection of B6-S3 and E5 corresponds to B6-S3-E5 formulated at 60 wt/wt. In the control row, the control under E4 corresponds to FuGENE® HD, and the control listed under E7 corresponds to Lipofectamine™ 2000. Increased orange intensity corresponds to increased toxicity of the nanoparticle formulations.

	E1	E3	E4	E5	E6	E7	E8	E9	E10	E12
Controls			75.1			80.4				
B3-S3o	83.7	86.0	82.5	80.3	80.8	75.0	84.3	16.1	98.6	92.3
B3m-S3o	87.5	97.3	97.1	92.3	92.4	91.1	100.6	34.5	76.5	91.9
B4-S3o	108.4	115.9	100.3	106.1	103.1	99.1	94.2	5.7	64.5	83.5
B5-S3o	121.2	98.6	92.9	105.9	122.5	101.8	104.5	11.6	78.2	112.9
B6-S3o	107.1	88.4	60.1	70.0	85.8	79.3	68.4	12.7	42.3	79.4
BL1-S3o	98.8	110.5	108.6	95.9	101.0	95.5	99.0	1.6	74.9	101.2
BL1-S3o	114.7	59.2	64.6	7.3	29.5	8.2	7.8	0.5	3.3	14.7
BH1-S3o	58.1	3.5	3.1	0.2	0.7	-0.1	0.1	3.8	0.2	0.0
B3-S3	70.8	70.6	79.0	96.9	96.8	103.1	106.9	6.5	86.6	114.0
B3m-S3	89.8	102.4	106.8	103.1	110.1	112.0	111.3	2.1	79.5	115.5
B4-S3	68.5	78.2	100.0	95.9	99.9	103.8	110.0	20.5	43.2	90.2
B5-S3	5.3	4.0	4.3	4.0	3.8	3.1	3.5	3.1	2.9	2.9
B6-S3	71.5	92.5	93.8	102.4	95.5	91.8	113.4	2.1	4.2	69.0
BL1-S3	6.6	4.6	5.1	5.1	6.1	6.4	6.6	5.4	5.7	6.0
BL2-S3	9.1	6.0	5.7	9.2	11.3	6.3	12.5	8.8	11.7	12.1
BH1-S3	100.3	89.7	99.2	95.7	89.9	87.8	91.0	58.0	83.5	89.4
B3-S4	87.6	97.7	93.4	91.7	96.8	94.7	100.6	19.0	100.1	109.1
B3m-S4	104.4	84.3	83.1	85.3	72.9	93.0	82.7	85.5	86.2	80.7
B4-S4	124.5	106.7	92.3	101.6	84.3	102.9	92.7	60.4	83.6	84.1
B5-S4	104.9	86.3	80.0	87.3	75.5	78.1	79.7	95.4	78.4	84.7
B6-S4	97.3	54.9	69.6	60.7	59.5	48.8	44.7	63.8	32.1	65.5
BL1-S4	-0.9	-1.1	-1.0	-0.9	-1.3	-1.3	-0.9	1.8	-0.9	-0.2
BL2-S4	2.2	1.8	2.3	1.8	1.7	1.4	1.0	1.8	1.7	1.4
BH1-S4	84.9	88.7	84.9	85.2	75.2	80.3	76.1	1.8	65.0	65.9
B3-S5	96.5	82.3	75.1	63.0	57.3	50.7	49.4	-1.1	46.9	64.7
B3m-S5	41.2	56.8	12.4	52.5	10.2	49.3	75.9	1.3	28.9	98.9
B4-S5	68.3	79.0	88.2	74.6	110.6	111.5	98.2	0.0	9.3	95.7
B5-S5	78.3	87.5	77.5	77.1	78.1	71.8	96.1	3.6	91.0	116.0
B6-S5	62.4	75.4	70.7	71.7	76.6	78.1	61.9	-1.5	40.3	60.9
BL1-S5	-1.1	-0.4	0.4	0.4	-0.8	-1.4	-1.3	9.7	1.5	-0.2
BL2-S5	-0.6	-1.2	-1.0	-1.4	-0.9	-1.3	-1.4	-0.3	-0.5	-0.2
BH1-S5	118.8	127.1	114.5	134.0	122.5	122.9	117.8	24.3	104.0	107.0

Table 4.6. Solubility maximum in 25 mM NaAc for E7 end modified polymers and their corresponding transfection efficacy.

	Solubility (mg/ml)	Luminescence (RLU/well)
B3-S3-E7	12.5	5.90E+03
B3m-S3-E7	10	1.36E+04
B4-S3-E7	5	1.78E+04
B5-S3-E7	6.25	4.49E+05
B6-S3-E7	5	1.10E+05
B3-S4-E7	6.25	8.96E+04
B3m-S4-E7	2.5	8.15E+04
B4-S4-E7	5	1.32E+04
B5-S4-E7	7.14	5.73E+05
B6-S4-E7	5	2.89E+05
B3-S5-E7	6.25	1.43E+06
B3m-S5-E7	6.25	2.24E+06
B4-S5-E7	6.25	5.63E+05
B5-S5-E7	7.14	9.00E+05
B6-S5-E7	7.14	4.29E+05

Table 4.7. Calculated non-parametric (Spearman) correlation coefficients and 2-tailed p-values comparing each end-modified amine

	E1	E3	E4	E5	E6	E7	E8	E9	E10	E12
E1		0.968	0.792	0.649	0.859	0.811	0.878	0.663	0.586	0.772
E3	0.968		0.821	0.728	0.922	0.874	0.931	0.749	0.635	0.772
E4	0.792	0.821		0.905	0.814	0.853	0.811	0.797	0.720	0.699
E5	0.649	0.728	0.905		0.783	0.831	0.711	0.759	0.492	0.575
E6	0.859	0.922	0.814	0.783		0.902	0.914	0.838	0.633	0.821
E7	0.811	0.874	0.853	0.831	0.902		0.941	0.850	0.678	0.801
E8	0.878	0.931	0.811	0.711	0.914	0.941		0.795	0.704	0.843
E9	0.663	0.749	0.797	0.759	0.838	0.850	0.795		0.802	0.809
E10	0.586	0.635	0.720	0.492	0.633	0.678	0.704	0.802		0.868
E12	0.772	0.772	0.699	0.575	0.821	0.801	0.843	0.809	0.868	

	E1	E3	E4	E5	E6	E7	E8	E9	E10	E12
E1		2.6E-12	3.1E-05	3.6E-03	1.3E-06	1.5E-05	3.6E-07	1.4E-03	6.6E-03	2.8E-04
E3	2.6E-12		9.1E-06	6.2E-04	7.8E-09	4.9E-07	2.7E-09	1.5E-04	2.7E-03	2.8E-04
E4	3.1E-05	9.1E-06		2.5E-07	1.3E-05	1.8E-06	1.5E-05	2.6E-05	3.4E-04	1.8E-03
E5	3.6E-03	6.2E-04	2.5E-07		1.2E-04	2.0E-05	9.4E-04	2.6E-04	3.8E-02	2.5E-02
E6	1.3E-06	7.8E-09	1.3E-05	1.2E-04		5.4E-08	1.7E-08	4.1E-06	2.7E-03	5.3E-05
E7	1.5E-05	4.9E-07	1.8E-06	2.0E-05	5.4E-08		6.3E-10	2.1E-06	1.0E-03	1.1E-04
E8	3.6E-07	2.7E-09	1.5E-05	9.4E-04	1.7E-08	6.3E-10		2.8E-05	5.3E-04	2.1E-05
E9	1.4E-03	1.5E-04	2.6E-05	2.6E-04	4.1E-06	2.1E-06	2.8E-05		2.2E-05	8.5E-05
E10	6.6E-03	2.7E-03	3.4E-04	3.8E-02	2.7E-03	1.0E-03	5.3E-04	2.2E-05		6.4E-06
E12	2.8E-04	2.8E-04	1.8E-03	2.5E-02	5.3E-05	1.1E-04	2.1E-05	8.5E-05	6.4E-06	

Table 4.8. Transfection efficacy of newly synthesized polymers (n = 4), evaluated by flow cytometry. Increased green intensity corresponds to increased transfection efficacy. In panel (a), polymers were formulated at 30 wt/wt; in panel (b), polymers were formulated at 60 wt/wt; in panel (c), polymers were formulated at 90 wt/wt.

(a)	E1	E3	E4	E5	E6	E7	E8
B3-S5	7.41	40.97	41.21	59.00	63.82	56.21	56.73
B3m-S5	44.01	40.49	41.35	72.66	64.92	69.33	60.80
B4-S5	74.76	66.97	58.60	49.00	70.65	76.50	71.60
B5-S5	29.29	35.85	9.64	37.65	31.65	31.17	34.40
B6-S5	33.82	2.44	11.92	7.16	2.96	2.73	1.80
(b)	E1	E3	E4	E5	E6	E7	E8
B3-S5	64.46	59.59	38.01	69.37	66.82	66.95	63.13
B3m-S5	53.40	64.05	42.11	63.11	68.92	67.24	66.84
B4-S5	65.52	67.63	76.68	35.15	61.64	72.54	68.94
B5-S5	11.63	31.56	0.87	25.34	22.44	36.89	16.29
B6-S5	60.28	59.31	55.84	44.07	40.66	38.29	51.38
(c)	E1	E3	E4	E5	E6	E7	E8
B3-S5	68.60	71.38	72.25	40.46	70.14	74.51	71.46
B3m-S5	37.38	59.45	35.52	57.40	60.31	46.45	56.99
B4-S5	68.92	75.84	45.29	55.39	67.84	61.67	59.86
B5-S5	10.46	24.66	1.87	8.47	29.53	2.60	5.51
B6-S5	25.74	19.08	37.30	51.27	54.81	26.53	55.00

4.6 References

1. Check, E., *Gene therapy put on hold as third child develops cancer.* Nature, 2005. **433**(7026): p. 561.
2. Thomas, C.E., A. Ehrhardt, and M.A. Kay, *Progress and problems with the use of viral vectors for gene therapy.* Nat Rev Genet, 2003. **4**(5): p. 346-58.
3. Check, E., *A tragic setback.* Nature, 2002. **420**(6912): p. 116-118.
4. *Gene Therapy Clinical Trials World Wide*. Journal of Gene Medicine 2011 May 19, 2011; March 2011:[Available from: http://www.wiley.com/legacy/wileychi/genmed/clinical/.
5. Sunshine, J.C., C.J. Bishop, and J.J. Green, *Advances in polymeric and inorganic vectors for nonviral nucleic acid delivery.* Therapeutic Delivery, 2011. **2**(4): p. 493-521.
6. Putnam, D., *Polymers for gene delivery across length scales.* Nat Mater, 2006. **5**(6): p. 439-51.
7. Lynn, D.M. and R. Langer, *Degradable poly(beta-amino esters): Synthesis, characterization, and self-assembly with plasmid DNA.* Journal of the American Chemical Society, 2000. **122**(44): p. 10761-10768.
8. Akinc, A., et al., *Synthesis of poly(beta-amino ester)s optimized for highly effective gene delivery.* Bioconjug Chem, 2003. **14**(5): p. 979-88.
9. Yang, F., et al., *Gene delivery to human adult and embryonic cell-derived stem cells using biodegradable nanoparticulate polymeric vectors.* Gene Ther, 2009. **16**(4): p. 533-46.
10. Green, J.J., et al., *Biodegradable polymeric vectors for gene delivery to human endothelial cells.* Bioconjug Chem, 2006. **17**(5): p. 1162-9.
11. Yang, F., et al., *Genetic engineering of human stem cells for enhanced angiogenesis using biodegradable polymeric nanoparticles.* Proceedings of the National Academy of Sciences of the United States of America, 2010. **107**(8): p. 3317-3322.
12. Green, J.J., et al., *Combinatorial Modification of Degradable Polymers Enables Transfection of Human Cells Comparable to Adenovirus.* Advanced Materials, 2007. **19**(19): p. 2836-2842.
13. Huang, Y.H., et al., *Nanoparticle-delivered suicide gene therapy effectively reduces ovarian tumor burden in mice.* Cancer Res, 2009. **69**(15): p. 6184-91.
14. Sawicki, J.A., D.G. Anderson, and R. Langer, *Nanoparticle delivery of suicide DNA for epithelial ovarian cancer therapy.* Adv Exp Med Biol, 2008. **622**: p. 209-19.
15. Tzeng, S.Y., et al., *Non-viral gene delivery nanoparticles based on Poly(beta-amino esters) for treatment of glioblastoma.* Biomaterials, 2011. **32**(23): p. 5402-5410.
16. Lee, J.S., et al., *Gold, Poly(beta-amino ester) Nanoparticles for Small Interfering RNA Delivery.* Nano Letters, 2009. **9**(6): p. 2402-2406.
17. Hawkins, A.M., et al., *Synthesis and analysis of degradation, mechanical and toxicity properties of poly(beta-amino ester) degradable hydrogels.* Acta Biomaterialia, 2011. **7**(5): p. 1956-1964.

18. Safranski, D.L., et al., *Effect of poly(ethylene glycol) diacrylate concentration on network properties and in vivo response of poly(beta-amino ester) networks.* Journal of Biomedical Materials Research Part A, 2011. **96A**(2): p. 320-329.
19. Min, K.H., et al., *Tumoral acidic pH-responsive MPEG-poly(beta-amino ester) polymeric micelles for cancer targeting therapy.* J Control Release. **144**(2): p. 259-66.
20. Zugates, G.T., et al., *Gene delivery properties of end-modified poly(beta-amino ester)s.* Bioconjug Chem, 2007. **18**(6): p. 1887-96.
21. Sunshine, J., et al., *Small-Molecule End-Groups of Linear Polymer Determine Cell-Type Gene-Delivery Efficacy.* Advanced Materials, 2009. **21**(48): p. 4947-+.
22. Bhise, N.S., et al., *The relationship between terminal functionalization and molecular weight of a gene delivery polymer and transfection efficacy in mammary epithelial 2-D cultures and 3-D organotypic cultures.* Biomaterials, 2010. **31**(31): p. 8088-8096.
23. Anderson, D.G., et al., *Structure/property studies of polymeric gene delivery using a library of poly(beta-amino esters).* Mol Ther, 2005. **11**(3): p. 426-34.
24. Green, J.J., R. Langer, and D.G. Anderson, *A combinatorial polymer library approach yields insight into nonviral gene delivery.* Accounts of Chemical Research, 2008. **41**(6): p. 749-759.
25. Fortune, J.A., T.I. Novobrantseva, and A.M. Klibanov, *Highly effective gene transfection in vivo by alkylated polyethylenimine.* J Drug Deliv, 2011. **2011**: p. 204058.
26. Forrest, M.L., et al., *Partial acetylation of polyethylenimine enhances in vitro gene delivery.* Pharm Res, 2004. **21**(2): p. 365-71.
27. Gabrielson, N.P. and D.W. Pack, *Acetylation of polyethylenimine enhances gene delivery via weakened polymer/DNA interactions.* Biomacromolecules, 2006. **7**(8): p. 2427-35.
28. Eliyahu, H., et al., *Novel dextran-spermine conjugates as transfecting agents: comparing water-soluble and micellar polymers.* Gene Ther, 2005. **12**(6): p. 494-503.
29. Santos, J.L., et al., *Functionalization of poly(amidoamine) dendrimers with hydrophobic chains for improved gene delivery in mesenchymal stem cells.* J Control Release, 2010. **144**(1): p. 55-64.
30. Wang, B., et al., *Effects of hydrophobic and hydrophilic modifications on gene delivery of amphiphilic chitosan based nanocarriers.* Biomaterials, 2011. **32**(20): p. 4630-8.
31. Liu, Z.H., et al., *Hydrophobic modifications of cationic polymers for gene delivery.* Progress in Polymer Science, 2010. **35**(9): p. 1144-1162.
32. Zou, S., et al., *Lipid-mediated delivery of RNA is more efficient than delivery of DNA in non-dividing cells.* International Journal of Pharmaceutics, 2010. **389**(1-2): p. 232-243.
33. Doroud, D., et al., *Cationic Solid Lipid Nanoparticles Loaded by Cysteine Proteinase Genes as a Novel Anti-Leishmaniasis DNA Vaccine Delivery System: Characterization and In Vitro Evaluations.* Journal of Pharmacy and Pharmaceutical Sciences, 2010. **13**(3): p. 320-335.

34. Parham, J.H., et al., *Optimization of transient gene expression in mammalian cells and potential for scale-up using flow electroporation.* Cytotechnology, 1998. **28**(1-3): p. 147-155.

5 Chapter 5: Uptake and transfection with polymeric nanoparticles are dependent on polymer end-group structure, but largely independent of nanoparticle physical and chemical properties

5.1 Introduction

Gene therapy is the treatment of disease through insertion or modification of DNA in cells. This treatment has tremendous implications for improving human health because almost all human diseases have a genetic component, including cancer. The fundamental challenge for successful gene therapy is finding both a safe and effective delivery system [1]. The traditional method for gene therapy has been viral gene delivery. Viruses have evolved to transduce cells with high efficacy but are limited by low cargo capacity, resistance to repeated infection, difficulty in production and quality control, and safety concerns [2].

All of these challenges can be overcome with non-viral methods that utilize biomaterials, which can be designed to deliver genes similar to a synthetic virus. Biodegradable cationic polymers such as poly(ester amines) and poly(amido amines) are promising for non-viral gene delivery due to their ability to condense plasmid DNA into small and stable nanoparticles, their ability to promote cellular uptake, facilitate escape from the endosome, and allow for DNA release in the cytoplasm [3] Studying these

---

This chapter contains excerpts from an article that was published as Sunshine JC, Peng DY, and Green JJ. "Uptake and Transfection with polymeric nanoparticles are dependant on polymer end-group structure, but largely independent of nanoparticle physical and chemical properties." *Molecular Pharmaceutics.* 2012; 9(11), 3375-3383.

properties is integral to understanding how to design biomaterials for optimal transfection efficacy. In order to deliver its plasmid cargo to the nucleus of the target cell, a particle must be able to cross the cell membrane, escape endocytosis, and release the plasmid intracellularly to allow for trafficking to the nucleus. Each of these steps is essential, and the contribution of small changes to the chemical structure of the polymers to these mechanistic steps will be examined in this manuscript.

There are multiple necessary components for effective gene delivery using cationic polymers. First, the polymers must bind strongly to the DNA, encapsulating or condensing it to prevent its degradation. A cationic polymer, through positively charged amine groups, allows for electrostatic interactions with anionic DNA. Cationic polymers such as poly-L-lysine (PLL) have been demonstrated to form stable polymer/DNA complexes [4]. The next step is cellular uptake, where the polymer/DNA nanoparticles must penetrate the lipid bilayer plasma membrane. These polyplexes or nanoparticles are generally taken into cells through endocytosis. Positively charged particles are important for attraction to anionic proteoglycans on the cell surface. Both particle size and surface charge play key roles in this step. Other potential uptake methods include ligand-specific / receptor-specific mediated endocytosis through various particle coatings [5, 6] or covalent attachment [7, 8].

Once in the endosome, the particles are then subjected to the endosomal-lysosomal pathway, where the complexes need to avoid being enzymatically degraded by lysosomes or recycled out of the membrane. Bypassing lysosomal degradation has been a bottleneck in improving intracellular gene delivery. It has been shown that polymer/DNA particles can escape the endosome into the cytoplasm through the “proton sponge

effect"[9]. Inside of the endosome, the pH drops from 7.4 to around 5.1, where a polymers' secondary and tertiary amine groups can buffer the acidification [10]. An influx of ions into the endosome can lead to osmotic swelling and eventual bursting to release the polyplexes into the cytoplasm [11]. The buffer capacity of titratable amine groups can effectively facilitate endosomal rupture, inducing efficient gene expression [10, 12]. An example of the importance of buffer capacity is that polyethylenimine (PEI) has an advantage over PLL in transfection due to its high buffering capacity. Studies have shown that polymers with secondary or tertiary amines are either able to provide more time to escape the endosome or mediate endosomal escape. Other strategies that have been utilized to promote endosomal escape include functionalizing polymers with endosomolytic peptides [13, 14], which utilize pH sensitive conformational changes that promote endosomal escape.

Once inside the cytoplasm, it is beneficial for the polymer to degrade to enhance release of the DNA to prevent polymer-mediated cytotoxicity. For effective plasmid release, polymers can be designed to degrade hydrolytically through ester linkages [15] or reducibly through disulfide linkages [16]. Amine-containing polymers that can degrade hydrolytically have shown to have much higher transfection and lower cytoxicity than polymers such as PEI [17] and degradable versions of PEI have shown improved efficacy and lower cytotoxicity than non-degradable versions [18]. The DNA plasmid must then overcome nuclear import. This is more easily achievable in dividing cells when the nuclear envelope breaks down during mitosis. Another strategy for nuclear import is appending nuclear localization signals (NLS) to DNA which may help carry it into the

nucleus [19, 20]. Measuring gene expression ensures that all of these intracellular barriers have been crossed including transcription and translation of the exogenous DNA.

Biodegradable cationic polymers such as end-modified poly(beta-amino ester)s have been demonstrated as promising biomaterials for non-viral gene delivery among various cell types [21-23]. End-modification with diamine monomers has shown that some of these polymers can rival adenovirus for gene delivery *in vitro* [17]. Additionally, PBAEs have been shown to have promise in the treatment of cancer *in vitro* and *in vivo* [24, 25] However, while previous studies have investigated certain physical and biological parameters [26-28], they have not fully looked at the chemical properties and mechanistic details that may fully explain the advantages that the lead structures possess [29] In particular, differences in polymer buffering capacity, polymer degradation, and the mechanistic differences between the same linear polymers with acrylate end-groups compared to differing amine-containing small molecules as end-groups needed to be more fully evaluated. This study aims to elucidate the polymer properties and biological process most responsible for the high gene delivery efficacy of end-modified PBAEs.

5.2 Materials and Methods

5.2.1 Cell Culture

COS-7 cells were cultured in Dulbecco's Modified Eagle Medium (DMEM) with L-glutamine and sodium pyruvate (DMEM 11995, Invitrogen, Carlsbad, CA) supplemented with 10% fetal bovine serum (FBS) and 1% penicillin/streptomycin. Cells were grown at 37°C in a humid 5% CO_2 atmosphere.

5.2.2 **Materials**

Monomers were purchased from commercial vendors and used as received. 4-amino-1-butanol (S4), 5-amino-1-pentanol (S5), 1,4-butanediol diacrylate (B4), 1,6-hexanediol diacrylate (B6), 1-(3-aminopropyl)-4-methylpiperazine (E7) were purchased from Alfa-Aesar, Ward Hill, MA. 1,3-propanediol diacrylate (B3) and 1,5-pentanediol diacrylate (B5) were purchased from Monomer-Polymer and Dajac Laboratories (Trevose, PA). 2-methyl-1,5-diaminopentane (E4) was purchased from TCI America (Portland, OR). 2-(3-aminopropylamino)ethanol (E6) and branched 25 kDa poly(ethylene imine) (PEI) were purchased from Sigma Aldrich (St. Louis, MO). Enhanced green fluorescent protein plasmid driven by a CMV promoter (eGFP) was obtained from Aldevron (Fargo, ND). CellTiter 96 AQueous One MTS assay was purchased from Promega (Fitchburg, WI) and used according to manufacturer's instructions.

5.2.3 **Polymer Synthesis**

Polymers were synthesized using a two-step procedure (**Figure 5.1**). As an example, acrylate-terminated poly(1,4-butanediol diacrylate-co-4-amino-1-butanol), B4-S4, was first synthesized in a solvent-free fashion at different acrylate: amine monomer molar ratios (1.2:1, 1.1:1, 1.05:1). Reactions took place in glass vials in the dark under magnetic stirring for 24 h at 90°C. As a second step, amine-containing small molecules were individually conjugated to the ends of each polymer. Excess amine is used to fully end-modify the base polymer. 80 mg of polymer in 480 μL of DMSO was mixed with 320 μL of a 0.5M solution of the end capping amine in DMSO in 1.5 mL eppendorf tubes in a multi-tube vortexer with constant agitation for 1 h at room temperature. As an

example, B4-S4 synthesized at a 1.1:1 ratio was end-modified by E7, and formed the B4-S4-E7 1.1:1 end-modified polymer. Polymers were stored at 100 mg/ml in anhydrous DMSO at -4°C with desiccant until use. Polymer nomenclature refers to the number of carbons between functional groups as we have previously described [29, 30]. For example, polymer B4-S4 contains 4 carbons between acrylate groups in the polymer backbone, "B", and 4 carbons between the amine and alcohol groups in the side chain, "S." Polymer structure was characterized on a Bruker spectrometer by ^{1}H NMR spectroscopy (400 MHz, d_6-DMSO) and completion of end-modification was verified by elimination of the peaks corresponding to the acrylate termini of the polymer (at 5.9-6.4 ppm) [30]. Spectra for B3-S5-Ac (acrylate-terminated base polymer) and B3-S5-E7 can be found in **Figure 5.2**.

5.2.4 Particle Size and Charge

Particle size was determined both by dynamic light scattering (DLS) using a Mavern Zetasizer Nano ZS (Malvern Instruments, Malvern, UK, detection angle 173°, 633 nm laser) and by nanoparticle tracking analysis (NTA) using a Nanosight NS500 (Amesbury, UK, 532 nm laser). Particle charge was determined using a Mavern Zetasizer Nano ZS (Malvern Instruments, Malvern, UK). Polymer/DNA nanoparticles were made at a 60 w/w ratio in 25 mM sodium acetate buffer (pH = 5.0) at 30 ng/μL DNA and diluted into 150 mM PBS, pH 7.4. For the measurements on the Zetasizer, particles were diluted 5-fold into PBS, and particle size is reported as the intensity-weighted Z-averaged of the particle diameter in nm. Average electrophoretic mobilities were measured at 25°C and zeta potentials were analyzed using the Smoluchowsky model. For the NTA analysis,

particles were diluted 50 to 100 fold into PBS such that particle number would be between 10^8 and 10^9 particles/mL, and particle size is determined from a 60s movie from which the Brownian motion of the particles was assessed as previously described [28].

5.2.5 **Gel Electrophoresis**

The gel electrophoresis experiments were conducted in 1% agarose gels made with 1 μg/ml ethidium bromide in the gel. Particles were formed at 30 ng/μL DNA and at a 60 w/w ratio (polymer:DNA; 1.8 μg polymer/μL) and allowed to complex for 10 minutes before glycerol was added, with or without bromophenol blue (15 mg/mL), a negatively charged dye used to visualize the extent that the gel runs, and then immediately added to the gel. The gels were run for 40 min with 100 V applied. Gels were visualized with a Visi-Blue™ transilluminator (UVP, Upland, CA).

5.2.6 **Buffering Capacity**

The buffering capacities of the polymers were determined through acid-base titration. Ten micrograms of polymer in DMSO at 100 mg/mL was dissolved in 10 mL of 0.1 M NaCl solution. The pH of polymer solutions was set to pH 3 using 1 M HCl and titrated to pH 11 using 0.1 M NaOH. The pH of solutions was measured after each addition using a Mettler Toledo S20 pH meter. Buffer capacity was calculated in two ways: by taking the ratio of total protons buffered between pH 7.4 and 5.1 to the total amines of the polymer and by taking the ratio of protons buffered between pH 7.4 and 5.1 to total polymer mass. Titration of NaCl without the presence of polymer was used as background control. For end-modified PBAEs, the buffering contribution from excess

free end-capping amine monomer was subtracted out to characterize the buffering of the polymers.

5.2.7 Degradation Studies

Two and a half milliliters of a 100 mg/ml solution of polymer in DMSO was added to 247.5 mL of phosphate buffered saline (PBS) solution at 37°C, and magnetically stirred to mix. At each time point, 25 mL of this solution was removed and frozen, then lyophilized to remove the water. This sample was dissolved in 1 mL of a solution of 94% THF, 5% DMSO and 1% piperidine, and organic phase permeation chromatography (GPC) was performed using the same solvent as an eluent at a flow rate of 1 mL/minute. The detector (Waters 2414 refractive index detector) and columns (three Waters Styragel columns, HR1, HR3, and HR4, in series) were maintained at 40°C throughout the runs. Polymer molecular weights presented are relative to monodisperse polystyrene standards (Shodex, Japan).

5.2.8 GFP transfections, with and without labeled plasmid

Fifteen thousand COS-7 cells were plated in 100 μL per well in clear 96-well tissue culture plates (Starstedt) to allow for overnight adhesion. For transfection experiments, eGFP pDNA was diluted into 25 mM NaAc buffer (pH 5.0) to form a final concentration of 60 ng/μL. Polymers stored at 100 mg/ml in DMSO were aliquoted out into 96-well plates and diluted to 3.6 μg/μL in 25 mM NaAc, and equal volumes of diluted polymers and diluted DNA were mixed by pipetting up and down in another 96-well plate. Ten minutes after mixing DNA and polymer solutions, 20 μL of nanoparticles

were added to 100 μL of media (DMEM containing 10% FBS, 1% penicillin/streptomycin v/v) on the cells for a final pDNA dose of 600 ng/well. PEI/DNA complexes were formed at a 3:1 polymer to DNA weight ratio and formed in 150 mM NaCl as previously described [23], and PEI/DNA complexes were added to the cells for a final pDNA dose of 600 ng/well. Four hours after transfection, the cells were washed with PBS and 100 μL of fresh media was added to the cells. Forty-eight hours after transfection, gene expression was measured using flow cytometry (Accuri C6 with HyperCyt high-throughput adaptor); gating was performed on FlowJo software and GFP+ cells were gated as a subpopulation of cells by two-dimensional gating of FL1 vs FL2 separate increased autofluorescence signal from increased signal (for examples, see **Figure 5.3**).

For DNA uptake studies, eGFP pDNA was labeled with Cy3 using the Label IT® Tracker™ kit (Mirus Biopharma) following manufacturer's instructions, and diluted into unlabeled pDNA resulting in a net ratio of 331 nucleotides / dye. Particles were formulated the same was as with the transfection experiment (but with labeled DNA), except that after washing the cells and changing the media 4 hours post transfection, the cells were washed again 2x, trypsin was added, and the cells were run on flow cytometry as above. Gating was performed on FlowJo 7.6.5 software and uptake was determined by two-dimensional gating (as a subpopulation of cells) of FL1 vs FL2 to separate increased autofluorescence signal from increased signal (for examples, see **Figure 5.3**).

5.2.9 Cell viability testing

For cell viability testing, transfection was performed as normal, but twenty-four hours after transfection, cell viability was measured by the AQueousOne CellTiter MTS assay; after addition of the CellTiter reagent (20 μL/well), cells were incubated at 37°C for 1 hour and then absorbance at 490 nm was measured on a plate reader (Synergy 2). Background absorbance from media and reagent were subtracted off, and the absorbance was normalized to untreated cells.

5.2.10 Statistical Analysis

Assays were performed in quadruplicate, and presented data are mean ± SD. All statistics were performed using the GraphPad Prism 5 software package. To examine multiple comparisons, such as differences between nanoparticle size with Acrylate (Ac) and Amine (Am) terminated polymers, we performed 1-way ANOVA with Bonferroni post tests.

5.3 Results and Discussion

5.3.1 Synthesis and Characterization of Polymer Array

PBAEs have been extensively investigated in a high-throughput fashion for their ability to mediate non-viral gene delivery *in vitro*, but significant characterization of the polymer properties that lead to overcoming the barriers to intracellular gene delivery have not been fully explored [3, 27, 31, 32]. PBAEs have achieved transfection efficacies comparable to adenovirus for transfection of human endothelial cells [17], have been used systems for efficient siRNA mediated gene knockdown [33, 34], and have been used

to target cancer *in vitro* and *in vivo* [24, 25]. Hydrophobicity appears to play a significant role in the ability of PBAEs to mediate efficient gene delivery [30] and the number of plasmids per particle that PBAEs form can also play a role [28].

To evaluate in greater detail why PBAEs are effective for non-viral gene delivery and to determine how subtle changes to structure affect efficacy, we synthesized an array of polymers with single carbon changes to the backbone, side chain, and small changes to the end-modifying amine (**Figure 5.1**). We synthesized 4 polymers with single carbon changes to the backbone (B3-S5-Ac, B4-S5-Ac, B5-S5-Ac, B6-S5-Ac) and end-modified each of those with E7 (B3-S5-E7, B4-S5-E7, B5-S5-E7, B6-S5-E7). We also synthesized two polymers with single carbon difference to the side chain (B4-S4 and B4-S5) and end-modified those polymers with 3 end-capping amines (E4, E6, E7), and finally we synthesized B4-S4 at three different amine:acrylate ratios (1.2, 1.1, 1.05) to generate different molecular weight versions of the base polymer, and end-capped those with a single end-capping amine (E7). We then studied polymer properties that we hypothesized would be related to the ability to overcome the barriers to intracellular gene delivery. We evaluated at nanoparticle size, zeta potential, and ability to retard DNA from moving on a gel to look at stable particle formation. We studied the PBAEs' buffering capacity to investigate how these polymers might be able to escape the endosome, and the polymer degradation rate to assess the ability of the polymer to promote release of DNA as well as avoid cytotoxicity. Finally, we evaluated particle uptake, viability, and transfection efficacy as biological outcomes, and as a way to assess where in the process particular polymer structure were failing or succeeding in overcoming barriers to gene delivery.

5.3.2 Particle size and charge

Previous work with cationic polymers for DNA delivery has indicated that formation of small, positively charged nanoparticles is a prerequisite for efficient transfection [1, 35]. However, too high of a charge density can lead to unwanted toxicity, and there may be some intermediate, optimal charge density depending on the polymer of interest. These competing effects can been seen in HPMA-oligolysine copolymers [36] and cationic glycopolymers [37], polymers synthesized by Reversible Addition-Fragmentation chain Transfer (RAFT) polymerization.

In a series of cationic glycopolymers with either a positively charged pendant group or a sugar, Ahmed et al. showed that increased carbohydrate content significantly reduces toxicity but also reduces transfection efficacy [37]. Studies on a library of HPMA-oligolysine copolymers revealed that size of the charged moieties matters; 5- and 10-lysine long oligocations were more effective than 15-lysine long oligocations. Shorter lysine chains were more salt stable (5 > 10 > 15). However, polymers with 10 lysine long oligocations were the best at transfection, followed by 5, then 15, indicating that there was some medium optimum between even distribution of charge and larger charged groups [36]. In addition, poly(glycoamidoamine) (PGAA) polymers, synthesized with repeating ethylenamines, were shown to be optimal transfection reagents when there were 4 ethylenamines; having 5 or 6 ethylenamines does not increase transfection but does increase toxicity [38].

All polymers in this study spontaneously formed positively-charged (+21 to +29 mV zeta potential) nanoparticles in the 130-150 nm diameter range (**Figure 5.4**). Previous studies have indicated that a zeta potential of greater than +10 mV was required

for PBAE nanoparticle transfection [27]. Acrylate-terminated polymers were found to be slightly larger than their end-modified versions by dynamic light scattering measurements; on average, E7-modified B3/4/5/6-S5 polymers were 170±20 nm in diameter, versus 221±8 nm for acrylate-terminated versions. There is a statistically significant difference between B4-S5-E7 and B4-S5-Ac ($p < 0.05$), but no statistically significant difference between the other pairs. There was no statistical difference between any of the polymers when looking at size by nanoparticle tracking analysis. In this study, we measured particle size in two ways: dynamic light scattering (DLS) and nanoparticle tracking analysis (NTA). NTA directly measures number-averaged size, thus the average particle size by number-weighting is the same for all acrylate and amine pairs. DLS measurements are intrinsically intensity-weighted, where large infrequent particles can cause a disproportionate contribution to the average size. Thus, particle formulations where DLS and NTA measurements are the same, such as B4-S5-E7, are monodisperse and formulations such as B4-S5-E6 are more polydisperse and have a minority component of slightly larger particles. It is only in case of B4-S5-E7 and B4-S5-Ac that the presence of a minority component of larger particles is statistically significant by end-group, and in this case, the number-average size remains the same.

Not surprisingly given the relatively narrow distribution of particle sizes and zeta potentials, particle size and zeta potential was not correlated with particle uptake or transfection efficacy to any significant degree (**Figure 5.5a-c**). However, particle size by dynamic light scattering appeared to be relatively negatively correlated with particle uptake (**Figure 5.5d**), indicating that smaller particles (as measured by DLS) tended to get taken up more efficiently than larger ones; this remains a weak trend. One potential

explanation is that as DLS size is intensity-weighted, a relatively small number of larger particles would skew the DLS average much more than NTA number average. Thus, if these larger particles are particularly inefficient at being taken up by the cells, and they segregate DNA away from the smaller particles, these formulations overall would be less efficient in being taken up by cells. Generally, these nanoparticles were found to all be very similar in surface charge and particle size, yet they had substantial differences in uptake and transfection as will be further described below.

5.3.3 Gel electrophoresis

In addition to a basic requirement to form small, positively charged nanoparticles, for efficient DNA delivery, the particles must bind to and protect DNA effectively. At 60 w/w, all of the 14 polymers completely retarded the DNA except for B3-S5-Ac (**Figure 5.6a)**. When bromophenol blue was added to the lanes containing particles, the most hydrophobic polymers containing B5 and B6 diacrylates in their backbone were able to retard the DNA (B5-S5-Ac, B5-S5-E7, B6-S5-Ac, B6-S5-E7) as well as B4-S4-E6 and B4-S5-E7. The remaining polymers were unable to completely retard the DNA migration (**Figure 5.6b**). Interestingly, acrylate terminated polymers and their amine-terminated counterparts bound DNA in similar patterns, with the largest discrepancy occurring with respect to the difference between B3-S5-Ac and B3-S5-E7. In this, even with no competition, B3-S5-Ac was unable to retard the DNA electrophoresis, up to a 150 w/w ratio, while the end-modified polymer was able to retain the DNA even at a low 15 w/w ratio (**Figure 5.7**). Hydrophobicity of the polymer seemed to play a large role in polymer binding affinity, as the four most hydrophobic polymers (B5-S5-Ac, B5-S5-E7, B6-S5-

Ac, B6-S5-E7) were all able to retain the DNA even after addition of the bromophenol blue. This may indicate a significant hydrophobic effect for the binding of PBAEs with DNA. Previous studies have demonstrated that hydrophobicity plays a strong role in enhancing gene delivery with PBAEs, generally increasing transfection efficacy but also increasing cytotoxicity [30]; these data may provide a mechanism for this effect.

5.3.4 Polymer buffering capacity

In order to escape the endosome, there needs to be a mechanism of endosomal escape. The ability of a polymer to buffer the endosome has been shown to be highly correlated with the amount of secondary and tertiary amine groups the polymers contain [10], as these amines tend to be protonatable across relevant pH ranges. To assess the ability of the polymers to buffer the endosome, titration curves were determined for polymers using acid-base titration (**Figure 5.8**). Using the titration curves, the buffering capacities of the polymers were calculated through the percentage of amine groups protonated between pH of 7.4 and 5.1. As references, sodium chloride (NaCl) showed a curve with no buffering indicated by its vertical slope, while polyethylenimine (PEI) displayed significant buffering indicated by a gradual slope between pH 5.1 and 7.4. Because PEI has an abundance of secondary and tertiary amine groups, it can buffer many protons in the endosome, where the pH drops from 7.4 to 5.1. The buffering capacities of gene delivery polymers affect their ability to escape the endosome via the proton sponge effect [9, 11].

Although the polymers differ only by small structural changes, their buffering capacities were found to have significant differences (**Table 5.1**). B4-S5-E7 1.05:1 was

found to have the lowest buffering capacity on a per-amine basis and on a per-mass basis, while B6-S5-E7 1.1:1 was found to have the highest buffering on both measures, buffering 4.6 mmol H+/g and having a per-amine buffering capacity of 95%.

Additionally, when the buffering capacities of the PBAEs are compared to branched PEI on a per-mass basis, the comparison is initially not a favourable one. The PBAEs buffering capacity was concentrated in the relevant pH range (pH 5.1 – 7.4), with their per-amine buffering capacity varying from 34% to 95% as compared to 25 kDa polyethyleneimine (PEI), which only uses 25% of its amine content over that key range. However, due to the higher amine-density on PEI, on a per mass basis, all PBAEs buffered fewer protons than PEI (1.4-4.6 mmol H+/g for PBAEs vs 6.2 mmol H+/g for PEI). However, since the PBAEs are much less cytotoxic, and are typically formulated at 60 w/w compared to 1-3 w/w for PEI, the total buffering capacity of PBAE based particles significantly exceeds that of PEI. As an example, the PBAE with the lowest buffering capacity per mass can buffer 1.7 mmol H+/g, but on a formulation basis, since the PBAE formulation contain on average 20 times more polymer than PEI formulation, 60 w/w particles would be able to buffer 5.5-times as many protons as 3 w/w PEI.

The structure-function relationship for end-cap molecule and PBAE buffering extent per mass is clear (**Table 5.1**). Polymers end-capped with E7 generally have the highest buffer capacities, which is expected as the E7 group contributes two tertiary amines in its structure. Polymers end-capped with E6 also have relatively high buffer capacities as compared to E4, as each E6 group contributes an extra secondary amine group as opposed to an extra primary amine. Acrylate-terminated polymers showed only slightly lower buffering capacity compared to their end-modified counterparts (**Table 5.1,**

Figure 5.9). The buffering for the acrylate-terminated polymers are not the lowest of the samples, indicating that the base polymers themselves, rather than their end-groups, drive buffering in the range of pH 5.1-7.4. Further, these results reveal that the modest differences in buffering capacity observed with these different polymer structures do not strongly correlate to the relatively large differences in particle uptake and transfection also observed with these structures (**Fig. 5.5f,g**).

In the context of intracellular gene delivery, endosomal buffering is required to mediate endosomal escape and facilitate transfection of the cell. We hypothesized that low buffering capacity would result in the stranding of nanoparticles in the endosomal/lysosomal system, resulting in high uptake not allowing for high transfection. In general, however, this trend is not perfect due to other confounding factors, and demonstrates that high buffering capacity is likely necessary but not sufficient for effective transfection with PBAEs. As predicted, there is no correlation between buffering capacity (per mass) and particle uptake, but there is a weak positive correlation between buffering capacity per mass and transfection (**Fig. 5.5f**). This makes intuitive sense, as improvements in buffering capacity should improve endosomal escape, thus enhancing the transfection of cells that have already taken up particles. This correlation is not that strong because of the generally very strong correlation between uptake and transfection seen in this cell type.

5.3.5 Polymer degradation

Intracellular DNA delivery requires that the polymer forms stable complexes that can bind DNA, protect it from enzymatic degradation, and enter cells. However,

successful transfection also requires that the DNA be released for efficient transcription of mRNA [39]. Polymer degradation rate is an important chemical parameter as it determines the time scale that the polymers have to escape the endosome and enter the cytoplasm for effective transfection. It is also important to characterize the polymer degradation mechanisms to evaluate the basis of possible reduced cytotoxicity compared to other cationic polymers. Cationic polymers that cannot degrade effectively will likely not be as biocompatible with cells. An example of this is PEI, which typically mediates high uptake and has a very high total buffer capacity (**Table 5.1**), but has a lower transfection efficacy and higher toxicity than other polymers [40]. Polymer degradation can be helpful in terms of enhancing the release of DNA from the polymer and reducing cytotoxicity; but if degradation is too quick, it could decrease particle stability, DNA protection, and cellular uptake.

Generally, the PBAEs degrade very rapidly in aqueous conditions, with half-lives in PBS at 37°C ranging from 90 minutes to just over 6 hours (**Figure 5.10, Table 5.1**). We hypothesized that due to the trade off between wanting to increase particle stability extracellularly, but also promote DNA release intracellularly, we may find a biphasic response between polymer half-life and transfection efficacy. We found that a modest biphasic trend is demonstrated when we compare transfection to half-life (**Figure 5.5e**). In addition, the two polymers with the shortest half-lives (B5-S5-E7 at 1.2 h and B4-S4-S7 1.2:1 at 1.6 h) showed the largest discrepancy between uptake and transfection, which may suggest that modestly long (> 2 h) half lives are required to protect the DNA all the way to the nucleus. Overall, these degradation rates are surprisingly rapid. Faster than anticipated degradation of polymers is observed in other related systems such as

poly(glycoamidoamine) (PGAA) polymers, which contain hydroxyl groups alpha to the amide bonds and secondary amines in the backbone of the polymer, and show rapid hydrolysis at pH 7.4 (half-lives of around 20 hr), even though amide bonds should hydrolyze much more slowly than ester bonds [41]. Interestingly, there is faster degradation in pH 7.4 than in pH 5; this is attributed to the effect of the proximal –OH group [41]. In particular, the secondary amines in the PGAAs are located a similar distance away from the amide bonds as the tertiary amines in the PBAEs are to the ester bonds, supporting the theory that they could likely be responsible for the rapid degradation of the PBAEs seen here. This very rapid degradation rate could be another reason for the general effectiveness and low cytotoxicity seen with this class of polymers, but it does pose potential challenges for eventual *in vivo* translation of this technology.

5.3.6 Particle Uptake, Transfection Efficacy, and Cytotoxicity

In order to compare polymer properties to biological outcomes, we investigated the cellular uptake, transfection efficacy, and cytotoxicity of our nanoparticle formulations (**Figure 5.11**). Polymers B4-S5-E6, B4-S4-E7 1.1:1, B3-S5-E7, and B4-S5-E7 were all found to have superior uptake and transfection to PEI, and B6-S5-E7 was found to have superior uptake but comparable transfection to PEI (**Figure 5.11a,b**; $p < 0.05$ for all comparisons). Most of the tested polymers were non-cytotoxic at the formulation ratio and dose tested with the exceptions being B4-S5-E4, B4-S4-E7 1.1, B4-S4-E7, B4-S4-E7, and PEI, which showed increased cytotoxicity relative to untreated controls (**Figure 5.11c**; $p < 0.05$ for all comparisons).

Increasing the number of carbons along the polymer backbone from 3 through 6 and leaving the side chain length at 5 carbons tended to increase cytotoxicity without increasing transfection efficacy. This result mirrors previous findings in COS-7 cells and RPE cells, where there is a limit at which increasing hydrophobicity of the polymer backbone does not improve transfection efficacy and only increases toxicity [22, 30]. Increasing the side-chain length from 4 carbons to 5 carbons resulted in mixed effects; end-modification of B4-S4 with E6 leaded to superior cell uptake and transfection compared to end-modification of B4-S5 with E6, but end-modification of B4-S5 with E4 had superior cell uptake and transfection compared to end-modification of B4-S4 with E4.

Increasing initial polymer molecular weight also had mixed effects. We synthesized B4-S4-E7 at 3 different molar ratios of acrylate to amine, resulting in 3 different molecular weights for the same base polymer. B4-S4-E7 at 1.1:1 had the highest transfection and uptake, but it also was the most toxic. These results are evocative of the recent work by Eltoukhy, et al, where they showed that intermediate length PBAEs mediated optimal transfection [42].

Acrylate-terminated PBAEs were found to have significantly lower uptake and transfection than their amine-terminated counterparts ($p < 0.001$ for all comparisons). Previous studies had indicated that acrylate-terminated polymers showed significantly reduced transfection efficacies [26, 27, 43], but were not able to determine the specific cause. Our investigation shows that this difference in transfection efficacy is due to differential uptake of the acrylate-terminated polymer nanoparticles as compared to the amine end-capped polymers. This is particularly striking given that there were no significant differences in particle formation as measured by gel electrophoresis or in

nanoparticle properties with respect to particle sizes and zeta potentials. Furthermore, the acrylate-terminated polymers were non-cytotoxic. Therefore, end-capping linear PBAEs with small molecules containing amines is necessary for sufficient cell uptake and transfection in a manner largely independent from nanoparticle biophysical properties. Further studies on specific mechanisms of gene delivery uptake will help improve our understanding of how differential polymer structure affects transfection efficacy and we are currently undertaking these studies.

5.4 Conclusions

Development of non-viral nanoparticles for gene delivery requires a greater understanding of the properties that enable gene delivery nanoparticles to overcome the numerous barriers to intracellular DNA delivery. Here we evaluated the effects of small structural perturbations within an array of linear poly(beta-amino ester)s (PBAEs) on polymer properties which are related to the barriers to intracellular gene delivery. Previous work has not investigated PBAE buffering capacity or examined the degradation rate of PBAEs formed from Michael addition of a primary amine containing side chain and a diacrylate. Interestingly, the PBAE polymers generally showed very rapid degradation in physiological conditions ($t_{½}$ = 90 min – 6 hours). On a per mass basis, PBAEs buffered 1.4-4.6 mmol H+/g. When compared to 25 kDa polyethyleneimine (PEI), PBAEs buffer significantly fewer protons/mass. However, since the PBAEs are much less cytotoxic and degrade so rapidly, they can be formulated at significantly higher weight ratios without substantial toxicity, and thus total buffering capacity of PBAE based particles significantly exceeds that of PEI. This may explain the

requirement for higher w/w ratios to achieve optimal efficacy using PBAEs compared to other polymer systems, and the rapid degradation rate may explain the low toxicity observed with large amounts of polymer.

Acrylate-terminated base polymers were much less efficacious than corresponding small molecule amine-containing end-capped versions, both in terms of uptake and transfection, even though there are minimal differences between acrylate and amine-terminated polymers in terms of DNA retardation in gel electrophoresis, nanoparticle size, nanoparticle zeta potential, polymer buffering capacity and cytotoxicity. This is a very interesting finding, and further investigation into the source of the considerable difference in efficacy seen here would be important. These studies further elucidate the role of polymer structure for gene delivery and highlight that small molecule end-group modification of a linear polymer can be critical for cellular uptake in a manner that is largely independent of polymer/DNA binding, particle size, and particle surface charge.

5.5 Figures

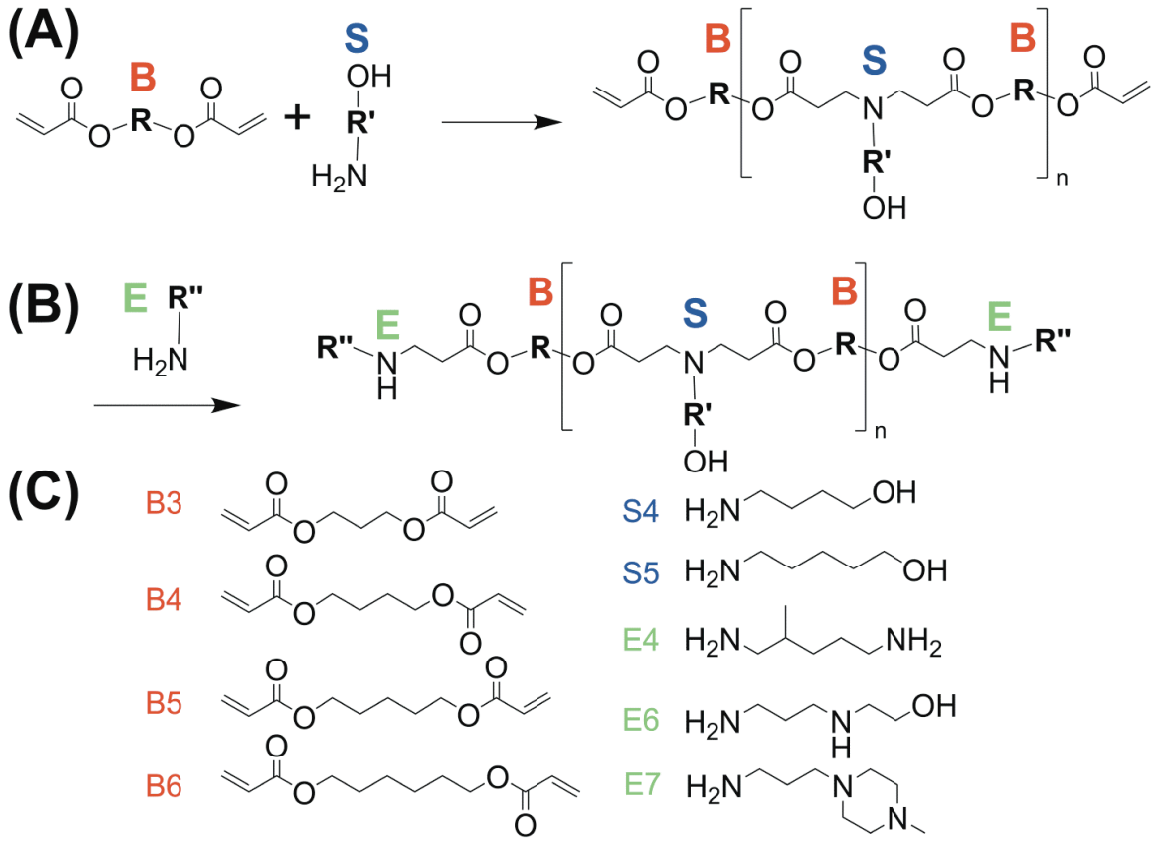

Figure 5.1. PBAE polymer library synthesis, and monomers used in Chapter 5. (A) The base polymer is formed via Michael addition of diacrylates ("B") and primary amines ("S"); the diacrylates are added in excess to form an acrylate terminated precursor. (B) In a second step, the diacrylate terminated base polymer is end-modified with an end capping amine ("E"), to form the end-modified polymer. (C) Monomers used in this study.

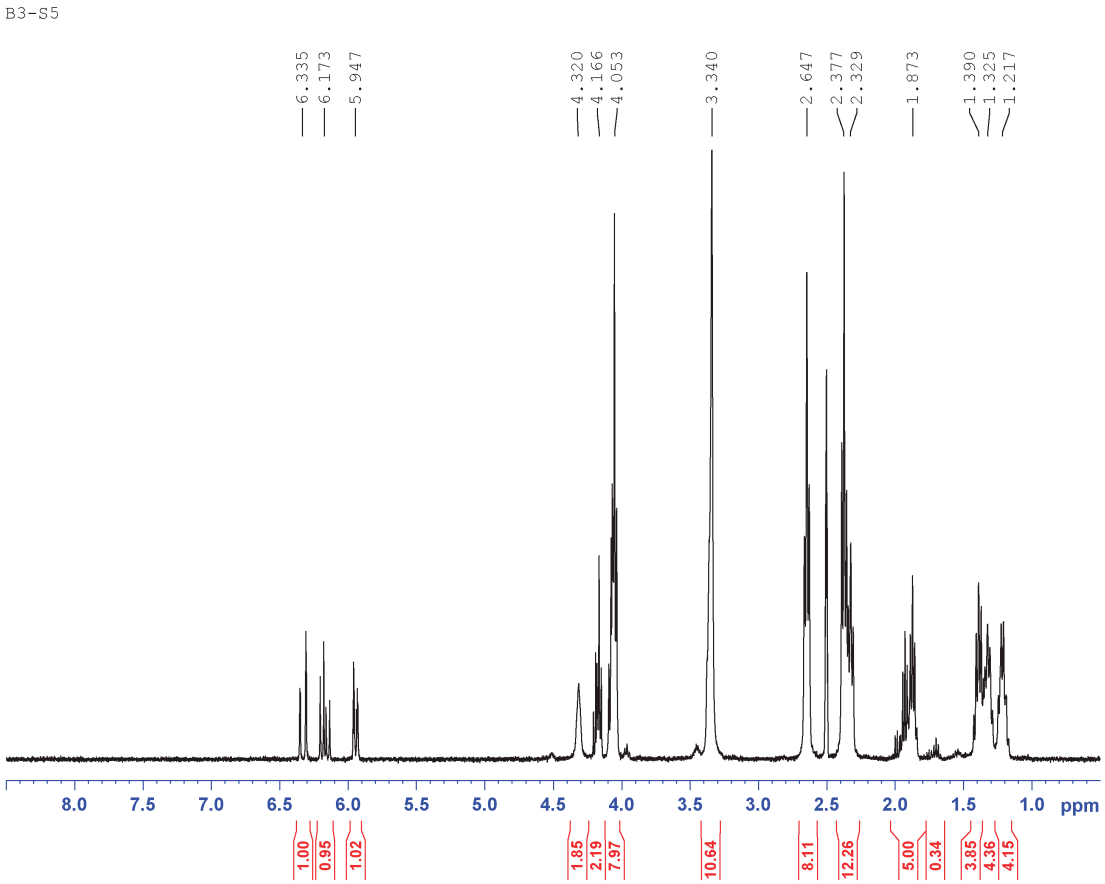

Figure 5.2a: NMR of B3-S5-Ac
1.15-1.25 (2H, quint, $NCH_2CH_2C\boldsymbol{H}_2CH_2CH_2OH$),
1.25-1.35 (2H, quint, $NCH_2C\boldsymbol{H}_2CH_2CH_2CH_2OH$),
1.35-1.45 (2H, quint, $NCH_2CH_2CH_2C\boldsymbol{H}_2CH_2OH$),
1.85-1.95 (2H, quint, $CH_2CH_2NCH_2CH_2(COO)CH_2C\boldsymbol{H}_2CH_2(COO)$),
2.3-2.4 (6H, t, $C\boldsymbol{H}_2CH_2NCH_2C\boldsymbol{H}_2(COO)CH_2CH_2CH_2(COO)$ and t,
$NC\boldsymbol{H}_2CH_2CH_2CH_2CH_2OH$),
2.6-2.7 (4H, t, $CH_2C\boldsymbol{H}_2NC\boldsymbol{H}_2CH_2(COO)CH_2CH_2CH_2(COO)$),
3.3-3.4 (2H, obsc, $NCH_2CH_2CH_2CH_2C\boldsymbol{H}_2OH$),
3.45 (t, $CH_2CH_2NCH_2CH_2(COO)CH_2CH_2C\boldsymbol{H}_2OH$)
4.0-4.1 (4H, t, $CH_2CH_2NCH_2CH_2(COO)C\boldsymbol{H}_2CH_2C\boldsymbol{H}_2(COO)$),
5.9-6 (d, $COOCH=C\boldsymbol{H}_2$),
6.1-6.2 (dd, $COOC\boldsymbol{H}=CH_2$),
6.3-6.4 (d, $COOCH=C\boldsymbol{H}_2$)

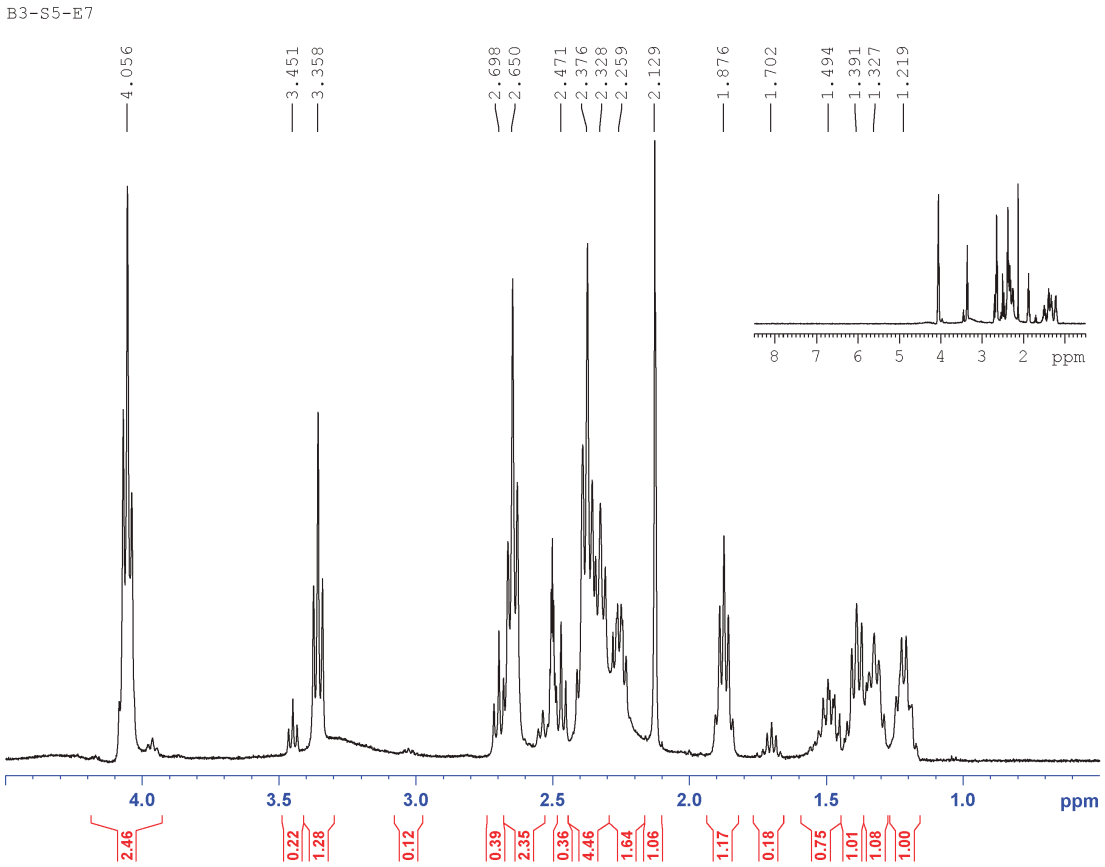

Figure 5.2b: NMR of B3-S5-E7

1.15-1.25 (2H, quint, $NCH_2CH_2C\boldsymbol{H}_2CH_2CH_2OH$),
1.25-1.35 (2H, quint, $NCH_2C\boldsymbol{H}_2CH_2CH_2CH_2OH$),
1.35-1.45 (2H, quint, $NCH_2CH_2CH_2C\boldsymbol{H}_2CH_2OH$),
1.50 (2H, quint, $-NHCH_2C\boldsymbol{H}_2CH_2N<(CH_2CH_2)_2>NCH_3$)
1.85-1.95 (2H, quint, $CH_2CH_2NCH_2CH_2(COO)CH_2C\boldsymbol{H}_2CH_2(COO)$),
2.13 (3H, s, $-NHCH_2CH_2CH_2N<(CH_2CH_2)_2>NC\boldsymbol{H}_3$)
2.3-2.4 (6H, t, $C\boldsymbol{H}_2CH_2NCH_2C\boldsymbol{H}_2(COO)CH_2CH_2CH_2(COO)$ and t, $NC\boldsymbol{H}_2CH_2CH_2CH_2CH_2OH$ and $-NHCH_2CH_2CH_2N<(C\boldsymbol{H}_2C\boldsymbol{H}_2)_2>NCH_3$ and $-NHCH_2CH_2C\boldsymbol{H}_2N<(CH_2CH_2)_2>NCH_3$),
2.47 (2H, t, $-NHC\boldsymbol{H}_2CH_2CH_2N<(CH_2CH_2)_2>NCH_3$)
2.6-2.7 (4H, t, $CH_2C\boldsymbol{H}_2NC\boldsymbol{H}_2CH_2(COO)CH_2CH_2CH_2(COO)$),
3.06 (br m, $-CONHCH_2-$)
3.3-3.4 (2H, t, $NCH_2CH_2CH_2CH_2C\boldsymbol{H}_2OH$),
3.45 (t, $CH_2CH_2NCH_2CH_2(COO)CH_2CH_2C\boldsymbol{H}_2OH$)
4.0-4.1 (4H, t, $CH_2CH_2NCH_2CH_2(COO)C\boldsymbol{H}_2CH_2C\boldsymbol{H}_2(COO)$)

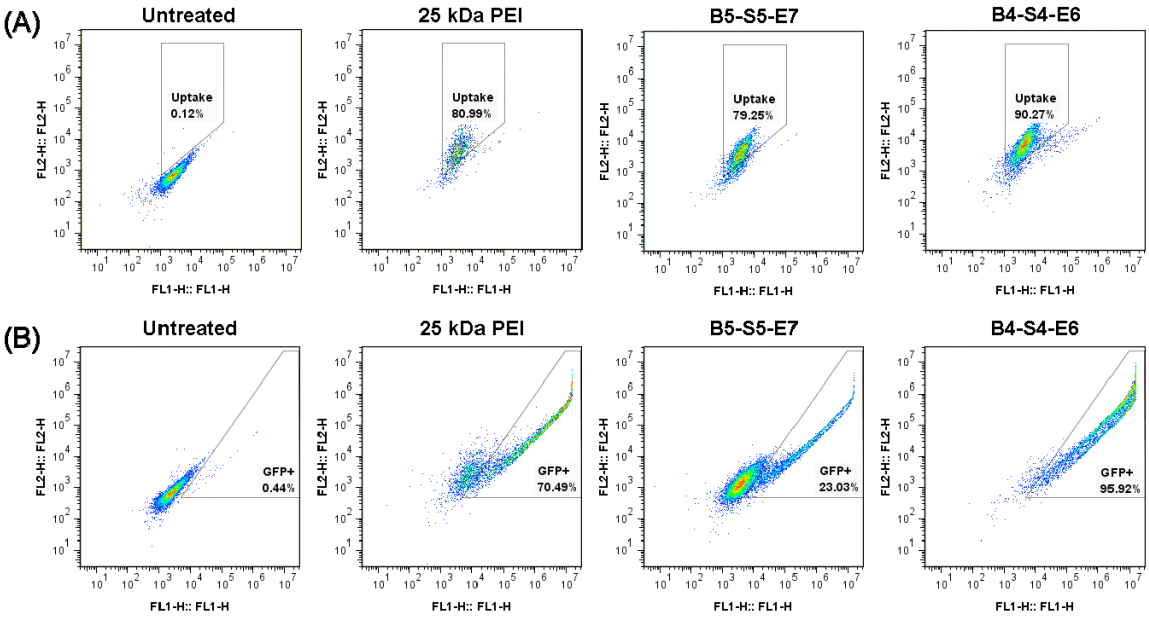

Figure 5.3. Example flow cytometry plots for (A) uptake of Cy3-labeled eGFP plasmid (5 hours post transfection) and (B) transfection of eGFP reporter plasmid (48 hours post transfection) 2D-gating analysis.

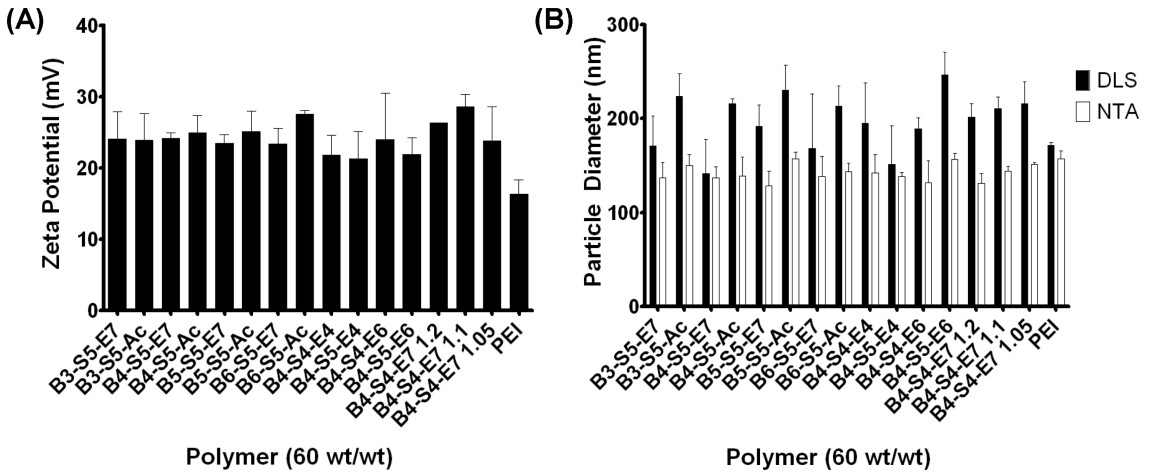

Figure 5.4. (A) Zeta potential of selected polymers. (B) Nanoparticle diameters measured using dynamic light scattering and nanoparticle tracking analysis.

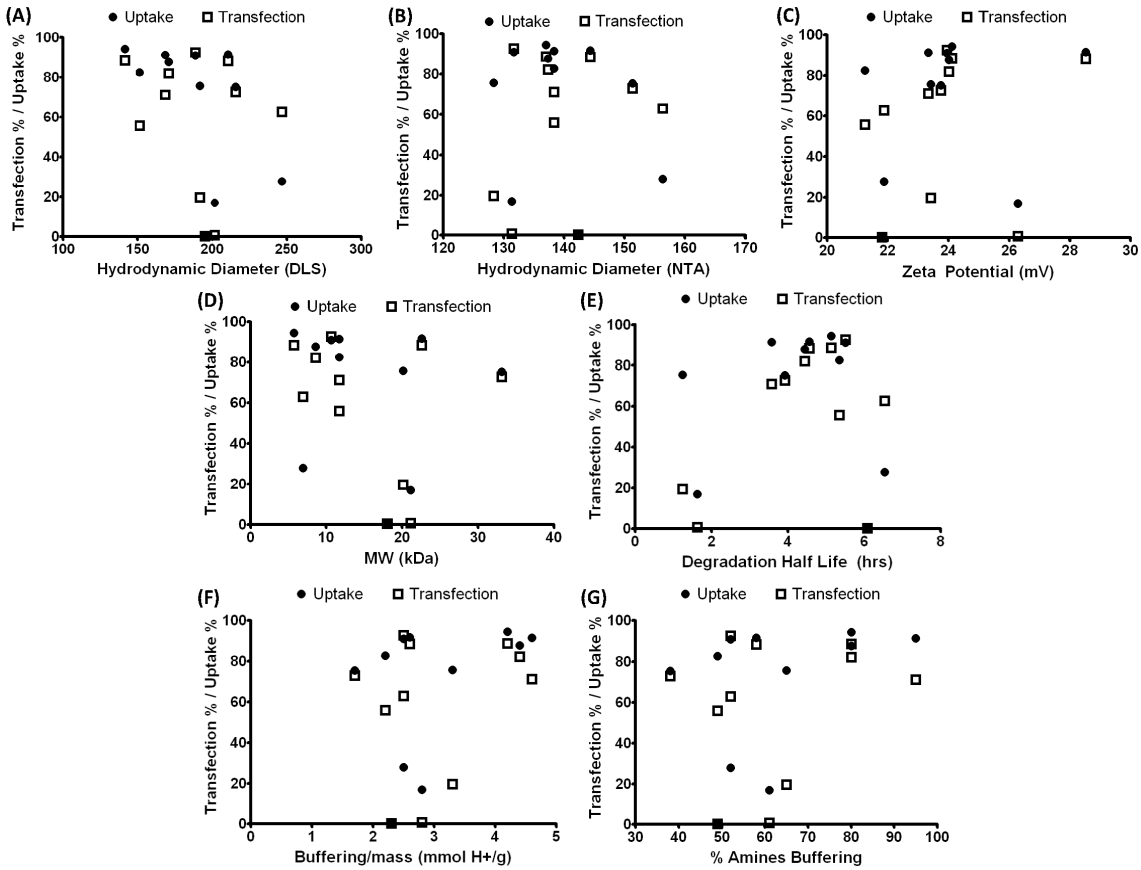

Figure 5.5. Comparison plots of various parameters vs. uptake and transfection. Transfection and uptake vs. (A) particle diameter, as measured by dynamic light scattering (DLS); (B) particle diameter, as measured by nanoparticle tracking analysis (NTA); (C) zeta potential; (D) polymer molecular weight; (E) polymer half-life; (F) buffering/mass; (G) % amines buffering.

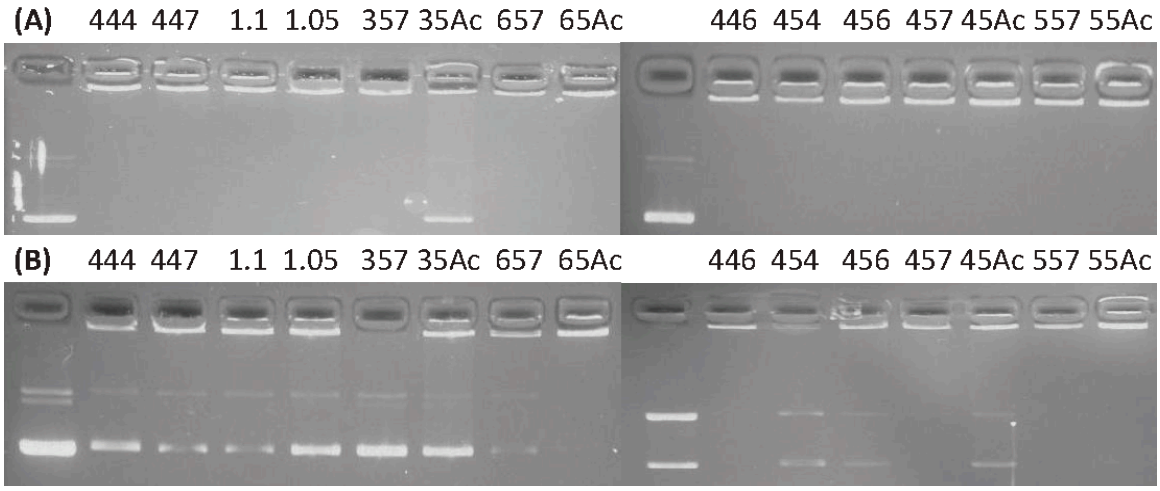

Figure 5.6. Gel electrophoresis of PBAE/DNA nanoparticles formed at 60 w:w (polymer:DNA ratio) (A) without bromophenol blue and (B) with bromophenol blue. For brevity, polymer names were shortened to remove the B-S-E designation, such that 444 is B4-S4-E4 and 357 is B3-S5-E7.

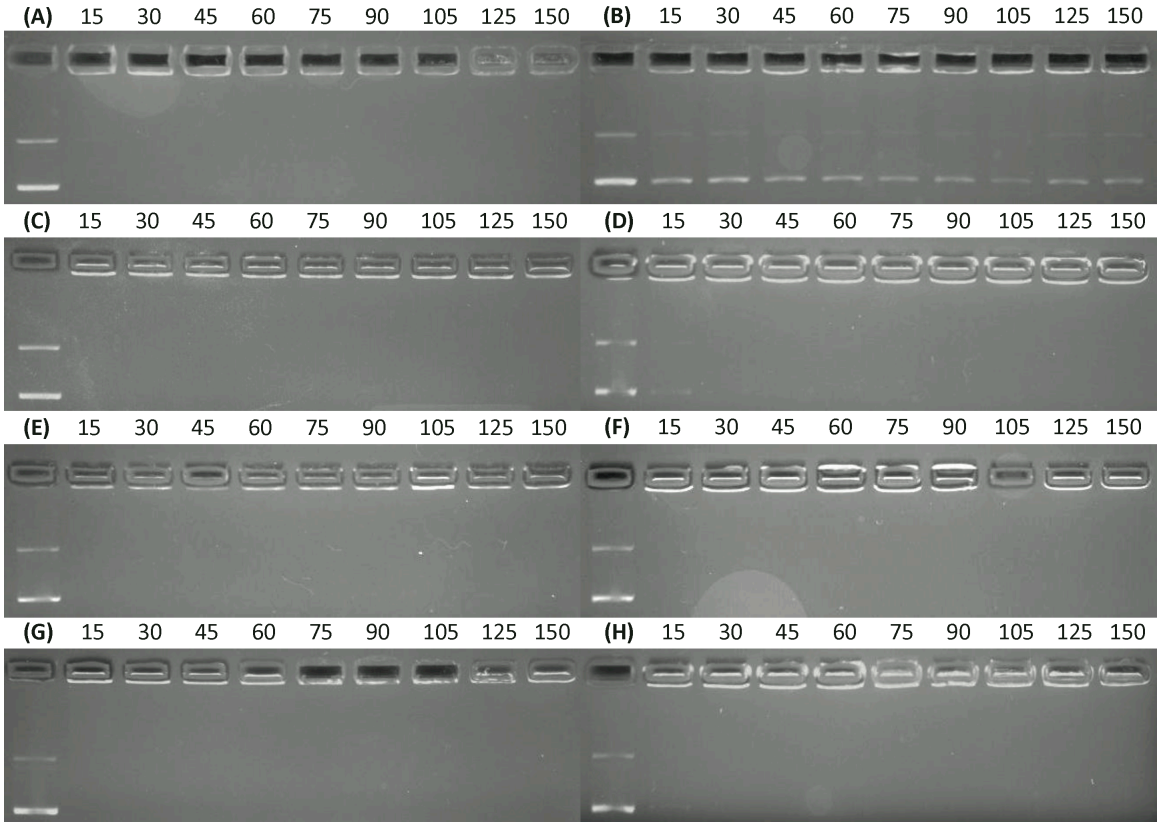

Figure 5.7. Gel electrophoresis of acrylate terminated and E7-end modified PBAE/DNA nanoparticles formed at the polymer:DNA ratio listed above the lane without bromophenol blue; 15 indicates that 15-fold more mass of polymer was used relative to the DNA mass. Each gel is from a single polymer. (A) B3-S5-E7 (B) B3-S5-Ac (C) B4-S5-E7 (D) B4-S5-Ac (E) B5-S5-E7 (F) B5-S5-Ac (G) B6-S5-E7 (H) B6-S5-Ac.

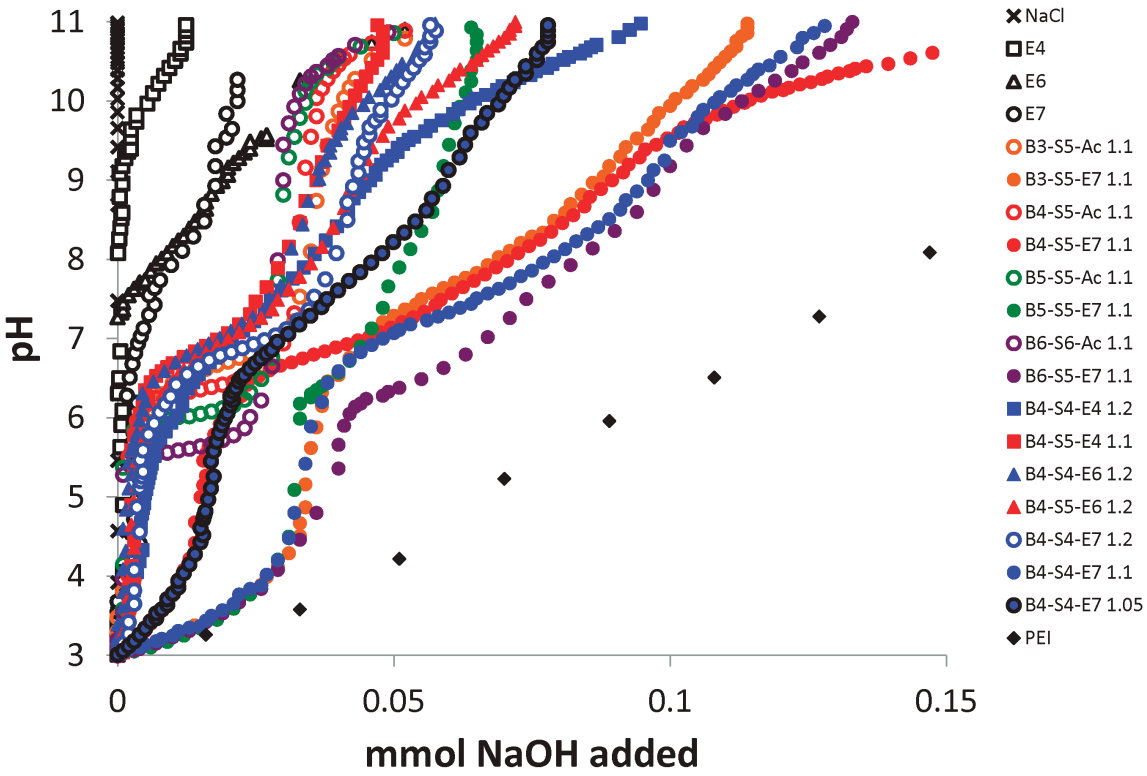

Figure 5.8. Acid-base titration curves for selected polymers and normalized for 150 mM aqueous NaCl. Measurements were taken using a Mettler Toledo S20 pH meter. pH was adjusted to pH 3 with HCl, then titrated with NaOH.

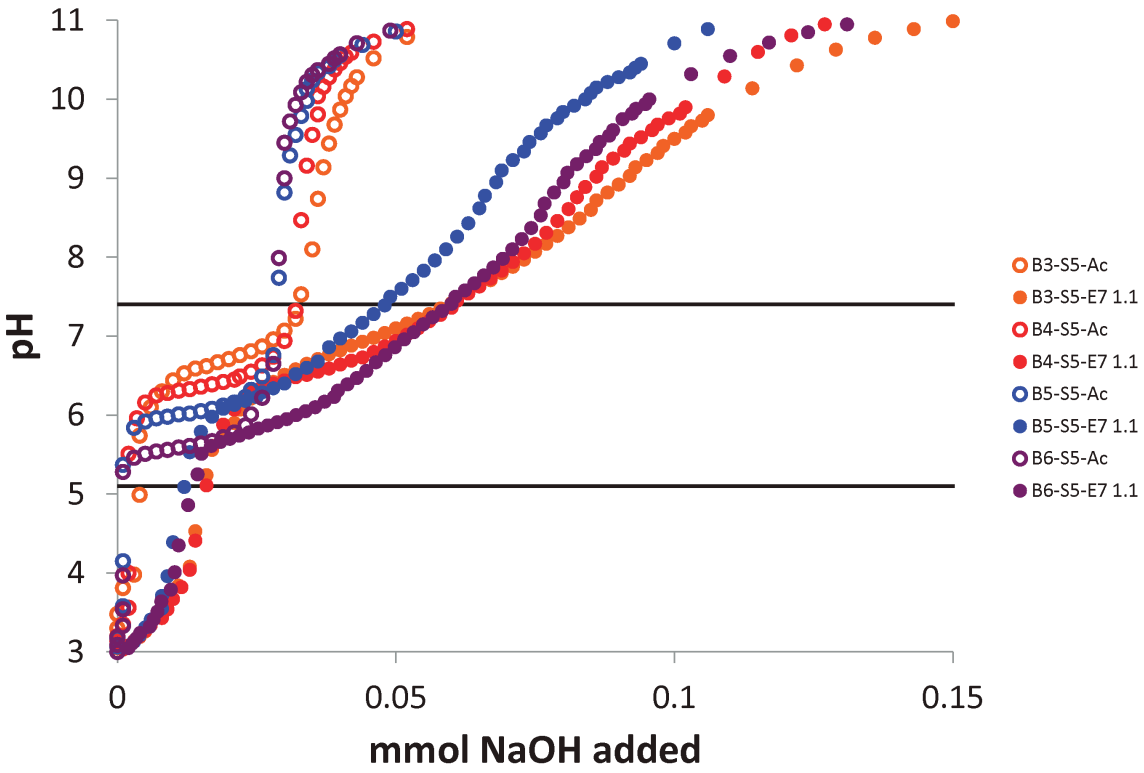

Figure 5.9. Acid-base titration curves for acrylate-terminated polymers and their E7-end modified counterparts normalized for 150 mM aqueous NaCl. Measurements were taken using a Mettler Toledo S20 pH meter. pH was adjusted to pH 3 with HCl, then titrated with NaOH. Horizontal lines correspond to pH 5.1 and 7.4 which were used for analysis.

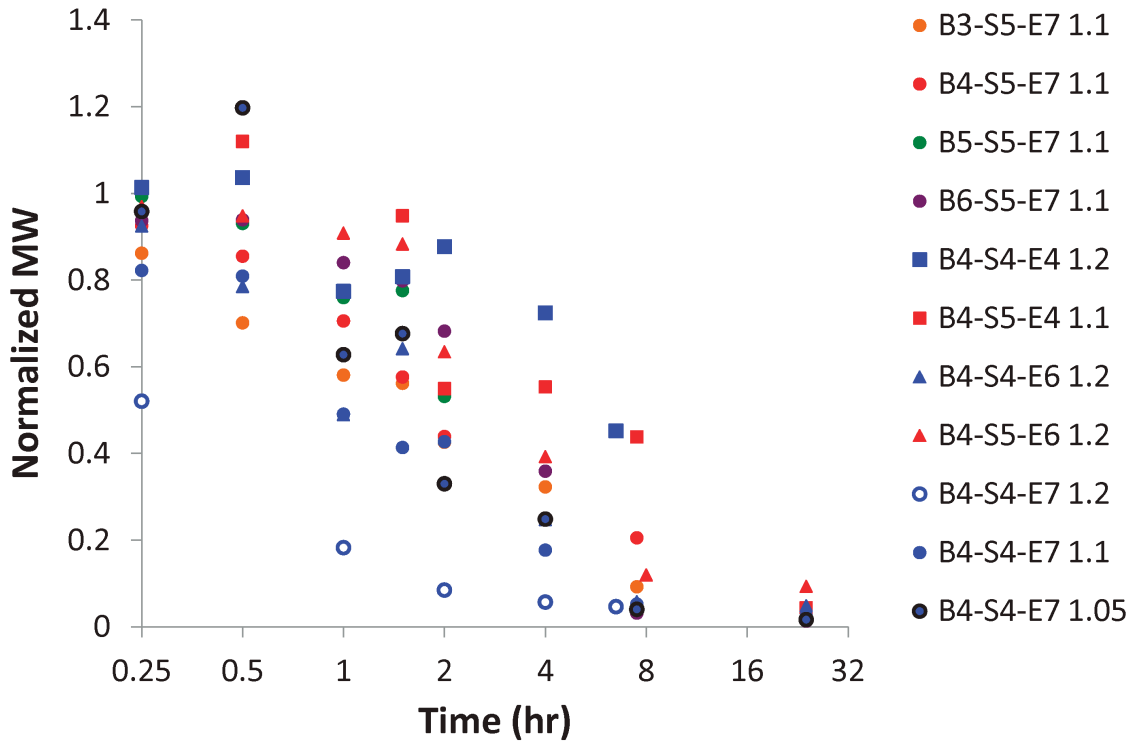

Figure 5.10. Degradation of polymers over time by GPC. MW is normalized (set = 1) to initial MW at t = 0. The majority of polymers showed extensive degradation by 4 hours.

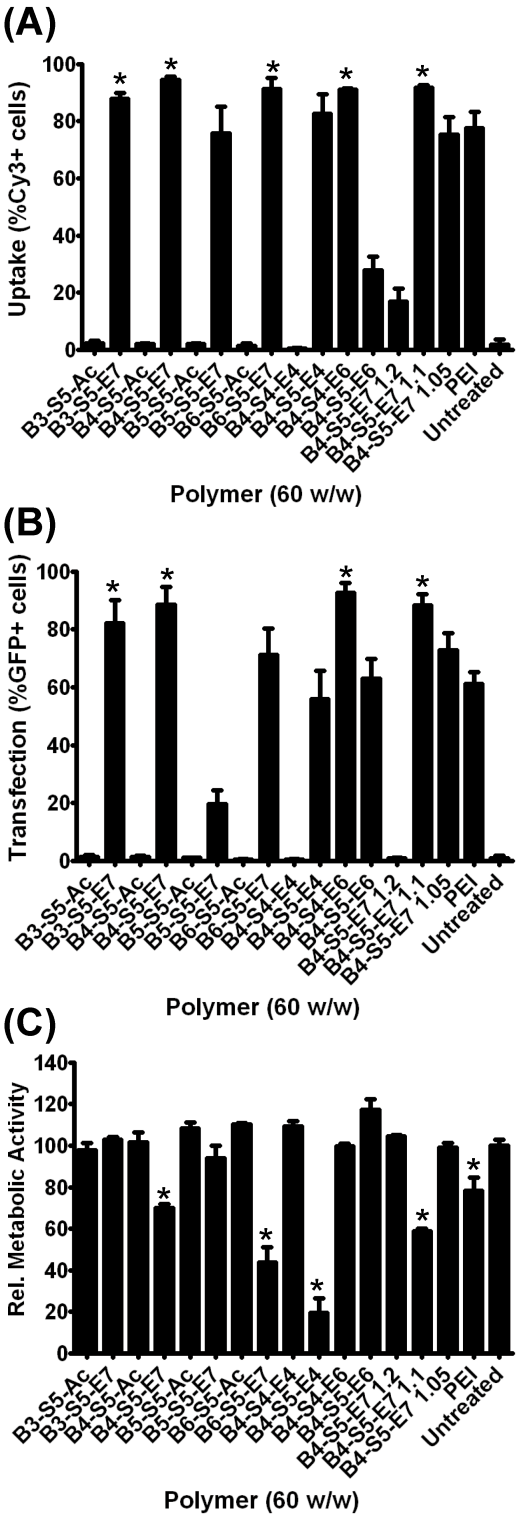

Figure 5.11. DNA nanoparticle uptake (A), cellular transfection (B), and cellular viability (C) after application of nanoparticles to cells. Data are presented as mean ± SEM. * Statistically significant improvement ($p < 0.05$) vs. 25 kDa PEI control for uptake and transfection plots; statistically significantly increased cytotoxicity ($p < 0.05$) vs. untreated control.

Table 5.1. Buffer capacities, molecular weights, and degradation half-lives of polymers. Buffer capacities of selected polymers were calculated using the titration curves found in Figure 5.4, and the half-lives were calculated from the GPC curves in Figure 5.10.

Polymer	**Buffer Capacity Per Amine**	**Buffer Capacity Per Mass**	**MW (kDa)**	**Half Life (h)**
B3-S5-E7	80	4.4	8.8	4.4
B3-S5-Ac	64	2.8		
B4-S5-E7	80	4.2	5.8	5.1
B4-S5-Ac	72	3.0		
B5-S5-E7	65	3.3	20.1	1.2
B5-S5-Ac	69	2.7		
B6-S5-E7	95	4.6	11.7	3.6
B6-S5-Ac	73	2.7		
B4-S4-E4	49	2.3	18.0	6.1
B4-S5-E4	49	2.2	11.7	5.3
B4-S4-E6	52	2.5	10.7	5.5
B4-S5-E6	52	2.5	6.9	6.5
B4-S4-E7 1.2	61	2.8	21.1	1.6
B4-S4-E7 1.1	58	2.6	22.6	4.6
B4-S4-E7 1.05	38	1.7	33.1	3.9
PBAEs	**34-95**	**1.4-4.6**	**5.8-33.1**	**1.6-6.5**
PEI	**26**	**6.2**	**25.0**	

5.6 References

1. Putnam, D., *Polymers for gene delivery across length scales.* Nature Materials, 2006. **5**(6): p. 439-51.
2. Check, E., *Gene therapy put on hold as third child develops cancer.* Nature, 2005. **433**: p. 561-561.
3. Green, J.J., R. Langer, and D.G. Anderson, *A combinatorial polymer library approach yields insight into nonviral gene delivery.* Accounts of Chemical Research, 2008. **41**(6): p. 749-759.
4. Park, T., *Current status of polymeric gene delivery systems.* Advanced Drug Delivery Reviews, 2006. **58**: p. 467-486.
5. Shmueli, R., *Electrostatic Surface Modifications to Improve Gene Delivery.* Expert Opinion Drug Delivery, 2010. **7**: p. 535-550.
6. Zhou, J., et al., *Biodegradable poly(amine-co-ester) terpolymers for targeted gene delivery.* Nature Materials, 2012. **11**(1): p. 82-90.
7. Ogris, M., et al., *DNA/polyethylenimine transfection particles: Influence of ligands, polymer size, and PEGylation on internalization and gene expression.* Aaps Pharmsci, 2001. **3**(3): p. art. no. 21.
8. Kagaya, H., et al., *Impact of polyplex micelles installed with cyclic RGD peptide as ligand on gene delivery to vascular lesions.* Gene Therapy, 2012. **19**(1): p. 61-9.
9. Boussif, O., *A versatile vector for gene and oligonucleotide transfer into cells in culture and in vivo: polyethylenimine.* Proc. Natl. Acad. Sci. U.S.A., 1995. **92**: p. 7297-7301.
10. Ou, M., *A family of bioreducible poly(disulfide amine)s for gene delivery.* Biomaterials, 2009. **30**: p. 5804-5814.
11. Sonawane, N.D., F.C. Szoka, and A.S. Verkman, *Chloride accumulation and swelling in endosomes enhances DNA transfer by polyamine-DNA polyplexes.* Journal of Biological Chemistry, 2003. **278**(45): p. 44826-44831.
12. Akinc, A., et al., *Exploring polyethylenimine-mediated DNA transfection and the proton sponge hypothesis.* Journal of Gene Medicine, 2005. **7**(5): p. 657-663.
13. Ogris, M., et al., *Melittin enables efficient vesicular escape and enhanced nuclear access of nonviral gene delivery vectors.* The Journal of biological chemistry, 2001. **276**(50): p. 47550-5.
14. Meyer, M., et al., *Breathing life into polycations: functionalization with pH-responsive endosomolytic peptides and polyethylene glycol enables siRNA delivery.* Journal of the American Chemical Society, 2008. **130**(11): p. 3272-3.
15. Lynn, D.M. and R. Langer, *Degradable poly(beta-amino esters): Synthesis, characterization, and self-assembly with plasmid DNA.* J Am Chem Soc, 2000. **122**: p. 10761-10768.
16. Lin, C. and J.F. Engbersen, *Effect of chemical functionalities in poly(amido amine)s for non-viral gene transfection.* Journal of controlled release : official journal of the Controlled Release Society, 2008. **132**(3): p. 267-72.

17. Green, J.J., et al., *Combinatorial modification of degradable polymers enables transfection of human cells comparable to adenovirus.* Adv. Mater., 2007. **19**(19): p. 2836-2842.
18. Forrest, M.L., J.T. Koerber, and D.W. Pack, *A degradable polyethylenimine derivative with low toxicity for highly efficient gene delivery.* Bioconjug Chem, 2003. **14**(5): p. 934-40.
19. Zanta, M.A., *Gene delivery: A single nuclear localization signal peptide is sufficient to carry DNA to the cell nucleus.* Proc. Natl. Acad. Sci. U.S.A., 1999. **96**: p. 91-96.
20. Dean, D.A., D.D. Strong, and W.E. Zimmer, *Nuclear entry of nonviral vectors.* Gene Ther, 2005. **12**(11): p. 881-90.
21. Sunshine, J., et al., *Small molecule end groups of linear polymer determine cell-type gene delivery efficacy.* Advanced Materials, 2009. **21(48)**: p. 4947-4951.
22. Sunshine, J.C., et al., *Poly(beta-Amino Ester)-Nanoparticle Mediated Transfection of Retinal Pigment Epithelial Cells In Vitro and In Vivo.* PloS one, 2012. **7**(5): p. e37543.
23. Bhise, N.S., et al., *The relationship between terminal functionalization and molecular weight of a gene delivery polymer and transfection efficacy in mammary epithelial 2-D cultures and 3-D organotypic cultures.* Biomaterials, 2010. **31**(31): p. 8088-96.
24. Showalter, S.L., et al., *Nanoparticulate delivery of diphtheria toxin DNA effectively kills Mesothelin expressing pancreatic cancer cells.* Cancer Biol Ther, 2008. **7**(10): p. 1584-90.
25. Tzeng, S.Y., et al., *Non-viral gene delivery nanoparticles based on poly(beta-amino esters) for treatment of glioblastoma.* Biomaterials, 2011. **32**(23): p. 5402-10.
26. Zugates, G.T., et al., *Gene delivery properties of end-modified poly(beta-amino ester)s.* Bioconjugate Chemistry, 2007. **18**(6): p. 1887-96.
27. Anderson, D.G., et al., *Structure/property studies of polymeric gene delivery using a library of poly(beta-amino esters).* Molecular Therapy, 2005. **11**(3): p. 426-34.
28. Bhise, N.S., et al., *A novel assay for quantifying the number of plasmids encapsulated by polymer nanoparticles.* Small, 2012. **8**(3): p. 367-73.
29. Green, J.J., *2011 Rita Schaffer Lecture: Nanoparticles for Intracellular Nucleic Acid Delivery.* Annals of Biomedical Engineering, 2012. **40**(7): p. 1408-18.
30. Sunshine, J.C., et al., *Effects of base polymer hydrophobicity and end-group modification on polymeric gene delivery.* Biomacromolecules, 2011. **12**(10): p. 3592-600.
31. Akinc, A., et al., *Parallel synthesis and biophysical characterization of a degradable polymer library for gene delivery.* Journal of the American Chemical Society, 2003. **125**(18): p. 5316-23.
32. Anderson, D.G., D.M. Lynn, and R. Langer, *Semi-automated synthesis and screening of a large library of degradable cationic polymers for gene delivery.* Angew Chem Int Ed Engl, 2003. **42**(27): p. 3153-8.
33. Lee, J.S., et al., *Gold, poly(beta-amino ester) nanoparticles for small interfering RNA delivery.* Nano Letters, 2009. **9**(6): p. 2402-6.

34. Tzeng, S.Y., et al., *Synthetic poly(ester amine) and poly(amido amine) nanoparticles for efficient DNA and siRNA delivery to human endothelial cells.* International journal of nanomedicine, 2011. **6**: p. 3309-22.
35. Sunshine, J.C., C.J. Bishop, and J.J. Green, *Advances in polymeric and inorganic vectors for nonviral nucleic acid delivery.* Therapeutic Delivery, 2011. **2**(4): p. 493–521.
36. Johnson, R.N., et al., *HPMA-oligolysine copolymers for gene delivery: optimization of peptide length and polymer molecular weight.* J Control Release, 2011. **155**(2): p. 303-11.
37. Ahmed, M. and R. Narain, *The effect of polymer architecture, composition, and molecular weight on the properties of glycopolymer-based non-viral gene delivery systems.* Biomaterials, 2011. **32**(22): p. 5279-90.
38. Ingle, N.P., B. Malone, and T.M. Reineke, *Poly(glycoamidoamine)s: a broad class of carbohydrate-containing polycations for nucleic acid delivery.* Trends Biotechnol, 2011. **29**(9): p. 443-53.
39. Schaffer, D.V., et al., *Vector unpacking as a potential barrier for receptor-mediated polyplex gene delivery.* Biotechnology and Bioengineering, 2000. **67**(5): p. 598-606.
40. Moghimi, S.M., et al., *A two-stage poly(ethylenimine)-mediated cytotoxicity: implications for gene transfer/therapy.* Mol Ther, 2005. **11**(6): p. 990-5.
41. Liu, Y. and T.M. Reineke, *Degradation of poly(glycoamidoamine) DNA delivery vehicles: polyamide hydrolysis at physiological conditions promotes DNA release.* Biomacromolecules, 2010. **11**(2): p. 316-25.
42. Eltoukhy, A.A., et al., *Effect of molecular weight of amine end-modified poly(beta-amino ester)s on gene delivery efficiency and toxicity.* Biomaterials, 2012. **33**(13): p. 3594-603.
43. Akinc, A., et al., *Synthesis of poly(beta-amino ester)s optimized for highly effective gene delivery.* Bioconjug Chem, 2003. **14**(5): p. 979-88.

6 Chapter 6: Gene delivery nanoparticles specific for human microvasculature and macrovasculature

6.1 Introduction

Endothelial cells play important roles in various ocular diseases, such as age-related macular degeneration, diabetic retinopathy, and retinoblastoma [1]. The dysregulation and subsequent angiogenic proliferation of these ocular microvascular endothelial cells represents the key step in most retinal causes of blindness. Regulation of this angiogenesis by anti-angiogenic drugs such as ranibizumab is now the first-line therapy and there is continued interest in more effective anti-angiogenic therapies [2]. Gene delivery is one such alternative method for delivery of antiangiogenic factors to endothelial cells, such as endostatin, angiostatin, and vascular endothelial growth factor-binding protein [3, 4]. In addition, gene therapy can be used to correct specific genetic deficiencies within the endothelial cell population. In this strategy, therapeutic genes that can either add or block a function are delivered to a targeted cell population. Additionally, such gene delivery methods can also be very useful in the study of cellular biology and disease.

Non-viral transfection of human retinal endothelial cells (HRECs) remains a challenge as does transfection of many other cell types. For example, one recent report using lipid coated magnetic nanoparticles achieved only ~5% transfection efficacy [5]. Leading commercial reagents, such as Lipofectamine 2000, can improve the transfection

---

This chapter contains excerpts from an article that was published as Shmueli RB*, Sunshine JC*, Xu Z, Duh EJ, Green JJ. "Gene delivery nanoparticles specific for human microvasculature and macrovasculature." *Nanomedicine: Nanotechnology, Biology, and Medicine*. 2012; 8(7):1200-1207.

of HRECs. One study found that this approach could lead to 42%-67% knockdown of a target receptor's surface expression following plasmid transfection [6]. Macrovascular (human umbilical vein endothelial cells, HUVECs) are also generally difficult to transfect as a lead polymer (polyethylenimine) plus magnetofection yielded transfection efficacy of only 39% positive cells [7]. New nanomedicines are needed to further increase the effectiveness of non-viral gene delivery.

Certain poly(β-amino esters) (PBAEs) have recently shown good transfection efficacy to a variety of cell types, including hard to transfect cell types like human mammary epithelium in 2D and 3D [8], human brain cancer cells [9], and HUVECs [10]. Particular polymers formulations have shown selectivity in terms of transfecting brain cancer cells as compared to normal astrocytes [9]. In addition, polymer end-group modification has been suggested as a tool to tune transfection efficacy [10-12]. The objectives of this study were to investigate the endothelial and retinal cell-type specificities of PBAE-based nanoparticles and also to identify novel nanoparticles that can achieve high transfection of human endothelial cells with minimal toxicity. A new PBAE combinatorial polymer library was synthesized and evaluated to discover nanoparticles that can transfect either macrovascular (HUVECs) or microvascular (HRECs) human endothelial cells or both.

6.2 Materials and Methods

6.2.1 Materials

All chemicals and solutions were used as received unless otherwise indicated. Monomers and vendors used for synthesis are the following: from Acros Organics [1-(3-

aminopropyl)pyrrolidine (E8)], Alfa Aesar [3-amino-1-propanol (S3), 4-amino-1-butanol (S4), 5-amino-1-pentanol (S5), 1,4-butanediol diacrylate (B4), 1,6-hexanediol diacrylate (B6), 1-(3-aminopropyl)-4-methylpiperazine (E7)], Fluka [2-(3-aminopropylamino)ethanol (E6)], Monomer-Polymer and Dajac Laboratories [1,3-propanediol diacrylate (B3), 1,5-pentanediol diacrylate (B5)], Sigma-Aldrich [1,3-diaminopropane (E1), 2,2-Dimethyl-1,3-propanediamine (E2), cystamine dihydrochloride (E10), 2-(1H-imidazol-4-yl)ethanamine (E12)], and TCI America [1,3-diaminopentane (E3), 2-methyl-1,5-diaminopentane (E4), (PEO)4-bis-amine (E5)]. Anhydrous DMSO and 3 M sodium acetate buffer were purchased from Sigma Aldrich. Sodium acetate buffer was diluted to 25 mM and filtered through 0.2 μm filter. pCMV-eGFP DNA was purchased from Aldevron. PBS, 0.25% trypsin-EDTA, Fu-Gene HD, and Lipofectamine 2000 were purchased from Invitrogen. CellTiter 96® AQ_{ueous} One MTS assay was purchased from Promega. 96-well TCP and non-TCP round-bottom plates were purchased from Sarstedt. Human Umbilical Vein Endothelial Cells (HUVECs) and EGM-2 Bullet Kit and Reagent Pack were purchased from Lonza. Human retinal endothelial cells (HRECs) were obtained from Cell Systems and cultured in EGM2-MV (from Lonza), as previously described [13, 14]. The immortalized human RPE cell line, ARPE-19, was obtained from the Dr. James Handa [15].

6.2.2 Synthesis of Poly(beta-amino ester) (PBAE)

The structures of these polymers were chosen so that there are ester linkages to ensure degradability of the polymers and amine groups to ensure the ability to bind DNA and form nanoparticles. The base polymers were synthesized by mixing diacrylates, labeled

as ‘B#’ in the text, and amino alcohols, ‘S#’, at a molar ratio of 1.2:1 in glass scintillating vials with teflon stir bars, forming ‘B#-S#’ base polymers (**Figure 6.1a**). The reaction was run at 90^{o}C for 24 hours. The base polymer was then dissolved at 167mg/mL in DMSO. In the last step of the reaction, 480 μL containing 80 mg of the base polymer and 320 μL of 0.5 M end-capping amine, ‘E#’, were mixed in a 1.5 mL eppendorf tubes in a shaker for 1 hour (**Figure 6.1b**). Completed polymers were aliquoted into smaller volumes and stored at 4^{o}C. The completed polymers are designated as ‘B#-S#-E#’; for example, B3-S5-E1 is an end-modified PBAE formed from the B3-S5 base polymer which is then end-modified with the end-capping amine E1 (**Figure 6.1c**). Polymer molecular weights were typically ~10 kDa as we previously have reported and among these polymers we have found that molecular weight is not correlated to transfection efficacy [16]. We have recently published the polymer characterization of these synthetic biomaterials including ^{1}H-NMR and Gel Permeation Chromatography of each polymer [16].

6.2.3 Nanoparticle Sizing

DNA was diluted in 25 mM sodium acetate buffer to 0.01 mg/mL. Polymer was diluted in sodium acetate buffer to either 30 or 60 times that concentration (30 and 60 weight to weight, w/w, ratios), added to the DNA solution and incubated at room temperature for 10 minutes. Nanoparticles were then diluted 20 fold into PBS and loaded into NS500 nanosight tracking analysis (NTA) system. Nanosight videos were captured for 60 seconds and then analyzed used the NTA software, version 2.2.

6.2.4 Transmission Electron Microscopy (TEM) imaging

Nanoparticles were prepared the same way as for sizing by NTA. 10 uL of sample was dropped onto carbon coated copper grids and left to dry in chemical hood for 2 hours. Unstained TEM imaging was then performed using the Philips CM120 system. Nanoparticle sizing was performed using ImageJ software.

6.2.5 Green Fluorescent Protein (GFP) transfection

HUVECs and HRECs were seeded at 2,500-5,000 cells/well onto 96-well plates and allowed to adhere overnight, in 100 μL of the appropriate media per well (EGM-2 for HUVECs and EGM-2 MV for HRECs). Immediately before transfection, media in plates were replaced with 10% supplemented FBS HUVEC media, 100 μL per well. For RPE transfections, ARPE-19 cells were seeded at 15,000 cells/well and allowed to grow to confluence over 3 days, and then transfected in DMEM with 10% supplemented FBS. Polymers and pCMV-eGFP DNA were diluted in 25mM sodium acetate buffer. The final DNA concentration of the mixture was 0.03 mg/mL, with PBAEs at either at 0.9 or 1.8 mg/mL (30 w/w and 60 w/w ratios, respectively). Solution was mixed, incubated for 10 minutes at room temperature and then 20 μL were added per well. FuGene HD and Lipofectamine 2000 were screened to find best formulation by following the manufacturer's guidelines. FuGene HD-DNA ratio of 4-1 was used, with 10 μL added per well, while Lipofectamine 2000-DNA ratio of 1.5-1 was used, with 10 μL added per well. Plates then incubated for 4 hours, after which nanoparticle loaded media was removed and fresh EGM-2 and EGM-2 MV media were added, 100 μL/well. Each experimental condition was evaluated in quadruplicate. Duplicate plates were made for

each experimental group to use one each for cell viability and transfection efficiency measurements.

6.2.6 Cell metabolism/viability

Twenty-four hours after transfection, designated plates were used for the CellTiter 96® AQ_{ueous} One MTS assay. 10 µL of the aliquoted assay solution was added per well. Plates were incubated for 1-4 hours, after which absorbance at 490 nm was measured using the BioTek Synergy 2 Plate Reader. Absorbance measurements were corrected from background media signal and normalized by untreated groups. Each experimental condition was evaluated in quadruplicate.

6.2.7 Flow cytometry

Forty-eight hours after transfection, flow cytometry was performed using the Accuri C6 flow cytometer with IntelliCyt high-throughput attachment. Cells were washed with 1x PBS and trypsinized with 30 µL/well of 0.25% trypsin-EDTA. 170 µL FACS buffer (2% FBS, 1x PBS) was added to cells and 200 µL/well transferred to 96-well round-bottom plates. The plates were centrifuged at 1000 rpm for 5 minutes, after which 170 µL/well of the supernatant was removed. The pellets were re-suspended in the remaining 30µL of buffer. Plates were then placed onto the IntelliCyt high-throughput attachment and HyperCyt software was to acquire and process data. FlowJo was used to analyze the flow cytometry data.

6.3 Results and Discussion

6.3.1 Polymer and Nanoparticle Synthesis

A polymer library was synthesized for gene delivery, such that a large diversity of structures could be investigated, each with small differential structural changes from each other. The structures of these polymers were chosen so that there are ester linkages to ensure degradability of the polymers and amine groups to ensure the ability to bind DNA and form nanoparticles. These polymers were synthesized from a pool of 4 acrylate monomers, 3 side chain monomers, and 12 end-chain capping molecules as described in the methods. The synthetic polymers are referred to by a 'B' number, a 'S' number, and an 'E' number, each referring to their constituent monomers. The number following the 'B' or the 'S' corresponds to the number of carbons between functional groups in the diacrylate or amino-alcohol monomers; thus 'B4-S5' is a polymer formed from a base diacrylate with 4 carbons between each acrylate group, and an amino-alcohol with 5 carbons between the amine and the alcohol functional groups.

Nanoparticles are formed through electrostatic self-assembly, due to attractive interactions between cationic polymers and anionic DNA. We use relatively high polymer to DNA weight ratios (w/w) such that the polymers encapsulate 100% of the DNA as we have recently described [17]. Representative polymers of interest were chosen for sizing measurements. Even though polymer structure varied, nanoparticle size was found to be similar with these different types of polymers (**Figure 6.2A**). Hydrodynamic diameter of the nanoparticles was approximately 150 nm, with a range of 110-190 nm in the particle distributions that was dependent on polymer to DNA weight-to-weight (w/w) formulation ratio. The average diameter of a nanoparticle formed from

B3-S5-E1 at 60 w/w as measured by TEM was 147 nm (**Figure 6.2B**), which closely matches the results found from NTA. There was no correlation between the sizes of nanoparticles that transfected the cells well (B3-S5-E# and B4-S4-E# series) as compared to those that transfected the cells less well (B3-S4-E# series). Therefore, we hypothesize that chemical structure, not nanoparticle physical properties, is the driver of the differences seen in transfection efficacy.

6.3.2 Nanoparticle-mediated Gene Delivery

Leading polymeric nanoparticles were found to be very effective for gene delivery to human microvascular and macrovascular endothelial cells. Significantly, transfection efficiencies of up to 85% for HRECs and 65% for HUVECs were observed as opposed to 49% (HREC) and 32% (HUVEC) with a leading commercially available reagent, Lipofectamine 2000 (**Figure 6.3A and 6.3B**). Lipofectamine 2000 was also more toxic than the PBAE nanoparticles (**Figures 6.3C and 6.3D**). The polymeric nanoparticles were found to display a wide range of transfection efficacies with both HRECs and HUVECs, which was dependent on polymer structure. Both the choice of base polymer and end-capping groups had a large effect on the transfection efficacy. The B4, B5, and B6 diacrylates differ by one carbon, yet there are significant differences in toxicity and transfection efficacy. A similar effect was observed when changing the side-chain amines. For example, B3-S4-based polymeric nanoparticles had very low transfection (< 10%), but a single carbon added to each of the side-chain monomers (B3-S5-based polymeric nanoparticles) resulted in highly effective gene delivery for both HRECs (up to 76%) and HUVECs (up to 64%). The end-group of the polymer made a

big difference to endothelial cell gene delivery as well, where the best formulations usually contained E5, E6, and E7.

In order to better isolate the effects from changing each component of the polymer, the data were averaged together across two of the three polymer elements that compose each synthetic polymer. In general, B4 and B5 based polymers had the highest gene delivery efficacy (**Figure 6.4A**) and reveal an optimal base diacrylate length. On the other hand, we observe an increasing monotonic trend with increasing length for the various side-chain amines used in this experiment, with S5 based polymers performing best (**Figure 6.4B**). Unlike with the structure of the base polymers, a clear trend in the structure of the end-group with transfection efficacy is not observed (**Figure 6.4C**). However, there are some end-capping amines, such as E6, which dramatically improve delivery, and others, such as E12, that are much less effective. These results motivate further studies on how polymer structure affects endothelial cell gene delivery.

6.3.3 Endothelial Cell-specific Gene Delivery

Comparing the transfection efficiencies between the different cell types and tissues revealed interesting trends (**Figure 5.4**). In this study, the HREC and HUVEC transfection profiles were positively correlated (linear regression, R^2= 0.81), with greater transfection efficiencies for HRECs overall. Similar viability profiles were also observed between HUVECs and HRECs. On the other hand, using the same set of nanoparticles, there is very little correlation between the transfection efficacies for gene delivery to HRECs as compared to retinal pigment epithelium (RPEs, linear regression, R^2 = 0.21), or HUVECs as compared to RPEs (linear regression, R^2 = 0.23). Polymers that

performed better on the endothelial cell types as compared the regression line include B4-S4 and B3-S5, as well as some B4-S5-based polymers (upper left hand corner of **Figures 6.5b and 6.5c**). As a group, these polymers were synthesized by diacrylate monomers that were less hydrophobic and contained 3 or 4 carbons between diacrylate monomer groups. On the other hand, there are some polymers that work better on the epithelial cells, such as B6-S5 (lower right hand corner of **Figures 6.5b and 6.5c**). This polymer is more hydrophobic than the polymers that tend to be better at transfecting endothelial cells and this polymer contains 6 carbons between its diacrylate monomer groups. The polymers that work well on both endothelial and epithelial cell types include B5-S5 based-polymers (upper right hand corner of **Figures 6.5B and 6.5C**), which have an intermediate level of hydrophobicity and 5 carbons between its diacrylate monomer groups. Strikingly, these structural changes are quite subtle and they do not influence nanoparticle size (**Figure 6.2)**.

6.4 Conclusions

Synthesis and testing of a PBAE library resulted in the identification of polymeric nanoparticles that can transfect human endothelial cells, HRECs and HUVECs, with high efficiency as compared to current commercially available standards. The best polymers (both good transfection and viability), B3-S5-E# and B4-S4-E# series, are new PBAE structures that were able transfect at least as well as the commercially available reagents and in some cases with less toxicity. Additionally, Small molecular changes to polymer backbone, side chain or end-group structure dramatically changed transfection efficiency. The best polymers were ones that contained B4 and B5, and S4 and S5, with a few

different E# groups. The most hydrophilic polymers, such as B3-S4, were not good at transfecting the cells, while their toxicity was also minimal. On the other hand, the most hydrophobic polymers, such as the B6-S5 series, were usually relatively toxic to the endothelial cells, subsequently also reducing the transfection efficiency. This trend is mirrored when looking at the effects of the different diacrylate monomers used (**Figure 6.4A**), where B4 and S5 performed best. While among certain structures, high hydrophobicity correlated to increased cytotoxicity and reduced transfection, overall, when all the data is evaluated together, there is not a strong correlation between transfection efficiency and viability (R^2 =0.06, data not shown).

Interestingly, the gene delivery efficacy across the entire polymer library was highly correlated between transfection of HREC and HUVEC cells – nanoparticle formulations that performed well for HRECs also performed well for HUVECs (R^2 = 0.81). This is dramatically different when compared to the performance of the same nanoparticles with retinal pigment epithelium, indicating that formulations could potentially be found which selectively transfect one ophthalmic cell type and not the other, as can be observed in Figures 6.5B and 6.5C. To our knowledge, this phenomenon, that specific ocular cell types can be targeted directly by fine-tuning of the polymer structure that composes nanoparticles, is striking and surprising. This finding also suggests that biomaterial-mediated targeting from this class of materials may be able to be combined with other methods of gene delivery targeting such as ligand or coating-mediated cell uptake [18-20] and transcriptional targeting [21, 22] to further improve specificity and efficacy to only one specific type of cell.

In particular, we show that the polymers in the middle of the hydrophobicity scale for this PBAE library worked very well for the endothelial cells, but much less so for the epithelial cells. On the other hand, those that were more hydrophobic, such as the B6-S5, worked well for the epithelial cells. Taken together, these correlations indicate that there may be natural cell type specificity for polymeric nanoparticles of this class.

Safe and effective gene delivery vehicles can have a large impact on biological studies and for the treatment of diseases. For example, researchers have developed a system for gene delivery of sFLT using adeno-associated virus (AAV) to bind VEGF in monkeys as a potential treatment for age-related macular degeneration [23]. However, viral gene therapy has limitations that may preclude many clinical applications due to carrying capacity constraints and safety concerns [24]. In contrast, our study reveals premiere non-viral nanoparticles that are enabling technologies for transfection of endothelial cells *in vitro* and are promising for use *in vivo* as delivery vehicles for genetic nanomedicines. We also show that polymer structure itself, may enable cell-specific non-viral gene delivery.

6.5 Figures

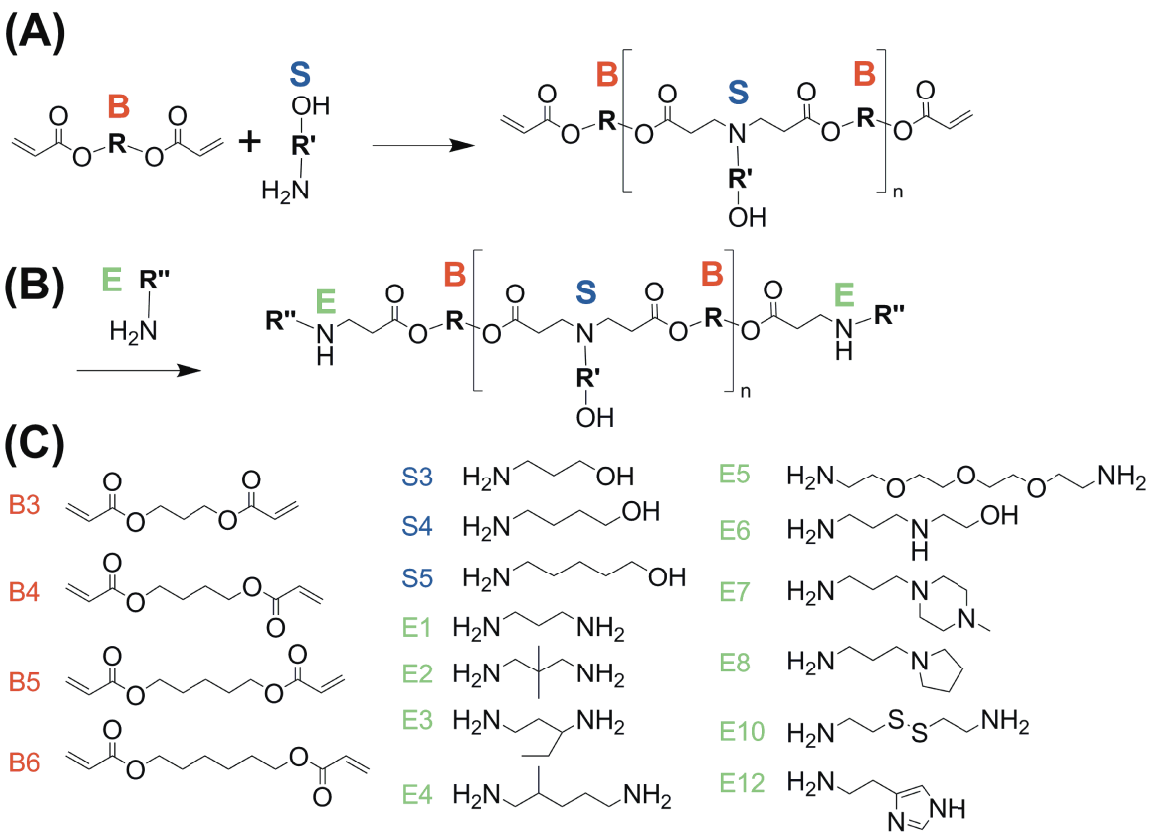

Figure 6.1. Polymer synthesis schematic and monomers used in Chapter 6. (A) Polymers were synthesized by reacting a diacrylate, 'B#', with an amino alcohol, 'S#'; (B) These were then reacted with an end-group, 'E#'; (C) Monomer structures.

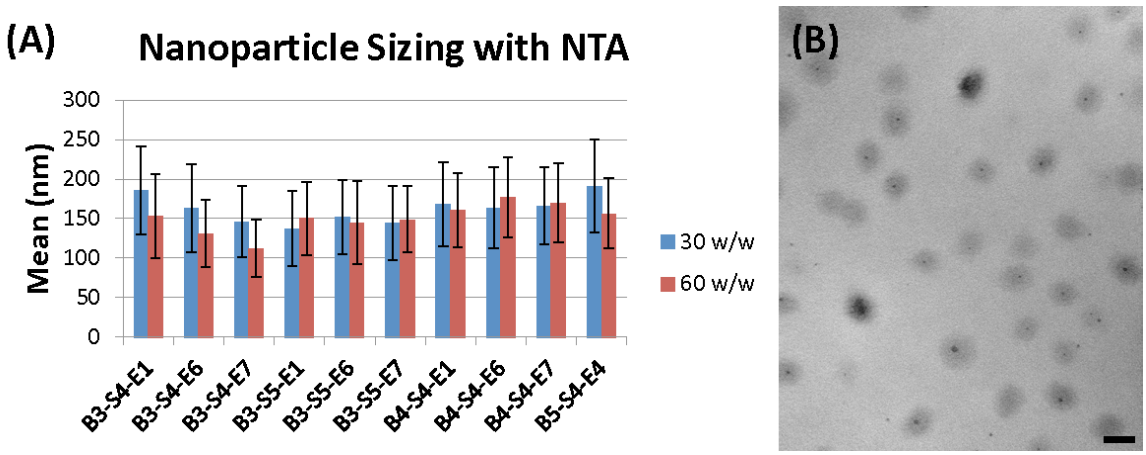

Figure 6.2. (A) Hydrodynamic diameter by nanoparticle tracking analysis. (B) Transmission Electron Microscopy of nanoparticles formed from B3-S5-E1 (60 w/w); scale bar is 200nm.

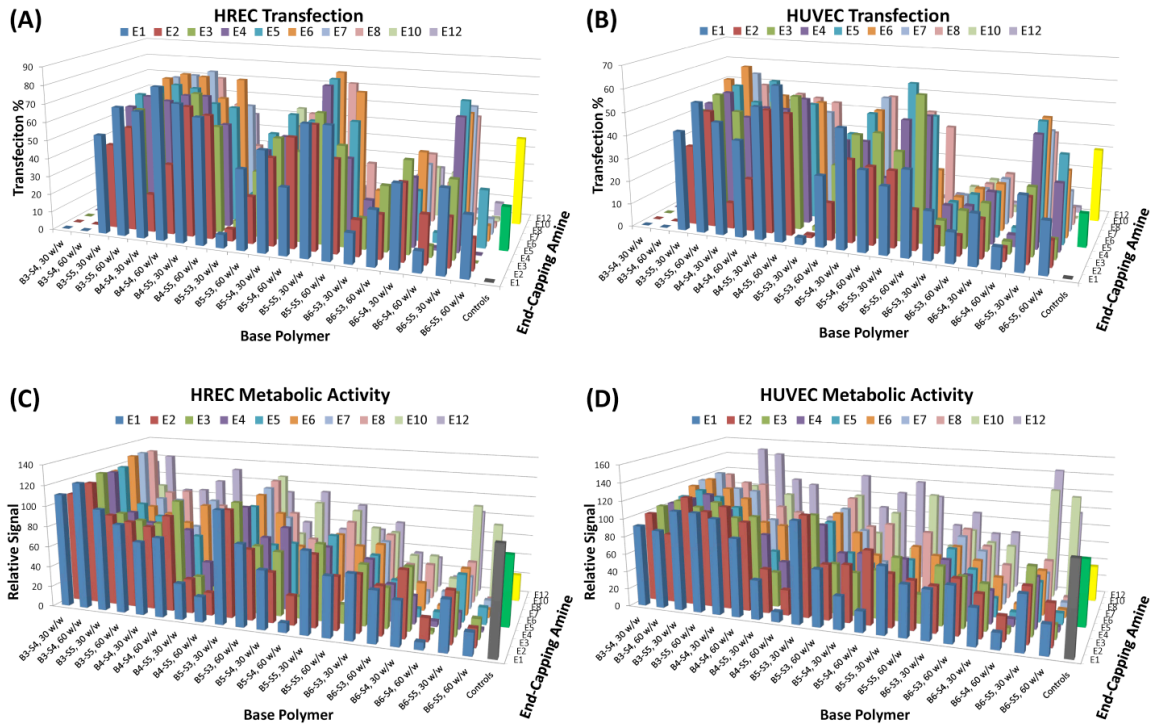

Figure 6.3. **Transfection efficiency (% GFP$^+$ cells) for transfection of HREC and HUVEC cells with the polymer library.** (A) HUVEC and (B) HREC transfection percentage. (C) HREC and (D) HUVEC metabolic activity relative to untreated control. Controls: Gray=untreated, Green=FuGene HD, Yellow=Lipofectamine 2000.

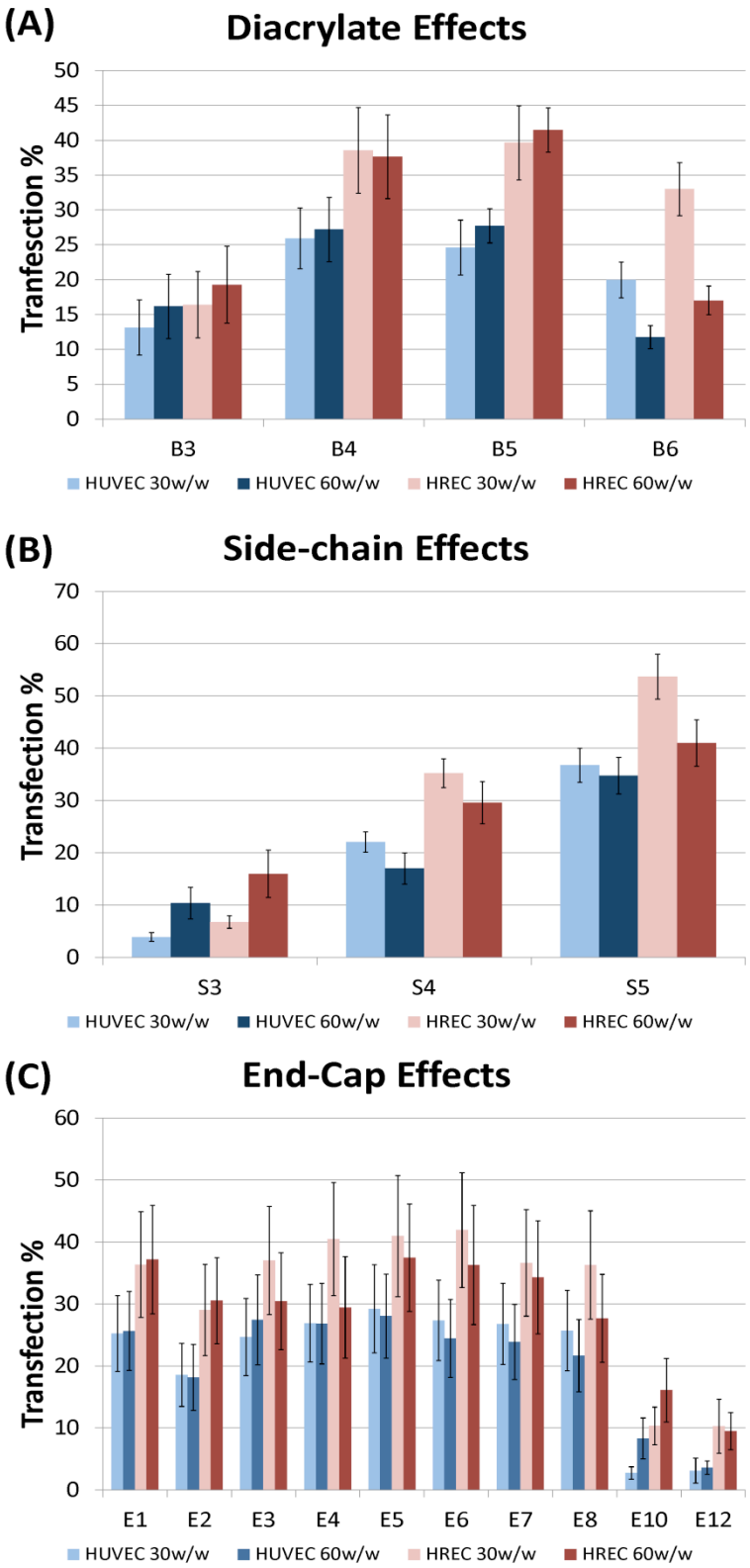

Figure 6.4. Panel of monomer effects on transfection %. Collapsing (averaging) two of three types of monomers attempt to isolate effects of each monomer change. (A) Diacrylate base, (B) Side-chain amine base, (C) End-group amine.

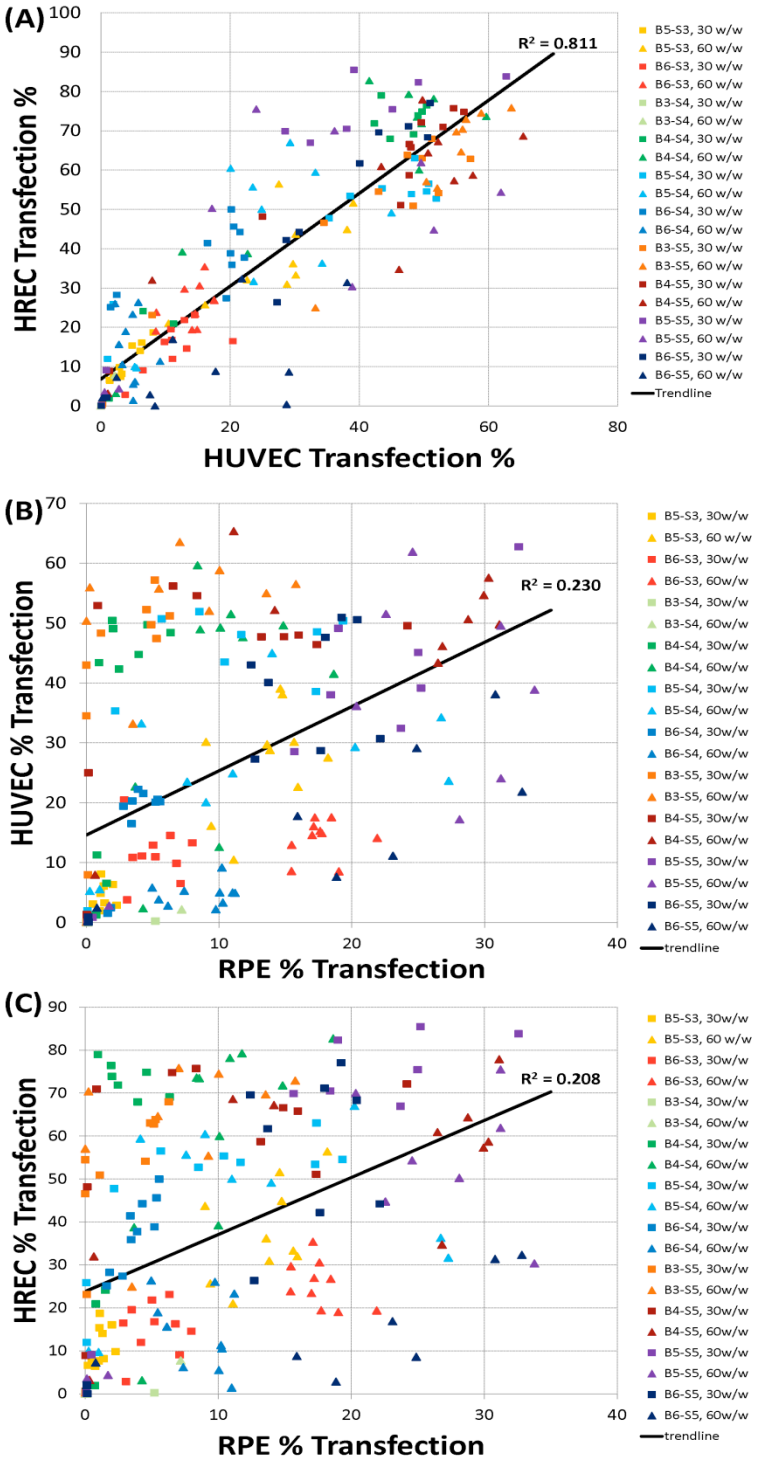

Figure 6.5. Correlation between transfection of HUVEC, HREC, and RPE cells with the polymer library. (A) There is a strong correlation between transfection of HUVEC and HRECs and (B) a much weaker correlation when compared to transfection of RPEs, or when comparing (C) HREC to RPEs.

6.6 References

1. Jo, D.H., J.H. Kim, and J.H. Kim, *How to Overcome Retinal Neuropathy: The Fight against Angiogenesis-related Blindness.* Archives of Pharmacal Research, 2010. **33**(10): p. 1557-1565.
2. Bhise, N.S., et al., *Drug delivery strategies for therapeutic angiogenesis and antiangiogenesis.* Expert Opinion on Drug Delivery, 2011. **8**(4): p. 485-504.
3. Adhim, Z., et al., *E10A, an adenovirus-carrying endostatin gene, dramatically increased the tumor drug concentration of metronomic chemotherapy with low-dose cisplatin in a xenograft mouse model for head and neck squamous-cell carcinoma.* Cancer Gene Ther, 2011.
4. Campochiaro, P.A., *Gene transfer for ocular neovascularization and macular edema.* Gene Ther, 2011.
5. Prow, T., et al., *Construction, gene delivery, and expression of DNA tethered nanoparticles.* Mol Vis, 2006. **12**: p. 606-15.
6. Spoerri, P.E., et al., *Effects of VEGFR-1, VEGFR-2, and IGF-IR hammerhead ribozymes on glucose-mediated tight junction expression in cultured human retinal endothelial cells.* Mol Vis, 2006. **12**: p. 32-42.
7. Krotz, F., et al., *Magnetofection potentiates gene delivery to cultured endothelial cells.* Journal of Vascular Research, 2003. **40**(5): p. 425-34.
8. Bhise, N.S., et al., *The relationship between terminal functionalization and molecular weight of a gene delivery polymer and transfection efficacy in mammary epithelial 2-D cultures and 3-D organotypic cultures.* Biomaterials, 2010. **31**(31): p. 8088-96.
9. Tzeng, S.Y., et al., *Non-viral gene delivery nanoparticles based on Poly(beta-amino esters) for treatment of glioblastoma.* Biomaterials, 2011. **32**(23): p. 5402-5410.
10. Sunshine, J., et al., *Small-Molecule End-Groups of Linear Polymer Determine Cell-Type Gene-Delivery Efficacy.* Advanced Materials, 2009. **21**(48): p. 4947-4951.
11. Green, J.J., et al., *Biodegradable polymeric vectors for gene delivery to human endothelial cells.* Bioconjugate Chemistry, 2006. **17**(5): p. 1162-1169.
12. Green, J.J., R. Langer, and D.G. Anderson, *A combinatorial polymer library approach yields insight into nonviral gene delivery.* Accounts of Chemical Research, 2008. **41**(6): p. 749-759.
13. Maiti, D., Z. Xu, and E.J. Duh, *Vascular endothelial growth factor induces MEF2C and MEF2-dependent activity in endothelial cells.* Invest Ophthalmol Vis Sci, 2008. **49**(8): p. 3640-8.
14. Xu, Z., Y. Yu, and E.J. Duh, *Vascular endothelial growth factor upregulates expression of ADAMTS1 in endothelial cells through protein kinase C signaling.* Invest Ophthalmol Vis Sci, 2006. **47**(9): p. 4059-66.
15. Handa, J.T., et al., *The advanced glycation endproduct pentosidine induces the expression of PDGF-B in human retinal pigment epithelial cells.* Exp Eye Res, 1998. **66**(4): p. 411-9.

16. Sunshine, J.C., et al., *Effects of Base Polymer Hydrophobicity and End-Group Modification on Polymeric Gene Delivery.* Biomacromolecules, 2011.
17. Bhise, N.S., et al., *A Novel Assay for Quantifying the Number of Plasmids Encapsulated by Polymer Nanoparticles.* Small, 2011.
18. Green, J.J., et al., *Electrostatic ligand coatings of nanoparticles enable ligand-specific gene delivery to human primary cells.* Nano Letters, 2007. **7**(4): p. 874-9.
19. Harris, T.J., et al., *Tissue-specific gene delivery via nanoparticle coating.* Biomaterials, 2010. **31**(5): p. 998-1006.
20. Shmueli, R.B., D.G. Anderson, and J.J. Green, *Electrostatic surface modifications to improve gene delivery.* Expert Opin Drug Deliv, 2010. **7**(4): p. 535-50.
21. Huang, Y.H., et al., *Nanoparticle-delivered suicide gene therapy effectively reduces ovarian tumor burden in mice.* Cancer Research, 2009. **69**(15): p. 6184-91.
22. Showalter, S.L., et al., *Nanoparticulate delivery of diphtheria toxin DNA effectively kills Mesothelin expressing pancreatic cancer cells.* Cancer biology & therapy, 2008. **7**(10): p. 1584-90.
23. MacLachlan, T.K., et al., *Preclinical Safety Evaluation of AAV2-sFLT01-A Gene Therapy for Age-related Macular Degeneration.* Molecular Therapy, 2011. **19**(2): p. 326-334.
24. Thomas, C.E., A. Ehrhardt, and M.A. Kay, *Progress and problems with the use of viral vectors for gene therapy.* Nature reviews. Genetics, 2003. **4**(5): p. 346-58.

7 Chapter 7: Transfection Of Retinal Pigment Epithelial Cells With A Combinatorial Library Of Poly(β-amino ester)s

7.1 Introduction

Many of the most debilitating ocular diseases are caused by gene deletion mutations. The ability of an ocular disease to be treated with a single gene replacement therapy was shown to be successful in principle in a canine model of Leber's Congenital Amaurosis in which RPE 65 was replaced using a recombinant adeno associated viral (AAV) delivery system that resulted in visual restoration in these animals [1]. Furthermore, early phase clinical trials studying this therapy in people suggest that gene therapy is a feasible potential strategy for retinal dystrophies [2]. A variety of genetic diseases of the retina, including retinitis pigmentosa, Best's disease, and Stargardt's disease might be excellent targets for gene replacement therapy.

Despite the initial success of gene replacement, gene delivery methods need to be optimized. There are significant limitations to viral delivery systems such as the AAV vector. The AAV vector is limited in what ocular diseases it could potentially treat because it is capable of optimally carrying 4.7-4.9 kilobases (kb) with a maximum carrying capacity of 5.2 kb [3-5] while many ocular diseases are caused by mutations to genes that are larger than 5 kb. Notable examples include Best's disease, caused by a mutation in Bestrophin-1 (14.6 kb) [6], or Stargardt's disease, caused by a mutation in the

This chapter contains excerpts from an article that was published as Sunshine JC*, Sunshine SB*, Handa JT, Green JJ. "Poly(β-amino ester)-Nanoparticle Mediated Transfection Of Retinal Pigment Epithelial Cells *in vitro* and *in vivo*." *PLoS ONE*. 2012; 7(5), e37543

ABCA4 gene (6.8kb) [7]. To address this problem, we recently reported that our non-viral delivery system using poly(beta-amino) esters (PBAEs) can accommodate large inserts to deliver up to 100 plasmids and ~500 kbp of nucleic acid per nanoparticle [8].

Non-viral systems for gene delivery offer a host of potential advantages over viruses, including reduced toxicity [9], reduced immunogenicity [10], and ease of production. However, to date, most non-viral systems are significantly less efficient at transfecting hard to transfect cell types compared to viral methods, so the major challenge remains finding an effective non-viral delivery system [11, 12]. Multiple alternative non-viral gene delivery approaches have been reported in the literature for *in vitro* transfection of retinal pigment epithelial (RPE) cells, with limited success. One report on transfection of the established RPE cell line, ARPE-19 cells, with solid lipid nanoparticles details difficulty in uptake of the particles that resulted in a transfection efficacy of only 2.5% [13]. Another study looked at optimizing several different commercially available reagents (Tfx-50, Lipofectin, Lipofectamine, Cellfectin, and DMRIE-C) for the transfection of primary RPE cells [14]. This study utilized serum free-conditions and non-confluent RPE cultures, which are associated with higher transfection efficacy [15], yet the best reagent formulated optimally, Tfx-50 at 3:1 DNA:liposome ratio, only achieved 12-15% transfection efficiency [14]. Another study looking at the transfection of primary RPE cells showed transfection efficiencies of less than 1% for Lipofectin, between 1 and 3% for DOTAP/DOGS, and up to 5% by using degraded dendrimers [15]. This limited success in transfection of ARPE-19 cells or primary RPE cells *in vitro* indicates a need for improved transfection reagents for use in the lab.

Poly(beta-amino) esters (PBAEs) [16] have shown great potential as gene delivery reagents and are easily synthesized, rapidly screened, and can be transfected into a wide variety of cell types with high efficacy *in vitro* [17-21]. PBAE nanoparticles have several advantages which help to overcome the barriers to intracellular plasmid DNA (pDNA) delivery [12]. PBAEs, when added to pH 5 buffer, are positively charged and can spontaneously form positively-charged nanoparticles (generally less than 200 nm) when added to negatively charged pDNA [8]. They get taken up via endocytosis, and enable endosomal escape by buffering the endosome [22]. They are degraded by hydrolysis of the ester bonds in the polymer backbone, enabling reduced cytotoxicity when compared to non-degradable controls [16]. Previous studies have indicated that not only was the base polymer important to its gene delivery properties, but that modification of the polymer ends can further improve transfection efficiency [17-19, 22]. We have recently found that PBAEs are highly effective (65%-85%) for the transfection of human macrovascular cells (human umbilical vein endothelial cells) and human microvascular cells (human retinal endothelial cells) and that although the efficacies of these nanoparticles are highly correlated between human vascular cell types, their efficacies are uncorrelated to human retinal pigment epithelial cells, which are also a more difficult cell type to transfect [23].

In this study, we synthesized and evaluated an expanded combinatorial library of PBAEs for evaluation of transfection efficacy and toxicity in ARPE-19 cells to identify lead polymer structures and transfection formulations for this difficult-to-transfect cell type. We discovered a lead polymer, polymer (1-(3-aminopropyl)-4-methylpiperazine-end-modified poly(1,5 pentanediol diacrylate-co-5-amino-1-pentanol) (B5-S5-E7) and

characterized it for the first time in terms of polymer molecular weight, polymer half-life, nanoparticle size, nanoparticle zeta potential, and vitro efficacy compared to leading commercially available reagents. To validate the *in vitro* screen and to evaluate the efficacy of a PBAE-based nanoparticle for gene delivery to the eye for the first time, nanoparticles were administered to mouse RPE *in vivo* by subretinal injection. Lyophilized DNA nanoparticles, utilizing a technology designed to enhance the stability and shelf-life of the biodegradable nanoparticles, were used for the *in vivo* injections. These novel nanoparticles offer opportunity both for studying diseases in the laboratory and as a potential treatment modality.

7.2 Materials and Methods

7.2.1 Materials

All reagents and solvents were obtained from commercial suppliers and used as received. Monomers were purchased from Acros Organics, Alfa Aesar, Fluka, Monomer-Polymer and Dajac Laboratories, Sigma-Aldrich, and TCI America. CMV-eGFP was amplified by Aldevron (Fargo, ND). X-tremeGENE HP DNA, Lipofectamine 2000, and Opti-MEM I were purchased from Invitrogen and used according to the manufacturer's instructions. 25 kDa PEI was purchase from Sigma Aldrich and diluted to a stock solution at 1 mg/ml in deionized water. 96 AQ_{ueous} One MTS assay was purchased from Promega and used according to the manufacturer's instructions. Dulbecco's Modified Eagle Medium (DMEM) F12 was purchased from Invitrogen and supplemented with 10% fetal bovine serum (FBS; Invitrogen).

7.2.2 Polymer Synthesis

The library of PBAEs was synthesized by adding primary amines to diacrylate compounds (1.2:1 molar ratio of diacrylate:amine) at 90^{o}C for 24h **(Figure 7.1a)**. The base polymerization reaction was performed without the use of any solvent in 20 mL glass scintillation vials, in an oven in the dark under magnetic stirring. By providing excess diacrylate in the initial polymerization reaction, diacrylate-terminated polymer was synthesized. We have recently described the synthesis and characterization of these materials [19]. The naming convention used here is designed to describe the chemical structure of each polymer. The diacrylates form the base ("B") chain of the polymer, and the primary amines form the side ("S") chains of the forming polymer. To further identify the structure of the base or side chain, a number corresponding to the number of carbons in the hydrocarbon portion of the "B" or "S" is appended; thus, B5 is a base diacrylate with 5 carbons in it's hydrocarbon portion between acrylate groups, and B5-S5 is a base polymer with 5 carbons in the hydrocarbon portion of its side chain between the amine and alcohol groups as well as 5 carbons in its hydrocarbon portion of its base chain between acrylate groups. In a second step, the acrylate ends of the polymer intermediates are modified by a second amine, resulting in the final end-modified polymers (**Figure 7.1b)**. The base polymers were end-capped by end-capping ("E") amines (at 10-fold molar excess of amine to diacrylate termini) at room temperature in DMSO at 100 mg/ml for 1 hr **(Figure 7.1b).** Specifically, 80 mg of base polymer was dissolved in 400 µl of DMSO, and combined with 320 µl of a 0.5M solution in DMSO of the end-capping amine, and placed on a multitube vortexer (VWR) and vortexed for 1 hr at 1000 RPM. The library of monomers used here is shown **(Figure 7.1c)**. For the end capping amines,

the number is simply sequential; B5-S5-E7 is an end-modified polymer with 5 carbons in the base, 5 carbons on the side chain, and which was end-modified with the E7 end-capping amine. For this study we synthesized a combinatorial library of PBAEs using 5 diacrylates, 3 amino-alcohol side chains, and 11 end-modifying amines to form 165 end-modified polymers with only small, single carbon changes to the backbone and side chains, and small modifications at the ends of the polymers. Base polymerization of all base polymers and end-capping of one base-polymer with all end-capping amines was verified by NMR; for spectra, see [19].

7.2.3 In vitro Polymer Library Transfection Screening

ARPE-19 cells were maintained as previously described [24], plated at 100,000 cells/cm^2 in 96-well plates, and allowed to grow for 72 hr until visually confluent prior to transfection with nanoparticles containing eGFP pDNA. To form the particles, polymer stock solutions at 100 mg/ml in DMSO and pDNA stock solutions at 1 mg/ml in water were separately dissolved in 25 mM sodium acetate (NaAc) buffer at pH 5.0, then combined and mixed by pipeting. Ten minutes later, 20 μl of particle solution containing 600 ng pDNA and 36 μg polymer was added to 100 μl of medium on the cells and allowed to incubate for 4 hr, when the medium was then replaced with fresh medium. For the commercially available lipid based controls Lipofectamine 2000 and X-tremeGENE HP DNA, reagents were formulated as specified by the company (at 100 ng pDNA/ well), and also tested at the same DNA dose as used in our screening (600 ng/well) to ensure that optimal, comparable controls were chosen. For PEI transfection, a PEI stock solution at 1 mg/ml was diluted in Opti-MEM I, and mixed with pDNA in Opti-MEM. The

solution was then vortexed and allowed to stand for 20 minutes before being added to cells. 24 hr post-transfection, cell viability was analyzed by the CellTiter 96® AQ_{ueous} One MTS assay using a plate reader (BioTek® Synergy 2), and is reported as a reduction in cell viability relative to untreated wells (100% - absorbance of well/untreated, normalized to no cells in the well). 48 hr post-transfection, transfection efficacy was analyzed by flow cytometry (Accuri C6 with Hypercyte high-throughput plate adaptor).

7.2.4 Preparation of lyophilized nanoparticles

Freeze dried pDNA nanoparticles were prepared by dissolving 36 µl of 100 mg/ml polymer in DMSO in 324 µl of 25 mM sodium acetate buffer (pH 5.0), and then adding 60 µl of 1 mg/ml pDNA (total 60µg) with 60 µl of 25 mM sodium acetate buffer (pH 5.0). The mixture was vortexed, and allowed to self-assemble for 10 minutes. The nanoparticles were split into two batches and 120 µl of 90 mg/ml sucrose was added to each. The sample was then flash-frozen in liquid nitrogen, and placed on a lyophilizer for freeze-drying. The dried particles (containing 30 µl pDNA) were then resuspended to 30 µl total volume in deionized water (thus resulting in a particle DNA concentration of 1 mg/ml) just prior to subretinal injection.

7.2.5 Particle Sizing and Zeta Potential measurements

Particle sizing was performed using a NanoSight NS500 (NanoSight Ltd. Wiltshire, UK). Each sample was diluted 1:50 from the transfection concentrations (n=3); for the lyophilized samples, each sample was diluted to the same DNA concentration as the freshly prepared samples. For zeta potential measurements, 800 microliters of particle

solution containing 5 micrograms of pDNA was diluted into PBS to a total volume of 800 μl and added to a disposable zeta cuvette, and measured in using a Malvern Zetasizer NanoZS.

7.2.6 Polymer Degradation

250 ml of a 100 mg/ml solution of B5-S5-E7 in DMSO was added to 250 mL of phosphate buffered saline (PBS) solution at 37^{o}C. At each time point, 25 mL of this solution was removed and frozen, then lyophilized to remove the water. This sample was dissolved in a solution of 94% THF, 5% DMSO and 1% piperidine, and organic phase permeation chromatography (GPC) was performed using the same solvent as an eluent at a flow rate of 1 mL/minute. The detector (Waters 2414 refractive index detector) and columns (three Waters Styragel columns, HR1, HR3, and HR4, in series) were maintained at 40°C throughout the runs. Polymer molecular weights presented are relative to monodisperse polystyrene standards (Shodex, Japan).

7.2.7 Subretinal Injections

Subretinal injections were performed in both eyes of 3 month old C57Bl6 mice using a Pico-Injector (PL1-100, Harvard apparatus, Holliston, MA). Mice were anesthetized by intramuscular (IM) injection of Ketamine (80mg/kg)/Xylazine (16mg/kg). Pupils were dilated using 2.5% Phenylephrine Hydrochloride Ophthalmic solution (AK-DILATE, Akorn, Lake Forest, IL) followed by administration of 0.5% Tetracaine Hydrochloride Ophthalmic solution (Phoenix Pharmaceutical Inc., St. Joseph, MO) eye drops just before the injection. The conjunctiva adjacent to the cornea was grasped with

forceps to allow optimal exposure of the injection site. A hole was made at the pars plana with the tip of a 30-gauge sterile (PrecisionGlide) needle. A 20~30μm (I.D.) micropipette glass needle tip mounted on a Pico-Injector holder was inserted in the hole, through the vitreous, and into the potential subretinal space. One ml of PBAE nanoparticles with eGFP pDNA and/or naked eGFP pDNA (at 1 mg/ml DNA, as described above in "Preparation of lyophilized nanoparticles") was then delivered. The retinal area injected was visualized as a retinal bleb or a slight retinal detachment. Subretinal injections were made under direct observation aided by a Zeiss dissecting microscope at 6x magnification. Immediately following injection of the nanoparticles, a small amount of Bacitracin Zinc and Polymyxin B Sulfate Ophthalmic ointment (Akorn, Buffalo Grove, IL) was applied to the eye. Mice were sacrificed 72 hr later with ether and cervical dislocation. Eyes were enucleated, and the cornea and lens were removed. The retina and RPE/choroid were dissected and prepared for RNA extraction. The fellow eye was prepared for flat mount using confocal microscopy. Fluorescence intensity was analyzed with ImagePro software. The eyes with surgical complications were excluded from the study.

7.2.8 Statistical Analysis

GraphPad Prism 5 software was used for all statistical analysis. For comparison of best polymer formulation (B5-S5-E7 at 60 w/w) with commercially available controls with respect to transfection and reduction in cell metabolic activity, we performed a 1-way ANOVA with a Dunnet post-test using B5-S5-E7 at 60 w/w as the control column. For comparison of base polymer structural effects with respect to transfection and reduction in cell metabolic activity, we performed a 2-way ANOVA with a Bonferroni

post-test to compare all columns to each other. A student's T-test was used for comparison of mRNA expression after subretinal injection of nanoparticles versus pDNA alone.

7.3 Results

7.3.1 Transfection efficacy and cytotoxicity in ARPE-19 cells

The transfection efficacy of the nanoparticle formulations (30 and 60 w/w polymer:DNA ratio, 600 ng/well DNA dose in a 96 well plate) ranged from 0-44% GFP+ cells (**Figure 7.2**), with only small, single carbon changes to the backbone of the polymer structure or small changes to the ends of the polymers. To look at the effects of single carbon changes along the base polymer with respect to transfection efficacy, we averaged across the various end-modified versions of the same base polymer (**Figure 7.3**) and performed a 2-way ANOVA to examine the trends statistically (**Table 7.1**). Generally, transfection efficacy tended to increase with increasing hydrophobicity of the diacrylate or side chain in the base polymer. Interestingly, for the least hydrophobic backbones (B3b, B4) the biggest changes (and the only statistically significant ones) with respect to transfection efficacy occurred when increasing the side chain hydrocarbon length from 3 to 4 carbons, whereas with the more hydrophobic backbones (B5, B6), the only statistically significant increases in transfection efficacy occurred when increasing the side chain hydrocarbon length from 4 to 5 carbons. Only intermediately hydrophobic base diacrylates B4 and B5 showed strong statistically significant improvements when increasing the side chain length from 3 to 5 carbons.

The vast majority of the nanoparticle formulations showed only small reductions in cell metabolic activity compared to untreated controls (**Figure 7.4**), with the exception of some of the B6-S4, B6-S5 and E9-end modified polymers. To look at the effects of single carbon changes along the base polymer with respect to cell cytotoxicity, we averaged across the various end-modified versions of the same base polymer (**Figure 7.5**) and performed a 2-way ANOVA to examine the trends statistically (**Table 7.1**). Cytotoxicity, like transfection efficacy, also tended to increase with increasing hydrophobicity of the diacrylate or side chain in the base polymer (**Figure 7.5**). There was increased cytotoxicity with the most hydrophobic side chain, S5 ($p<0.001$ for 60 w/w with B3, B4, B5 and B6) as compared to the least hydrophobic side chain S3. Interestingly, The least hydrophobic backbones (B3, B3b) only showed increased cytotoxicity when the side chain length increased from 4 to 5 carbons and not from 3 to 4 carbons at 60 w/w, whereas the more hydrophobic backbones (B4, B5, and B6) showed increased cytotoxicity when the side chain length increased from 3 to 4 carbons ($p < 0.01$ for all 3), but no significant increase in cytotoxicity with side chain length increasing from 4 to 5 carbons. Cytotoxicity also increased with increasing hydrophobicity of the base diacrylate, although there seems to be no increase in toxicity when the backbone contains 4 carbons (B4) between diacrylate groups as compared to only 3 (B3).

The formulation with the highest transfection efficacy was B5-S5-E7 at 60 w/w polymer:DNA (44±5%), and it was also relatively non-toxic (23% cell cytotoxicity) following transfection. This is significantly higher transfection than has been previously reported in the literature [13-15], and was significantly higher than optimized formulations of FuGeneHD (Roche) or Lipofectamine 2000 (Invitrogen), two of the

leading commercially available, cationic lipid based transfection reagents, or 25 kDa branched polyethyleneimine (**Figure 7.6**). Lipofectamine 2000 was optimal at a 4 to 1 ratio of lipid:DNA and enabled 26±7% transfection and 16±3% toxicity. X-tremeGENE HP DNA was optimal at a 600 ng DNA dose with a 5 to 1 ratio of lipid:DNA, yielding 22±6% transfection and 32±9% toxicity. Branched 25 kDa polyethyleneimine (PEI) performed optimally at a 3:1 ratio at 600 ng DNA/well, only achieving 8±1% transfection efficacy with 25±6% toxicity. A 1-way ANOVA with a Dunnet post-test with B5-S5-E7 as the control column showed that B5-S5-E7 at 60 w/w was significantly more efficacious than any of the positive controls ($p < 0.001$) but maintained comparable cell viability ($p > 0.05$ for all controls at 600 ng/well except for Lipofectamine 200 at a ratio of 2:1).

In general, increased transfection brought with it concomitant increased cytotoxicity (**Figure 7.7**), but many formulations were either ineffective but moderately toxic or effective but fairly non-toxic. In general, among the base polymers which enabled high transfection, polymers containing B3-S5 were on the "bad" side of the best fit line (higher cytotoxicity relative to their transfection) and B4-S5 containing polymers were on the "good" side of the best fit line (lower cytotoxicity relative to their transfection). This can also vary by end group – B5-S5-E7 achieved the highest transfection efficacy (44±5%) with relatively low cytotoxicity (23±6%), but B5-S5-E4, with the same base polymer but different end group, transfected only 22% of cells with 39% cytotoxicity.

7.3.2 Nanoparticle Physical Characterization

Our lead polymer from the *in vitro* study, B5-S5-E7, when prepared in a large batch and purified, is moderately polydisperse, with a polydispersity index of 3.2, a number averaged molecular weight of 25,000 Da, and a weight-averaged molecular weight of 80,000 Da. It is hydrolytically degradable, with a free polymer half-life of 4.6 hr in physiological salt solution at 37^{o}C (**Figure 7.8**). When complexed with pDNA, it forms nanoscale particles (hydrodynamic diameter of 180 nm), which are positively charged (zeta potential of +26 mV). The particles, when lyophilized, retain these characteristics, showing very comparable zeta potential and particle size after undergoing the freeze-drying process and being resuspended (**Figure 7.9**).

7.3.3 Subretinal Injection of Lyophilized GFP-Nanoparticles

A successful subretinal injection caused a bleb or retinal detachment of approximately 1/8 to 1/4 of the retina. Subretinal injection (n=5) of 1 μl of 1 mg/ml lyophilized pDNA nanoparticles (60 w/w B5-S5-E7:DNA) resulted in significant transfection in the area of injection (**Figure 10b**), and quantitatively increased by over 1000-fold the expression of GFP mRNA by RT-PCR in both the retina ($p < 0.001$) and the RPE/choroid ($p = 0.003$; **Figure 10c**) 72 hr post injection as compared to control subretinal injections of pDNA alone (n=3).

7.4 Discussion

Standard non-viral transfection protocols for *in vitro* transfection of RPE cells achieve only limited to moderate success in terms of transfection efficiency. In addition,

unlike typically optimal *in vitro* transfection conditions, where the transfection is done without serum and with cells in a sub-confluent state to maximize transfection, *in vitro* conditions were chosen here to more closely match the *in vivo* state. As RPE cells in the mature eye are not rapidly dividing and particles will come into contact with proteins before reaching cell surfaces, we used confluent cells in the presence of serum for our *in vitro* studies.

Figures 2-6 show interesting trends to guide the design of polymeric nanoparticles for transfection of retinal pigment epithelial cells. As seen previously in studies looking at transfection of COS-7 monkey kidney cancer cells [19], we can see interplay between the hydrophobicity of the base diacrylates and the side chain amino-alcohols (for statistical analysis, see **Table 7.1**). For example, relatively hydrophilic base polymers containing the shortest side chain, S3, were generally ineffective, and required the most hydrophobic base diacrylates, B5 and B6, to see any transfection efficacy. They were also non-toxic. On the other hand, polymers containing the most hydrophobic side chain, S5, were nearly all reasonably effective in transfection. Optimal transfection for many end-groups was achieved with the intermediately-hydrophobic base-diacrylates B4 and B5 and most hydrophobic side chain S5. End-modified polymers with the most hydrophobic base group (B6) did not tend to be as effective and also were associated with more cytotoxicity, and B3-S5 end-modified polymers were not as efficacious but were non-toxic. Interestingly, increasing the hydrophobicity of the side chain from 3 to 4 carbons in length tended to increase the transfection efficacy of polymers containing the least hydrophobic base diacrylates without increasing the cytotoxicity, whereas increasing the side chain length from 4 carbons to 5 carbons for the most hydrophobic

base diacrylate only increased the cytotoxicity of the formulation without increasing transfection efficacy. Taking this together suggests that polymer hydrophobicity plays a key role in the transfection efficacy of these complexes, but that there is a limit at which polymer hydrophobicity no longer increases transfection efficacy as fast as it increases cytotoxicity, such that there is an optimal hydrophobicity for PBAE based non-viral gene delivery vectors.

End-modification of the polymers had a clear and strong effect, with polymers end-modified with E1 and E3-E8 tending to be more successful, and polymers modified with E9, E10, and E12 end-modifications tending to be less effective. Increasing polymer to pDNA weight ratio from 30 w/w to 60 w/w tended to both increase transfection efficacy and cytotoxicity; however, even at 60 w/w the cytotoxicity was moderate for most transfection conditions. Molecular weight was previously found to not vary the transfection efficacy of these materials [19], so that these differences in efficacy are likely due directly to the small changes in chemical structure that we observe. These small changes in structure may play a role in changing the DNA/polymer binding properties, changing the particle size, and changing the degradation rate of the nanoparticles, all of which could play a significant role in the observed gene delivery properties of the polymer library.

We next sought to test the most successful type of nanoparticle *in vivo*. However, *in vivo* injections into the eye require low volumes and highly concentrated pDNA nanoparticles. The maximum volume that can be injected into the mouse eye is 1 μL. Simply scaling down our transfection protocol to the 1 μl volume required for the subretinal injections would have allowed us to deliver only 30 ng of DNA to the eye. Due

to the hydrophobicity of the polymers, formulation of particles at greater than 30-fold higher concentration (which would be required for our desired 1 μg dose to the eye) in standard aqueous conditions is not possible due to polymer solubility constraints. However, our lab has recently developed a protocol to formulate PBAE-based nanoparticles by adding sucrose as a cryoprotectant and then freeze-drying the particles. This process has been shown to allow long-term storage of the particles, with complete retention of transfection efficiency in glioblastoma cells after 3 months [20]. Although *in vitro* transfection efficacy has been validated using this procedure, *in vivo* efficacy of these lyophilized PBAE nanoparticles is unknown. Since the dry polymer/DNA nanoparticles can be resuspended following lyophilization in minimal water volumes, we hypothesized that we could increase nanoparticle concentration using this procedure. This is likely because resuspension of the nanoparticles requires formation of a colloidal suspension of polymer/DNA nanoparticles and does not require solvation of free polymer at the same concentrations. The cryoprotectant is also required for this step, as particles formed without cryoprotectant were unable to be resuspended. We were able to formulate 60 w/w particles with 30 μg of pDNA, add sucrose, freeze dry the particles, and then resuspend the particles to 30 μl total volume in water, thus allowing the injection of 1 μg of DNA in 1 μl. This technique has several advantages beyond simply increasing the concentration of the particles, such as easy storage and low risk of degradation.

Significant transfection of the RPE and retina was achieved with subretinal injection of 1 μl of 1 mg/ml DNA nanoparticles, in the area of injection (**Figure 9b**). Quantitatively, there was over 1000-fold increase in expression of GFP mRNA by RT-PCR in both the retina and the RPE/choroid (**Figure 9c**). The relative expression of GFP

mRNA varied between the different mice (86-3800 fold increase in the retina, and 50-5000 fold increase in the RPE/choroid), compared to naked eGFP DNA injection. Nonetheless even the lowest transfection is significantly higher than other delivery systems. A recent article by Muna Naash's laboratory studied CK30PEG10k complexed with eGFP to transfect RPE and found a 2.5 fold increase in eGFP expression in the RPE compared to a naked pDNA control [25]. Interestingly, they found similar uptake of GFP with CK30PEG10k as with naked GFP due to the RPE cell's ability to phagocytoze naked GFP, and attributed their 2.5-fold improvement in transfection to improvements in downstream nuclear import [25]. Here, we are able to show a >1000-fold increase in GFP expression in the retina and RPE with our nanoparticles, which are specifically designed for improved intracellular delivery. PBAE nanoparticles are believed to improve intracellular delivery by binding and protecting pDNA, and facilitating both endosomal escape and the release of the DNA to the cytoplasm [22].

Here we show that poly(beta-amino) ester-based nanoparticles have great promise for delivery of plasmids to RPE cells. These nanoparticles are small in size (180 nm), have a positive zeta potential (+26 mV), and easily degrade in water. Many polymer formulations showed transfection efficacy that was significantly superior to Lipofectamine 2000 and FuGeneHD, two of the lead commercially available alternatives for non-viral gene delivery, with comparable cellular viability. The lead polymer, 1-(3-aminopropyl)-4-methylpiperazine-end-modified poly(1,5 pentanediol diacrylate-co-5-amino-1-pentanol) (B5-S5-E7), at 60 w/w polymer:DNA ratio was able *in vitro* to transfect 44% of ARPE-19 cells that were visually confluent with minimal cytotoxicity. Therefore, this novel nanoparticle has many potential benefits to further investigate

ocular diseases. The successful transfection of the RPE *in vivo* with lyophilized nanoparticles using this polymer formulation suggests that this technology could be useful in the future *in vivo* both in the lab and possibly in the clinic, to help ameliorate genetic diseases of the retina.

7.5 Figures

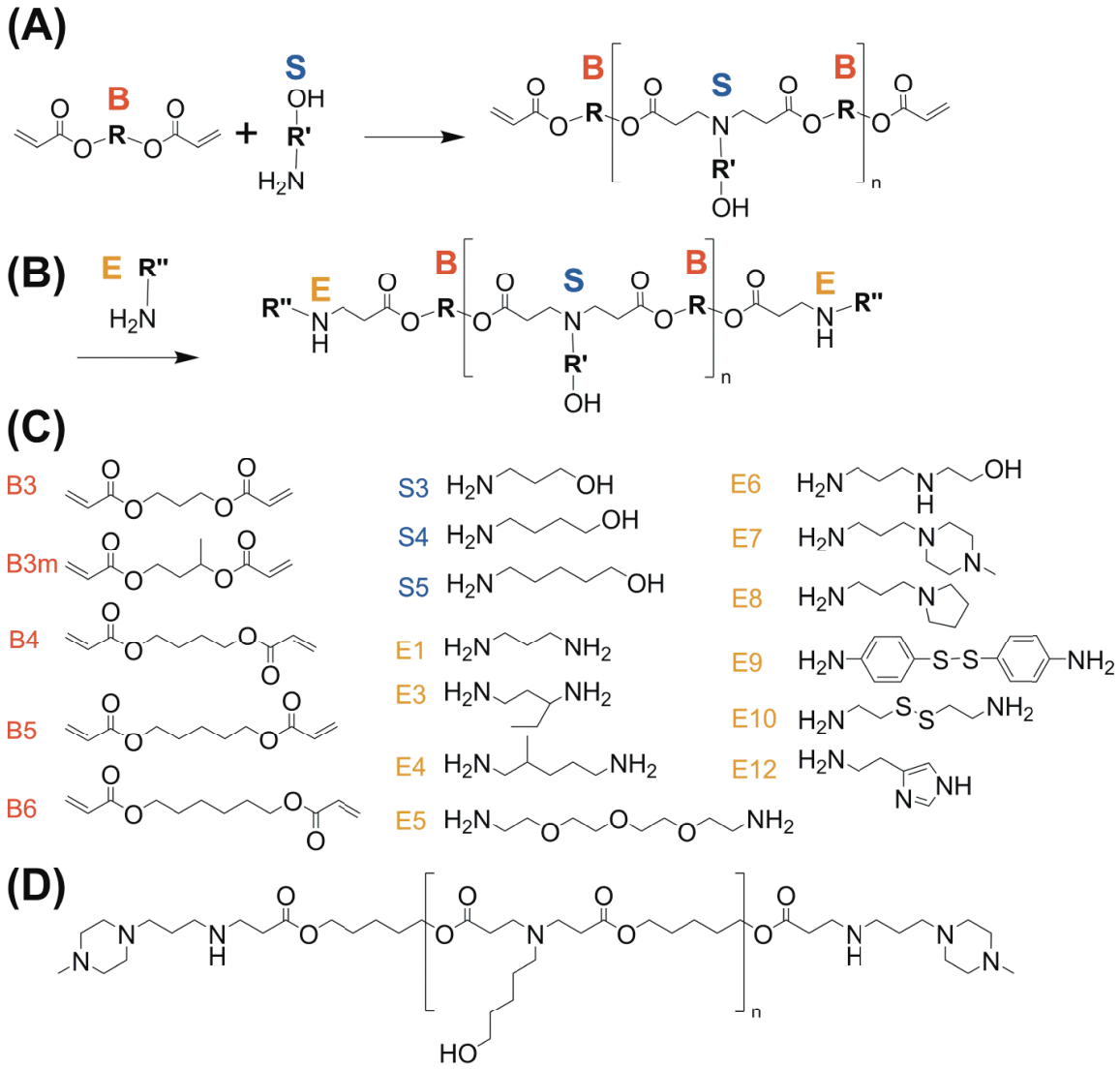

Figure 7.1: Schematic showing polymerization scheme and monomers used in Chapter 7. (A) Diacrylates ("B") were added to primary-amine containing amino-alcohol side chains ("S") to form the base polymers. (B) Base polymers were end-capped with amine monomers ("E") to form the final, end-modified polymers. (C) The base diacrylate ("B"), amino-alcohol side chain ("S"), and end-modifying amines ("E") used in the polymer library are listed here. (D) The full structure of B5-S5-E7 (1-(3-aminopropyl)-4-methylpiperazine-end-modified poly(1,5 pentanediol diacrylate-co-5-amino-1-pentanol) is shown here.

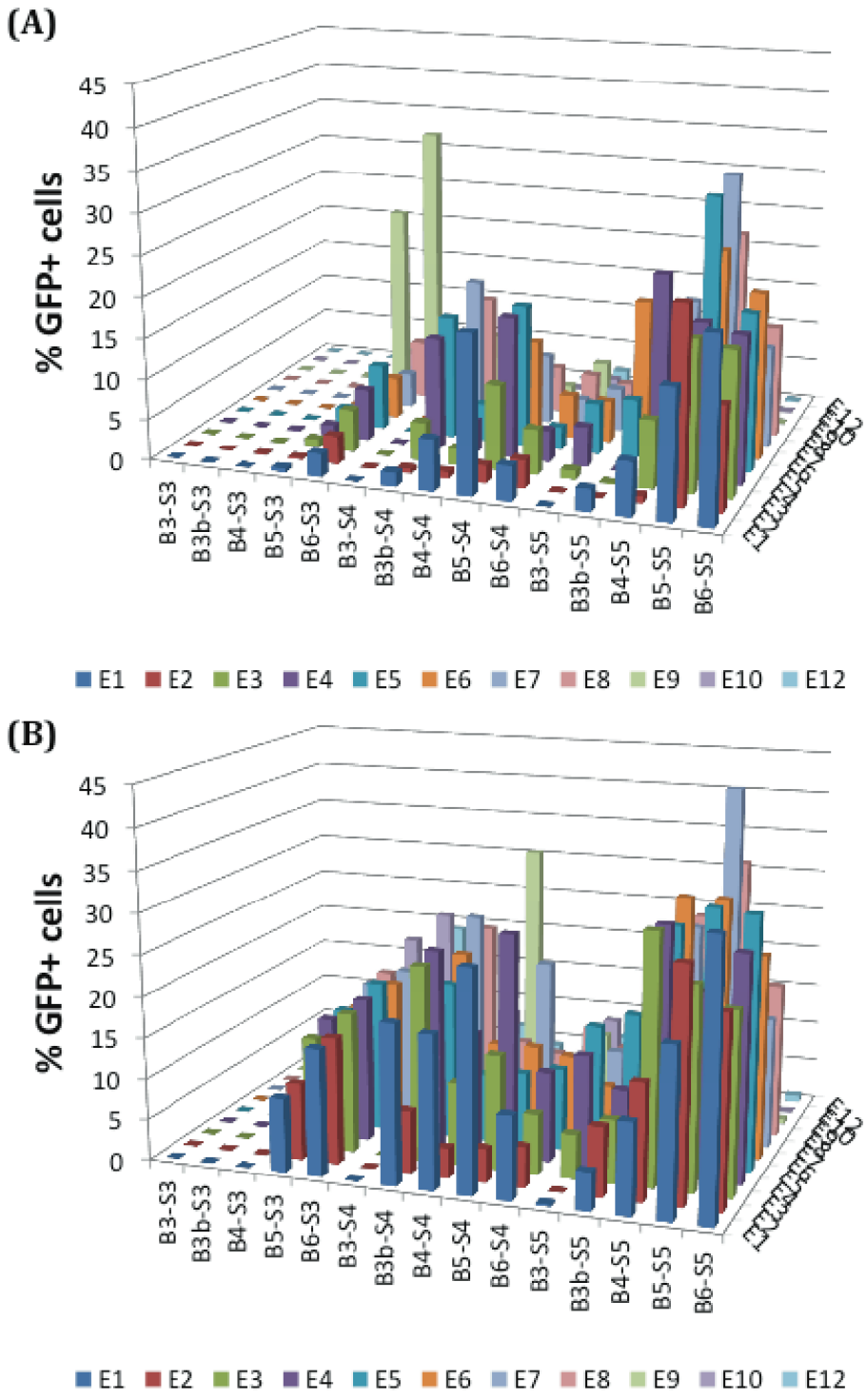

Figure 7.2: Bar graph displaying confluent ARPE-19 cell-sheet transfection efficacy (%GFP+ cells by FACS) of polymer formulations (n=4) in our library screen. (a) Transfection efficacy of polymer library formulated at 30 w/w ratio. (b) Transfection efficacy of polymer library formulated at 60 w/w ratio. Optimal formulation B5-S5-E7 at 60 w/w resulted in 44% transfection efficacy as compared to 26% for Lipofectamine 2000, 22% for ExtremeGENE HP DNA, and 8% for branched 25 kDa PEI.

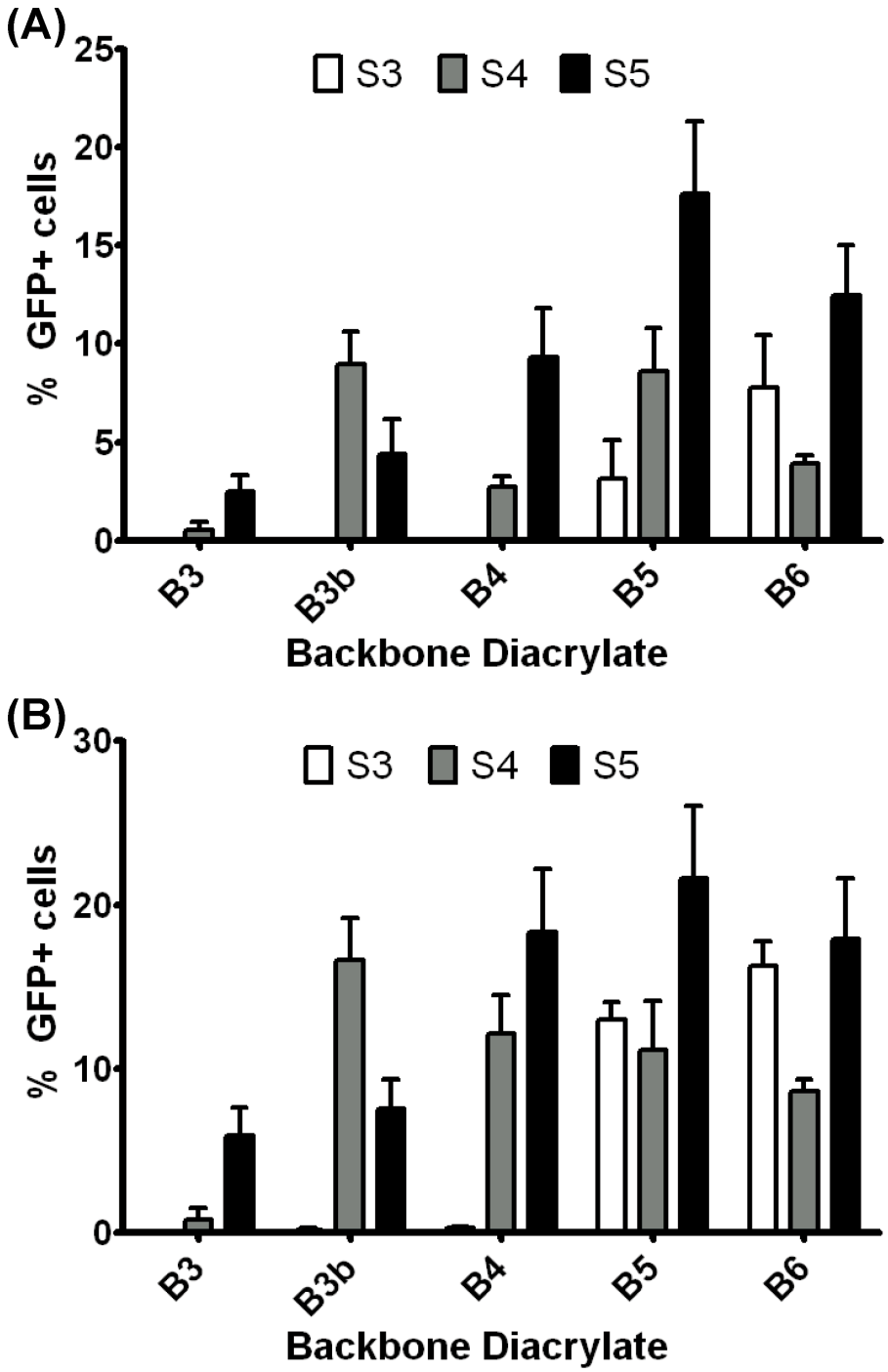

Figure 7.3: Comparison of base polymer structure with transfection efficacy. Each bar represents the average transfection efficacy associated with the end-modified polymers that contained the base polymer shown (n=11; error bar = SEM). Base diacrylate and side chain amino-alcohols are shown from least hydrophobic to most hydrophobic from left to right. (a) Transfection efficacy of 30 w/w formulations averaged over 11 end-modified amines containing the base polymer shown. (b) Transfection efficacy of 60 w/w formulations averaged over 11 end-modified amines containing the base polymer shown. For statistical analysis, see Table 1.

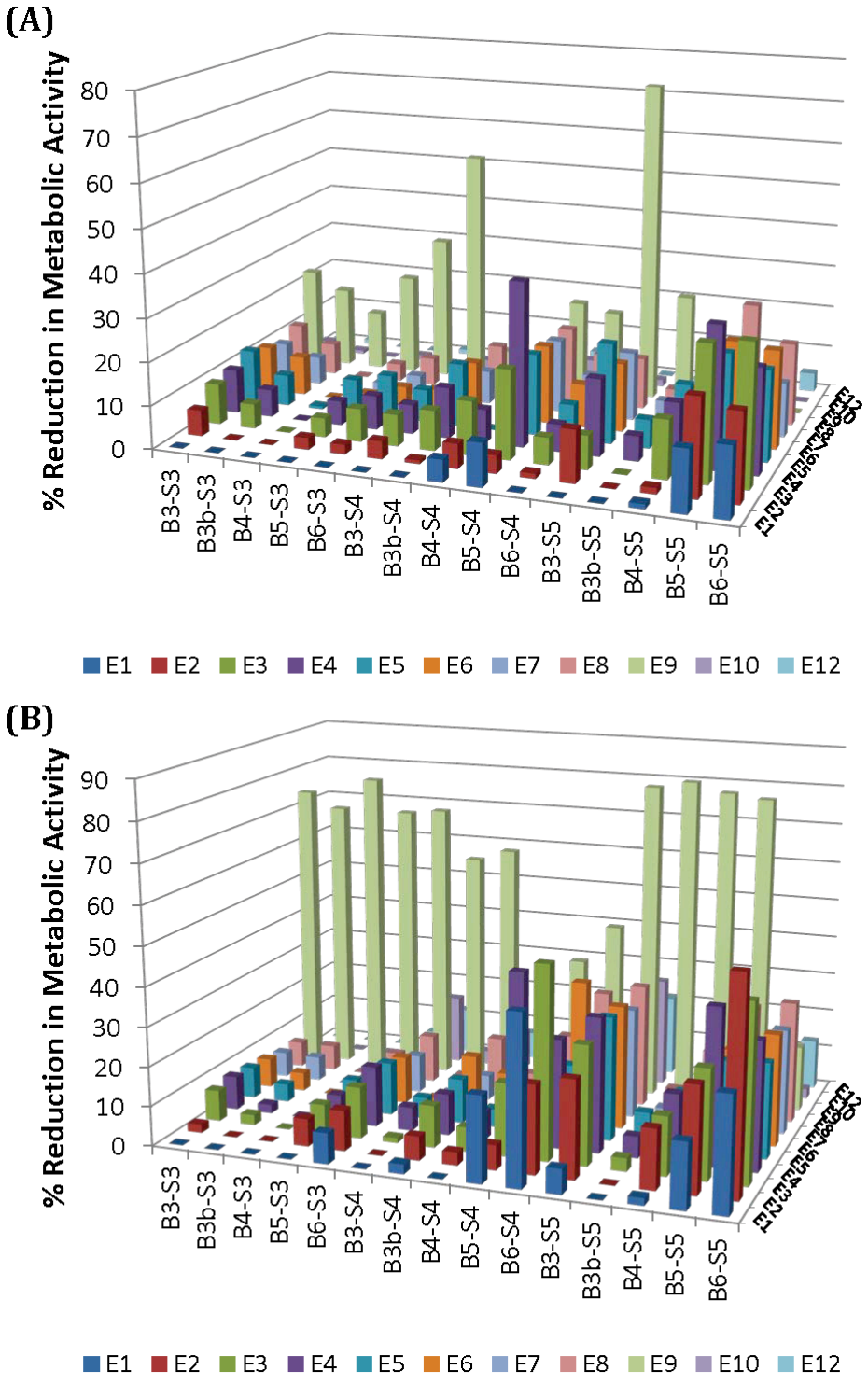

Figure 7.4: Reduction in metabolic activity following PBAE nanoparticle administration. Formulations plotted at 0% reduction of metabolic activity here had equivalent or slightly higher metabolic activity than untreated controls. (a) Reduction in metabolic activity post transfection with polymer library formulated at 30 w/w ratio (n=4). (b) Reduction in metabolic activity post transfection with polymer library formulated at 60 w/w ratio (n=4).

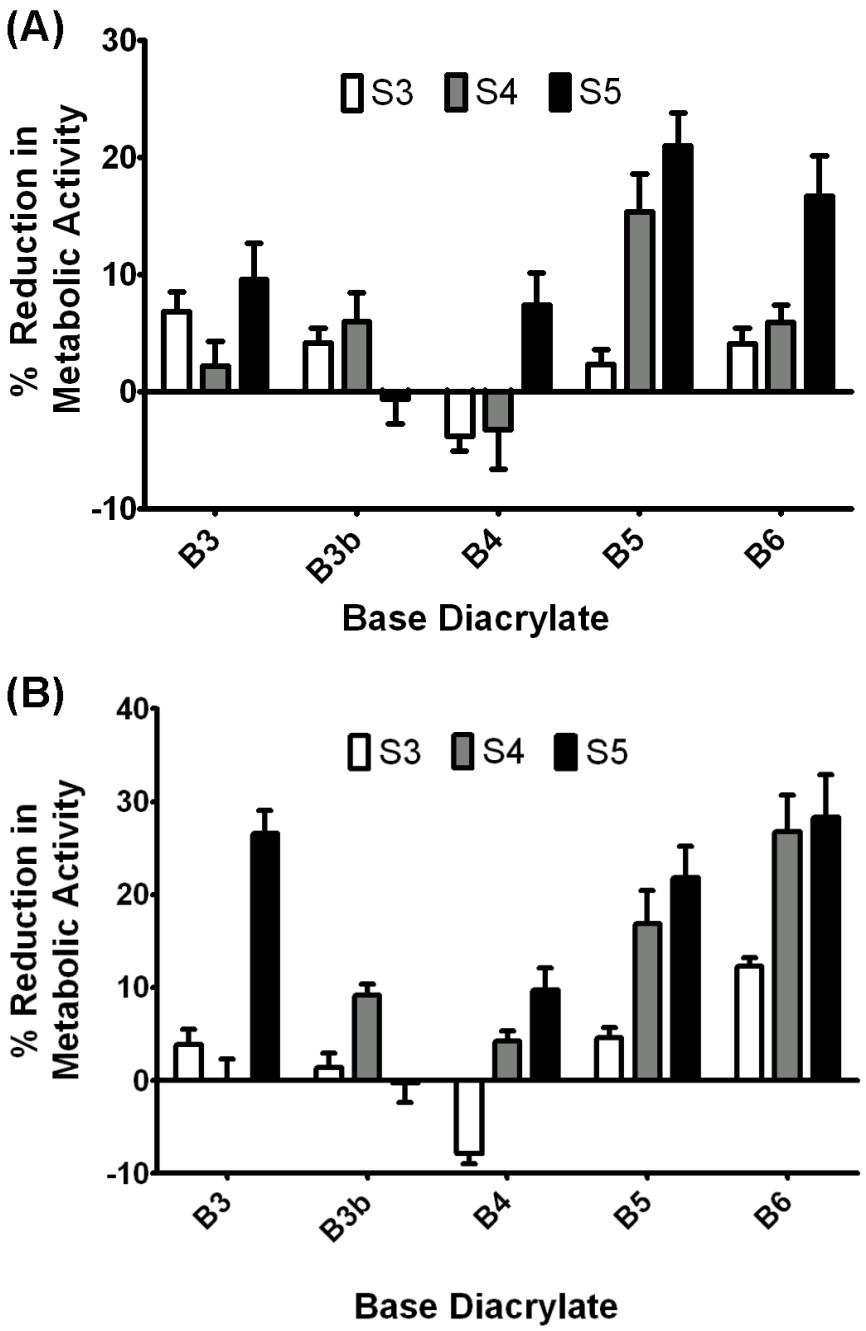

Figure 7.5: Comparison of base polymer structure with reduction in metabolic activity. Each bar represents the average toxicity associated with the end-modified polymers that contained the base polymer shown (n=11; error bar = SEM). Base diacrylate and side chain amino-alcohols are shown from least hydrophobic to most hydrophobic from left to right. (A) Reduction in metabolic activity of 30 w/w formulations averaged over 10 end-modified amines containing the base polymer shown. (B) Reduction in metabolic activity of 60 w/w formulations averaged over 10 end-modified amines containing the base polymer shown. For statistical analysis, see **Table 7.1**.

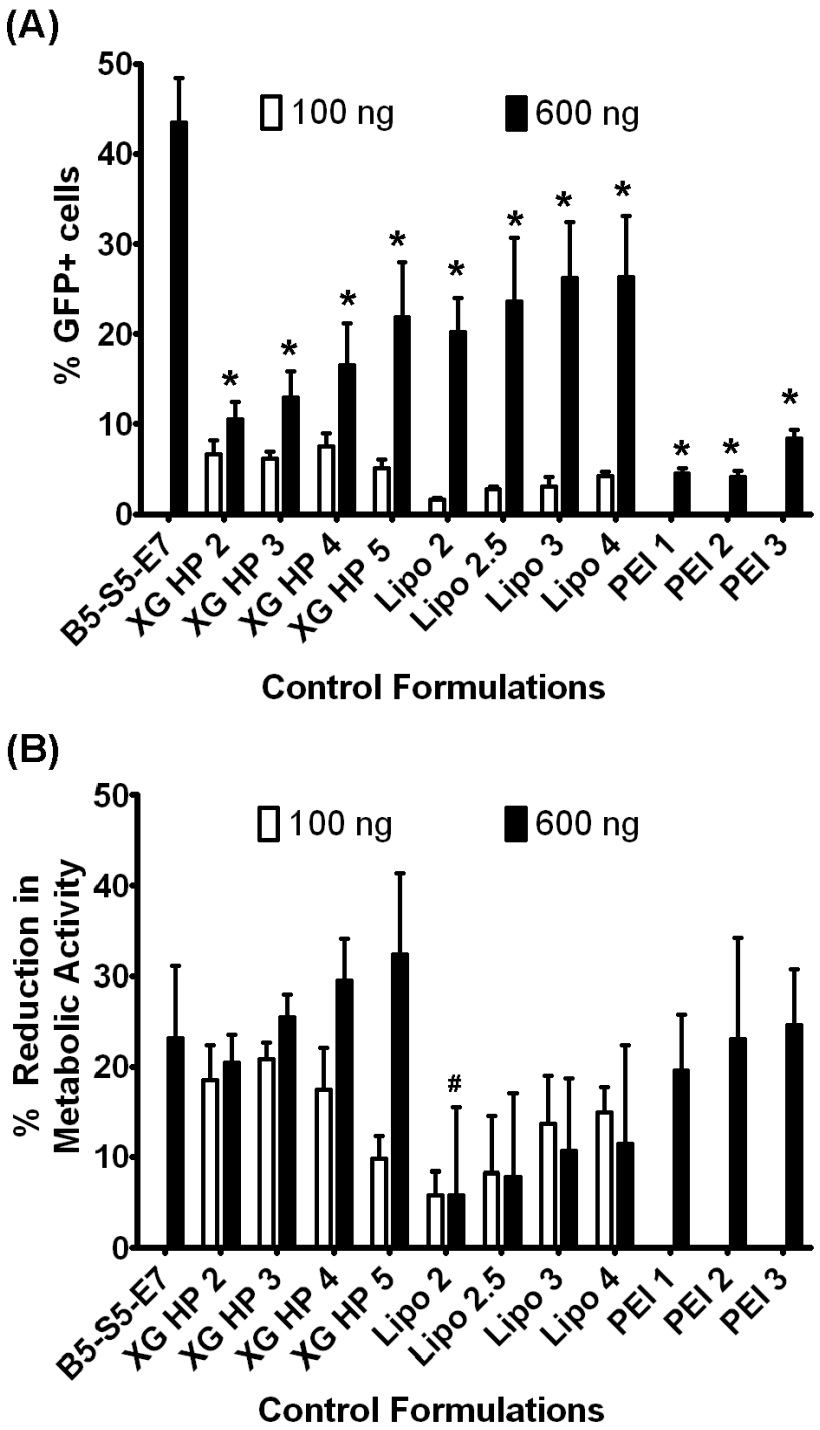

Figure 7.6: Comparison to commercially available transfection reagents. (XG HP = XtremeGENE HP; Lipo = Lipofectamine 2000; PEI = 25 kDa branched polyethyeleneimine). The numbers next to the reagent name corresponds to the ratio of lipid (v/v) or polymer (w/w) to DNA used. (A) Transfection efficacy of control formulations and B5-S5-E7 at 60 w/w (n=4); * indicates $p < 0.001$ vs. B5-S5-E7 at 60 w/w. (b) Reduction of metabolic activity of control formulations and B5-S5-E7 at 60 w/w (n=4); # indicates $p < 0.05$ vs. B5-S5-E7 at 60 w/w.

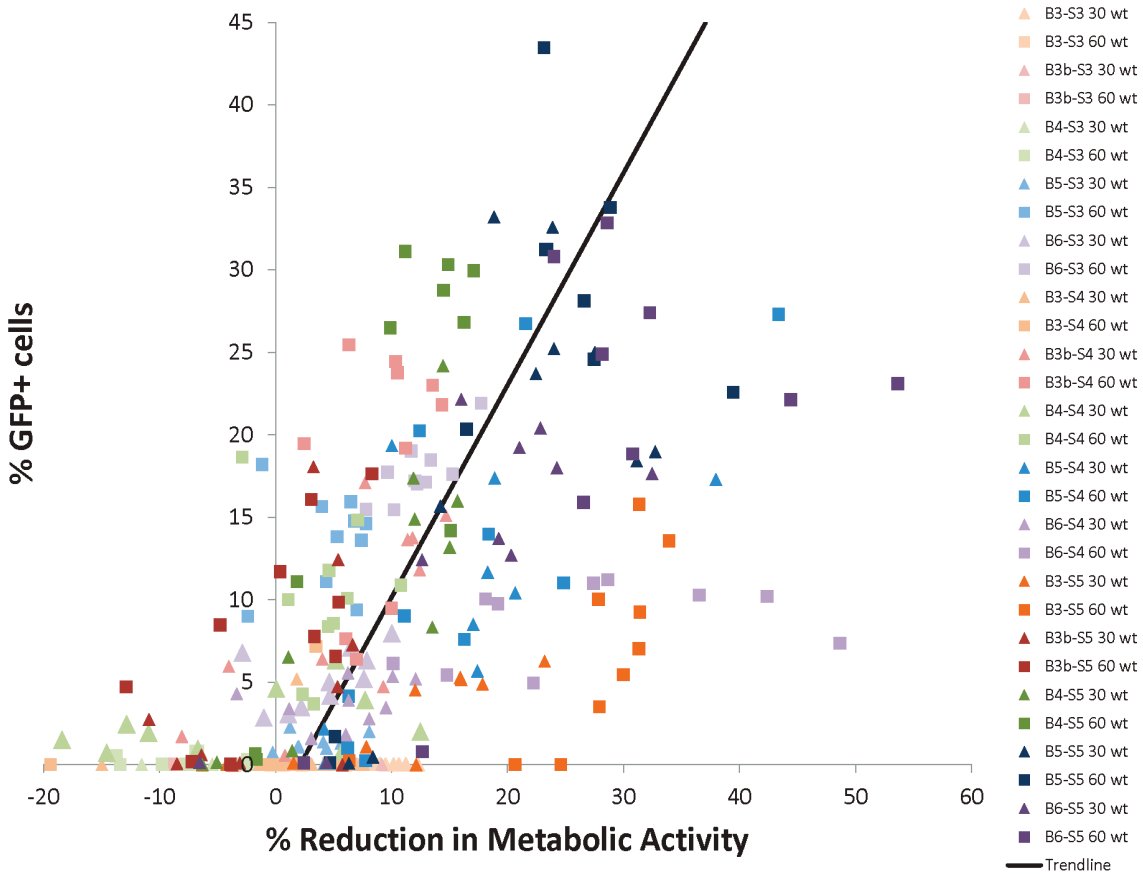

Figure 7.7: Comparison of transfection efficacy to reduction in metabolic activity of the polymers in the polymer library. There is an overall trend of increasing cytotoxicity with increasing transfection efficiency (the best-fit line represents a 0.77% decrease in cell metabolic activity with every 1% increase in transfection efficiency of the formulation) but the trend only explains a portion of the results ($R^2 = 0.37$). A number of polymer formulations exhibited high transfection efficiencies and low concomitant cytotoxicities.

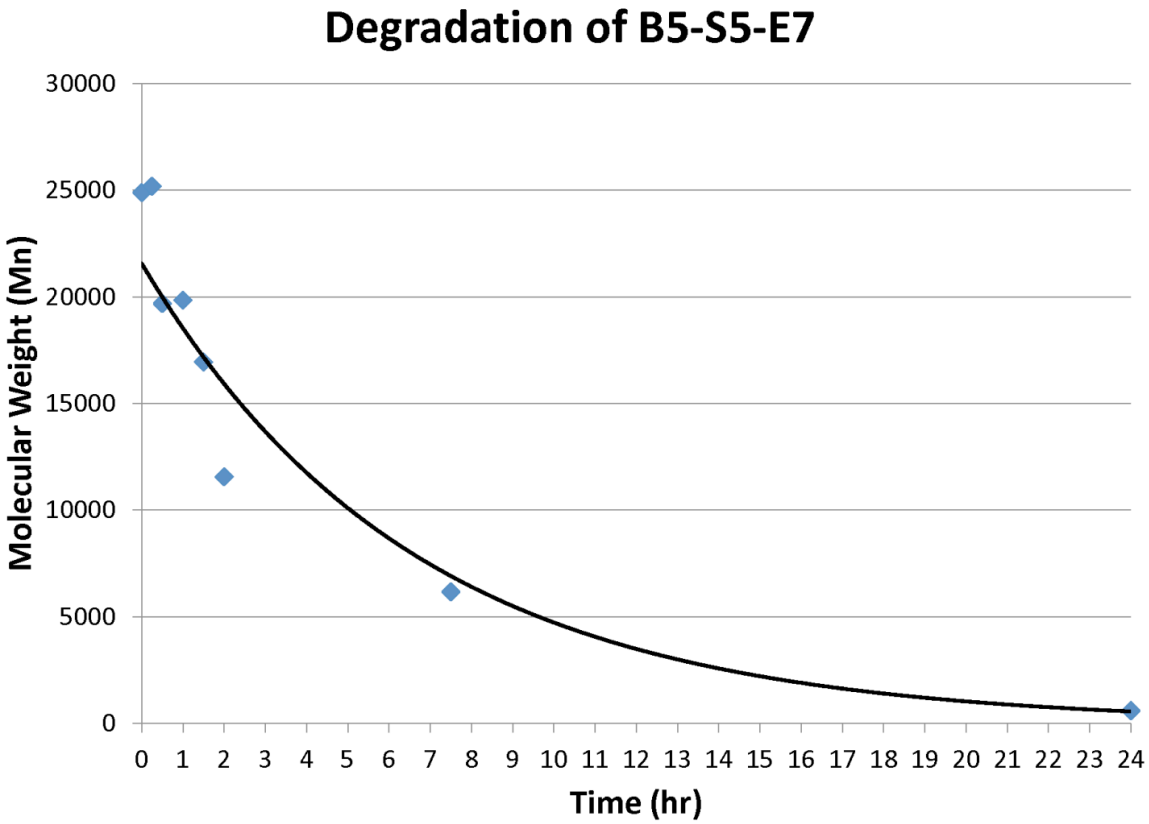

Figure 7.8: Number-averaged molecular weight versus time of B5-S5-E7 in PBS at 37C with agitation. The half-life of the polymer in solution was 4.6 hr ($R^2 = 0.984$), and the polymer was almost completely degraded within 1 day.

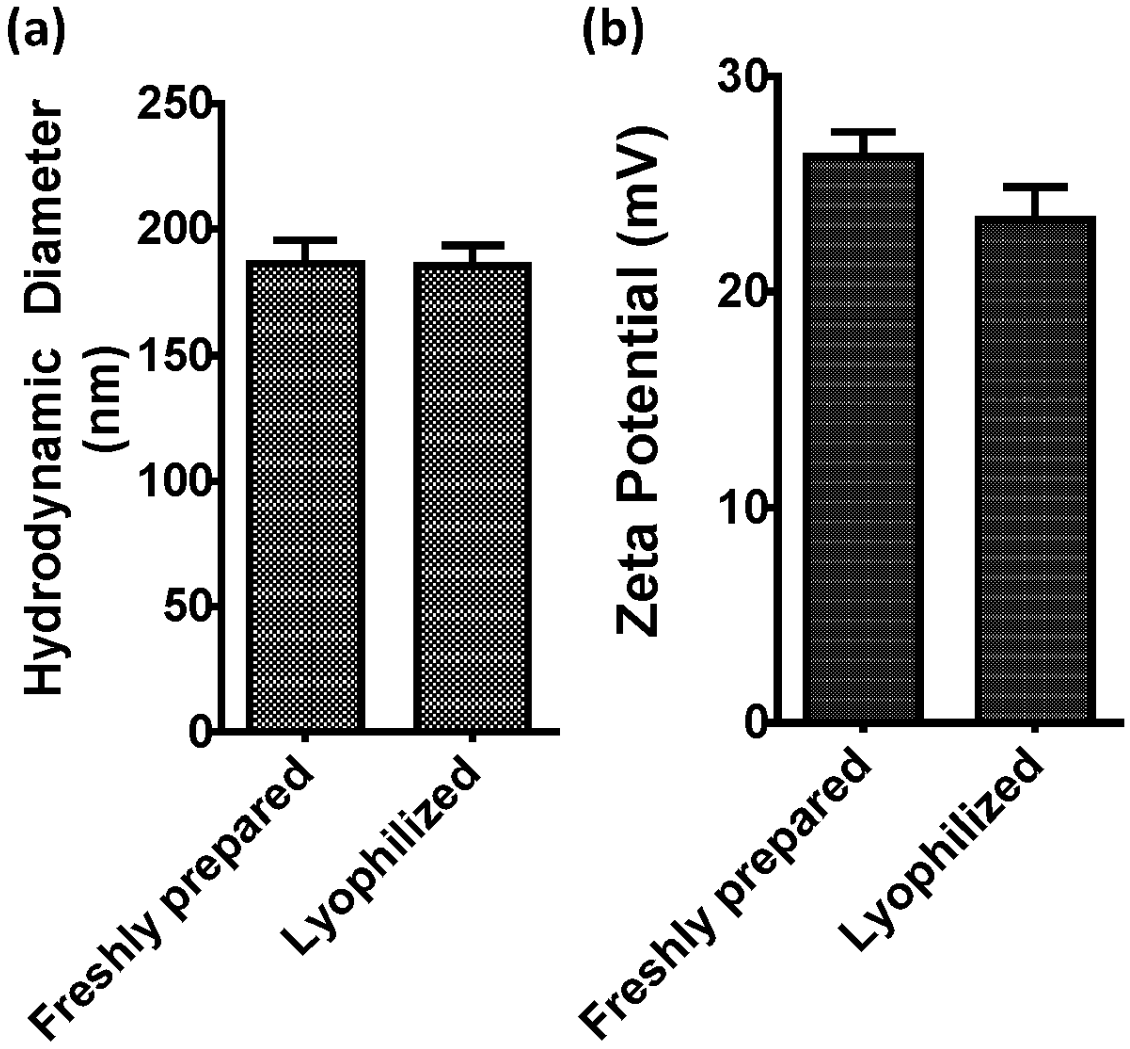

Figure 7.9: Comparison of freshly prepared to lyophilized particles by particle size and charge. (a) Hydrodynamic diameter of freshly prepared DNA/B5-S5-E7 particles versus lyophilized particles (n=3; bars are standard error). (b) Zeta potential of freshly prepared DNA/B5-S5-E7 particles versus lyophilized particles (n=3; bars are standard error). Differences in particle size (p=1) and zeta potential (p=0.05) are not significant.

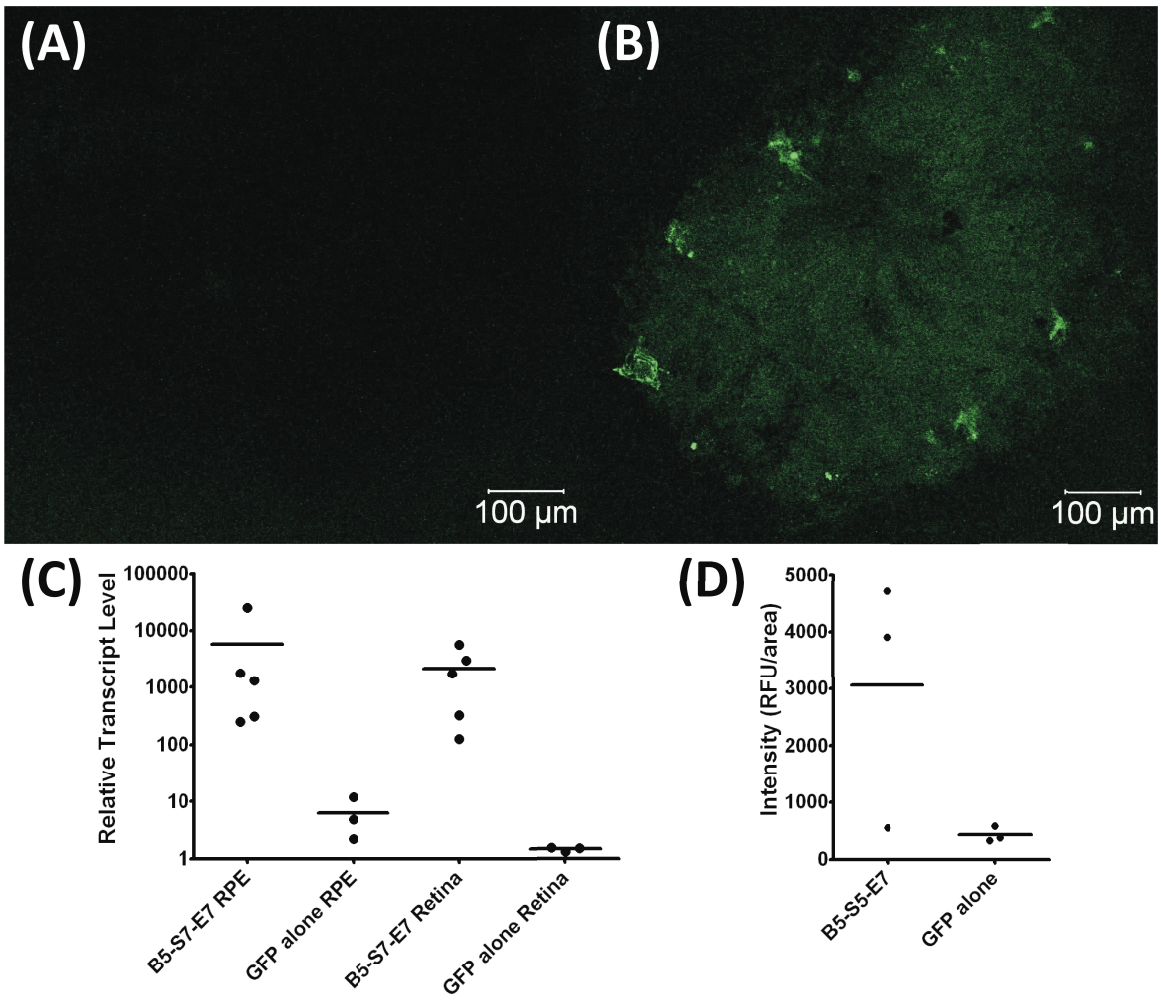

Figure 7.10: **Subretinal injection of PBAE nanoparticles.** Confocal image of RPE/choroid flat mount post subretinal injections; green corresponds to fluorescence due to GFP expression. Both images were taken with the same camera settings. (A) pDNA alone. (B) pDNA/nanoparticle injection. (C) Relative transcript level to GAPDH (set at 10,000) of GFP mRNA expression after subretinal injection of PBAE eGFP nanoparticles and subretinal injection of naked DNA. Each injection is diplayed as a separate point, and the mean relative transcript level is displayed as a bar. Subretinal injections using lyophilized GFP-PBAE nanoparticles resulted in $1.1\pm1x10^3$-fold and $1.5\pm0.7x10^3$-fold increased GFP expression in the RPE/choroid and neural retina, respectively, compared to injection of DNA alone ($p = 0.003$ for RPE/choroid, $p < 0.001$ for neural retina). (D) Relative fluorescence intensity of retinal flat mounts after subretinal injection with GFP nanoparticles and GFP plasmid alone ($n = 3$).

Table 7.1: Results of 2-way ANOVA examining the effect of increased hydrophobicity of the side chain with respect to the base diacrylate it is paired with. NS is non-significant; $P < 0.05$ is *; $P < 0.01$ is **; $P < 0.001$ is ***.

Reduction in Metabolic Activity				**Transfection Efficacy**			
30 w/w	S3->S4	S4->S5	S3->S5	**30 w/w**	S3->S4	S4->S5	S3->S5
B3	NS	NS	NS	B3	NS	NS	NS
B3b	NS	NS	NS	B3b	**	NS	NS
B4	NS	*	**	B4	NS	NS	**
B5	***	NS	***	B5	NS	**	***
B6	NS	**	**	B6	NS	**	NS
60 w/w	S3->S4	S4->S5	S3->S5	**60 w/w**	S3->S4	S4->S5	S3->S5
B3	NS	***	***	B3	NS	NS	NS
B3b	NS	*	NS	B3b	***	NS	NS
B4	**	NS	***	B4	*	NS	***
B5	**	NS	***	B5	NS	**	*
B6	***	NS	***	B6	NS	*	NS

7.6 References

1. Acland, G.M., et al., *Gene therapy restores vision in a canine model of childhood blindness.* Nat Genet, 2001. **28**(1): p. 92-5.
2. Jacobson, S.G., et al., *Gene Therapy for Leber Congenital Amaurosis Caused by RPE65 Mutations: Safety and Efficacy in 15 Children and Adults Followed Up to 3 Years.* Arch Ophthalmol, 2011.
3. Wu, Z., H. Yang, and P. Colosi, *Effect of genome size on AAV vector packaging.* Mol Ther, 2010. **18**(1): p. 80-6.
4. Ostedgaard, L.S., et al., *Cystic fibrosis transmembrane conductance regulator with a shortened R domain rescues the intestinal phenotype of CFTR-/- mice.* Proc Natl Acad Sci U S A, 2011. **108**(7): p. 2921-6.
5. Pacak, C.A. and B.J. Byrne, *AAV vectors for cardiac gene transfer: experimental tools and clinical opportunities.* Mol Ther, 2011. **19**(9): p. 1582-90.
6. Bitner, H., et al., *A homozygous frameshift mutation in BEST1 causes the classical form of Best disease in an autosomal recessive mode.* Invest Ophthalmol Vis Sci, 2011. **52**(8): p. 5332-8.
7. Briggs, C.E., et al., *Mutations in ABCR (ABCA4) in patients with Stargardt macular degeneration or cone-rod degeneration.* Invest Ophthalmol Vis Sci, 2001. **42**(10): p. 2229-36.
8. Bhise, N.S., et al., *A Novel Assay for Quantifying the Number of Plasmids Encapsulated by Polymer Nanoparticles.* Small, 2011.
9. Check, E., *Gene therapy put on hold as third child develops cancer.* Nature, 2005. **433**(7026): p. 561.
10. Check, E., *A tragic setback.* Nature, 2002. **420**(6912): p. 116-118.
11. Putnam, D., *Polymers for gene delivery across length scales.* Nature Materials, 2006. **5**(6): p. 439-451.
12. Sunshine, J.C., C.J. Bishop, and J.J. Green, *Advances in polymeric and inorganic vectors for nonviral nucleic acid delivery.* Therapeutic Delivery, 2011. **2**(4): p. 493–521.
13. del Pozo-Rodriguez, A., et al., *Solid lipid nanoparticles for retinal gene therapy: transfection and intracellular trafficking in RPE cells.* Int J Pharm, 2008. **360**(1-2): p. 177-83.
14. Abul-Hassan, K., R. Walmsley, and M. Boulton, *Optimization of non-viral gene transfer to human primary retinal pigment epithelial cells.* Curr Eye Res, 2000. **20**(5): p. 361-6.
15. Urtti, A., et al., *Gene delivery and expression in human retinal pigment epithelial cells: effects of synthetic carriers, serum, extracellular matrix and viral promoters.* J Drug Target, 2000. **7**(6): p. 413-21.
16. Lynn, D.M. and R. Langer, *Degradable poly(beta-amino esters): Synthesis, characterization, and self-assembly with plasmid DNA.* Journal of the American Chemical Society, 2000. **122**(44): p. 10761-10768.
17. Bhise, N.S., et al., *The relationship between terminal functionalization and molecular weight of a gene delivery polymer and transfection efficacy in*

mammary epithelial 2-D cultures and 3-D organotypic cultures. Biomaterials, 2010. **31**(31): p. 8088-8096.
18. Sunshine, J., et al., *Small-Molecule End-Groups of Linear Polymer Determine Cell-Type Gene-Delivery Efficacy.* Advanced Materials, 2009. **21**(48): p. 4947-4951.
19. Sunshine, J.C., et al., *Effects of base polymer hydrophobicity and end-group modification on polymeric gene delivery.* Biomacromolecules, 2011. **12**(10): p. 3592-600.
20. Tzeng, S.Y., et al., *Non-viral gene delivery nanoparticles based on Poly(beta-amino esters) for treatment of glioblastoma.* Biomaterials, 2011. **32**(23): p. 5402-5410.
21. Green, J.J., et al., *Combinatorial modification of degradable polymers enables transfection of human cells comparable to adenovirus.* Advanced Materials, 2007. **19**(19): p. 2836-+.
22. Green, J.J., R. Langer, and D.G. Anderson, *A combinatorial polymer library approach yields insight into nonviral gene delivery.* Accounts of Chemical Research, 2008. **41**(6): p. 749-759.
23. Shmueli, R.B., et al., *Gene delivery nanoparticles specific for human microvasculature and macrovasculature.* Nanomedicine, 2012.
24. Handa, J.T., et al., *The advanced glycation endproduct pentosidine induces the expression of PDGF-B in human retinal pigment epithelial cells.* Exp Eye Res, 1998. **66**(4): p. 411-9.
25. Koirala, A., et al., *Nanoparticle-mediated gene transfer specific to retinal pigment epithelial cells.* Biomaterials, 2011. **32**(35): p. 9483-93.

8 Chapter 8: Particle shape determines efficient T cell activation and enhances tumor immunotherapy by artificial Antigen Presenting Cells

8.1 Introduction

Geometry and spatial organization are critical components in many biological systems. The cytoskeleton, its organization, and the physical cues that it can transmit, result in dramatic effects on cell fate [1]. This is seen within the immune system in a variety of ways including during the interaction of a T cell with an antigen presenting cell (APC), which is a critical determinant of T cell fate and effector function. With activation, APC such as dendritic cells have major changes in their cell morphology resulting in significant increases in their overall cell surface area facilitating interaction with naïve T cells to direct T cell fate. Once an initial contact has been made by a T cell and an APC or some other target cell, T cell activation is further modulated by the formation of the immune synapse, a large surface area of close membrane apposition between the DC and T cell membrane, with concomitant cytoskeletal rearrangement and clustering of surface proteins [2-6]. Materials science approaches have helped to elucidate how the spatial organization and clustering of ligands that make up this synapse are important [7]. Thus, taking into account the geometry and spatial organization at cell-cell interfaces is important in studying biological responses.

This chapter contains excerpts from an article that was published as Sunshine JC*, Perica K*, Schneck JP, Green JJ. "Particle shape dependence of CD8+ T cell activation by artificial Antigen Presenting Cells." Biomaterials. 2013. http://dx.doi.org/10.1016/j.biomaterials.2013.09.050

Reductionist systems have facilitated the study of effective immune responses. One such system is the acellular artificial antigen presenting cell (aAPC). aAPCs have been made by coupling proteins required for T cell activation to particles. Minimally, T cell activation requires two sets of receptor-receptor interactions. One interaction, Signal 1, is the binding of major histocompatibility complexes (MHC) or a surrogate, such as anti-CD3, to bind the T cell receptor (TCR). A second interaction, Signal 2, is the binding of co-stimulatory receptors on the APC, such as B7.1, to ligands on the T cell, such as CD28. aAPC have been generated by coupling proteins that deliver Signal 1 and 2 to the surface of particles (**Fig. 8.1A**) made from a range of materials, including magnetic microparticles [8, 9], polystyrene particles [10] and PLGA microparticles [11-13]. Such systems have been broadly applied to tumor immunotherapy, vaccination, and immunosuppression, and are amenable to *in vivo* or *ex vivo* T cell stimulation and offer possible novel translational approaches to immunotherapy [9, 14-18].

While useful, the Signal 1 and 2 paradigms alone do not capture aspects of spatial organization or the geometry of interactions. Previous work developing aAPCs have not attempted to re-capitulate these aspects of APC behavior. As a result, all aAPCs tested thus far have used spherical particles for their aAPC platforms, which unlike DCs minimize surface area for a given volume (**Fig. 8.1B**).

Particle shape has only recently become a design parameter of interest in the field of material design for drug delivery. Shape can play a role in tuning the rate and mechanism of cellular uptake [19], can dramatically reduce internalization by phagocytic cells such as macrophages [20, 21], can change the biodistribution of the drug delivery vehicle [22, 23], and has been posited as potentially modulating the ability of a particle to

bind a cell in part by increasing the surface area for interaction [22, 24]. In fact, a recent study by Barua et al showed that antibody coated polystyrene nanorods had higher specific and reduced non-specific uptake than spherical counterparts, demonstrating a significant relationship between particle shape and cell binding/unbinding [25].

We adapted a method for controlling the shape of microparticles made from biocompatible polymer poly (lactic-co-glycolic) acid (PLGA)[26] to generate ellipsoid aAPCs with varying long axis lengths and aspect ratios (ARs)(**Fig. 8.1C,D**). These ellipsoidal aAPC were successful at stimulating T cells, modulating both significantly enhanced T cell expansion *in vitro* and tumor rejection *in vivo*. Confocal imaging of cell-aAPC interactions indicates that this effect may be due to improved interaction along the long axis of the aAPC. These findings suggest that particle geometry is a critical design criterion in the generation of aAPC, and may offer insight into the essential role of geometry involved in the interaction between T cells and biological APCs.

8.2 Results

8.2.1 Ellipsoidal aAPC synthesis and characterization

Ellipsoidal, biodegradable aAPCs were synthesized by first fabricating PLGA microparticles which were then stretched into ellipsoids using a film stretching method [26] This method offers the advantage of allowing a direct comparison of particle shape and surface area, while retaining equivalent volumes.

The single emulsion PLGA (50:50 LA/GA, MW 38,000-54,000) microparticle synthesis resulted in spherical microparticles (**Fig. 8.1D, spheres**) with a number-weighted average diameter of 4.3 μm and a volume-weighted diameter of 6.7 μm (**Fig.**

8.1E). We were able to control the aspect ratio (AR) of ellipsoidal microparticles with a high degree of accuracy by imposing different degrees of stretch (STR) onto the film (**Fig. 8.1D**). This technique exhibits a high correlation between predicted AR and empirically measured AR (by SEM) for a fixed volume ellipsoid that has been elongated in one direction ($AR = STR^{1.5}$) (**Fig. 8.1F**). This indicates that particle stretching is a feasible, controllable process that allows for flexibility in specifying the shape of the resulting particles. Ellipsoidal and spherical microparticles were then made into aAPCs by EDC/sulfo-NHS mediated covalent coupling of a dimeric MHC-Ig fusion protein[27] and an antibody against CD28 to free carboxyl groups on the particle surface.

Key parameters to evaluate these aAPCs include characterizing the total protein on the surface, the protein density, the dimer/anti-CD28 antibody ratio and the surface distribution on the spherical and ellipsoidal aAPCs. To characterize the conjugation efficiency with different amounts of protein added, we synthesized spherical and ellipsoidal (STR 2/AR 2.8) aAPC with fluorescently labeled MHC-Ig dimer and unlabeled anti-CD28 antibody, and characterized the particles by fluorimetry (**Fig. 8.1G**). By increasing the amount of MHC-Ig used during synthesis, we achieved protein coupling of up to 0.75 mg MHC-Ig/mg PLGA (**Fig. 8.1G**). Coupling efficiency was 15-20% over the entire range of protein analyzed, and there were no statistically significant differences between spherical and ellipsoidal aAPC in terms of their total protein content or protein density ($p > 0.35$ for all comparisons) (**Fig. 8.1G**). PLGA microparticles showed only minor auto-fluorescence and did not interfere with dye emission (**Fig. 8.S1**).

To evaluate whether spherical or ellipsoidal aAPCs might show differences in dimer/anti-CD28 antibody ratio or surface distribution of the two proteins, we

synthesized spherical or ellipsoidal aAPCs with fluorescently labeled MHC-Ig dimer and unlabeled anti-CD28 antibody, and characterized the particles by fluorimetry and by confocal microscopy (**Fig.** 8.**S2**). Spherical and ellipsoidal aAPC did not show significant differences in MHC-dimer amount or density, anti-CD28 amount or density, or MHC-dimer/anti-CD28 ratio (**Fig. 8.S2**). Approximately 85-90% of the protein on the surface required the EDC/NHS pre-activation step (**Fig. 8.S2**). The fluorescence signals from the two proteins were co-localized in both cases (quantified here by the Pearsons correlation), and the distribution pattern was equivalent between the two groups (**Fig. 8.S2**). Taken together with the modest (16%) increase in total surface area for 2-fold stretched particles (AR 2.8) as compared to spherical particles (**Table 8.1**), the protein surface characterization data indicate that there are not substantial differences between spherical and ellipsoidal particles with respect to protein density, total protein amount, protein organization, or surface release.

While bulk polymer degradation from PLGA microparticles have been well investigated in the drug delivery field [28-30], the effect of degradation on release of surface-coupled proteins is less well studied. For aAPCs, presentation of immobilized proteins are critical for T cell activation and thus it is important to study release of these proteins [10]. To characterize surface degradation, aAPCs bearing fluorescently labeled MHC-Ig were incubated for varying amounts of time at 37°C. Supernatants were recovered through centrifugation of the aAPCs and released protein quantified by protein fluorescence. For both spherical aAPCs and ellipsoidal aAPCs, 60-70% of the protein that was conjugated to the surface was released over 7 days, with 30-40% of the protein released in the first 3 days. At 7 days, 30-40% of the protein remained on the surface of

the aAPCs, as quantified by total fluorimetry from the particles (**Fig. 8.1H**). There was no significant difference in this release profile between ellipsoidal and spherical aAPCs.

We characterized the stability of the ellipsoidal aAPC shape by analyzing their relaxation rate to the more stable spherical shape. Previous studies have indicated that relaxation rates are dependent on surface characteristics, molecular weight, polymer composition, and temperature [26]. We observed very little shape relaxation for high aspect ratio ellipsoidal aAPC over 1 week at 37°C in PBS, indicating that the shape transition is slow for ellipsoidal aAPCs with the chosen lactide to glycolide ratio (**Fig. 8.S3**). This agrees with published relaxation timescales for high aspect ratio PLGA with hydrophilic surfaces, such as those used here [26].

8.2.2 High aspect ratio aAPCs efficiently induce T cell proliferation

In order to assess the impact of particle elongation, we measured the ability of aAPC to induce antigen specific T cell expansion of pMEL TCR transgenic T cells. Spherical and 2-fold stretched (AR = 2.8) ellipsoidal aAPCs were synthesized at 3 different cognate MHC-peptide densities by adding 4, 1, and 0.5 μg of Db-Ig GP100/mg PLGA with corresponding amounts of anti-CD28 antibody, resulting in spherical and ellipsoidal aAPC with 0.75, 0.14, and 0.08 μg of MHC-dimer/mg PLGA (**Fig. 8.1G**). Spherical aAPCs bearing non-cognate Db-Ig ASN at the highest protein density were used as a negative control. The aAPCs were added to pMEL TCR transgenic T cells at 3 aAPC to cell ratios (1, 0.1 and 0.01 mg aAPC/10^5 cells). Proliferation was assessed at day 4 by CFSE dilution (see methods for details) and on day 7 by cell counts. Day 4 CFSE dilution for a representative Db-Ig density (0.75 ug Db-Ig/mg PLGA) is shown at each

aAPC:cell ratio (**Fig. 8.2A**), while day 7 fold proliferation data are shown for all three parameters of aAPC shape, aAPC:cell ratio, and Db-Ig density (**Fig. 8.2B**).

At a subsaturating dose of aAPC, 0.01 mg/10^5 cells, ellipsoidal but not spherical aAPCs induced T cell proliferation as measured by CFSE dilution (**Fig. 8.2A 0.01mg**). This was reflected in Day 7 cells counts, with only ellipsoidal aAPC bearing 0.75 or 0.14 μg Db-Ig/mg PLGA inducing T cell expansion, of 22-fold and 11-fold expansion, respectively (**Fig. 8.2B 0.01mg;** $p<0.001$ and $p<0.01$ for 0.75 and 0.14 μg Db-Ig/mg, respectively**)**. At an intermediate aAPC:cell ratio (0.1 mg/10^5 cells), ellipsoidal aAPC also induced higher levels of CFSE dilution (**Fig. 8.2A 0.1mg**) than spherical aAPC. Cell counts indicated ellipsoidal aAPC conferred an approximately 3-fold increase in total T cell expansion by day 7 compared to spherical aAPCs (**Fig. 8.2B 0.1mg;** $p<0.001$ and $p<0.01$ for 0.75 and 0.14 μg Db-Ig/mg, respectively). At saturating high aAPC:cell ratios (1 mg/10^5 cells) and the highest Db-Ig density, differences between ellipsoidal and spherical aAPCs were substantially smaller but still statistically significant ($p<0.05$) (**Fig. 8.2A/2B, 1mg**). However, when Db-Ig density on aAPC was titered to 0.1 mg Db-Ig/mg PLGA, ellipsoidal aAPC regained their advantage, stimulating significantly more T cell expansion than spherical aAPC ($p<0.001$). aAPC bearing non-cognate MHC-peptide did not induce CFSE dilution or T cell proliferation (**Fig. 8.2A left**).

Two parameters that are important in T cell activation are total amount of antigen-MHC complex and antigen density [31-33]. We wanted to study the impact of shape independent of total antigen-MHC complex or antigen density. To separate the effect of shape from the effect of total antigen-MHC dose or antigen density, we replotted the expansion data from **Fig. 8.2B** versus total antigen-MHC dose (**Fig. 8.2C**) and antigen

density (**Fig. 8.2D**). Increasing total dose results in increased CTL expansion, but at all total doses, ellipsoidal aAPC (in red) outperform their spherical counterparts (in black) (**Fig. 8.2C**). For example, at a total dose of MHC near 0.1 μg/10^5 cells, all 3 ellipsoidal formulations showed higher fold-expansion than the 3 spherical formulations. There is also a positive correlation between increased antigen density and T cell proliferation at a given particle dose (**Fig. 8.2D**), but across the probed density ranges, ellipsoidal particles (in red) show higher fold-expansion than comparable spherical particles (in black). For example, in **Fig. 8.2D 0.1mgs**, ellipsoidal particles with an MHC density of 400±140 and 240±70 MHC-Ig dimer/μm^2 displayed higher fold expansion (19.7±0.7 and 6.3±0.8 fold respectively) than spherical particles with an intermediate MHC density of 350±60 MHC-Ig dimer/μm^2 (2.3±1 fold expansion). Thus, across a range of total antigen doses and protein densities, when controlling for dose and density, ellipsoidal aAPC were more efficient at inducing T cell expansion than spherical aAPC.

To further study the importance of AR on T cell stimulation, PLGA microparticles were synthesized, stretched varying amounts, and made into aAPCs. There was a striking correlation between increased AR and increased T cell proliferation (**Fig. 8.3**). Interestingly, the greatest gain in T cell numbers was seen by increasing the aspect ratio of the ellipsoidal aAPC by increasing the applied stretch from 1.5-fold to 2-fold, which resulted in approximately 2 fold expansion up to approximately 20 fold T cell expansion at a 0.01 mg aAPC/10^5 cells dose (**Fig. 8.3C**). Analysis of the number of divisions from the CFSE dilution data (**Fig. 8.3A**) revealed that increasing AR further resulted in a larger percentage of cells have gone through significantly greater number of divisions (**Fig. 8.3B**). The fraction of non-responders (generations 0-1) progressively

decreases with increasing AR, eventually resulting in only 11% non-responders for the 3.5-fold stretched (AR 6.6) aAPCs. The number of cells undergoing 4-5 or 6-7 divisions also increases with every additional .5-fold increase in applied film stretch. This effect was also saturable with very high doses of aAPCs (**Fig. 8.S4**). Therefore, increasing aspect ratio of the aAPCs resulted in increased T cell expansion consistently up to 3.5 fold stretched aAPCs (AR 6.6), with the greatest improvement in overall T cell expansion seen when going from 1.5-fold to 2-fold applied stretch, which corresponds to a change in AR from 1.8 to 2.8.

Thus, increasing aspect ratio of ellipsoidal aAPC results in improved T cell activation, and this enhanced proliferation that is mediated by ellipsoidal aAPC is primarily dependent on aAPC geometry rather than potential subtle differences in the density or amount of conjugated surface protein.

T cell quality, as reflected by the amount and diversity of cytokines and cytotoxic markers produced when T cells are re-challenged by antigen, is a critical parameter for assessing responses [34]. To determine the functional status of the expanded T cell population, we re-challenged aAPC-activated T cells with peptide-pulsed splenocytes and measured the production of a key cytokine, IFNγ, as well as measured the degranulation marker, CD107a in an intracellular cytokine staining (ICS) assay. Function tracked with proliferation; there was no significant difference in the quality of T cells generated from spherical or ellipsoidal aAPCs as determined by IFNγ or CD107a expression (**Fig. 8.S5**). There was no significant difference when comparing T cell quality after equal doses of aAPCs (which resulted in higher proliferation with the ellipsoidal aAPC) or when comparing equal proliferation (from lower doses of ellipsoidal aAPC).

8.2.3 High aspect ratio ellipsoidal aAPCs enhance T cell conjugate formation

Antigen recognition on APC is known to trigger coordinated cytoskeletal rearrangements in both T cells and APCs, leading to close apposition of their cellular membranes. The resulting interactions mediate T cell activation and, when visualized by imaging or flow cytometry, are termed cell-cell conjugates [35].

To evaluate the formation of T cell-aAPC conjugates, naïve T cells were incubated at 37°C with spherical or ellipsoidal aAPCs. Cell-aAPC interactions were visualized after a one-hour incubation by confocal imaging. In the presence of ellipsoidal aAPCs bearing cognate MHC/peptide, T cell membranes could be observed in close apposition to the aAPC's long but not short axis, creating a T cell "cap", characteristic of conjugate formation (**Fig. 8.4A**).

Conjugate formation was observed for T cells incubated in the presence of either ellipsoidal (**Fig. 8.4B**) or spherical (**Fig. 8.4C**) aAPC. Importantly, conjugate formation was a process driven by recognition of cognate antigen, as neither spherical nor ellipsoidal aAPCs bearing non-cognate MHC/peptide induced cap formation (**Fig. 8.4D, E**). When quantitated, conjugate formation was approximately 2.5-fold more frequent with ellipsoidal aAPC, with 4.6 ± 0.9% of the T cells forming conjugates with the ellipsoidal aAPC compared to 1.8 ± 0.4% with spherical aAPC ($p = 0.01$, **Fig. 8.4F**). In addition to being 2.5-fold more frequent, we observed a significant increase ($p = 0.01$, **Fig. 8.4G**) in the contact length between the T cells and the ellipsoidal aAPC (3.6 ± 0.6 μm/interface) as compared to spherical aAPC (1.9 ± 0.2 μm/interface).

Time-lapsed imaging revealed a striking reorientation and rearrangement of the T

cell surface against the aAPC long axis. Initially, the T cell appears to contact the aAPC along the short axis but with time migrates along the long axis rearranging its membrane against the long axis of the ellipsoidal aAPCs (**Fig. 8.4H**). Membrane reorientation and alignment against the long axis of ellipsoidal aAPC strongly suggests a preference for the flat surface presented by the long axis of ellipsoidal aAPC. We thus observe that ellipsoidal aAPCs generate increased biomimetic interactions with T cells compared to spherical aAPCs, and suggests that the improved T cell expansion seen *in vitro* is due to increased frequency and size of T cell-aAPC contact along the long axis of the ellipsoidal aAPCs.

8.2.4 High aspect ratio, ellipsoidal aAPCs enhance tumor killing *in vivo*

To test the activity of high aspect ratio aAPCs *in vivo*, we utilized a subcutaneous B16 melanoma tumor model. We injected a dose of aAPC subcutaneously 3 days before and a second dose 3 days after tumor injection into the hindlimb (see **Fig. 8.5A**). Treatment with either ellipsoidal ($p = 0.0009$ vs. non-cognate) or spherical ($p = 0.02$ vs. non-cognate) cognate aAPCs led to significant reductions in tumor size as compared to controls that received control non-cognate aAPCs or T cells alone (**Fig. 8.5B**). By day 19, cognate ellipsoidal aAPC treated tumors had only reached a size of 42.5 ± 14.9 mm^2, compared to 90.5 ± 33.8 mm^2 for cognate spherical, 164.5 ± 28.6 mm^2 for non-cognate ellipsoidal, and 154.4 ± 35.4 mm^2 for T cell alone treated mice. Area under the curve (AUC) of tumor growth over the course of the entire experiment showed a similar pattern, with tumors growing a total of 44.3 ± 15.6 mm^2, compared to 105.3 ± 34.7 mm^2 for cognate spherical, 251.0 ± 46.6 mm^2 for non-cognate ellipsoidal, and 238.0 ± 46.6 mm^2

for T cell alone treated mice. Cognate ellipsoidal aAPCs thus reduced tumor size more than spherical aAPCs, but this effect did not achieve statistical significance ($p = 0.13$).

Survival studies revealed statistically significant differences in survival between mice injected with ellipsoidal cognate aAPC over spherical cognate aAPC (**Fig. 8.5C**)($p=0.05$), as well as ellipsoidal non-cognate control aAPCs ($p=0.004$). 25% of the animals in the cognate ellipsoidal aAPC group completely cleared tumor by day 19 and survived the course of the experiment, which did not occur in any other treatment or control groups. Furthermore, ellipsoidal aAPC treatment led to a significant delay in tumor growth, with no mice reaching substantial tumor burden until 22 days after tumor injection, compared to 19 days for the other three groups.

Critically, this demonstrates that increased aspect ratio acellular aAPCs, which only differ in their shape (and importantly not in their volume or significantly in their protein content or antigen density) as compared to spherical controls, not only engender enhanced antigen specific activation *in vitro* but *in vivo* as well, and this enhanced activation has functional consequences which lead to reduced tumor burden and enhanced survival.

8.3 Conclusion

The key consideration in cancer immunotherapy remains the efficient stimulation of antigen (Ag)-specific cytotoxic T cells (CTLs). *In vivo*, a key interaction for generation of activated, effector Ag-specific CTLs is the interaction between antigen presenting cells, such as dendritic cells or macrophages, with T cells. In the development of acellular systems for CTL stimulation, previous literature has focused predominantly

on the proteins involved in the interaction between APCs and T cells [8, 9, 13, 36-38], and recent studies extended this to release of cytokines [12, 39].

However, the biological interaction between T cells and their targets is distinctly not an interaction that is most appropriately represented by two spheres interacting. We evaluated the effect of 1-dimensional stretching of aAPCs on the ability of these acellular, biodegradable aAPCs to induce T cell proliferation *in vitro* and tumor killing *in vivo*. In this study, antigen dose, antigen density, protein ratio, protein colocalization, and particle volume are held essentially equivalent between spherical and ellipsoidal aAPCs, and yet, at sub-saturating aAPC doses, high aspect ratio ellipsoidal aAPCs show significantly enhanced activity beyond spherical aAPCs. Increasing the aspect ratio of ellipsoidal aAPCs shows enhanced activity up to AR 6.6. This enhanced activity was also reflected *in vivo*, where ellipsoidal cognate aAPCs caused increased survival in mice compared to ellipsoidal non-cognate aAPCs ($p=0.004$) as well as cognate spherical aAPCs ($p=0.05$). One key parameter that is altered in with particle stretching is increases in surface area (**Table 8.1B**). However, while total surface area increases modestly with stretching, with a maximum increase in net surface area of the aAPCs of 50% for AR 6.6 aAPCs, stretching the aAPCs dramatically increases surface flatness along the long axis of the aAPCs, with the radius of curvature increasing 23-fold over the same range (**Table 8.1E**). Confocal imaging suggests that the observed improvement in T cell activation is due to improved interaction along this flatter, long axis of the biomimetic, ellipsoidal aAPCs.

These findings indicate that shape matters and that aAPC geometry is a critical design criterion to consider in the synthesis of biomimetic acellular aAPC systems. While particle-based T cell stimulation systems have yielded crucial insights regarding early

activation events [36, 40], aAPC that more closely mimic endogenous cell-cell interactions may provide a more complete understanding of the underlying process, such as the role of close membrane apposition and a large surface area of contact in the APC/T cell interation. aAPCs thus may not only be an enabling tool for antigen-specific immunotherapy, but also for studying basic aspects of T cell biology.

8.4 Materials and Methods

8.4.1 Microparticle fabrication

The poly(lactide-glycolide) (PLGA) microparticles were made by dissolving 200 mg of acid-terminated PLGA (50:50 LA/GA, MW 38,000-54,000, Sigma-Aldrich) in 5 ml of dicholoromethane (ACS grade, Sigma-Aldrich). The dissolved PLGA was then added dropwise to 50 ml of an ice-cold 1% poly(vinyl alcohol) (PVA) solution, which was homogenized at 5,000 rpm. After dropwise addition, the solution was allowed to homogenize for an additional minute, and then added to a 100 ml solution of 0.5% PVA which was stirring at 500 rpm in the cold room (at 4°C). After stirring for 4 hours to allow for solvent evaporation, the particles were centrifuged (4000 rpm for 5 min) and washed 3x, resuspended in 5 mL of deionized water and lyophilized.

For confocal imaging, tetramethyl rhodamine (TAMRA) loaded microparticles were synthesized via single emulsion as follows: The TAMRA was dissolved in dichloromethane at 1 mg/ml. 200 mg of acid-terminated PLGA was dissolved in 4.9 ml of DCM and 100 µl of TAMRA solution was added to the PLGA DCM phase. Particle synthesis otherwise followed the same protocol as the single emulsion particles above.

8.4.2 Preparation of MHC-Ig Dimers

Briefly, Db-Ig molecules were stripped under mildly acidic conditions (pH 6.5) and refolded in the presence of 40 fold molar excess peptide and 2-fold molar excess of human β2-microglobulin. Peptides GP100 (KVPRNQDWL; the "cognate" peptide) and ASN (ASNENMETH; a "non-cognate" peptide) were purchased from Genscript (Piscataway, NJ). Protein concentration was determined after labeling by size exclusion High Performance Liquid Chromatography.

8.4.3 Film formation and particle stretching

Lyophilized microparticles were added to a solution containing 10% PVA and 2% glycerol by weight at 5 mg/ml (particles/ml solution). The solution was poured on a flat surface and allowed to dry overnight. After drying, strips of the resulting film were cut out and placed on an aluminum-stretching device consisting of two aluminum blocks that can be separated by sliding on aluminum rods. The film and custom-made stretcher were placed in a 90°C oven for 10 minutes and then the film was slowly stretched inside of the oven to the desired stretch ratio by separating the two blocks. After allowing the film to cool down to room temperature, the film was removed and dissolved in 10 ml of deionized water, then the particles were centrifuged (4000 rpm for 5 min) and washed 3x, and finally resuspended in deionized water, frozen, and lyophilized. Spherical particles in all experiments were also prepared similarly; they were heated along side of the ellipsoidal particles but simply not stretched.

8.4.4 aAPC synthesis

Soluble MHC-Ig dimers were prepared and loaded with peptide as described.[41] Spherical and ellipsoidal microparticles were resuspended in coupling buffer (0.1M MES pH 6.0), and activated with EDC (1-Ethyl-3-(3-dimethylaminopropyl)carbodiimide, Sigma-Aldrich) and sulfo-NHS (N-hydroxysulfosuccinimide). As an example, 5 mg of microparticles were resuspended in 1 ml of coupling buffer and activated with 10 mg of EDC and 13 mg of sulfo-NHS for 15 min at 1000 rpm on a multitube vortexer (VWR). Activated microparticles were then centrifuged, the supernatant was removed, and the activated particles were resuspended in 1 ml PBS (pH 7.4) and transferred to a 5 mL glass scintillation vial for coupling. As an example, 8 μg of MHC-dimer and 10 μg of anti-CD28 antibody (always in this ratio) were added to 2 μg of activated PLGA microparticles, and then the reaction was allowed to proceed in the cold room (4°C) for 4 hours. After 4 hours, the aAPCs (here, 2 mg of aAPCs) were centrifuged and washed 2x with PBS, then centrifuged, re-suspended in 200 μl of 0.2 mm-filtered sterilized 100 mg/ml endotoxin-free sucrose solution, frozen, and lyophilized overnight.

8.4.5 Characterization of aAPCs

8.4.5.1 Measuring size and aspect ratio by SEM

Lyophilized particle samples were spread on conductive carbon tape mounted on aluminum SEM mounts (Eletron Microscopy Sciences, Hatfield, PA). Samples were sputter coated with a chromium sputter coater and imaged on a Leo/Zeiss Field emission SEM in the Johns Hopkins Core Microscopy facility. Particle size and aspect was quantified using ImageJ software. For spherical particles, a single diameter was measured

for each particle. For ellipsoidal particles, two diameters were measured (long-axis and short-axis) and the aspect ratio was calculated by dividing the two.

8.4.5.2 Surface protein quantification and release

Surface protein quantification was performed by conjugation of unlabeled anti-CD28 mAb and fluorescently labeled MHC-IgG dimer to the surface of pre-activated 2-fold stretched (AR 2.8) ellipsoidal or spherical PLGA microparticles for 4 hours at 4C. These aAPC were centrifuged washed 3x, and then their fluorescence was characterized on a Synergy 2 plate reader (Biotek, Winooski, VT). Release from surface was characterized by incubating 10 mg of aAPC (spherical, ellipsoidal) with labeled dimer in 500 µl PBS at 37°C for 1 week. At 3 days and 7 days, the particles were centrifuged and the supernatant was removed and stored for subsequent analysis. At 7 days, the supernatant was removed, and then the aAPC were resuspended the fluorescence was characterized.

***8.4.5.3** Intracellular cytokine staining*

Six days after primary stimulation with aAPC, T cell functional activity was assessed by re-challenge with peptide-pusled C57Bl/6j splenocytes. Splenocytes were pulsed with the indicated concentration of peptide for 2 hours at 37°C then washed. 200,000 aAPC-activated T cells were incubated in complete RPMI with 200,000 splenocytes for 4 hours in a round bottom 96 well plate in the presence of 0.2 µl GolgiPlug, 0.2 ul GolgiStop, and anti-CD107a-fitC (BD Biosciences, Mountain View, CA). Cells were washed and fixed using a BD Cytofix/Cytoperm kit (BD Biosciences)

according to the manufacturer's instructions, then stained with anti-IFNγ PE (BioLegend). Cytokine staining was assessed by flow cytometry and frequency of cytokine functional cells was assessed by comparison with an unstimulated control in FlowJo (TreeStar).

8.4.6 *In vitro* CTL induction and CFSE dilution

T cells used were obtained from homogenized mouse spleens after depletion of RBC by hypotonic lysis. Cytotoxic lymphocytes were isolated using a CD8-negative isolation kit and magnetic enrichment column from Miltenyi Biotec (Cologne, Germany) and labeled with carboxyfluorescein succinimidyl ester (CFSE) for 15 minutes at 37°C, then washed extensively. Cells and aAPCs at the indicated amounts and dosages were mixed and cultured for 4-7 days in complete RPMI media supplemented with T cell factor, a cytokine cocktail harvested from human plasma [42]. Cell proliferation was quantified by manual cell counting, and final T cell count was divided by the initial T cell count for fold-change data.

8.4.7 aAPC-T cell conjugate formation evaluation

For confocal imaging, PLGA microparticles with encapsulated 5(6)-carboxy-tetramethylrhodamine dye (TAMRA, Nova Biochem, San Diego, CA) were synthesized (see supplemental methods). These labeled particles were then cast into a film, and the film stretching and subsequent sythesis of aAPC from spherical and ellipsoidal TAMRA-loaded particles were done as before. $1x10^6$ CFSE-labeled T cells were incubated with 1 mg spherical or ellipsoidal aAPC for 60 minutes at 37^oC in a No. 1.5 glass bottom dish (MatTek, Ashland, MA). Images were acquired on a Zeiss LSM 510 META (Zeiss,

Oberkochen, Germany) laser scanning confocal at 40x magnification at the Johns Hopkins School of Medicine Microscopy Facility. aAPC/T cell areas of contact were quantitated by image analysis on ImageJ.

8.4.8 *In vivo* activity of aAPCs

We performed a subcutaneous B16 melanoma tumor prevention mouse model (**Fig 6a**). The animals were preinjected intravenously (i.v.) with naïve pmel T cells (day -1, $2x10^6$ cells/animal), subcutaneously (s.c.) in the flank with aAPCs (day 0, 2 mg aAPCs/animal), then injected with $2x10^5$ tumor cells in the hindlimb (day 3). Responses were boosted with subsequent s.c. injection of a second aAPC batch (day 6, 2 mg aAPCs/animal), and tumor growth over the course of the experiment was followed by measurement with external calipers. Once the tumor size reached 200 cm^2, the mice were sacrificed. Treatment groups consisted of ellipsoidal and spherical cognate aAPC (n=8), and control groups consisted of ellipsoidal non-cognate (n=8) and T cell alone groups (n=5).

8.4.9 Statistics

All statistics were performed in GraphPad Prism. For analysis of surface protein quantification, we performed pairwise t-tests. For analysis of specific T cell proliferation in response to specified aAPC dose, protein density, and shape of aAPC, we performed two-tailed t-tests with a Bonferroni correction for multiple comparisons. For analysis of quantification of cognate formation and area of contact between aAPCs and T cells, we performed pairwise t-tests. For analysis of tumor size, we performed a 1-way ANOVA

with Tukey post test. For *in vivo* survival analysis, we used the Log-rank (Mantel-Cox) test. Data in text are presented as mean ± SEM.

8.5 Figures

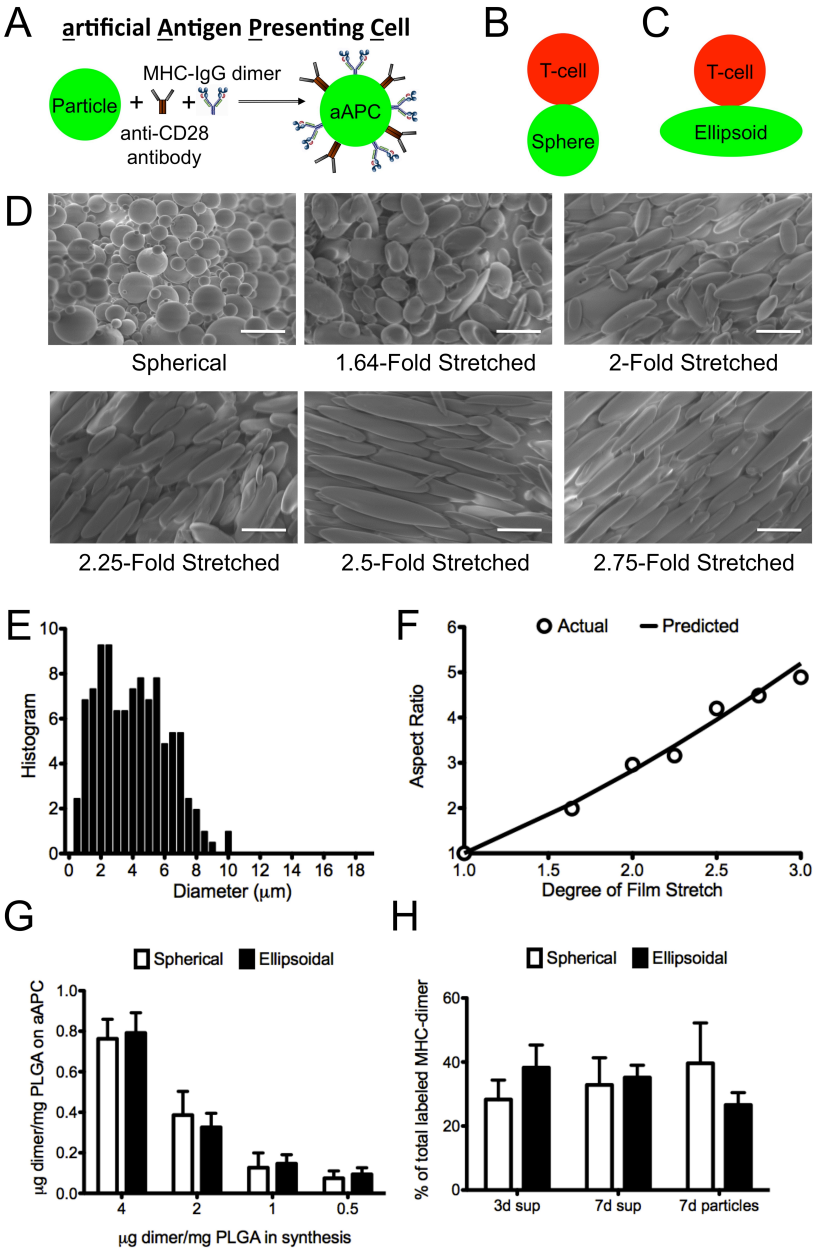

Figure 8.1: (A) Schematic of an aAPC. (B-D) Schematic of the interaction between a T cell, modeled as a sphere, interacting with (B) a sphere; (C) an ellipsoid (AR 2.83; stretch ratio 2). (D) Characterization by SEM (2000x magnification) of spherical and ellipsoidal aAPCs. Scale bar corresponds to 10 μm. (E) Size distribution of aAPCs. (G) Comparison of degree of stretch imposed on the film (STR) with the aspect ratio (AR) of the generated ellipsoidal aAPCs. Predicted AR = $STR^{3/2}$ (F) Coupling efficiency for protein during synthesis of aAPC from spherical and ellipsoidal microparticles (n=2). (G) Protein release from the surface of aAPC at 37°C in PBS (pH 7.4) over the course of 1 week.

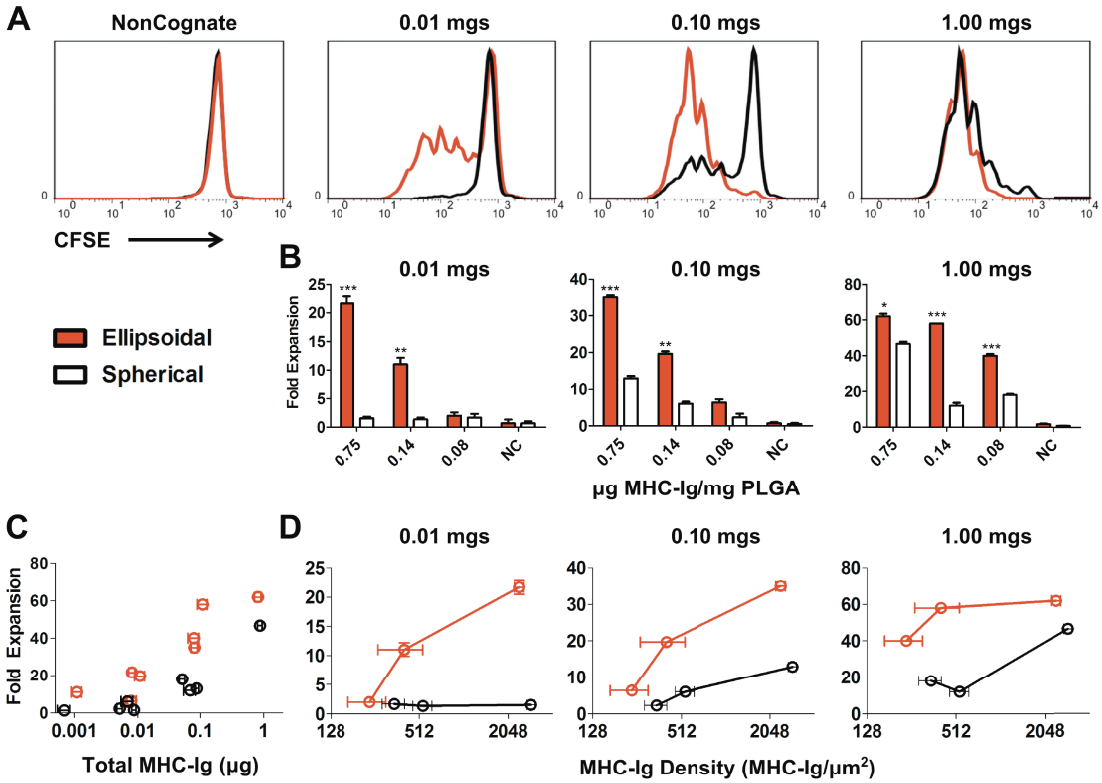

Figure 8.2: Specific T cell proliferation in response to specified aAPC dose, protein density, and shape of aAPC. (A) CFSE dilution data for ellipsoidal (red) and spherical aAPC (black) at the highest protein dose (4µg dimer/mg PLGA during conjugation) at 3 doses of aAPC (0.01 mg, 0.1mg, and 1mg/10^5 $CD8^+$ *pmel* T cells) compared to non-cognate. (B) T cell proliferation (fold expansion/10^5 cells) 7 days after aAPC addition to T cells with indicated doses, shapes (ellipsoidal in red, spherical in white), and protein densities. (For comparison of ellipsoid vs. spherical, * $p<0.05$, ** $p<0.01$, *** $p<0.001$; n=3). (C) T cell proliferation (fold expansion/10^5 cells) versus total MHC-dimer dose (in µg) for ellipsoidal (red) and spherical (black) aAPCs. (D) T cell proliferation (fold expansion/10^5 cells) versus MHC-dimer density (in MHC-Ig/µm^2) for ellipsoidal (red) and spherical (black) aAPC at 3 doses of aAPC (0.01 mg, 0.1mg, and 1mg/10^5 $CD8^+$ *pmel* T cells).

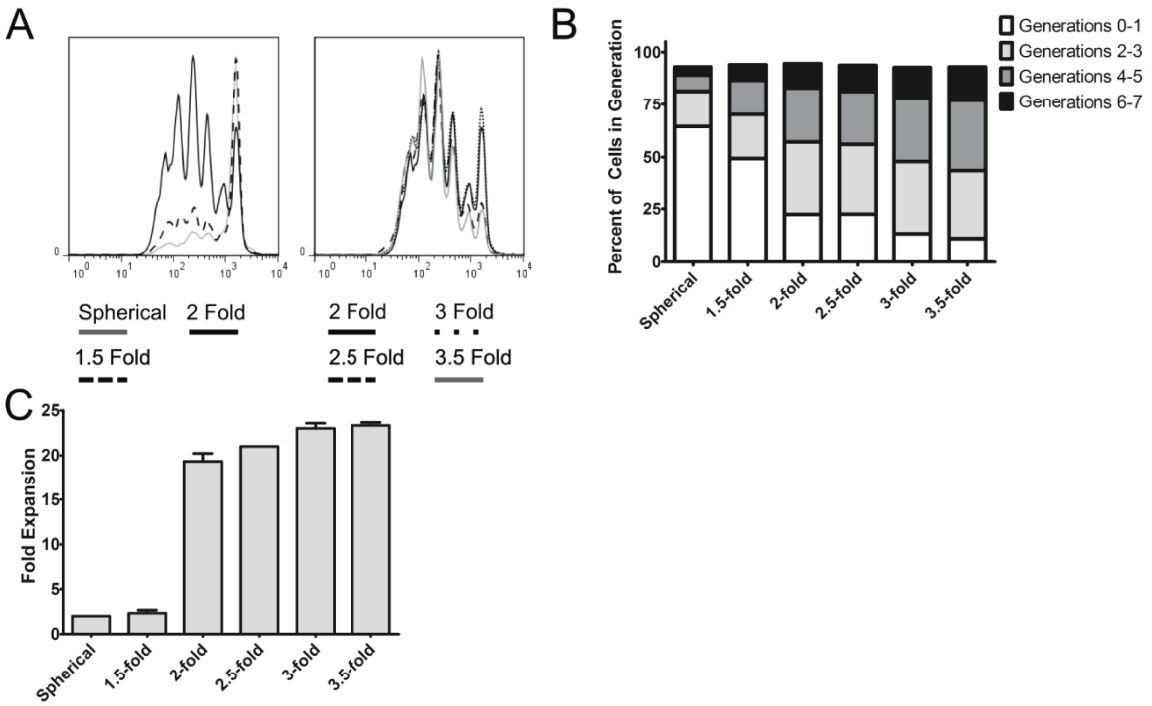

Figure 8.3: **Response to differential stretching.** Specific T cell proliferation in response to 0.01 mg particles/100,000 cell dose for ellipsoidal aAPCs with different applied stretch compared to spherical aAPCs. (A) CFSE dilution after aAPC addition to T cells. (B) Fraction of cells which underwent 0-1, 2-3, 4-5, 6-7 rounds of proliferation after aAPC addition to T cells. (C) T cell proliferation (fold expansion/100,000 cells) 7 days after aAPC addition to T cells.

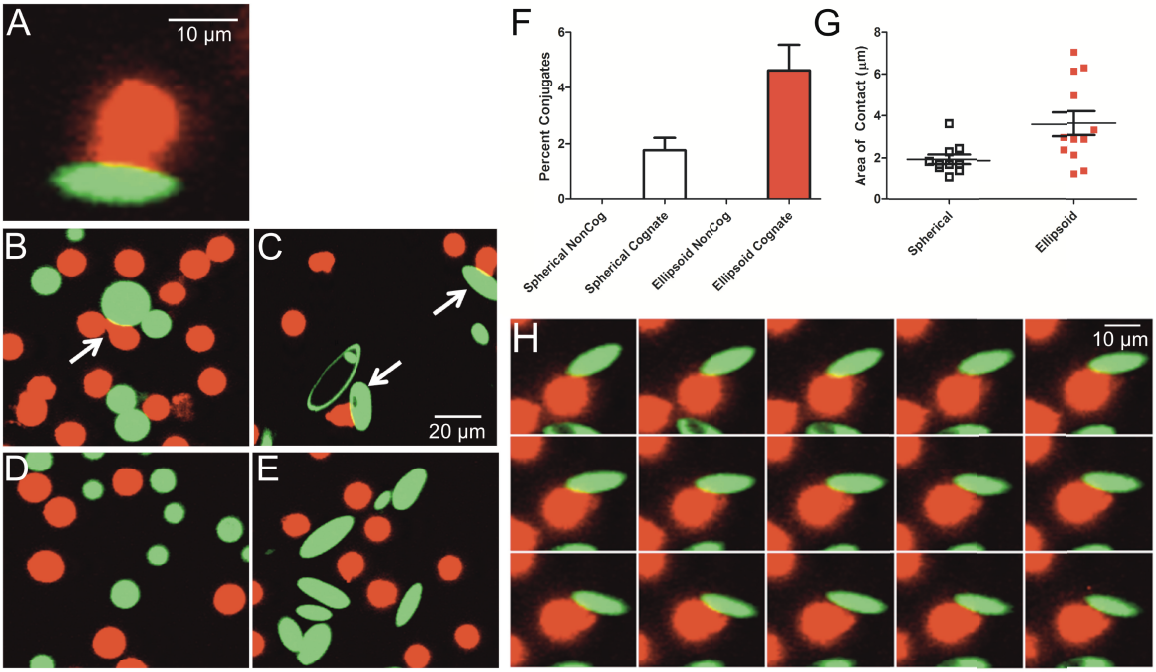

Figure 8.4: Confocal imaging of aAPC (green) conjugate formation to T cells (red). (A) Conjugates appear as areas of close membrane apposition between aAPC and cells, with T cell morphology rearrangement into a distinctive cap. (B) Spherical and (C) ellipsoidal aAPC form cell-bead conjugates, which are more frequently observed with ellipsoidal aAPC. (D-E) Conjugate formation is not observed with aAPC bearing non-cognate MHC-peptide. (F) 4.6 ± 0.9% of T cells incubated with ellipsoidal aAPC (red) compared to 1.8 ± 0.4% with spherical aAPC (unfilled) were observed to have formed conjugates (p=0.01). (G) The area of contact between cells and aAPC was 1.9 ± 0.2 μm for spherical (unfilled) and 3.6 ± 0.6 μm for ellipsoidal (red) cognate aAPC (p = 0.01). (H) Time-lapse image of a single T cell interacting with one ellipsoidal cognate aAPC; images acquired 2 s apart.

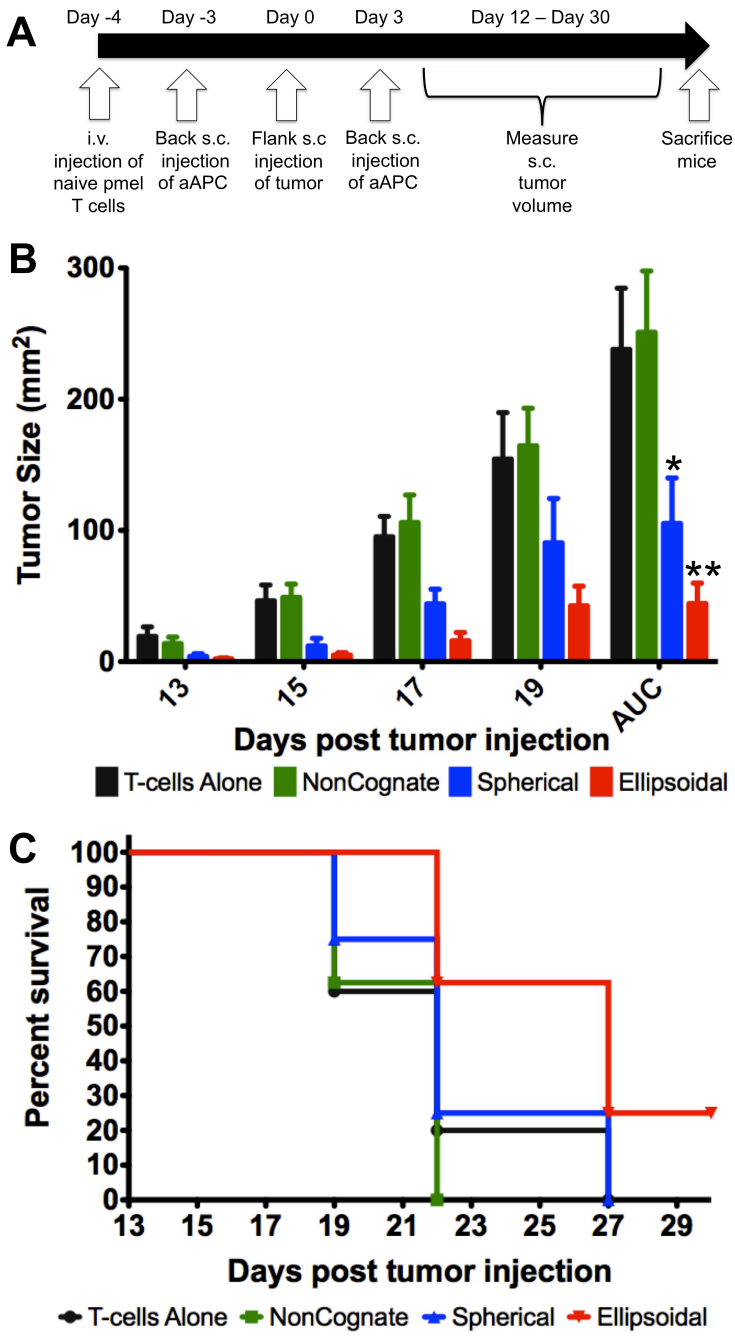

Figure 8.5: In vivo tumor-prevention model. (A) Experimental protocol and timeline. (B) Tumor size measurements for mice injected with cancer and T cells alone or also injected with non-cognate ellipsoidal (NonCognate), cognate spherical (Spherical), and cognate ellipsoidal aAPC (Ellipsoidal). AUC = area under the curve. * p = 0.02 vs. non-cognate; ** p = 0.0009 vs. non-cognate. For comparison of ellipsoidal cognate and spherical cognate by AUC, p = 0.13. (C) Survival curve – mice were sacrificed and declared "dead" when tumor size reached 200 mm^2. Subcutaneous injection of ellipsoidal aAPC resulted in increased survival vs. spherical non-cognate particles (p=0.05), ellipsoidal non-cognate particles (p=0.004), and T cells alone (p=0.05).

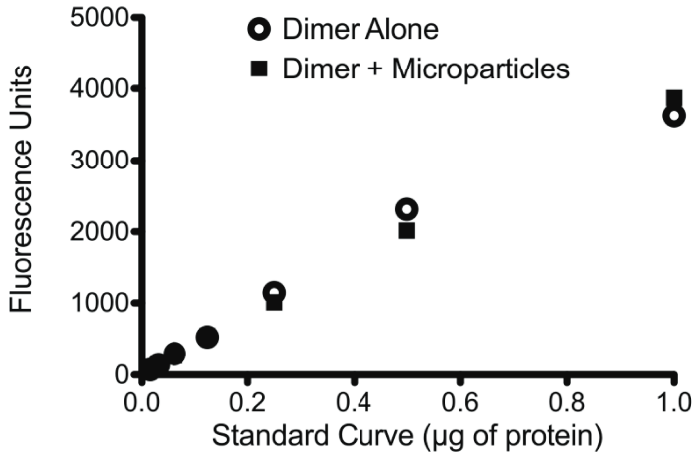

Figure 8.S1: Standard curves for fluorescently labeled MHC dimer or for dimer + 2 mg microparticles per well.

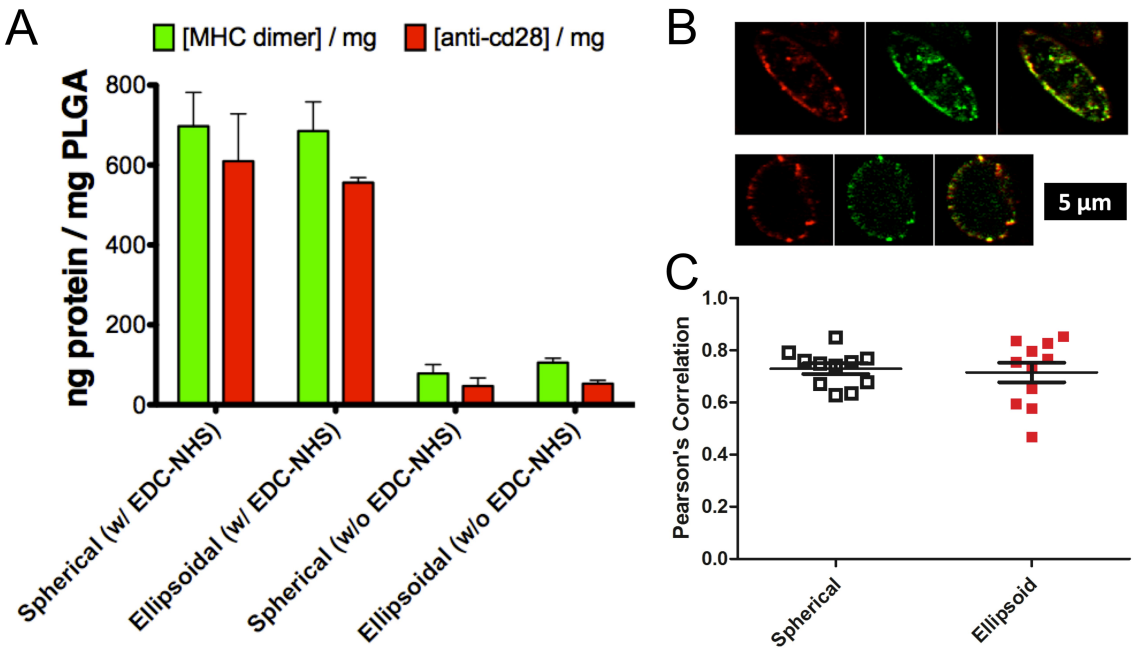

Figure 8.S2: Surface MHC-dimer (fluorescently labeled with alexa 488) and anti-CD28 (fluorescently labeled with APC) quantification by fluorescence. (A) Spherical and ellipsoidal aAPC synthesized with EDC/NHS chemistry did not have significant differences in MHC-dimer amount ($p = 0.92$) or density ($p = 0.42$), anti-CD28 amount ($p = 0.70$) or density ($p = 0.39$), or MHC-dimer/anti-CD28 ratio ($p = 0.72$). Approximately 85-90% of the protein on the surface required the EDC/NHS pre-activation step. (B) Representative confocal images of ellipsoidal and spherical aAPC showing anti-CD28 (red), MHC-dimer (green), and overlay of the two channels. (C) Pearson's correlation between the red and green channels for spherical and ellipsoidal aAPC (value?)

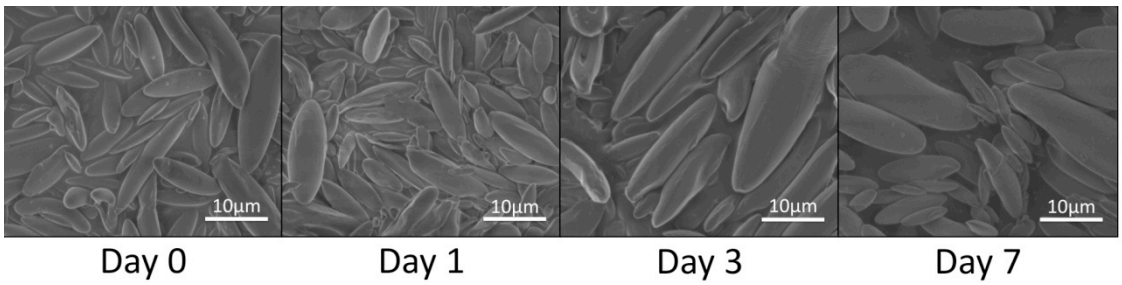

Figure 8.S3: aAPCs do not change their shape in physiological conditions over one week. SEM of freshly prepared aAPCs (a) and aAPCs incubated in PBS at 37°C for (b) 1 day, (c) 3 days, (d) 7 days. The calculated ARs were: (a) 3.57; (b) 3.31; (c) 3.34; (d) 3.23.

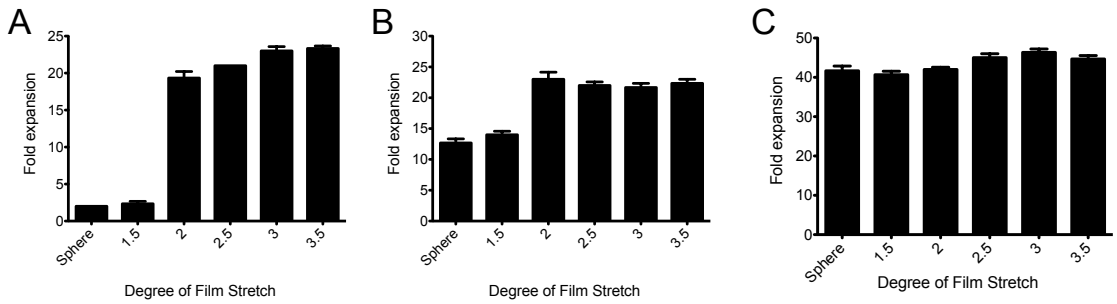

Figure 8.S4: Fold expansion of PMEL T cells post incubation with (A) 0.01 mg / 100,000 cells, (B) 0.1 mg / 100,000 cells, and (C) 1 mg / 100,000 cells of differentially stretched ellipsoidal aAPC as indicated. Negative controls with non-cognate peptide-in-MHC showed no expansion.

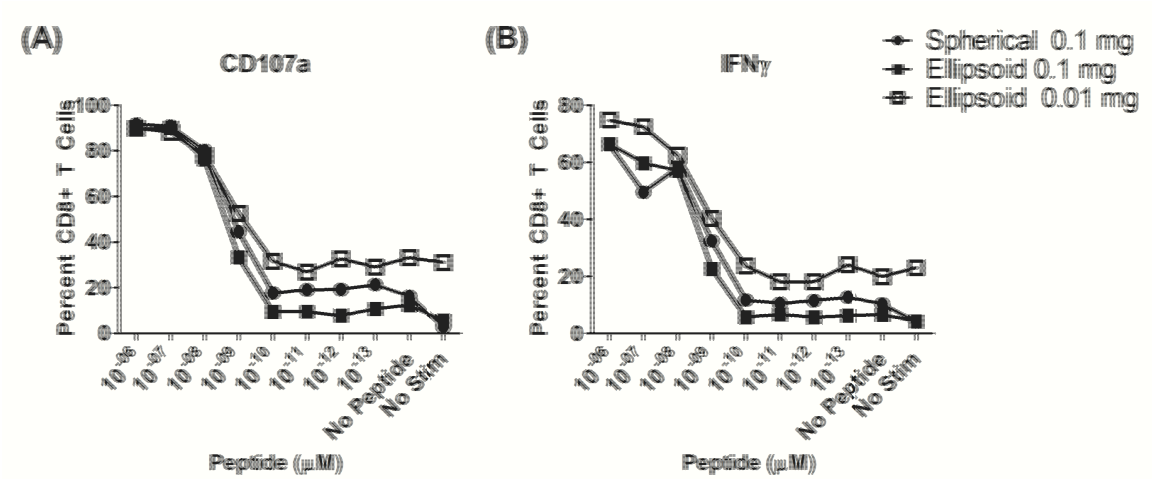

Figure 8.S5: Intracellular cytokine staining after stimulation of aAPC-activated T cells. CD8+ isolated splenocytes were activated with 0.1 mg spherical aAPC (filled circle), 0.1 mg of ellipsoidal aAPC (filled square), or 0.01 mg of ellipsoidal aAPC (unfilled square). Seven days later, T cells were restimulated with splenocytes from C57BLACK6 mice pulsed with the indicated dose of cognate GP100 peptide. Unpulsed splenocytes (No Peptide) or no splenocytes (No Stim) were used as controls. Cytokine production is reported as percentage of T cells making indicated cytokine.

Table 8.1: Key physical parameters altered by stretching of particles: (a) Aspect ratio (AR). (b) Surface area (SA) of ellipsoidal particles, relative to spheres. (c) Protein density on surface of aAPC with equivalent total protein content relative to spheres. (d-f) Radius of curvature, R, for the tip of the ellipsoid (R_a), and for the flat face of the prolate spheroid in either direction (R_b, R_c). For equations used, and description of derivations, see **Supplemental calculation**.

Stretch	AR	Rel. SA	Rel. Density	R_a	R_b	R_c
Sphere	1	1	1	1	1	1
1.5	1.84	1.06	0.94	0.44	2.8	0.82
2	2.83	1.16	0.86	0.25	5.7	0.71
2.5	3.95	1.27	0.78	0.16	9.9	0.63
3	5.20	1.38	0.72	0.11	16	0.58
3.5	6.55	1.48	0.67	0.08	23	0.53

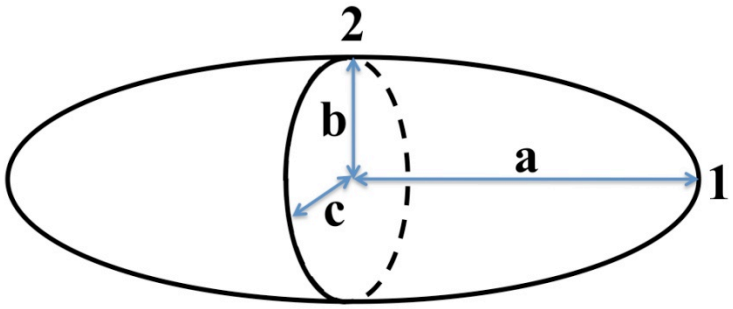

Figure 8.S6: A prolate ellipsoid (a > b = c) with axes labeled and key points numbered.

Supplemental calculation: See Fig. S6 for the identities of *a*, *b*, *c*, **1**, and **2**.
Determining the lengths of a, b, c: For a spheroid that has been elongated in 1 dimension, since total volume is conserved from a sphere, the length of the short axes is related to the length of the long axis by $b = c = \frac{1}{\sqrt{a}}$

Surface area of a prolate spheroid: Since the geometrical shape corresponds to a prolate spheroid (a > b = c), the surface area of the spheroid can be determined by the following formula[43]:

$$SA = 2\pi b^2 + 2\pi \frac{ab}{e} \sin^{-1} e \text{ where } e = \sqrt{1 - \frac{b^2}{a^2}}$$

This surface area was then normalized by the surface area of a sphere with radius 1.

Equivalent protein density: Equivalent protein density with total protein content held constant is the inverse of the normalized surface area (density = 1/SA).

Radius of curvature: The radius of curvature is the radius of a circle with the same curvature as the observed curve at that point. Thus, for flatter curves, the radius of curvature increases, as that flatness requires a larger circle to describe it.

An ellipse can be described parametrically by $\begin{matrix} x(t) = a\cos(t) \\ y(t) = b\cos(t) \end{matrix}$.

For any parameterized equation of the form $\begin{matrix} x = x(t) \\ y = y(t) \end{matrix}$,

the radius of curvature can be calculated[44] from:

$R = \frac{((x')^2 + (y')^2)^{3/2}}{|x'y'' - y'x''|}$, where $\begin{matrix} x' = dx/dt \\ y' = dy/dt \end{matrix}$ and $\begin{matrix} x'' = d^2x/dt^2 \\ y'' = d^2y/dt^2 \end{matrix}$.

So for an ellipse:

$$R = \frac{(a^2\sin^2(t) + b^2\cos^2(t))^{3/2}}{ab\sin^2(t) + ab\cos^2(t)} = \frac{(a^2\sin^2(t) + b^2\cos^2(t))^{3/2}}{ab}$$

To calculate the radius of curvature at the tip, since t = 0 corresponds to point **1** (**Fig. S5**), R_a can be calculated using *a* and *b* as the two axes of the ellipse. To calculate the radius of curvature at the tip, since t = π/2 corresponds to point **2** (**Fig. S5**), R_b can be calculated using *a* and *b* as the two axes of the ellipse and plugging in t = π/2. Thus,

$$R_a = \frac{b^3}{ab} = \frac{b^2}{a}$$

$$R_b = \frac{a^3}{ab} = \frac{a^2}{b}$$

And since the bc plane at 2 is already described by a circle, $R_c = b = c$.

8.6 References

1. Fletcher, D.A. and R.D. Mullins, *Cell mechanics and the cytoskeleton.* Nature, 2010. **463**(7280): p. 485-92.

2. Dustin, M.L., *T-cell activation through immunological synapses and kinapses.* Immunol Rev., 2008. **221**(221): p. 77-89.

3. Dykstra, M., et al., *Location is everything: lipid rafts and immune cell signaling.* Annu Rev Immunol, 2003. **21**: p. 457-81.

4. Grakoui, A., et al., *The immunological synapse: a molecular machine controlling T cell activation.* Science, 1999. **285**(5425): p. 221-7.

5. Lee, K.H., et al., *T cell receptor signaling precedes immunological synapse formation.* Science, 2002. **295**(5559): p. 1539-42.

6. Monks, C.R., et al., *Three-dimensional segregation of supramolecular activation clusters in T cells.* Nature, 1998. **395**(6697): p. 82-6.

7. Doh, J. and D.J. Irvine, *Immunological synapse arrays: patterned protein surfaces that modulate immunological synapse structure formation in T cells.* Proceedings of the National Academy of Sciences of the United States of America, 2006. **103**(15): p. 5700-5.

8. Oelke, M., et al., *Ex vivo induction and expansion of antigen-specific cytotoxic T cells by HLA-Ig-coated artificial antigen-presenting cells.* Nat Med, 2003. **9**(5): p. 619-25. PMID: 12074385.

9. Ugel, S., et al., *In vivo administration of artificial antigen-presenting cells activates low-avidity T cells for treatment of cancer.* Cancer Res, 2009. **69**(24): p. 9376-84.

10. Mescher, M.F., *Surface contact requirements for activation of cytotoxic T lymphocytes.* J Immunol, 1992. **149**(7): p. 2402-5.

11. Han, H., et al., *A novel system of artificial antigen-presenting cells efficiently stimulates Flu peptide-specific cytotoxic T cells in vitro.* Biochem Biophys Res Commun, 2011. **411**(3): p. 530-5.

12. Steenblock, E.R., et al., *An artificial antigen-presenting cell with paracrine delivery of IL-2 impacts the magnitude and direction of the T cell response.* J Biol Chem, 2011. **286**(40): p. 34883-92.

13. Steenblock, E.R. and T.M. Fahmy, *A comprehensive platform for ex vivo T-cell expansion based on biodegradable polymeric artificial antigen-presenting cells.* Mol Ther, 2008. **16**(4): p. 765-72. PMID: 18334990.

14. Ndhlovu, Z.M., et al., *Dynamic regulation of functionally distinct virus-specific T cells.* Proc Natl Acad Sci U S A, 2010. **107**(8): p. 3669-74.

15. Ito, F., et al., *Antitumor reactivity of anti-CD3/anti-CD28 bead-activated lymphoid cells: implications for cell therapy in a murine model.* J Immunother, 2003. **26**(3): p. 222-33.

16. Lum, L.G., et al., *Immune modulation in cancer patients after adoptive transfer of anti-CD3/anti-CD28-costimulated T cells-phase I clinical trial.* J Immunother, 2001. **24**(5): p. 408-19.

17. Taylor, P.A., C.J. Lees, and B.R. Blazar, *The infusion of ex vivo activated and expanded CD4(+)CD25(+) immune regulatory cells inhibits graft-versus-host disease lethality.* Blood, 2002. **99**(10): p. 3493-9.

18. Balmert, S.C. and S.R. Little, *Biomimetic delivery with micro- and nanoparticles.* Advanced Materials, 2012. **24**(28): p. 3757-78.

19. Wang, J., et al., *More effective nanomedicines through particle design.* Small, 2011. **7**(14): p. 1919-31.

20. Champion, J.A. and S. Mitragotri, *Role of target geometry in phagocytosis.* Proc Natl Acad Sci U S A, 2006. **103**(13): p. 4930-4.

21. Sharma, G., et al., *Polymer particle shape independently influences binding and internalization by macrophages.* J Control Release, 2010. **147**(3): p. 408-12.

22. Champion, J.A., Y.K. Katare, and S. Mitragotri, *Particle shape: a new design parameter for micro- and nanoscale drug delivery carriers.* J Control Release, 2007. **121**(1-2): p. 3-9.

23. Devarajan, P.V., et al., *Particle shape: a new design parameter for passive targeting in splenotropic drug delivery.* J Pharm Sci, 2010. **99**(6): p. 2576-81.

24. Harris, B.J. and P. Dalhaimer, *Particle shape effects in vitro and in vivo.* Front Biosci (Schol Ed), 2012. **4**: p. 1344-53.

25. Barua, S., et al., *Particle shape enhances specificity of antibody-displaying nanoparticles.* Proc Natl Acad Sci U S A, 2013. **110**(9): p. 3270-5.

26. Yoo, J.W. and S. Mitragotri, *Polymer particles that switch shape in response to a stimulus.* Proc Natl Acad Sci U S A, 2010. **107**(25): p. 11205-10.

27. Schneck, J.P., et al., *Monitoring antigen-specific T cells using MHC-Ig dimers.*, in *Current protocols in immunology*, J.E. Coligan, Editor. 2011.

28. Rothstein, S.N., W.J. Federspiel, and S.R. Little, *A unified mathematical model for the prediction of controlled release from surface and bulk eroding polymer matrices.* Biomaterials, 2009. **30**(8): p. 1657-64.

29. Batycky, R.P., et al., *A theoretical model of erosion and macromolecular drug release from biodegrading microspheres.* Journal of Pharmaceutical Sciences, 1997. **86**(12): p. 1464-77.

30. von Burkersroda, F., L. Schedl, and A. Gopferich, *Why degradable polymers undergo surface erosion or bulk erosion.* Biomaterials, 2002. **23**(21): p. 4221-31.

31. Gottschalk, R.A., et al., *Distinct influences of peptide-MHC quality and quantity on in vivo T-cell responses.* Proc Natl Acad Sci U S A, 2012. **109**(3): p. 881-6.

32. Arens, R. and S.P. Schoenberger, *Plasticity in programming of effector and memory CD8 T-cell formation.* Immunol Rev, 2010. **235**(1): p. 190-205.

33. Bullock, T.N., D.W. Mullins, and V.H. Engelhard, *Antigen density presented by dendritic cells in vivo differentially affects the number and avidity of primary, memory, and recall CD8+ T cells.* J Immunol, 2003. **170**(4): p. 1822-9.

34. Seder, R.A., P.A. Darrah, and M. Roederer, *T-cell quality in memory and protection: implications for vaccine design.* Nat Rev Immunol, 2008. **8**(4): p. 247-58.

35. Kroger, C.J. and M.A. Alexander-Miller, *Cutting edge: CD8+ T cell clones possess the potential to differentiate into both high- and low-avidity effector cells.* J Immunol, 2007. **179**(2): p. 748-51.

36. Curtsinger, J., et al., *Artificial cell surface constructs for studying receptor-ligand contributions to lymphocyte activation.* J Immunol Methods, 1997. **209**(1): p. 47-57.

37. Maus, M.V., et al., *Ex vivo expansion of polyclonal and antigen-specific cytotoxic T lymphocytes by artificial APCs expressing ligands for the T-cell receptor, CD28 and 4-1BB.* Nat Biotechnol, 2002. **20**(2): p. 143-8.

38. Steenblock, E.R., et al., *Antigen presentation on artificial acellular substrates: modular systems for flexible, adaptable immunotherapy.* Expert Opin Biol Ther, 2009. **9**(4): p. 451-64. PMID: 19344282.

39. Suhoski, M.M., et al., *Engineering artificial antigen-presenting cells to express a diverse array of co-stimulatory molecules.* Mol Ther, 2007. **15**(5): p. 981-8.

40. Levine, B.L., et al., *Effects of CD28 costimulation on long-term proliferation of CD4+ T cells in the absence of exogenous feeder cells.* J Immunol, 1997. **159**(12): p. 5921-30.

41. Schneck, J.P., et al., *Monitoring antigen-specific T cells using MHC-Ig dimers*, in *Current protocols in immunology*, J.E. Coligan, Editor. 2001.

42. Durai, M., et al., *In vivo functional efficacy of tumor-specific T cells expanded using HLA-Ig based artificial antigen presenting cells (aAPC).* Cancer Immunol Immunother, 2009. **58**(2): p. 209-20.

43. Weisstein, E.W. *Prolate Spheroid*. MathWorld - A Wolfram Web Resource 2012; Available from: http://mathworld.wolfram.com/ProlateSpheroid.html.

44. Weisstein, E.W. *Radius of Curvature*. MathWorld - A Wolfram Web Resource 2012; Available from: http://mathworld.wolfram.com/RadiusofCurvature.html.

9 Chapter 9: Future Directions

9.1 Next generation artificial Antigen Presenting Cells for Tumor Immunotherapy

For the development of next-generation nanoengineered aAPCs special attention should be paid to particle size and particle shape, and at the protein level, surface density, spatial organization and dynamics are key parameters of interest (**Table 9.1**).

There are potentially many advantages to a nanosized immunostimulatory platform for use *in vivo*. Smaller particles (20-200 nm in diameter) can transit directly to the lymphatics after subcutaneous injection without the aid of phagocytosis [1], where they could reach the T cell population in the ideal setting for T cell expansion. Nanosized constructs are also potentially i.v. injectable, as micro-sized particles would potentially be trapped in the capillary bed of the lungs, blocking capillary flow. Additionally, control over surface topology on the nanoscale (shape), surface density, and surface organization, would more precisely mimic the biological setting. The fabrication of such technology would also allow for greater understanding about the role of geometry, protein surface organization, and dynamic rearrangement play with natural biological APCs.

9.1.1 Nanoscale surface patterning

Most aAPC systems utilize uniform presentation of ligands on the surface, due to ease of fabrication and simplicity of design. However, the interaction of a biological APC

[8] This chapter contains excerpts from an article that was published as Sunshine JC, Green JJ. "Nanoengineering approaches to the design of artificial antigen-presenting cells." Nanomedicine 2013, 8(7), 1173-1189.

with a T cell results in the formation of an organized, anisotropic arrangement of surface proteins termed the immunological synapse (IS) [2, 3]. When mature, the IS consists of two main distinct concentric rings of organized proteins. The central supramolecular activation cluster (cSMAC) consists primarily of TCRs in contact with peptide-MHC molecules on the APC surface and other costimulatory molecules (such as the B7:CD28 interaction). This is surrounded by a peripheral supramolecular activation cluster (pSMAC), formed by integrin:adhesion molecule interactions (principally LFA-1 on the T cell surface binding ICAM-1 on the APC surface). Taking advantage of these dynamic rearrangements and anisotropic protein arrangements could be of great advantage in future aAPC systems.

One potential way of mimicking the biomolecular organization of the immune synapse on aAPC systems would be to utilize recent advances in the synthesis and design of patchy particles [4]. By formation of particles with at least two distinct surface subdomains, one could synthesize a particle that had the components of the cSMAC (pMHC and various costimulatory molecules) in one subdomain, with the components of the pSMAC (principally ICAM-1) in the other subdomain. As these designs get more advanced, more precise biomimicry could be achieved with such systems.

Janus particles, named after the Roman god Janus who had two faces, are particles that have two distinct faces. The various synthetic approaches to Janus particles are helpfully reviewed by Walther and Muller [5], and these approaches to double sided particles could prove useful for the development of aAPCs.

Lithography has proved to be an incredibly useful tool in a number of fields, for computers, to microfulidics, to biology. In the 2D setting, researchers have developed

immunological synapse arrays, which are stimulatory patches surrounded by integrin fields in a flat lithographically patterned substrate [6], and used them to study how the disruption of these 2D immunological synapses might affect the response of T cells to these substrates. Complex particle lithography, on the micro- and particularly nano-scale, has proven to be challenging. However, some work has been done in this area to develop particles that might be suitable for nanoscale aAPC design. Snyder et al. used polyelectrolytes to cover the exposed surface of amine-functionalized PS spheres adhered to negatively charged cover slips as a mask [7]. Using microcontact printing techniques and PDMS molds, Cayre et al were able to synthesize dipolar particles [8]. In addition, they extended their method to allow printing of one colloidal layer onto another, which enables the formation of "raspberry" particles if the particles are of very dissimilar sizes [9].

Another approach to the formation of patchy particles with multiple patches involves the use of glancing angle deposition (GLAD) [10]. The GLAD technique involves the deposition of gold or silver vapor onto a close-packed colloidal monolayer at low pressure. The technique is referred to as "glancing angle" because the sample is angled with respect to the vapor deposition. Changing the angle allows alterations in the geometry of and location of the vapor deposition. To produce multiple patches of different functionalities, the vapor deposition is done in two steps. To position the second group differently, the angle of deposition is changed. This can allow for two separate patches on the same side of the particle that also interconnect. Patches can be produced on opposite poles of the particles by using a PDMS stamp to flip the particles and then allow vapor deposition to proceed on the opposite side [11]. These techniques have also

been applied to colloidal crystals. By using upper single or double layers in colloidal crystals as masks during the vapor deposition, Zhang et al. were able to develop patterns on the 3rd layer of nanoparticles with nanoscale feature resolution [12].

Recently, Kamalasanan et al. reported a novel technique to produce multiple circular patches on the surface of microspheres. The technique involves applying liquid polydimethylsiloxane (PDMS) to a 3D colloidal crystal or various 2D arrays of spherical polystyrene microparticles. During this process, selective solidification of the PDMS happens at particle interfaces, allowing for those sites to be selectively blocked by the PDMS masks (**Fig. 9.1**) [13]. This process allows ligand to be conjugated at the unblocked sites, followed by exposure of the PDMS patches, and addition of a second ligand or set of ligands to the newly exposed sites. The number of PDMS patches is determined by the coordination number of the particle in the colloidal crystal / 2D array [13].

Microfluidics has also been used to address the problem of synthesizing particles with multiple functionalities. Particles are synthesized by flowing multiple polymers or monomers into a single stream [14]. Janus and ternary particles can be synthesized by mixing of 2 or 3 monomers with photoinitiator in a microfluidic device. A surfactant-containing stream is flowed in outside of the monomer containing streams, and these streams are then forced through a narrow opening that causes the fluid to break up into droplets. The droplets are then polymerized by UV irraditation [15]. This approach does not, however, generate particles with nanoscale features, as the particle sizes generated were around 100 microns. Biphasic Janus particles were generated with nanoscale features by the use of simultaneous electrohydrodynamic jetting [16]. In this case, instead

of the particles being generated by being forced through a narrow opening, an electric field is applied and the nano-janus particles are collected on the collecting plate which houses the counter-electrode (**Fig. 9.2**) [16]. This method can be performed using two of the same polymers while loading in different drugs in each half, and/or can allow selective chemical modification of one portion of the particle, making this setup amenable to the generation of biphasic nano-scale aAPCs. This technique does not allow the precise patterning afforded by some of the printing strategies, but future advances in the technique may make this a viable option. In addition, one could envision using this dual approach to provide cytokine release from one portion of the nanoparticle and stable ligand presentation from another portion of the nanoparticle, successfully avoiding some of the compromises often required for controlled release and surface presentation of ligands. Critically, this type of approach allows generation of a "top" and "bottom" or "front" and "back" which can each contain appropriate surface molecules and in this manner better mimic biological cells.

9.1.2 Dynamic surface rearrangement – Liposomes and Protocells

More recent advances in the use of liposomes as aAPCs help to demonstrate additional parameters of likely importance for nanoengineered approaches to aAPC design. In particular, the signal 1-signal 2-signal 3 model which emphasizes the identity of the molecular signals involved in the directed signaling by an APC to a T cell may be supplemented by developing approaches to mimic other critical aspects of the biological system.

Liposomes afford two advantages to solid particle systems that mimic the biological system more directly. First of all, liposomal membrane fluidity enables the aAPC to dynamically rearrange the proteins on its surface, in a similar fashion as the dramatic protein rearrangements that occur during APC / T cell interaction and generate the immune synapse. In addition to the ability of liposomes to allow for biomimetic nanoscale reorganization of the proteins expressed on the surface, further advances in the ability to control initial organization of the expressed proteins might also be enabling. With respect to immune synapse formation, an innovative study using 2D SLBs showed that the imposition of patterned lines disrupted the geometry of the immune synapse [17]. These data indicate that initial TCR engagement is followed by formation of TCR microdomains, which are then followed by directed transport of microclusters to form the final cSMAC. Lipid rafts, which are small, 10-200 nm domains that are highly enriched in sterols (such as cholesterol) or sphingolipids [18], have shown to be critical organizing features of biological membranes [19, 20], and molecular simulations have indicated the importance of these nano-domains to improve protein-protein interaction [21]. In fact, biological APCs have been shown to pre-cluster antigen even in the absence of T cells [22], and concentration of MHC molecules into lipid rafts has been shown to improve antigen presentation in biological APCs [23]. Perhaps partitioning cSMAC components into small lipid rafts for initial TCR signaling and allowing flow in the membrane to rearrange into larger clusters might be a particularly effective method to mimic the biology and achieve optimal stimulation from aAPCs.

Giannoni et al. showed that preclustering of peptide-MHC and costimulatory signals in a nanoscale liposomal system resulted in higher T cell stimulation than with

soluble tetramers or liposomal aAPC without preclustering [24]. The beta subunit of cholera toxin interacts strongly with cholesterol, a major component of lipid rafts. Preclustering was accomplished by linking the surface proteins to cholera toxin by biotin-neutravidin interactions (with biotin on the antibodies, and neutravidin on the beta subunit of cholera toxin). Importantly, the distribution alone (with no alteration in the quantity of any ligand critically modulated the strength of the stimulation by the aAPC. A subsequent study where the same group added anti-LFA-1 (the major adhesion molecule involved) to anti-CD3 (for general T cell activation) and anti-CD28 (for costimulation) all preclustered in microdomains as before resulted in increased expansion of polyclonal T cells and MART-1-specific CD8+ T cells than commercially available systems [25]. Interestingly, this second approach of preclustering LFA-1 with cSMAC components does not allow for subsequent segregation of the LFA-1 into the surrounding pSMAC. Perhaps future experiments might investigate whether pre-clustering of signal 1 and signal 2 separate from adhesion molecules such as LFA-1 might more directly mimic the biological situation and further enhance activation.

A major difficulty that has hindered the use of liposomes as aAPC surrogates is their relative instability when compared to solid particles. One potential novel new solution, which has been used for drug delivery but has yet to be applied to the design of aAPC, is the concept of particle-supported lipid bilayers (pSLBs).

Particle systems which incorporate lipid monolayers or lipid bilayers on their surfaces have been developed which offer improved stability and drug delivery particles to standard liposomal formulations [26]. To synthesize aAPC, the focus is on supported lipid bilayers (SLB) as opposed to the systems that utilize only lipid monolayers at the

particles surface, because SLBs enable the replication of the fliuidity of biological membranes in artificial systems. In particular, for the design of future aAPCs, mimicking the biological situation that allows for large-scale protein rearrangement subsequent to TCR triggering is likely of significant benefit.

Supported lipid bilayers have been used extensively as a model system for the study of the molecular dynamics of immune synapses, as they provide a flexible platform that is compatable with modern imaging techniques and have most of the characteristics of a real APC membrane [27]. This technique, extensively studied in 2D, has been recently applied to the synthesis of nanoparticles with supported lipid bilayers on a hydrogel [28], silica particle [29, 30], or polymeric (PLGA) particle core [31]. These particle-supported lipid bilayers can be anchored (by covalently attaching the inner layer to the surface) or can be unanchored, with a lipid bilayer sitting on the surface of the silica or polymeric particle core.

Ashley et al. developed a "protocell" which consists of a nanoporous silica core and a supported lipid bilayer which can be modified with targeting ligand, fusogenic peptides, and polyethylene glycol (PEG) that enables increased stability and drug delivery capacity (**Fig. 9.3**) [32]. Interestingly, the nanoporous silica particles showed increased membrane fluidity when compared with protocells formed from non-porous solid silica nanoparticles or unsupported liposomes. These protocells can be loaded with a variety of cargoes, such as small molecule druges, siRNA, toxins, or quantum dots, and show vastly improved (10^6-fold) anticancer activity when compared to comparable liposomes. Critically, this indicates the potential to use this system to release immunomodulatory cytokines from the construct, potentially allowing the synthesis of a

system which can provide signal 1, signal 2, and signal 3 while replicating the fluidity of biological membranes in a stable fashion.

Porotto et al. have used larger (3 μm) protocells designed to inactivate enveloped viruses by presenting viral entry receptors on the surface of the protocells. This enables the protocells to act as cellular decoys, inactivating viruses that would otherwise infect healthy cells by triggering premature fusion of the viruses. Interestingly, at low temperatures (4 °C), the protocells were unable to activate virus, whereas at 37 °C, considerable inactivation was demonstrated. This indicates that membrane fluidity is required for protocell inactivation of the virus. Importantly, the protocells did not accumulate virus, but rather were renewable, as binding led directly to premature fusion and permanent inactivation of the viruses [33].

In addition to fully chemically synthesized supported lipid bilayers, natural erythrocyte membranes have been used to coat biodegradable polymeric microparticles [31], and leukocyte-membranes have been fused to silica cores [34]. These approaches present an alternative to the reductionist systems typically used in acellular aAPC systems, and offer the potential to generate particles which are coated with real DC membranes and perhaps subsequently modified to generate an off-the-shelf, acellular aAPC which has much of the benefits of an acellular system while retaining all the critical components of a real DC membrane.

9.1.3 Conclusion & Future Perspective

Acellular aAPC have particularly shown great initial promise for *ex vivo* activation of CTL and have been investigated for *in vivo* applications as well. The development of aAPCs has focused mainly on the choice of proteins to use for surface

presentation to T cells when conjugated to various spherical, micro-scale particles. Key recent advances have allowed for the development of acellular aAPCs that incorporate more biological cues than antigen recognition (signal 1) and costimulation (signal 2). aAPCs have been developed that incorporate secretable cues (cytokines, "signal 3") and surface geometric cues that operate from the nanoscale to the microscale, such as interfacial geometry, surface protein organization and segregation, and dynamic protein rearrangement. Early work has demonstrated a critical role for particle size, showing that the surface area available for contact is crucial in these systems. Additionally, preclustering of protein signals into nanodomains (lipid rafts) has been shown to be of substantial benefit for aAPC-based stimulation.

New synthetic particle technology has been developed to synthesize patchy particles with varying geometry and nanoscale features. These technologies may allow for the development of nanoscale anisotropic aAPCs with that mimic the physical segregation evident in the immune synapse.

Liposome based aAPCs, and lipid rafts, enable the generation of nanoclustered surface functionality, and the fluidity of the membranes allows for more biomimetic dynamic rearrangement of surface proteins upon contact with target cells. However, liposomes suffered from relative instability as compared to solid particles. Recent advances in the development of supported lipid bilayers might enable the generation of SLB based aAPCs that offer the advantages of liposomal systems with superior stability and improved drug release.

Biodegradable particles offer strong biocompatablility and are useful for release of secretable cues or other immunomodulatory factors. Recent advances in the

development of methods for the generation of non-spherical biodegradable particles may enable next-generation aAPC with interfacial geometry that more closely mimics the biological situation. In addition, non-spherical aAPC offer the potential of developing nanoparticles with interfacial geometry similar to successful microparticulate systems, with improved *in vivo* performance due to easy access to draining lymph nodes and suitability for intravenous injection.

Of particular interest may be an approach that combines all of these techniques to generate non-spherical supported lipid bilayers with sustained surface presentation on the micro- or nanoscales.

9.2 Figures

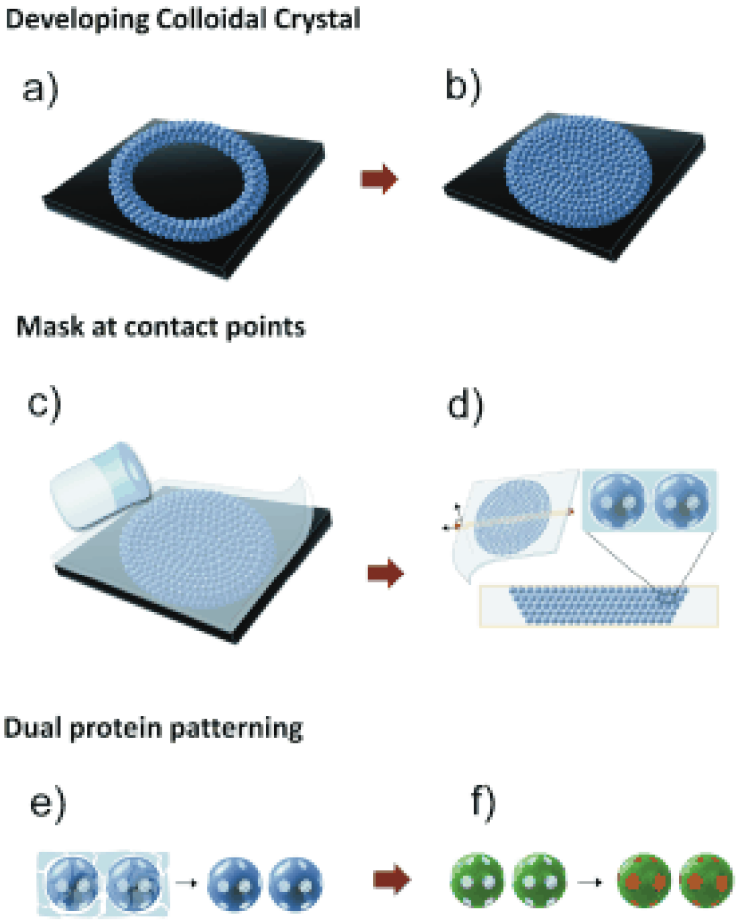

Figure 9.1: Patchy particles can be formed by filling a well with a colloidal crystal iteratively (a,b), then forming a PDMS mask by adding PDMS solution (c); as dewetting occurs at the interface between particles, PDMS patches form at the contact points (d). The particles can be separated from the scaffold (c) and two different proteins can be added by adding the first protein to the exposed region (f, green) followed by removal of the mask and addition of a second protein (f, red). Reproduced with permission from John Wiley and Sons: Angewandte Chemie International Edition [13], copyright 2011.

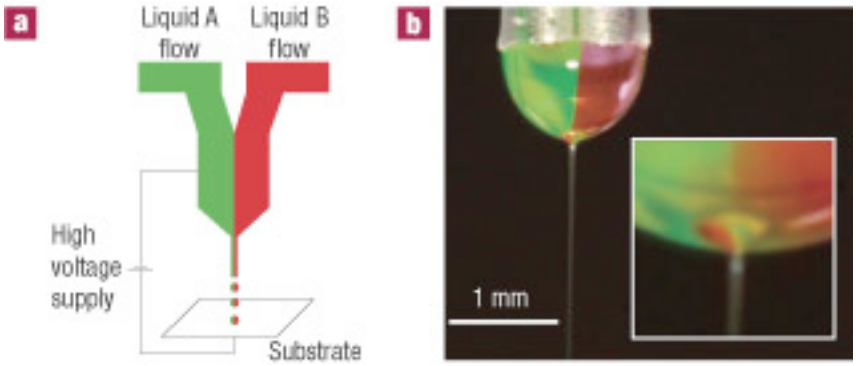

Figure 9.2: (a) The experimental setup used for generation of nanoscale biphasic Janus particles. The bipolar jetting fluid is exposed to applied electrical potential and the particles are collected on the counter electrode. (b) Digital image of the biphasic taylor cone with jet. Reproduced with permission from Macmillan Publishers Ltd: Nature Materials [16], copyright 2005.

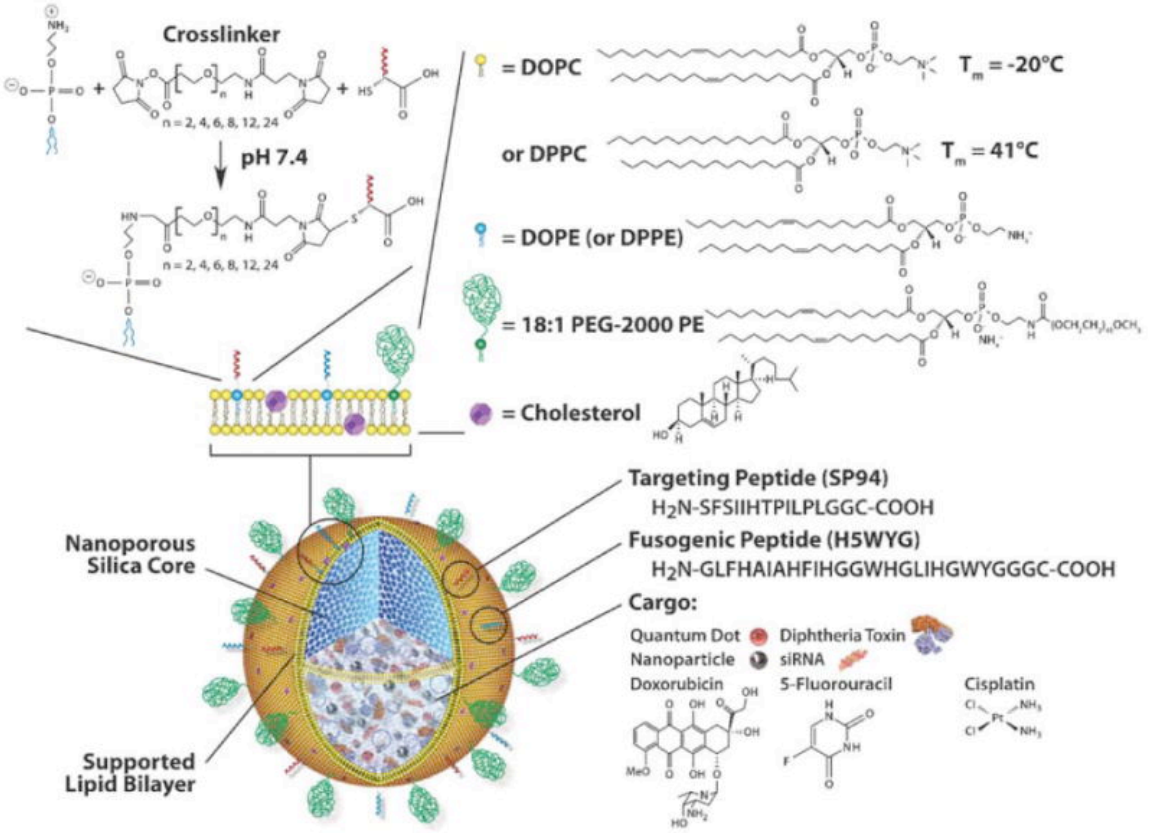

Figure 9.3: A schematic showing a particle supported lipid bilayer, with the range of cargoes and surface ligands that can be encapsulate or presented on the surface of the particle. Reproduced with permission from Macmillan Publishers Ltd: Nature Materials [32], copyright 2011.

Table 9.1: Key parameters for designing next-generation aAPCs

Key Parameter	Activated Biological APC / DC	Current aAPC	Future aAPC
Signal 1 - Recognition	Peptide-in-MHC (pMHC)	Antigen specific: pMHC/pMHC multimers General T cell targeting: anti-CD3 mAb	pMHC multimers
Signal 2 - Costimulation	B7.1, B7.2, etc.	Anti-CD28 mAb	Anti-CD28 mAb and others
Signal 3 – Secretable, Immunomodulatory Signals	Various (eg. IL-2) or chemokine (eg. CCL3, CCL4, etc.) [35]	IL-2 release[36]	Cytokine or chemokine release
Size	20 μm diameter	4-5 μm > 1 μm for spherical aAPC[37]	Micro- or nano-scale
Shape	Long, thin, sheet like projections/veils in many directions from the cell body; highly dynamic[38]	Spherical	Non-spherical
Density	Dynamic local density	2000 MHC/μm^2 > 10000 or 40000 MHC/μm [39]	Preclustered, intermediate density
Organization	Before T cell contact: Microclustering After contact with T cell: Dynamic reorganization; Immune synapse formation[2, 3, 17, 22, 23, 40]	Liposomes/lipid bilayers allow for preclustering, dynamic reorganization[24, 25]	Preclustered with dynamic reorganization via supported lipid bilayers

9.3 References

1. Manolova, V., et al., *Nanoparticles target distinct dendritic cell populations according to their size.* Eur J Immunol, 2008. **38**(5): p. 1404-13.
2. Grakoui, A., et al., *The immunological synapse: a molecular machine controlling T cell activation.* Science, 1999. **285**(5425): p. 221-7.
3. Lee, K.H., et al., *T cell receptor signaling precedes immunological synapse formation.* Science, 2002. **295**(5559): p. 1539-42.
4. Pawar, A.B. and I. Kretzschmar, *Fabrication, assembly, and application of patchy particles.* Macromol Rapid Commun, 2010. **31**(2): p. 150-68.
5. Walther, A. and A.H.E. Muller, *Janus particles.* Soft Matter, 2008. **4**(4): p. 663-668.
6. Doh, J. and D.J. Irvine, *Immunological synapse arrays: patterned protein surfaces that modulate immunological synapse structure formation in T cells.* Proc Natl Acad Sci U S A, 2006. **103**(15): p. 5700-5.
7. Snyder, C.E., et al., *Nanoscale functionalization and site-specific assembly of colloids by particle lithography.* Langmuir, 2005. **21**(11): p. 4813-5.
8. Cayre, O., V.N. Paunov, and O.D. Velev, *Fabrication of dipolar colloid particles by microcontact printing.* Chem Commun (Camb), 2003(18): p. 2296-7.
9. Cayre, O., V.N. Paunov, and O.D. Velev, *Fabrication of asymmetrically coated colloid particles by microcontact printing techniques.* Journal of Materials Chemistry, 2003. **13**(10): p. 2445-2450.
10. Zhao, Y.P., et al., *Novel nano-column and nano-flower arrays by glancing angle deposition.* Nano Letters, 2002. **2**(4): p. 351-354.
11. Pawar, A.B. and I. Kretzschmar, *Multifunctional patchy particles by glancing angle deposition.* Langmuir, 2009. **25**(16): p. 9057-63.
12. Zhang, G., D.Y. Wang, and H. Mohwald, *Patterning microsphere surfaces by templating colloidal crystals.* Nano Letters, 2005. **5**(1): p. 143-146.
13. Kamalasanan, K., et al., *Patchy, anisotropic microspheres with soft protein islets.* Angew Chem Int Ed Engl, 2011. **50**(37): p. 8706-8.
14. Serra, C.A. and Z.Q. Chang, *Microfluidic-assisted synthesis of polymer particles.* Chemical Engineering & Technology, 2008. **31**(8): p. 1099-1115.
15. Nie, Z.H., et al., *Janus and ternary particles generated by microfluidic synthesis: Design, synthesis, and self-assembly.* Journal of the American Chemical Society, 2006. **128**(29): p. 9408-9412.
16. Roh, K.H., D.C. Martin, and J. Lahann, *Biphasic Janus particles with nanoscale anisotropy.* Nature Materials, 2005. **4**(10): p. 759-763.
17. Mossman, K.D., et al., *Altered TCR signaling from geometrically repatterned immunological synapses.* Science, 2005. **310**(5751): p. 1191-1193.
18. Pike, L.J., *Rafts defined: a report on the Keystone Symposium on Lipid Rafts and Cell Function.* J Lipid Res, 2006. **47**(7): p. 1597-8.
19. Lingwood, D. and K. Simons, *Lipid Rafts As a Membrane-Organizing Principle.* Science, 2010. **327**(5961): p. 46-50.
20. Hancock, J.F., *Lipid rafts: contentious only from simplistic standpoints.* Nature Reviews Molecular Cell Biology, 2006. **7**(6): p. 456-462.

21. Nicolau, D.V., et al., *Identifying optimal lipid raft characteristics required to promote nanoscale protein-protein interactions on the plasma membrane.* Molecular and Cellular Biology, 2006. **26**(1): p. 313-323.
22. Vogt, A.B., S. Spindeldreher, and H. Kropshofer, *Clustering of MHC-peptide complexes prior to their engagement in the immunological synapse: lipid raft and tetraspan microdomains.* Immunol Rev, 2002. **189**: p. 136-51.
23. Anderson, H.A., E.M. Hiltbold, and P.A. Roche, *Concentration of MHC class II molecules in lipid rafts facilitates antigen presentation.* Nat Immunol, 2000. **1**(2): p. 156-62.
24. Giannoni, F., et al., *Clustering of T cell ligands on artificial APC membranes influences T cell activation and protein kinase C theta translocation to the T cell plasma membrane.* J Immunol, 2005. **174**(6): p. 3204-11.
25. Zappasodi, R., et al., *The effect of artificial antigen-presenting cells with preclustered anti-CD28/-CD3/-LFA-1 monoclonal antibodies on the induction of ex vivo expansion of functional human antitumor T cells.* Haematologica, 2008. **93**(10): p. 1523-34.
26. Tan, S., et al., *Lipid-enveloped hybrid nanoparticles for drug delivery.* Nanoscale, 2013.
27. Mossman, K.D., et al., *Altered TCR signaling from geometrically repatterned immunological synapses.* Science, 2005. **310**(5751): p. 1191-3.
28. Jin, T., P. Pennefather, and P.I. Lee, *Lipobeads: a hydrogel anchored lipid vesicle system.* FEBS Lett, 1996. **397**(1): p. 70-4.
29. Liu, J., et al., *Electrostatically mediated liposome fusion and lipid exchange with a nanoparticle-supported bilayer for control of surface charge, drug containment, and delivery.* J Am Chem Soc, 2009. **131**(22): p. 7567-9.
30. Mornet, S., et al., *The formation of supported lipid bilayers on silica nanoparticles revealed by cryoelectron microscopy.* Nano Letters, 2005. **5**(2): p. 281-5.
31. Hu, C.M., et al., *Erythrocyte membrane-camouflaged polymeric nanoparticles as a biomimetic delivery platform.* Proc Natl Acad Sci U S A, 2011. **108**(27): p. 10980-5.
32. Ashley, C.E., et al., *The targeted delivery of multicomponent cargos to cancer cells by nanoporous particle-supported lipid bilayers.* Nature Materials, 2011. **10**(5): p. 389-97.
33. Porotto, M., et al., *Synthetic protocells interact with viral nanomachinery and inactivate pathogenic human virus.* PLoS One, 2011. **6**(3): p. e16874.
34. Parodi, A., et al., *Synthetic nanoparticles functionalized with biomimetic leukocyte membranes possess cell-like functions.* Nat Nanotechnol, 2013. **8**(1): p. 61-8.
35. Castellino, F., et al., *Chemokines enhance immunity by guiding naive CD8+ T cells to sites of CD4+ T cell-dendritic cell interaction.* Nature, 2006. **440**(7086): p. 890-5.
36. Steenblock, E.R., et al., *An artificial antigen-presenting cell with paracrine delivery of IL-2 impacts the magnitude and direction of the T cell response.* J Biol Chem, 2011. **286**(40): p. 34883-92.

37. Mescher, M.F., *Surface contact requirements for activation of cytotoxic T lymphocytes.* J Immunol, 1992. **149**(7): p. 2402-5.
38. Banchereau, J. and R.M. Steinman, *Dendritic cells and the control of immunity.* Nature, 1998. **392**(6673): p. 245-52.
39. Engelhard, V.H., et al., *Induction of secondary cytotoxic T lymphocytes by purified HLA-A and HLA-B antigens reconstituted into phospholipid vesicles.* Proc Natl Acad Sci U S A, 1978. **75**(11): p. 5688-91.
40. Dustin, M.L. and J.T. Groves, *Receptor signaling clusters in the immune synapse.* Annu Rev Biophys, 2012. **41**: p. 543-56.

Vita

Joel Chaim Sunshine was born in Washington, D.C., on July 2, 1985, to Philip and Margot Sunshine. After spending kindergarten through 12th grade at the Charles E. Smith Jewish Day School in Rockville, M.D., he attended Brandeis University in Waltham, M.A., where he earned a Bachelor of Science in Biochemistry and a Masters of Science in Chemistry in May 2007. At Brandeis he also met his future wife, Sarah Brem, and they married in August 2007.

Interested in pursuing more engineering approaches to biological problems, he then worked in the Laboratory of Dr. Robert S. Langer at the Massachusetts Institute of Technology for one year. He then joined the M.D./Ph.D. program at the Johns Hopkins School of Medicine in September of 2008, and the Ph.D. program in Biomedical Engineering in September 2010. Under the guidance of his Ph.D. mentor, Dr. Jordan Green, he helped to develop a cationic polymer library for gene delivery applications, and developed a non-spherical platform for artificial antigen presentation, and plans to graduate and return to the clinic in May 2013. His passions outside of work include running, playing and watching sports, and spending time with family and friends.